

Beyond 5G White Paper

6G Radio Technology Project

“Repeater, metasurface, and RIS/IRS”

Version 1.0

May 7, 2025

XG Mobile Promotion Forum



Contents

Preface.....	6
I. Introduction.....	7
II. Use cases and scenarios	8
II.1. Introduction.....	8
II.2. Repeater.....	8
II.2.1. Operating mode.....	8
II.2.2. Use case.....	10
II.3. Metasurface and RIS/IRS	15
II.3.1. Operating mode.....	16
II.3.2. Use case.....	22
II.4. Operating environment and deployment scenarios	28
II.4.1. Operating environment.....	28
II.4.2. Deployment scenarios	29
III. Technology trend survey	30
III.1. Introduction.....	30
III.2. Categories of repeater, metasurface, and RIS/IRS.....	30
III.3. Publication summary.....	31
III.4. Overall trend	55
III.5. Technology trend on repeater.....	58
III.6. Technology trend on metasurface.....	63
III.7. Technology trend on RIS/IRS	68
IV. Standardization survey	72
IV.1. Network Controlled Repeater (NCR)	72
IV.2. Integrated Access and Backhaul (IAB).....	74
IV.3. RIS/IRS	75
IV.4. Summary	78
V. Recent activities in Japan	80
V.1. Repeater.....	81

GROUP A -- AF relay (NCR)	81
V.1.1. Field evaluation of mmWave relays in various topologies	82
V.1.2. mmWave massive analog relay MIMO	87
V.1.3. mmWave massive analog relay MU-MIMO with resource and user scheduling	93
V.1.4. Phased array antenna technology for 6G analog repeater system	99
V.1.5. Research on low latency relay technology to extend millimeter wave area	102
GROUP B -- Other relay technologies	108
V.1.6. Wireless transport technology for Xhaul.....	109
V.2. Metasurface and RIS/IRS	115
GROUP C -- Metasurface (static).....	115
V.2.1. Analysis of using transmissive metasurfaces toward 5G evolution and 6G	116
V.2.2. Optically transparent dual-band meta-surface reflector	123
V.2.3. Metasurface technologies for controlling radio waves in specific directions	126
V.2.4. Social implementation technology for passive reflector that support the Sub6 band and above, and the results of verification	132
V.2.5. Transparent & flexible metasurface reflector film	139
V.2.6. Reconfigurable metasurface reflector with multi sheets/sliding sheets	147
GROUP D -- RIS/IRS (programmable).....	154
V.2.7. An efficient beam searching in hybrid intelligent reflecting/refracting surfaces (IRS)-aided mmWave 6G network	155
V.2.8. Relay-related technologies in new radio network topology	161
V.2.9. Beamforming-based IRS control for Sub-Terahertz-band communications in indoor office environments.....	166
V.2.10. Beam squint-aware frequency resource allocation for IRS-aided communication	171
V.2.11. Prototype and evaluation of intelligent reflecting surface for 60 GHz band	175
V.2.12. Experimental evaluation of impact of intelligent reflecting surface for 60 GHz band on radio channel in Sub-6 GHz band	182
V.2.13. Performance evaluation of RIS-empowered 6G system by system-level and link- level simulations	187
V.2.14. Liquid crystal reconfigurable intelligent surface.....	195

V.2.15. Multishape radio and its experimental studies using Airy and Bessel beams in Sub-THz bands: RIS perspective on beam manipulation	199
VI. Summary	205
Abbreviation list.....	206

【Revision History】

Ver.	Date	Contents	Note
1.0	2025.5.7	Initial version	

【Editor List】

No.	Name	Affiliation	Note
1	Kei Sakaguchi	Institute of Science Tokyo	Chief editor
2	Yuichi Kawamoto	Tohoku University	Editor
3	Gia Khanh Tran	Institute of Science Tokyo	Editor
4	Takuya Ohto	KDDI Research, Inc.	Section II
5	Masamichi Yonehara	KYOCERA Corporation	Section II
6	Hiroshi Okamoto	KYOCERA Corporation	Section II
7	Kugo Morita	KYOCERA Corporation	Section II
8	Akira Sakai	VIAVI Solutions	Section II
9	Hiroaki Asano	Panasonic System Networks R&D Lab. Co., Ltd.	Section II
10	Shinjiro Fukuyama	Sekisui Chemical Co., Ltd.	Section II
11	Tomoki Murakami	NTT Corporation	Section III
12	Keisuke Sato	DKK Co., Ltd.	Section III
13	Yuichi Miyazaki	Dai Nippon Printing Co., Ltd.	Section III
14	Takahiro Ohyama	Panasonic System Networks R&D Lab. Co., Ltd.	Section III
15	Doohwan Lee	NTT Corporation	Section III
16	Takumi Yoneda	NTT Corporation	Section III
17	Daisuke Kitayama	NTT Corporation	Section III
18	Hiroki Maeda	Dai Nippon Printing Co., Ltd.	Section III
19	Masatoshi Sano	Sekisui Chemical Co., Ltd.	Section III
20	Takahiro Saiwai	KYOCERA Corporation	Section III
21	Jin Nakazato	The University of Tokyo	Section IV
22	Yuyuan Chang	NTT DOCOMO, INC.	Section IV
23	Kazuto Yano	Advanced Telecommunications Research Institute International	Section IV
24			
25			
26			
27			
28			
29			
30			
31			
32			
33			
34			
35			
36			
37			
38			
39			
40			
41			

Preface

This white paper is intended for telecom operators and vendors worldwide who will develop and deploy repeater, metasurface, and Reconfigurable Intelligent Surface (RIS)/Intelligent Reflecting Surface (RIS/IRS), for Beyond 5G and 6G. Based on insights gained from the deployment of mmWave 5G by four telecom operators in Japan since 2020, the 6G Radio Technology Project of XGMF has decided to publish this white paper as a comprehensive guide for the use of repeater, metasurface, and RIS/IRS, in mmWave deployment for Beyond 5G and 6G, including the contents to Beyond 5G White Paper Supplementary Volume "Relay and Reflector Technologies" published by XGMF in 2024.

As we embark on the journey towards Beyond 5G/6G technologies, repeater, metasurface, and RIS/IRS technologies emerge as one of key elements in this technological evolution. Japan's endeavor to overcome the challenges to realize the repeater, metasurface, and RIS/IRS technologies, coupled with its commitment to research and development in this domain, positions it at the forefront of this next-generation mobile communication revolution. This white paper aims to provide a comprehensive overview of the potential, challenges, and future directions of the repeater, metasurface, and RIS/IRS technologies for Beyond 5G and 6G, with a particular emphasis on their initiatives and advancements in Japan.

This white paper was prepared with the generous support of many people who participated in "Repeater, Metasurface, and RIS/IRS" Working Group of 6G Radio Technology Project, XGMF. The cooperation of telecommunications industry players and academia experts, as well as representatives of various industries other than the communications industry has also been substantial. Thanks to everyone's participation and support, this white paper was able to provide a lot of useful information for future business creation discussions between the industry, academia, and government, and for investigating solutions to social issues, not only in the telecommunications industry, but also across all industries. We hope that this white paper will help Japan create a better future for society and promote significant global activities.

Yuichi Kawamoto
Tohoku University

I. Introduction

As the world moves beyond 5G (B5G) and toward the realization of 6G networks, wireless communication systems must address unprecedented challenges in coverage expansion, spectral efficiency, energy optimization, and ultra-reliable low-latency communication (URLLC). The increasing adoption of high-frequency millimeter-wave (mmWave) and sub-terahertz (THz) bands introduces signal propagation challenges due to path loss, atmospheric absorption, and blockage effects. To overcome these limitations, relay and reflector technologies via repeater and intelligent metasurfaces are expected to play a vital role in enhancing network connectivity, extending coverage, and optimizing wireless transmission efficiency.

This Beyond 5G White Paper focuses on the “Repeater, metasurface, and RIS/IRS”, which integrates relay nodes, repeaters, intelligent reflecting surfaces (IRS), and metasurface technologies as key enablers of next-generation wireless networks. The paper explores various technological innovations, including network-controlled reflection/diffraction, decode-and-forward (DF) and amplify-and-forward (AF) relays, which facilitate efficient signal transmission in complex environments. Additionally, these technologies are highlighted as promising solutions to dynamically control radio wave propagation, mitigate interference, and enhance non-line-of-sight (NLOS) communications. These advancements will be crucial in achieving seamless connectivity in urban environments, high-speed mobility applications, and remote rural areas where traditional network infrastructure is limited.

The document also provides an overview of current standardization efforts, research trends, and experimental demonstrations in Japan, emphasizing the nation's commitment to driving B5G and 6G technological advancements. Key industry stakeholders and research institutions are actively exploring practical deployment scenarios, cost-effective implementation strategies, and energy-efficient architectures to make relay and reflector-assisted wireless communication viable for future mobile networks. The discussion extends to potential use cases, including ultra-dense urban networks, disaster recovery communication, autonomous vehicle connectivity, and non-terrestrial and terrestrial hybrid networks.

As Beyond 5G and 6G networks continue to evolve, the insights presented in this white paper will serve as a foundational guide for academia, industry, and government stakeholders working toward the next generation of wireless technologies. By leveraging relay and reflector-based solutions, the future of wireless communication can achieve greater efficiency, wider coverage, and seamless global connectivity, paving the way for a highly connected and intelligent digital society.

This paper is organized as follows. Chapter II, III and IV respectively presents surveys of use cases and scenarios where relaying technologies in this paper are required, latest technical trends of relay and reflector technologies, international standardization activities. Finally, Chapter V will individually introduce latest research achievements in Japan.

II. Use cases and scenarios

II.1. Introduction

In this section, we provide an overview of the use cases and scenarios for repeaters, metasurfaces and RIS/IRS. First, we will explain the operating modes for the repeaters, metasurfaces and RIS/IRS, followed by an introduction to their respective use cases. Finally, we discuss the operating environment and deployment scenarios.

II.2. Repeater

II.2.1. Operating mode

II.2.1.1. Decode and forward

Decode and Forward (DF) is a relaying mode to enhance signal reliability and coverage. It is a two-hop relaying technique where the relay node down-converts the received signals into baseband, decodes the received signal to remove the effect of noise at the repeater, re-encodes it, and then up-converts to the carrier frequency to forward the processed signal to the destination. This method mitigates noise propagation compared to amplify-and-forward, since the relay regenerates the transmitted data rather than forwarding a noisy version of the received signal, at the expense of introducing baseband signal processing at the repeater.

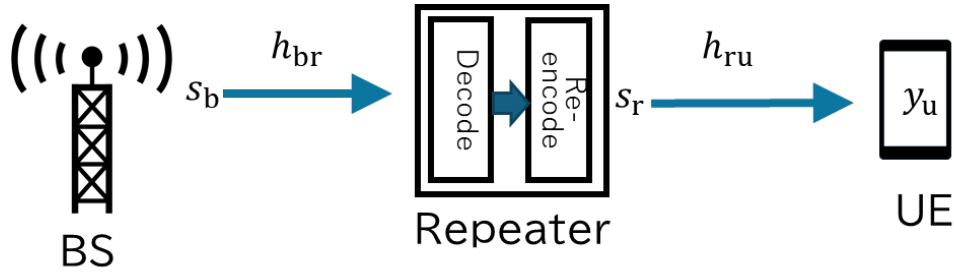


Fig. II.2.1-1 Decode and forward mode.

Mathematically, the transmission process in a DF mode can be represented as follows, where $s_b, s_r, y_r, y_u, n_r, n_u$ respectively represent the transmit signal at the transmitter, the regenerated transmit signal at the repeater, the receive signal at the repeater and the end user, noise at the repeater and the end user.

$$y_r = h_{br}s_b + n_r$$

$$s_r = \Delta(y_r, s)$$

$$y_u = h_{ru}s_r + n_u$$

Here, h_{br}, h_{ru} are respectively the channel responses between the transmitter/repeater and repeater/end user pairs, and $\Delta(y_r, s_b)$ denotes the process of estimating s_b from y_r and reconstructing them as s_r for retransmission.

II.2.1.2. Amplify and forward

Amplify and Forward (AF) is a relaying mode to improve signal coverage and reliability. In this technique, the relay node directly amplifies the received signal at carrier frequency and forwards it to the destination without performing any down-converting/decoding and re-encoding/up-converting. This method is computationally simpler compared to DF but suffers from noise amplification, as any noise introduced in the first hop is also forwarded to the destination.

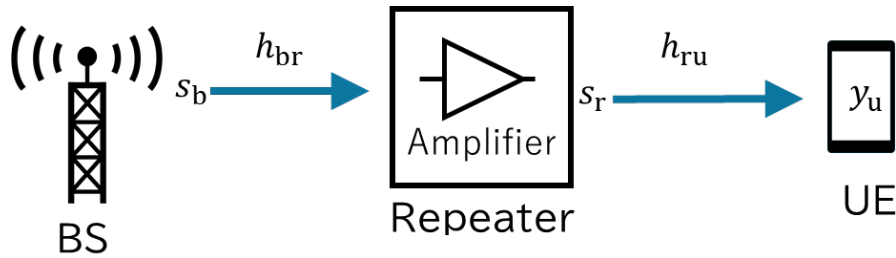


Fig. II.2.1-2 Amplify and forward mode.

Mathematically, the transmission process in an AF mode can be represented as follows, where β is an amplification coefficient at the repeater.

$$y_r = h_{br}s_b + n_r$$

$$s_r = \beta y_r$$

$$y_u = h_{ru}s_r + n_u$$

Different from DF, the received signal at the end user can be rewritten as.

$$y_u = \beta h_{ru}(h_{br}s_b + n_r) + n_u$$

$$= \beta h_{ru}h_{br}s_b + \beta h_{ru}n_r + n_u$$

As seen from the last equation, due to simple amplification at the repeater, the noise at the repeater propagates to the end user and accumulates with the noise at the receiver end, that substantially increases the noise level.

II.2.1.3. Beamforming

Beamforming mode can be additionally applied upon the two aforementioned relaying modes. In beamforming mode, the repeater is equipped with beamforming antennas at either receiving or retransmitting interfaces or both. The introduction of beamforming antennas with high directivities helps to furthermore boost the signal strength over the relaying path.

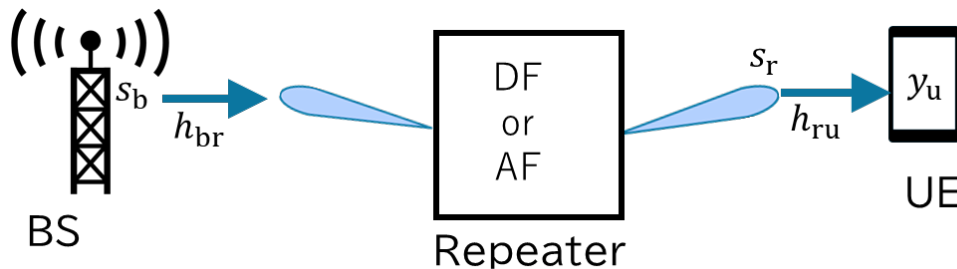


Fig. II.2.1-3 Beamforming mode.

II.2.2. Use case

II.2.2.1. Coverage enhancement

When constructing a wireless communication network, various obstacles such as buildings and trees pose a problem in forming a communication area. In areas with weak radio signal strength due to obstacles or distance attenuation, terminals cannot achieve sufficient throughput, making it difficult to ensure QoS.

As the frequency increases, the propagation loss becomes greater, making it difficult to maintain wireless quality. Additionally, the weakening of the diffraction effect makes it difficult for radio signals to bend around obstacles. One possible solution would be to install many base stations, but this would be disadvantageous in terms of cost and power consumption.

Repeaters present a viable solution to these challenges. For areas that are shaded by obstacles or are far from the base station, repeaters can be installed in locations where wireless quality from base stations can be ensured to relay radio signals. And it can provide sufficient wireless quality to terminals in the target area. Figure II.2.2-1 demonstrates the repeater relays radio signals between the base station (BS) and the terminal (UE), avoiding obstacles such as buildings and trees.

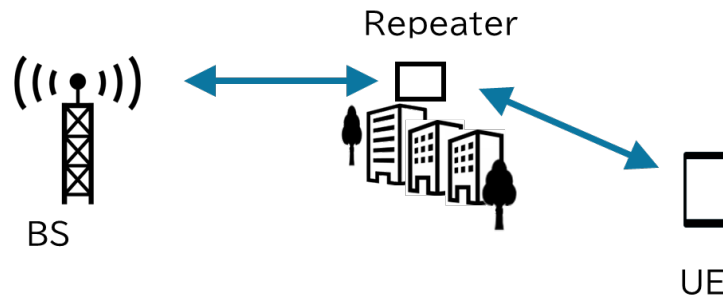


Fig. II.2.2-1. The repeater relays radio signals between BS and UE, avoiding obstacles such as buildings and trees.

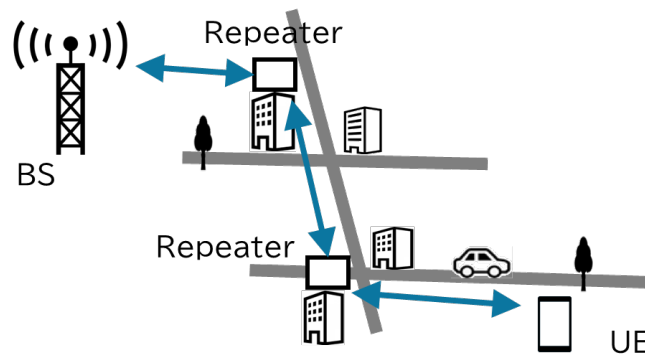


Fig. II.2.2-2. Repeaters in a multi-hop configuration relay radio signals between BS and UE.

In a wireless communication system utilizing repeaters, there are two configurations. One is a single hop, as shown in Figure II.2.2-1, and the other is a multi-hop, where radio signals are relayed through multiple repeaters. Figure II.2.2-2 illustrates the use of repeaters in a multi-hop configuration.

In addition to terrestrial buildings, repeaters can also be mounted on aerial platforms such as drones. By using repeaters mounted on aerial platforms, it is possible to flexibly change relay position according to location of UEs, thereby facilitating easy area expansion (e.g., [II.2.2-1]).

II.2.2.2. Spectral efficiency

(1) MIMO

In wireless communication networks, the number of eigen channels for parallel data transmission is limited when channels between transmitter antennas and receiver antennas may have strong correlation.

When using an amplify-and-forward repeater, it is possible to reduce channel correlation between BS and UE, thereby improving frequency utilization efficiency through spatial multiplexing. By deploying multiple repeaters and selectively using the optimal repeater, it is possible to expand communication capacity between BS and UE using MU-MIMO or SU-MIMO [II.2.2-2].

Additionally, when repeaters are mounted on drones, applying Asymmetry LOS MIMO technology allows for stable improvement in frequency utilization efficiency through spatial multiplexing, even if the distance between the BS and the repeater varies [II.2.2-3].

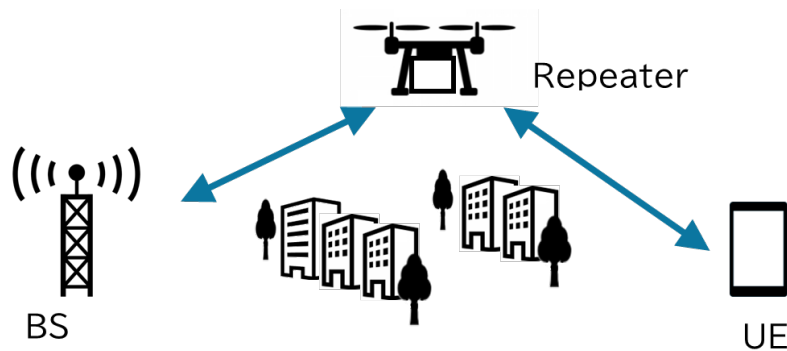


Fig. II.2.2-3. The repeater on the drone relays radio signals between BS and UE.

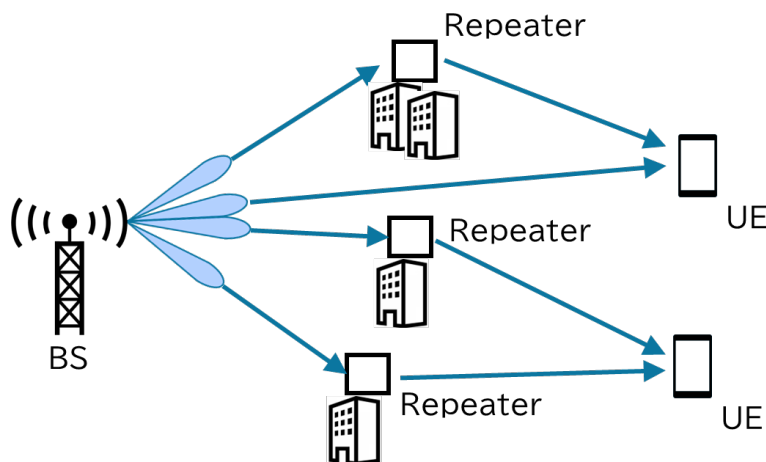


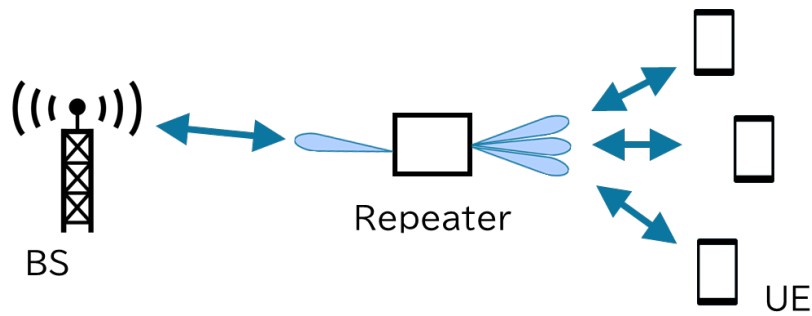
Fig. II.2.2-4. MU-MIMOs are realized with utilizing wireless links between BS and UE or wireless links via repeaters.

(2) AMC

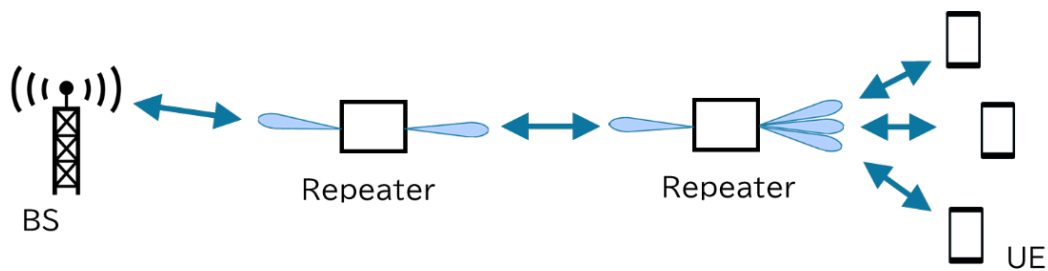
In wireless communication systems, Adaptive Modulation and Coding (AMC) technology, which adaptively controls the order of multi-level modulation according to the level of wireless quality, is widely used. Compared to not using repeaters, using repeaters ensures sufficient wireless quality and enables the use of higher-order adaptive modulation, thereby improving frequency utilization efficiency.

(3) Beam control

In high-frequency bands, beamforming technology is widely used to mitigate propagation loss in wireless transmission. Beam control, which enables appropriate use of beamforming at each node in a wireless communication system, reduces interference, improves wireless quality, and expands coverage area. It contributes to improve frequency utilization efficiency [II.2.2-4]. Beam control can be applied to both decode-and-forward repeaters and amplify-and-forward repeaters, in both relay links and access links.



(a) Beam control applied to a single hop repeater



(b) Beam control applied to a multi-hop repeater

Fig. II.2.2-5. To improve frequency utilization efficiency, beam control is applied to repeaters in single hop and multi-hop configurations.

II.2.2.3. Others

(1) Reliability

In a wireless communication network, deploying multiple repeaters to connect to UEs allows for redundant usage, thereby improving reliability. Compared to deploying multiple BSs, installing

repeaters enables the construction of a network that ensures reliability at a lower cost and with reduced complexity. When multiple repeaters are installed, reliability can be enhanced through coverage enhancement effects and improved spectral efficiency via MIMO/AMC.

(2) Energy efficiency

Future wireless communication networks will face significant challenges in reducing energy consumption due to increasing data capacity demands. To achieve sustainable wireless communication networks, many energy-efficient technologies are being considered. For repeaters, technologies are being explored that allow for the power-off of unnecessary repeater relay functions in coordination with BSs, depending on locations of UEs. Applying these technologies can reduce the overall power consumption of the wireless communication network [II.2.2-2] [II.2.2-4].

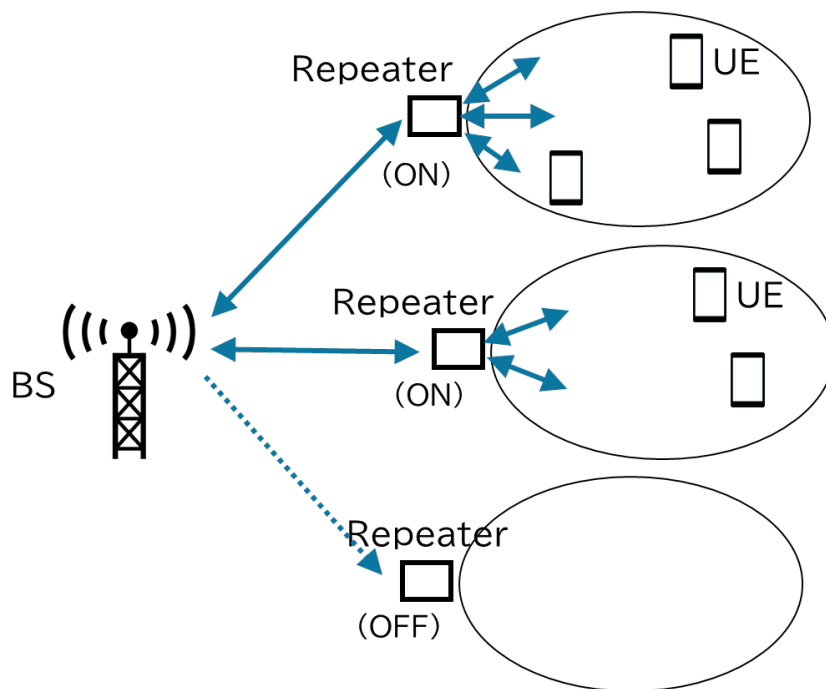


Figure II.2.2-6. Depending on locations of UEs, repeaters coordinate with the BS to power off the relay function of repeaters that are no longer needed and power on the relay function of repeaters that are needed, thereby reducing power consumption.

REFERENCE

- [II.2.2-1] Y. Ambe, Y. Okada, Y. Yokota, S. Abe, F. Kojima, T. Miyachi, "Radio-map-based flight planning of autonomous repeater drones for bridge inspection," IEEE PIMRC, 2022
- [II.2.2-2] Suwen Ke, Gia Khanh Tran, Zongdian Li, Kei Sakaguchi, "Millimeter-wave massive analog relay MU-MIMO with blocking-empowered user scheduling toward 6G," IEEE Open Journal of the Communications Society, vol.6, pp1-12, Dec., 2024
- [II.2.2-3] N. Matsumura, K. Nishimori, R. Taniguchi, T. Hiraguri, T. Tomura and J. Hirokawa, "Novel Unmanned Aerial Vehicle-Based Line-of-Sight MIMO Configuration Independent of Transmitted Distance Using Millimeter Wave," IEEE Access, Vol. 8, pp. 11679-11691, 2020.
- [II.2.2-4] 3GPP TS 38.106 V18.7.0, "NR; NR Repeater Radio Transmission and Reception," Dec. 2024.

II.3. Metasurface and RIS/IRS

The basic principle of devices that control the direction of propagation of electromagnetic waves by reflection or refraction (or transmission) is that multiple elements (meta-atoms) arranged within the device plane control the reflected wavefront (or transmitted wavefront) by having appropriate reflection phases (or transmission phases) each [Fig. II.3-1].

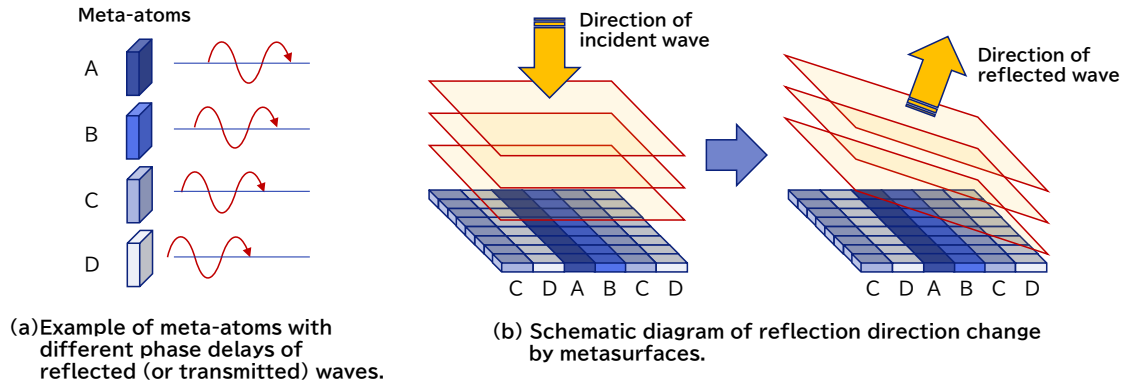


Fig. II.3-1. Illustration of why metasurfaces change the direction of propagation of electromagnetic waves.

In this case, if the reflection characteristics are set in advance during manufacturing and cannot be changed afterwards, it is called a static metasurface, and if the reflection characteristics can be changed afterwards, it is called a non-static metasurface. Among these, those whose reflection characteristics can be changed using electrical means are called programmable metasurfaces (RIS/IRS) [Fig. II.3-2].

In order for static devices to be effective, sufficient specification review is required before installation, but they are basically simple in structure and are more advantageous than variable types in terms of component and running costs. Non-static devices can adapt to changes in the surrounding environment after installation and to changes in the direction of the target to which electromagnetic waves are to be transmitted, and they are advantageous in that they can reduce the number of device types (number of products). In particular, programmable types are effective when it is necessary to change the communication environment frequently.

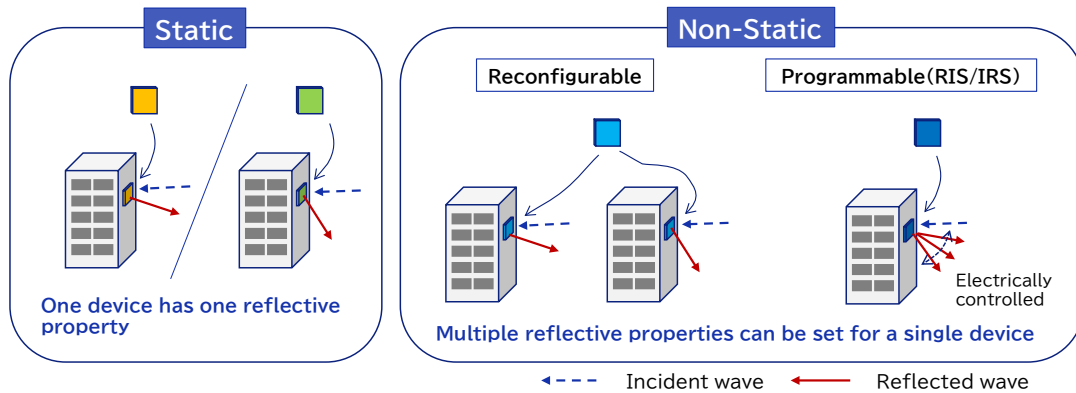


Fig. II.3-2. Example of classification of devices that control the direction of electromagnetic wave propagation with metasurfaces.

II.3.1. Operating mode

II.3.1.1. Passive

Passive-type electromagnetic wave direction control devices do not amplify incoming radio waves, but instead control the direction of reflection or refraction (transmission), or the reflection or transmission rate [Fig. II.3.1-3]. Because they do not amplify power, they cannot be used to extend the range of radio waves from the device, and their main uses are to deliver radio waves to areas that are in the shadow of structures, or to create new propagation paths in areas where radio waves are already being received. However, on the other hand, they have the advantage of being easy to introduce, as they are not subject to various restrictions on their use. Naturally, they also have the potential to reduce running costs.

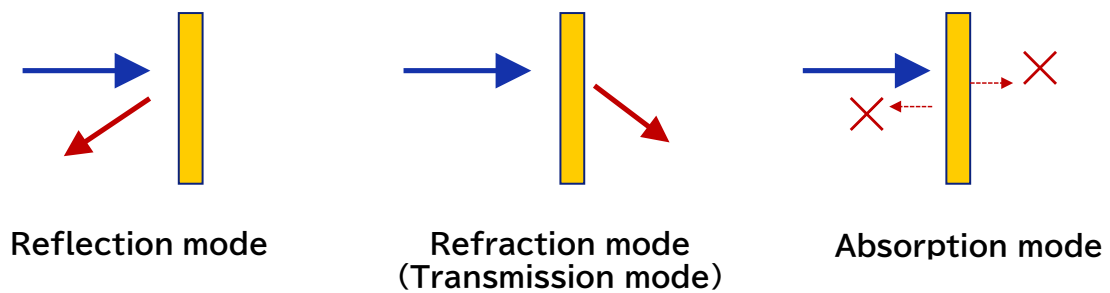


Fig. II.3.1-3. Typical modes of passive type electromagnetic wave propagation direction control devices.

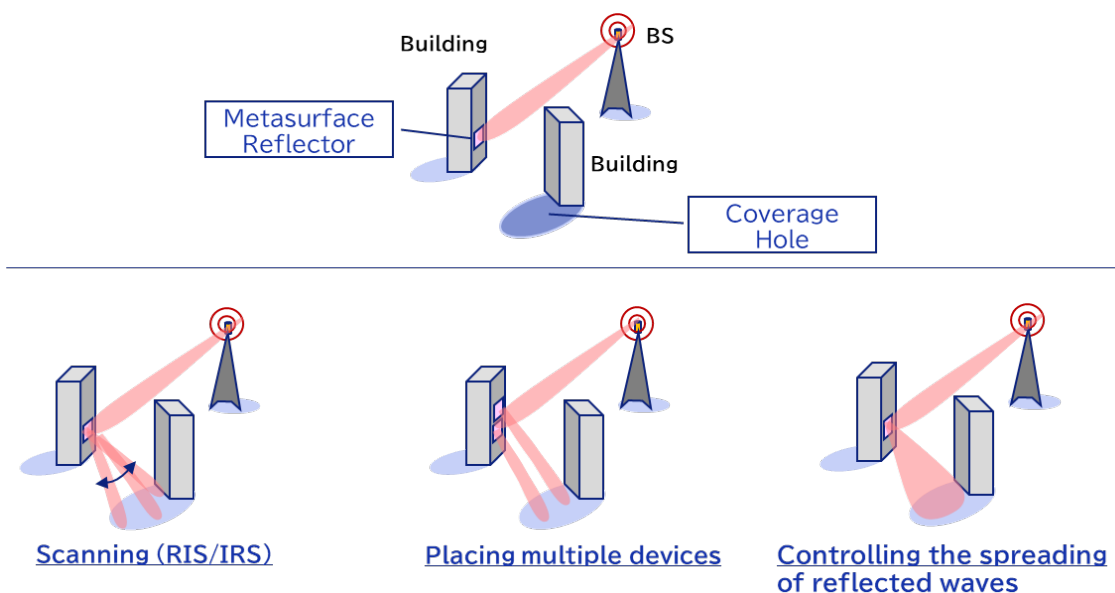


Fig. II.3.1-2. Examples of efficient ways to resolve a coverage hole.

- Reflection

Reflection mode controls the reflection characteristics by arranging the reflection phase of multiple elements (meta-atoms) in the device plane, and has the function of reflecting electromagnetic waves in the target frequency band in a set direction. The main applications are expected to be improving the communication environment in coverage holes and improving communication quality as part of MIMO. In addition, there are also studies on using multiple devices in combination with a single base station.

In reflection mode, the device basically has a ground layer, so it behaves like a metal plate in frequency bands other than the target band, and for this reason it can also be used as a shielding material. In addition, because the incident surface and the reflecting surface are the same, and there is a so-called “back surface” that does not affect incident or reflected waves, it can be attached to the wall of a structure, etc., when installed. There is also a type that transmits electromagnetic waves other than the target frequency, without using a ground layer, so it can be used differently depending on the installation environment. In addition, the use of transparent materials is being considered for installation in windows and other locations.

In reflection mode, the reflection efficiency decreases as the incident angle and reflection angle approach 90° , so it is necessary to consider the direction of installation and the size of the device that can be installed.

There are several ways to efficiently cover the area per device, such as scanning the reflected wave within the target area, arranging multiple devices with different reflection directions, and setting the spread of the reflected wave from the device to match the size of the target area. In particular, programmable RIS/RIS is used for scanning [Fig. II.3.1-2].

- Refraction

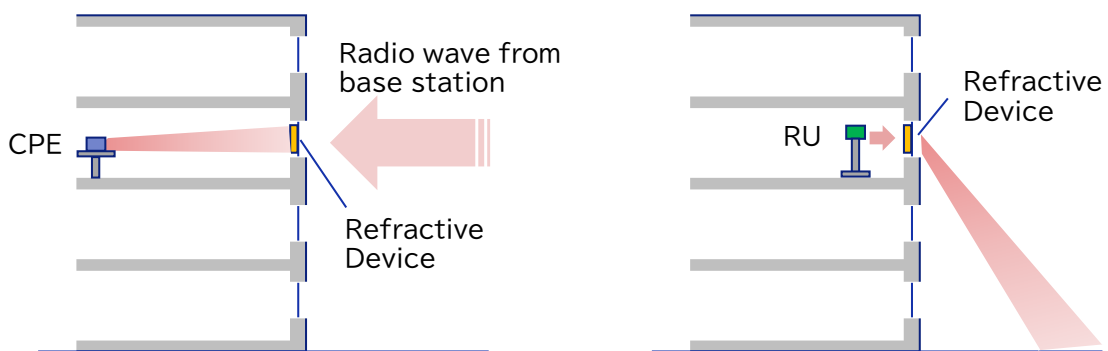


Fig. II.3.1-3. Examples of radio wave refraction device application

Refraction mode devices control the transmitted wavefront by arranging the transmission phase of multiple elements (meta-atoms) within the device plane, or by applying the Fresnel zone plate principle using a combination of transmission and shielding.

Devices in this mode have the incident and reflected surfaces on opposite sides, so they are not installed on walls that block radio waves, but are instead installed in windows or fixed in open spaces using installation jigs.

The main use is to improve coverage holes, but in particular, there are also studies underway on using it through windows, such as using it to concentrate radio waves from outside into CPE inside the building, or using it to transmit radio waves from base stations on upper floors of buildings through windows to the foot of the building. There are also studies underway on devices with light transmissivity, with the aim of installing them in windows [Fig. II.3.1-3].

- Omni Surface / STAR-RIS

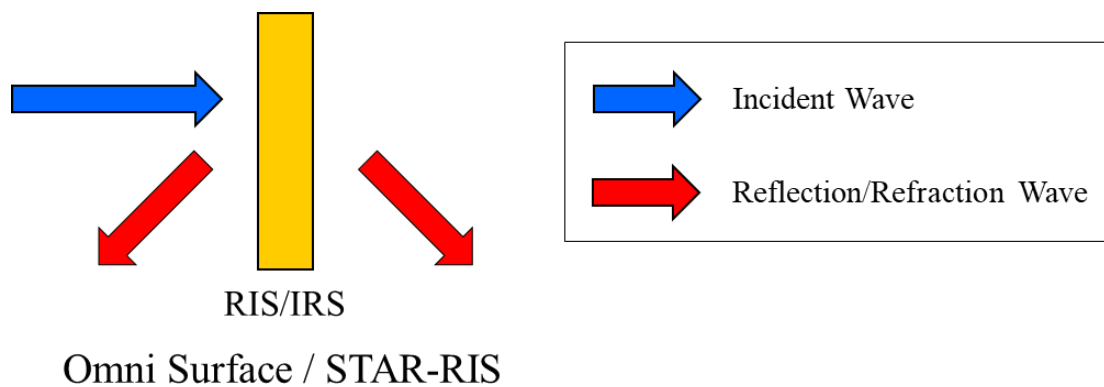


Fig. II.3.1-4. Typical modes of Omni Surface / STAR-RIS type electromagnetic wave propagation direction control devices.

RIS/IRS that are capable of simultaneously processing or switching between reflection and refraction signals are under consideration. These devices enable omnidirectional communication, allowing users to communicate regardless of the position of the RIS/IRS. Similar to the reflection mode, these devices utilize both sides and can be mounted on windows or fixed in open spaces using installation fixtures. The types of devices under consideration include the Omni Surface, which performs reflection and refraction simultaneously [II.2.1-1], the Simultaneously Transmitting And Reflecting RIS(STAR-RIS) [II.2.1-2], [II.2.1-3], and RIS/IRS capable of switching between reflection and refraction modes [II.2.1-4] [II.2.1-5].

- Absorption

Devices that absorb electromagnetic waves can be used to ensure security due to leaked radio waves and to suppress interference with adjacent base stations, but for some purposes, shielding can be substituted for absorption. The principle of absorbing electromagnetic waves includes those that absorb electromagnetic waves according to the properties of the material and those that apply the principle of metasurfaces to limit the frequency of absorption. Some types with variable absorption characteristics have also been proposed. The application of transparent absorbing devices, intended for installation in windows, is also being considered.

II.3.1.2. Active and hybrid

Active and Hybrid Type RIS/IRS amplifies signals by receiving external power supply. While it may result in increased power consumption, it enables long-distance transmission and high signal strength, which are challenging for passive RIS/IRS. Utilization in SU-MIMO [II.2.1-6], MU-MIMO [II.2.1-7], and the transmission and reception of signals discussed later is being considered.

Additionally, efforts to reduce power consumption are advancing. Considerations include methods where multiple elements share a single power amplifier while individually controlling phase shifts [II.2.1-8], power amplification methods using active load impedance [II.2.1-9], and approaches where only some elements are active components [II.2.1-10].

Describe the illustrative concept of Active and Hybrid modes as a substitute in Fig. II.2-6.

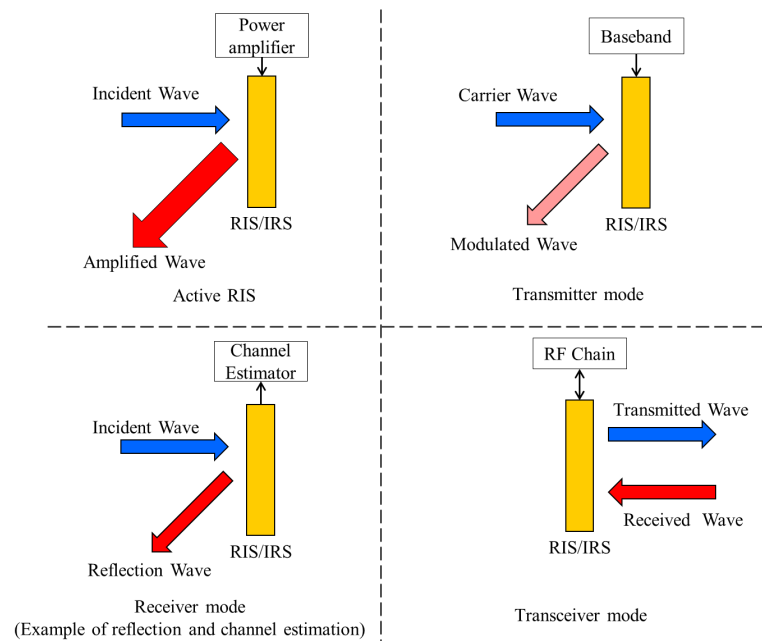


Fig. II.3.1-5. Typical modes of active and hybrid types of electromagnetic wave propagation direction control devices.

- **Transmitting**

The transmitter mode performs wireless transmission using RIS/IRS. RIS/IRS-based wireless transmitters can perform transmission, modulation and beamforming. Techniques such as MIMO-QAM [II.2.1-11], index modulation [II.2.1-12], and Passive Beamforming and Information Transfer (PBIT) [II.2.1-13] are being considered.

- **Receiving**

The reception mode performs wireless reception using RIS/IRS. RIS/IRS-based wireless receivers can perform reception, channel estimation, and sensing. By understanding the propagation environment, channel estimation enables beam direction control of the RIS/IRS without any overhead [II.2.1-14], [II.2.1-15], [II.2.1-16], [II.2.1-17]. Additionally, applications such as RF sensing [II.2.1-18] are also being considered.

- Transceiver

The transceiver mode performs wireless transmission and reception using RIS/IRS. The use of RIS/IRS is being considered as a solution to the cost and power consumption challenges in massive MIMO. Technologies such as Holographic MIMO Surface (HMIMOS) [II.2.1-19], [II.2.1-20] and Dynamic Meta-Surface Antennas (DMA) [II.2.1-21] are being explored.

REFERENCE

[II.2.1-1] S. Zhang *et al.*, "Intelligent Omni-Surfaces: Ubiquitous Wireless Transmission by Reflective-Refractive Metasurfaces," in *IEEE Transactions on Wireless Communications*, vol. 21, no. 1, pp. 219-233, Jan. 2022, doi: 10.1109/TWC.2021.3094869.

[II.2.1-2] X. Mu, Y. Liu, L. Guo, J. Lin and R. Schober, "Simultaneously Transmitting and Reflecting (STAR) RIS Aided Wireless Communications," in *IEEE Transactions on Wireless Communications*, vol. 21, no. 5, pp. 3083-3098, May 2022, doi: 10.1109/TWC.2021.3118225.

[II.2.1-3] M. Ahmed *et al.*, "A Survey on STAR-RIS: Use Cases, Recent Advances, and Future Research Challenges," in *IEEE Internet of Things Journal*, vol. 10, no. 16, pp. 14689-14711, 15 Aug. 2023, doi: 10.1109/JIOT.2023.3279357.

[II.2.1-4] NTT DOCOMO Press Release: "DOCOMO and AGC Use Metasurface — Dynamic wave manipulation and high transparency expected to optimize 5G network construction —," Jan. 2020.

[II.2.1-5] Reconfigurable Intelligent Sustainable Environments for 6G Wireless Networks (RISE-6G), 2022/7/29, "Deliverable 3.2, RIS designs, and first prototypes characterization", H2020-ICT-52/RISE-6G/D3.2

[II.2.1-6] C. You and R. Zhang, "Wireless Communication Aided by Intelligent Reflecting Surface: Active or Passive?," in *IEEE Wireless Communications Letters*, vol. 10, no. 12, pp. 2659-2663, Dec. 2021, doi: 10.1109/LWC.2021.3111044.

[II.2.1-7] Z. Zhang *et al.*, "Active RIS vs. Passive RIS: Which Will Prevail in 6G?," in *IEEE Transactions on Communications*, vol. 71, no. 3, pp. 1707-1725, March 2023, doi: 10.1109/TCOMM.2022.3231893.

[II.2.1-8] K. Liu, Z. Zhang, L. Dai, S. Xu and F. Yang, "Active Reconfigurable Intelligent Surface: Fully-Connected or Sub-Connected?," in *IEEE Communications Letters*, vol. 26, no. 1, pp. 167-171, Jan. 2022, doi: 10.1109/LCOMM.2021.3119696.

[II.2.1-9] R. Long, Y. -C. Liang, Y. Pei and E. G. Larsson, "Active Reconfigurable Intelligent Surface-Aided Wireless Communications," in *IEEE Transactions on Wireless Communications*, vol. 20, no. 8, pp. 4962-4975, Aug. 2021, doi: 10.1109/TWC.2021.3064024.

[II.2.1-10] N. T. Nguyen, Q. -D. Vu, K. Lee and M. Juntti, "Hybrid Relay-Reflecting Intelligent Surface-Assisted Wireless Communications," in *IEEE Transactions on Vehicular Technology*, vol. 71, no. 6, pp. 6228-6244, June 2022, doi: 10.1109/TVT.2022.3158686.

[II.2.1-11] W. Tang *et al.*, "MIMO Transmission Through Reconfigurable Intelligent Surface: System Design, Analysis, and Implementation," in *IEEE Journal on Selected Areas in Communications*, vol. 38, no. 11, pp. 2683-2699, Nov. 2020, doi: 10.1109/JSAC.2020.3007055.

[II.2.1-12] E. Basar, "Reconfigurable Intelligent Surface-Based Index Modulation: A New Beyond MIMO Paradigm for 6G," in *IEEE Transactions on Communications*, vol. 68, no. 5, pp. 3187-3196, May 2020, doi: 10.1109/TCOMM.2020.2971486.

[II.2.1-13] W. Yan, X. Yuan and X. Kuai, "Passive Beamforming and Information Transfer via Large Intelligent Surface," in *IEEE Wireless Communications Letters*, vol. 9, no. 4, pp. 533-537, April 2020, doi: 10.1109/LWC.2019.2961670.

[II.2.1-14] Alamzadeh, I., Alexandropoulos, G.C., Shlezinger, N. *et al.* A reconfigurable intelligent surface with integrated sensing capability. *Sci Rep* **11**, 20737 (2021). <https://doi.org/10.1038/s41598-021-99722-x>

[II.2.1-15] A. Taha, M. Alrabeiah and A. Alkhateeb, "Enabling Large Intelligent Surfaces With Compressive Sensing and Deep Learning," in *IEEE Access*, vol. 9, pp. 44304-44321, 2021, doi: 10.1109/ACCESS.2021.3064073.

[II.2.1-16] G. C. Alexandropoulos and E. Vlachos, "A Hardware Architecture For Reconfigurable Intelligent Surfaces with Minimal Active Elements for Explicit Channel Estimation," *ICASSP 2020 - 2020 IEEE International Conference on Acoustics, Speech and Signal Processing (ICASSP)*, Barcelona, Spain, 2020, pp. 9175-9179, doi: 10.1109/ICASSP40776.2020.9053976.

[II.2.1-17] G. C. Alexandropoulos, N. Shlezinger, I. Alamzadeh, M. F. Imani, H. Zhang and Y. C. Eldar, "Hybrid Reconfigurable Intelligent Metasurfaces: Enabling Simultaneous Tunable Reflections and Sensing for 6G Wireless Communications," in *IEEE Vehicular Technology Magazine*, vol. 19, no. 1, pp. 75-84, March 2024, doi: 10.1109/MVT.2023.3332580.

[II.2.1-18] J. Hu *et al.*, "Reconfigurable Intelligent Surface Based RF Sensing: Design, Optimization, and Implementation," in *IEEE Journal on Selected Areas in Communications*, vol. 38, no. 11, pp. 2700-2716, Nov. 2020, doi: 10.1109/JSAC.2020.3007041.

[II.2.1-19] C. Huang *et al.*, "Holographic MIMO Surfaces for 6G Wireless Networks: Opportunities, Challenges, and Trends," in *IEEE Wireless Communications*, vol. 27, no. 5, pp. 118-125, October 2020, doi: 10.1109/MWC.001.1900534.

[II.2.1-20] T. Gong *et al.*, "Holographic MIMO Communications: Theoretical Foundations, Enabling Technologies, and Future Directions," in *IEEE Communications Surveys & Tutorials*, vol. 26, no. 1, pp. 196-257, Firstquarter 2024, doi: 10.1109/COMST.2023.3309529.

[II.2.1-21] N. Shlezinger, G. C. Alexandropoulos, M. F. Imani, Y. C. Eldar and D. R. Smith, "Dynamic Metasurface Antennas for 6G Extreme Massive MIMO Communications," in *IEEE Wireless Communications*, vol. 28, no. 2, pp. 106-113, April 2021, doi: 10.1109/MWC.001.2000267.

II.3.2. Use case

II.3.2.1. Coverage enhancement

The typical configuration for coverage extension using a reflector is shown in the Fig. II.3.2-1. There are transmitting and receiving antennas for wireless communication, and there is an obstacle between the transmitting and receiving antennas that attenuates electromagnetic waves. In other words, the transmitting and receiving antennas are in a NLOS (Non-Line-of-Sight) condition. In such a situation, by placing a reflector at a position where both the transmitting and receiving antennas have LOS (Line-of-Sight), a propagation path that avoids attenuation due to the obstacle can be established.

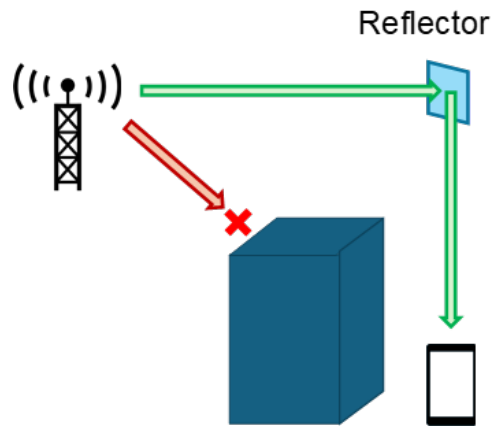


Fig. II.3.2-1 Typical configuration for coverage extension using a reflector

Another usage involves expanding the area by reflecting radio waves that have passed through a narrow path at a wide angle. There are also methods to adjust the directivity of reflection through meta-surface design, or to curve the reflector using flexible materials.

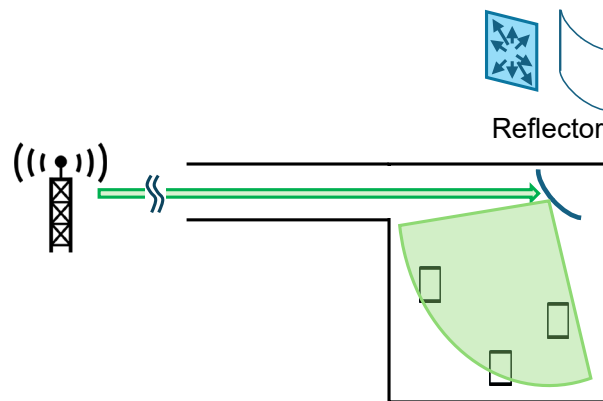


Fig. II.3.2-2 Coverage extension using a wide-angle reflector

II.3.2.2. Spectral efficiency

(1) MIMO

In high SNR channels such as line-of-sight (LOS), there is a problem that parallel data transmission cannot be utilized because the channel between the transmitting antenna and the receiving antenna is

strongly correlated. [II.3.2-1] By introducing RIS, multipaths arriving from various angles can be added to the channel, and the number of spatial multiplexing can be increased [II.3.2-2]. SU-MIMO [II.3.2-3], MU-MISO [II.3.2-4], MU-MIMO [II.3.2-5], Cell Free MIMO [II.3.2-6], etc.

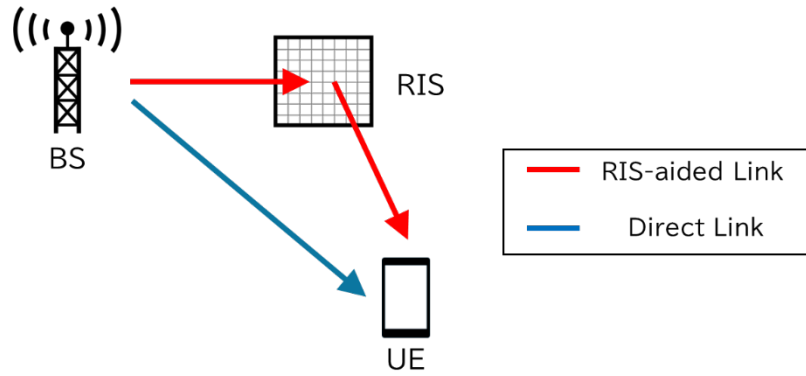


Fig. II.3.2-3 MIMO was achieved by using BS-UE's Direct Link or RIS support link via RIS.

(2) Beam Manipulation

Beam manipulation is a fundamental capability of Reconfigurable Intelligent Surface (RIS) technology, enabling precise control over the direction, shape, and focus of electromagnetic waves. Unlike traditional beamforming techniques, RIS passively reflects and reconfigures incident waves to achieve desired beam patterns, allowing for dynamic steering, splitting, and concentration of beams for various applications.

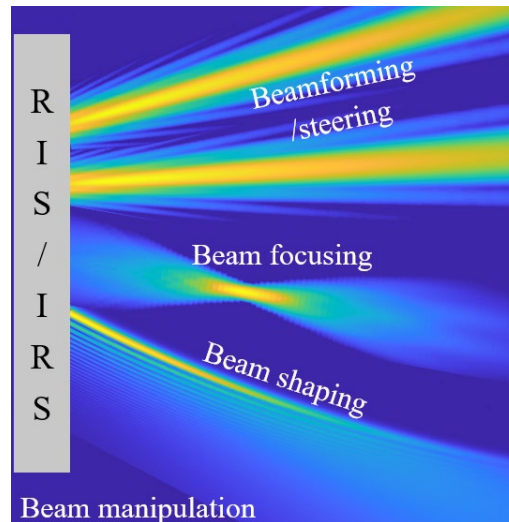


Fig. II.3.2-4 Concept of beam manipulation.

A key advantage of RIS-based beam manipulation is its precise control over wavefront propagation. Deploying RIS at the transmitter enables pre-configured beam shaping and directional transmission, reducing reliance on complex active beamforming architectures. Experimental results indicate that RIS can achieve an antenna gain of 19.1 dBi at 28 GHz, significantly enhancing millimeter-wave

communication efficiency [II.3.2-7]. By adjusting phase shifts, RIS can direct signals, focus energy, or generate multiple beams, thereby supporting localized energy delivery.

Furthermore, RIS dynamically adapts to environmental variations by modifying beam characteristics in response to obstacles or interference. The capability to generate multiple beams and mitigate interference further enhances communication robustness. For example, a 1024-element RIS operating at 26 GHz has demonstrated the ability to generate two independent beams, enabling dual-user communication in an ultra-massive MIMO prototype and achieving near-theoretical data rates [II.3.2-8]. Unlike conventional systems, which suffer from performance degradation due to reflections, RIS optimally reconfigures wave reflections to maintain superior performance.

Another critical aspect of RIS-based beam manipulation is its ability to independently control amplitude and phase, refining wavefront engineering. Unlike traditional designs that adjust only phase, advanced RIS architectures manipulate both phase and amplitude, enhancing beamforming accuracy and power efficiency. Experimental results have demonstrated improved wave steering and focusing precision, establishing RIS as a valuable tool for advanced wireless applications [II.3.2-9].

II.3.2.3. Others

(1) Reliability

In environments where metasurfaces and Reconfigurable Intelligent Surfaces (RIS/IRS) are not installed, the propagation paths between base stations and users can be obstructed due to blocking caused by the human body or vehicles, resulting in degraded communication quality [II.3.2-10]. Conversely, by implementing these technologies, even in the event of temporary obstructions, alternative paths can be established, thereby enhancing the reliability of wireless communication.

(2) Physical layer security

In wireless communication, data transmission is conducted using a common medium, space. Due to uncontrollable propagation characteristics, the transmitted data can be reached various locations. For example, the walls or ceilings close to user equipment reflect confidential signals to unwanted directions. This increases the risks of leakage of confidential signals to eavesdroppers.

To solve this problem, RIS becomes the candidate technology to enhance the physical security. By controlling the reflection direction of confidential signals to secure space, the risks of the leakage can be reduced to enhance the physical security [II.3.2-11].

(3) Sensing capabilities

In the 5G advanced and 6G wireless networks, demands for sensing performance as well as communication performance will be increased to provide many new applications. The Integrated Sensing And Communication (ISAC) systems have been gathering attention and is discussed in 3GPP rel. 19. In the ISAC systems, sensing performance depends on the Line of Sight (LoS) link between the transmitter and the target system. In other words, it is degraded in the NLoS areas. Because RIS

can provide artificial LoS links, the sensing capabilities will be enhanced by collaborating RIS and sensing systems [II.3.2-12].

(4) Energy efficiency

Energy efficiency and power consumption of wireless network has gathering great interests to provide green and sustainable service. RIS is utilized as a relay node to enhance the coverage. By utilizing passive RIS, which does not include any amplifier, the coverage can be enhanced with low power consumption compared to other relay node such as wireless repeater. In addition, since RIS can control the direction of electromagnetic (EM) waves, it has capabilities to enhance wireless power transfer efficiency of the NLoS links between transmitter and energy harvesting devices [II.3.2-13].

(5) Link management

Since RIS can control the path direction of EM waves, it also has capabilities for link management. For example, RIS can be deployed inside or inter racks of servers in a data center. RIS controls links between servers with millimeter wave or Terahertz to alleviate the cabling cost and decrease the connection complexity [II.3.2-11].

(6) Wave domain processing

Another key application of RIS is Wave Domain Processing, which enables direct manipulation of electromagnetic waves at the wavefront level. Unlike traditional digital signal processing (DSP), which operates after signals are received, Wave Domain Processing provides real-time control over wave properties, reducing latency and improving system performance.

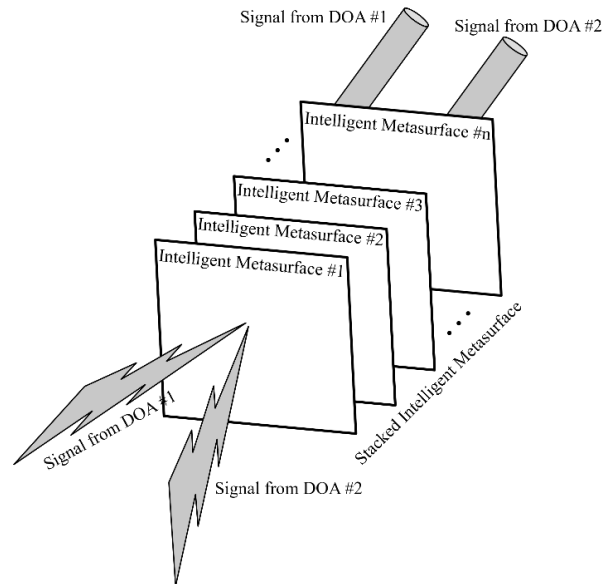


Fig. II.3.2-5 Illustration of wave domain processing of Direction of Arrival (DOA) estimation using SIMs.

One major advancement in Wave Domain Processing is the use of Stacked Intelligent Metasurfaces (SIMs) [II.3.2-15]. These multi-layered metasurfaces enable independent wave control across different

layers, allowing for beamforming, interference suppression, and signal enhancement at the wavefront level. By adjusting multiple signal paths, SIMs optimize multi-user communication, improving signal quality and reducing interference in congested environments.

For instance, Direction of Arrival (DOA) estimation can be effectively performed using SIMs. By leveraging 2D Discrete Fourier Transform (DFT) operations in the wave domain, SIMs achieve faster and more accurate DOA estimation than conventional methods. This capability is particularly valuable for applications requiring precise signal localization, such as radar and high-precision communication systems. However, successful deployment depends on environmental conditions and metasurface quality [II.3.2-16]. Another example is multi-user beamforming using SIMs. Studies have shown that stacked intelligent metasurfaces optimize wave domain beamforming by dynamically adjusting electromagnetic interactions for efficient multi-user management. This approach reduces hardware complexity while enhancing communication performance, making it a promising solution for future networks [II.3.2-17].

RIS and SIM-based Wave Domain Processing simplify wireless networks by eliminating the need for digital beamforming and high-resolution digital-to-analog converters at base stations. However, challenges such as scalability, cost, and manufacturing precision remain key considerations.

REFERENCE

- [II.3.2-1] A. Lozano, A. M. Tulino and S. Verdu, "High-SNR power offset in multiantenna communication," in *IEEE Transactions on Information Theory*, vol. 51, no. 12, pp. 4134-4151, Dec. 2005, doi: 10.1109/TIT.2005.858937
- [II.3.2-2] Ö. Özdoğan, E. Björnson and E. G. Larsson, "Using Intelligent Reflecting Surfaces for Rank Improvement in MIMO Communications," *ICASSP 2020 - 2020 IEEE International Conference on Acoustics, Speech and Signal Processing (ICASSP)*, Barcelona, Spain, 2020, pp. 9160-9164, doi: 10.1109/ICASSP40776.2020.9052904.
- [II.3.2-3] S. Zhang and R. Zhang, "Capacity Characterization for Intelligent Reflecting Surface Aided MIMO Communication," in *IEEE Journal on Selected Areas in Communications*, vol. 38, no. 8, pp. 1823-1838, Aug. 2020, doi: 10.1109/JSAC.2020.3000814
- [II.3.2-4] L. Wei, C. Huang, G. C. Alexandropoulos, C. Yuen, Z. Zhang and M. Debbah, "Channel Estimation for RIS-Empowered Multi-User MISO Wireless Communications," in *IEEE Transactions on Communications*, vol. 69, no. 6, pp. 4144-4157, June 2021, doi: 10.1109/TCOMM.2021.3063236.
- [II.3.2-5] Chen, Y. -C. Liang, H. V. Cheng and W. Yu, "Channel Estimation for Reconfigurable Intelligent Surface Aided Multi-User mmWave MIMO Systems," in *IEEE Transactions on Wireless Communications*, vol. 22, no. 10, pp. 6853-6869, Oct. 2023, doi: 10.1109/TWC.2023.3246264.
- [II.3.2-6] T. Van Chien, H. Q. Ngo, S. Chatzinotas, M. Di Renzo and B. Ottersten, "Reconfigurable Intelligent Surface-Assisted Cell-Free Massive MIMO Systems Over Spatially-Correlated Channels," in *IEEE Transactions on Wireless Communications*, vol. 21, no. 7, pp. 5106-5128, July 2022, doi: 10.1109/TWC.2021.3136925.

- [II.3.2-7] L. Dai et al., "Reconfigurable Intelligent Surface-Based Wireless Communications: Antenna Design, Prototyping, and Experimental Results," *IEEE Access*, vol. 8, pp. 45913-45923, 2020.
- [II.3.2-8] S. Zeng et al., "RIS-Based IMT-2030 Testbed for MmWave Multi-Stream Ultra-Massive MIMO Communications," *IEEE Wireless Communications*, vol. 31, no. 3, pp. 375-382, June 2024.
- [II.3.2-9] J. C. Liang, L. Zhang, Z. W. Cheng, P. Zhang, and T. J. Cui, "Flexible Beam Manipulations by Reconfigurable Intelligent Surface With Independent Control of Amplitude and Phase," *Frontiers in Materials*, vol. 9, p. 946163, 2022.
- [II.3.2-10] H. Hashida, Y. Kawamoto, N. Kato, M. Iwabuchi and T. Murakami, "Mobility-Aware User Association Strategy for IRS-Aided mm-Wave Multibeam Transmission Towards 6G," in *IEEE Journal on Selected Areas in Communications*, vol. 40, no. 5, pp. 1667-1678, May 2022.
- [II.3.2-11] M. Ahmed et al., "A Survey on STAR-RIS: Use Cases, Recent Advances, and Future Research Challenges," in *IEEE Internet of Things Journal*, vol. 10, no. 16, pp. 14689-14711, 15 Aug. 2023, doi: 10.1109/JIOT.2023.3279357.
- [II.3.2-12] P. Saikia, A. Jee, K. Singh, C. Pan, W. -J. Huang and T. A. Tsiftsis, "RIS-Aided Integrated Sensing and Communication Systems: STAR-RIS Versus Passive RIS?," in *IEEE Open Journal of the Communications Society*, vol. 5, pp. 7954-7973, 2024, doi: 10.1109/OJCOMS.2024.3515933.
- [II.3.2-13] H. Ren, Z. Zhang, Z. Peng, L. Li and C. Pan, "Energy Minimization in RIS-Assisted UAV-Enabled Wireless Power Transfer Systems," in *IEEE Internet of Things Journal*, vol. 10, no. 7, pp. 5794-5809, 1 April, 2023
- [II.3.2-14] ETSI, "Reconfigurable Intelligent Surfaces (RIS); Use cases, Deployment Scenarios and Requirements," ETSI GR RIS 001, v1.1.1, April, 2023.
- [II.3.2-15] M. Di Renzo, "State of the Art on Stacked Intelligent Metasurfaces: Communication, Sensing, and Computing in the Wave Domain," *arXiv preprint*, arXiv:2411.19687, 2024.
- [II.3.2-16] J. Zhao, Y. Liu, and X. Yang, "Stacked Intelligent Metasurface Performs a 2D DFT in the Wave Domain for DOA Estimation," *IEEE Transactions on Antennas and Propagation*, vol. 71, no. 4, pp. 3561-3572, Apr. 2023.
- [II.3.2-17] J. An, M. Di Renzo, M. Debbah, and C. Yuen, "Stacked Intelligent Metasurfaces for Multiuser Beamforming in the Wave Domain," in *Proc. IEEE International Conference on Communications (ICC)*, Rome, Italy, 2023, pp. 2834-2839.

II.4. Operating environment and deployment scenarios

II.4.1. Operating environment

(1) Indoor scenarios

For indoor scenarios, line-of-sight transmission cannot be guaranteed in some areas such as corridors, corners and stairs.

In addition, shadow fading may be serious due to the influence of obstacles such as human bodies and furniture.

Deploying RIS or repeater on the surface of walls or furniture can establish additional transmission links to improve coverage, increase received signal strength as well as SNR. Data rates can be improved for individual users and the overall system throughput can be improved as well. Indoor scenarios such as automated industrial factories may also benefit from the improvements in localization accuracy.

(2) Outdoor scenarios

For outdoor scenarios, mobile terminals and UEs at the edge of the cell or in the shadow area may suffer serious propagation loss including path loss and shadow fading caused by obstacles such as buildings or trees. RIS or repeaters can be deployed on the facade of the building or along with base stations to establish additional transmission links. In this way, the performance of these terminals can be significantly improved. However, the spread of radio waves beyond the area designated by the license may cause interference with adjacent areas.

In outdoor environment, mobility can become more significant than indoor scenarios, especially considering that UEs on high-speed trains can travel at a speed of 350 km/h. In this case, dynamically reconfigurable phase shift matrices on RIS are needed for fast beam tracking.

(3) Hybrid scenarios

Hybrid deployment scenarios for RIS or repeaters involve both indoor and outdoor environment, or describe a mixed environment which is hard to be characterized by any single scenario.

One example of hybrid scenario is the outdoor to indoor scenario. It is challenging for base stations deployed outdoors to serve indoor users due to the signal attenuation introduced by the walls or window glasses. The attenuation is more significant in FR2. One conventional solution is to deploy micro-BS inside the building, which is of high cost. In this scenario, RIS or repeaters are placed on facades of buildings or are manufactured as transparent surfaces which can also be used as window glasses. The RIS placed on facades can reflect signals to indoor environment of another building. RIS used as window glasses, which are usually transparent, can focus the incident signals into certain areas in the room and achieve good coverage. The focus points of such transparent RIS can be pre-configured according to indoor environment or dynamically changed based on real-time demands.

II.4.2. Deployment scenarios

(1) Static deployment

Typically, repeaters, metasurfaces, and Reconfigurable Intelligent Surfaces (IRS/RIS) are installed in a stationary manner. When deployed outdoors, it is anticipated that they will be mounted on rooftops or attached to poles such as streetlights and utility poles. For metasurfaces and IRS/RIS, installation on building walls, glass surfaces, and billboards is also assumed.

(2) Nomadic deployment

Another installation method that can be anticipated is a nomadic installation approach, where devices are mounted on UAVs (Unmanned Aerial Vehicles) and vehicles. This installation method enables temporary area enhancements and allows for the repositioning of devices in response to environmental changes. This is particularly effective during disasters or events. In particular, when installing repeaters on UAVs, opportunistic relay transmission and opportunistic ferry transmission become possible [II.4.2-1]. Furthermore, IRS/RIS installed on UAVs are referred to as aerial IRS/RIS and function similarly as relay nodes [II.4.2-2]. Additionally, unlike static deployment, in the case of nomadic deployment, the channels between BS or UE and the repeater (or metasurface, IRS/RIS) fluctuate depending on the position of the node, making beam control a challenge. Moreover, when using UAVs, challenges such as UAV node selection, UAV resource allocation, and interference avoidance arise.

REFERENCE

- [II.4.2-1] D. Liu et al., "Opportunistic UAV Utilization in Wireless Networks: Motivations, Applications, and Challenges," in IEEE Communications Magazine, vol. 58, no. 5, pp. 62-68, May 2020.
- [II.4.2-2] Y. Li, C. Yin, T. Do-Duy, A. Masaracchia and T. Q. Duong, "Aerial Reconfigurable Intelligent Surface-Enabled URLLC UAV Systems," in IEEE Access, vol. 9, pp. 140248-140257, 2021.

III. Technology trend survey

III.1. Introduction

This section provides an overview of the technology trends related to repeaters, metasurface and RIS/IRS. Specifically, we introduce the categories of repeaters, metasurface, and RIS/IRS. Next, we summarize the findings from the examination of technical documents such as research journals and conference papers and present the technological trends from a quantitative perspective. Finally, we highlight the technological trends related to repeaters, metasurface and RIS/IRS.

III.2. Categories of repeater, metasurface, and RIS/IRS

Relay types can be classified into several categories based on their method and structure. Here, classification is made into Repeater and Intelligent surface of metasurface and RIS/IRS, depending on whether they have amplification functionality or not.

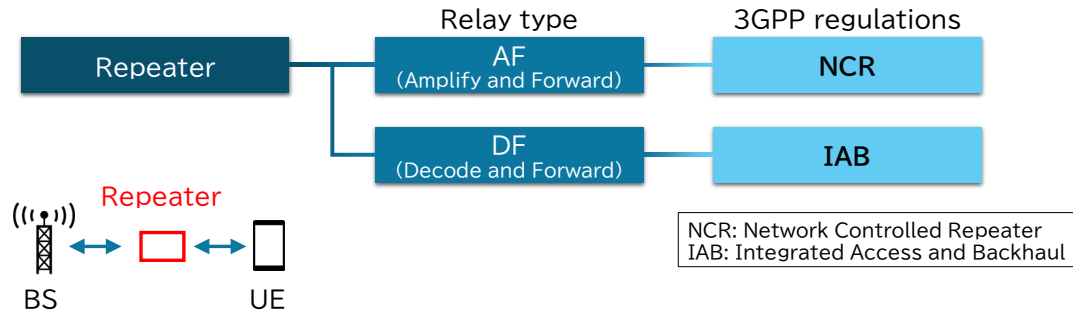


Fig. III.2-1. Category of Repeater.

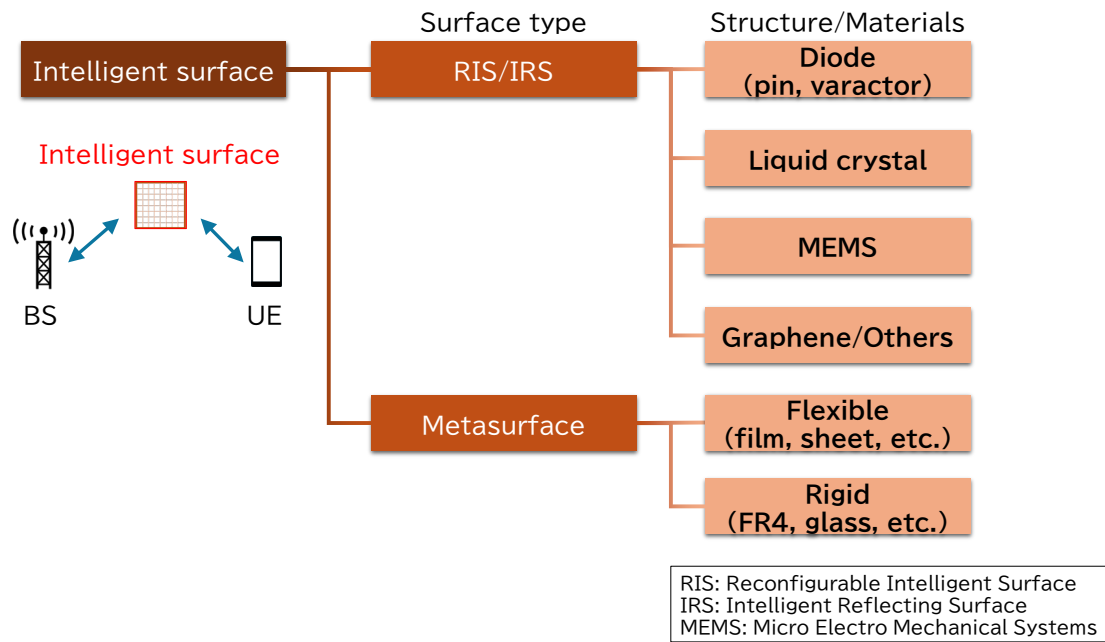


Fig. III.2-2. Category of metasurface and RIS/IRS.

Repeater is characterized by its ability to amplify received signals. There are different relay types: Amplify and Forward (AF), Decode and Forward (DF) as shown in Figure III.2-1. In AF, amplification and phase modification are performed in the analog processing, utilizing MIMO and beamforming techniques. DF is a method in which the received signal is demodulated, decoded, re-encoded, amplified, and then retransmitted. In 3GPP, AF and DF are defined as NCR (Network Controlled Repeater) and IAB (Integrated Access and Backhaul), respectively. It is necessary to select the appropriate method based on each specific use case.

As shown in Figure III.2-2, Intelligent surface, within the relay category, does not have the capability to amplify received signals but is characterized by its ability to reflect incident waves in various directions. There are different reflection types, including active RIS/IRS that can be controlled, passive metasurfaces (some of which are also active), and traditional metal reflectors. RIS/IRS can further be classified based on their structure and material. Diodes and Liquid Crystals (LC) are commonly used, and other methods include MEMS and Graphene applications. Metasurfaces are classified into flexible types, such as those applied to film materials or sheets, and fixed types, such as those applied to glass.

III.3. Publication summary

The results of the literature survey on wireless relay technology are shown in Table III.3-1.

Table III.3-1. Summary of research findings on wireless relay technology.

Active / Programmable	Category	Frequency	Research *1
Yes / Yes (Repeater)	AF	Up to 24GHz	[III.3-23][III.3-39]
		24 to 100GHz	[III.3-26][III.3-29][III.3-31][III.3-37][III.3-40][III.3-41][III.3-47][III.3-50][III.3-51][III.3-53][III.3-54][III.3-57][III.3-86][III.3-89]
		Above 100GHz	
		NA	[III.3-30][III.3-34][III.3-42][III.3-46][III.3-55][III.3-68][III.3-75][III.3-76][III.3-81][III.3-83]
	DF	Up to 24GHz	[III.3-78][III.3-84]
		24 to 100GHz	[III.3-66]
		Above 100GHz	
		NA	[III.3-34][III.3-43][III.3-49][III.3-58][III.3-59][III.3-60][III.3-63][III.3-71][III.3-72][III.3-79][III.3-80][III.3-82]
	NCR	Up to 24GHz	[III.3-91]
		24 to 100GHz	[III.3-1][III.3-2][III.3-3][III.3-4][III.3-5][III.3-11][III.3-22][III.3-27][III.3-28][III.3-38][III.3-87][III.3-88][III.3-90]
		Above 100GHz	
		NA	[III.3-6][III.3-7][III.3-21][III.3-24][III.3-25]
	IAB	Up to 24GHz	

		24 to 100GHz	[III.3-3][III.3-4][III.3-5][III.3-15] [III.3-16][III.3-17][III.3-28][III.3-32] [III.3-35][III.3-36][III.3-45][III.3-48] [III.3-52][III.3-56][III.3-65][III.3-67] [III.3-69][III.3-70][III.3-74][III.3-90]
		Above 100GHz	[III.3-33][III.3-36][III.3-77]
		NA	[III.3-6][III.3-12][III.3-14][III.3-18] [III.3-19][III.3-20][III.3-25][III.3-44] [III.3-61][III.3-62][III.3-64][III.3-73] [III.3-85]
	Others	Up to 24GHz	
		24 to 100GHz	[III.3-8]
		Above 100GHz	
		NA	[III.3-9][III.3-10][III.3-13]
No / No	Metasurface	Up to 24GHz	[III.3-96][III.3-104][III.3-106][III.3-118] [III.3-127][III.3-128][III.3-130][III.3-132] [III.3-133][III.3-134]
		24 to 100GHz	[III.3-94][III.3-100][III.3-101][III.3-103] [III.3-108][III.3-109][III.3-110][III.3-111] [III.3-112][III.3-113][III.3-114][III.3-116] [III.3-117][III.3-119][III.3-121][III.3-122] [III.3-123][III.3-131]
		Above 100GHz	[III.3-92][III.3-95][III.3-102][III.3-115] [III.3-124][III.3-125][III.3-126][III.3-129]
		NA	[III.3-93][III.3-97][III.3-98][III.3-99] [III.3-105][III.3-107][III.3-120]
No / Yes	RIS/IRS	Up to 24GHz	[III.3-138][III.3-145][III.3-147][III.3-149] [III.3-153][III.3-154][III.3-168][III.3-169] [III.3-170][III.3-175][III.3-176][III.3-177] [III.3-184][III.3-186][III.3-189][III.3-193] [III.3-194][III.3-195][III.3-196][III.3-198] [III.3-201][III.3-202][III.3-208][III.3-209] [III.3-210][III.3-211][III.3-212][III.3-218] [III.3-223][III.3-224][III.3-225][III.3-226] [III.3-227][III.3-228]
		24 to 100GHz	[III.3-135][III.3-136][III.3-137][III.3-140] [III.3-141][III.3-150][III.3-151][III.3-152] [III.3-155][III.3-156][III.3-157][III.3-158] [III.3-159][III.3-160][III.3-161][III.3-162] [III.3-163][III.3-164][III.3-165][III.3-172] [III.3-173][III.3-174][III.3-178][III.3-179] [III.3-180][III.3-181][III.3-182][III.3-183] [III.3-185][III.3-187][III.3-188][III.3-190] [III.3-191][III.3-192][III.3-216][III.3-217] [III.3-221]
		Above 100GHz	[III.3-139][III.3-142][III.3-143][III.3-144] [III.3-146][III.3-148][III.3-171][III.3-197] [III.3-204][III.3-205][III.3-206][III.3-207] [III.3-213][III.3-214][III.3-215][III.3-219] [III.3-220][III.3-229]
		NA	[III.3-166][III.3-167][III.3-199][III.3-200] [III.3-203]

*1 For RIS/IRS, literature numbers will be marked with the colors specified below, according to the phase shift implementation method:

* LC: Yellow

* Diode: Green

* Graphene: Light Blue

* MEMS: Pink

* Others or Simulation: White

Table III.3-2 organizes the correspondence between the technologies listed in Table III.3-1 and the use cases they enable. Within the RIS/IRS category, noteworthy are the use cases and control techniques for standalone RIS/IRS, which operate independently without external control, as explored in [III.3-158], [III.3-159], and [III.3-161]. Also, [III.3-158], [III.3-159], and [III.3-163] present techniques for sharing RIS/IRS among multiple communication operators. Methods for using quantum computing, which can solve specific problems with high speed and low power consumption, to control RIS/IRS are investigated in [III.3-155]-[III.3-159] and [III.3-199]-[III.3-203]. Furthermore, research on wave-domain computation and control techniques, typified by stacked intelligent metasurfaces (SIM), has been attracting attention in recent years, and the number of related studies is increasing [III.3-150][III.3-154][III.3-172]-[III.3-188].

Table III.3-2. Correspondence between wireless relay use cases and the technologies that enable them.

Category	Use case		Research
Repeater	Coverage enhancement	Single hop	[III.3-4][III.3-9][III.3-13][III.3-23][III.3-24] [III.3-25][III.3-27][III.3-30][III.3-31] [III.3-32][III.3-33][III.3-37][III.3-39] [III.3-41][III.3-47][III.3-52][III.3-53] [III.3-54][III.3-60][III.3-61][III.3-64] [III.3-68]
		Multi hop	[III.3-11][III.3-12][III.3-14][III.3-19] [III.3-65][III.3-67][III.3-69][III.3-70] [III.3-71][III.3-72][III.3-74][III.3-77]
	Spectral efficiency	MIMO	[III.3-18][III.3-28][III.3-29][III.3-75] [III.3-87][III.3-89]
		AMC	[III.3-42][III.3-43][III.3-46][III.3-56] [III.3-57][III.3-58][III.3-59][III.3-79] [III.3-81]
		Reliability	[III.3-6][III.3-8][III.3-20][III.3-36][III.3-38] [III.3-44][III.3-45][III.3-63][III.3-73] [III.3-76][III.3-84]
	Others	-	[III.3-10][III.3-15][III.3-16][III.3-17] [III.3-21][III.3-22][III.3-55][III.3-62] [III.3-66][III.3-78]
Metasurface	Coverage enhancement	-	[III.3-92][III.3-93][III.3-94][III.3-95] [III.3-96][III.3-97][III.3-98][III.3-99] [III.3-100][III.3-101][III.3-102][III.3-103]

			[III.3-104][III.3-105][III.3-106][III.3-107] [III.3-108][III.3-109][III.3-110][III.3-111] [III.3-112][III.3-113][III.3-114][III.3-115] [III.3-116][III.3-117][III.3-118][III.3-119] [III.3-120][III.3-121][III.3-122][III.3-123] [III.3-124][III.3-125][III.3-126][III.3-127] [III.3-129][III.3-130][III.3-132][III.3-133] [III.3-134]
	Spectral efficiency	MIMO	
		Beam Manipulation	
	Others	Reliability	
		Physical layer security	
		Sensing capabilities	
		Energy efficiency	[III.3-131]
		Link management	
		Wave domain processing	
		Others	[III.3-128]
RIS/IRS	Coverage enhancement	-	[III.3-136][III.3-137][III.3-138][III.3-139] [III.3-140][III.3-141][III.3-142][III.3-143] [III.3-145][III.3-148][III.3-158][III.3-199] [III.3-208][III.3-209][III.3-211][III.3-213] [III.3-214][III.3-217][III.3-220][III.3-222] [III.3-227]
	Spectral efficiency	MIMO	[III.3-151][III.3-152][III.3-153][III.3-157] [III.3-205][III.3-221]
		Beam Manipulation	[III.3-149][III.3-154][III.3-161][III.3-163] [III.3-165][III.3-168][III.3-189][III.3-190] [III.3-193][III.3-194][III.3-195][III.3-197] [III.3-201][III.3-212]
	Others	Reliability	[III.3-170][III.3-171][III.3-202][III.3-203]
		Physical layer security	[III.3-166][III.3-167][III.3-223]
		Sensing capabilities	[III.3-159][III.3-162]
		Energy efficiency	[III.3-200]
		Link management	[III.3-156][III.3-164][III.3-169]
		Wave domain processing	[III.3-172][III.3-173][III.3-174][III.3-175] [III.3-176][III.3-177][III.3-178][III.3-179] [III.3-180][III.3-181][III.3-182][III.3-183] [III.3-184][III.3-185][III.3-186][III.3-187] [III.3-188][III.3-192][III.3-196][III.3-198]
		Others	[III.3-135][III.3-144][III.3-146][III.3-147] [III.3-150][III.3-155][III.3-160][III.3-191] [III.3-204][III.3-206][III.3-207][III.3-210] [III.3-215][III.3-216][III.3-218][III.3-219] [III.3-224][III.3-225][III.3-226][III.3-228] [III.3-229]

REFERENCE

Repeater

- [III.3-1] L. Wang and C. E. Saavedra, "28–31 GHz Bi-directional amplifier for 5G wireless repeaters," *2017 IEEE 28th Annual International Symposium on Personal, Indoor, and Mobile Radio Communications (PIMRC)*, Montreal, QC, Canada, 2017, pp. 1-4.
- [III.3-2] J. Romeu *et al.*, "Lens-Based Switched-Beam Antenna for a 5G Smart Repeater," in *IEEE Antennas and Wireless Propagation Letters*, vol. 22, no. 10, pp. 2482-2486, Oct. 2023.
- [III.3-3] J. Potschka *et al.*, "A Switchable, Passively Tuneable 28 GHz to 39 GHz Upconversion Link for a 5G Repeater using a Broadside Coupler and Analog Predistortion in a 130 nm BiCMOS Technology," *2020 18th IEEE International New Circuits and Systems Conference (NEWCAS)*, Montreal, QC, Canada, 2020, pp. 30-33.
- [III.3-4] S. Maier, H. Schlesinger, W. Templ and H. Viswanathan, "Long distance and high bandwidth wireless link tests for a 39 GHz to 28 GHz 5G low-cost repeater," *2018 IEEE 5G World Forum (5GWF)*, Silicon Valley, CA, USA, 2018, pp. 338-342.
- [III.3-5] J. Potschka *et al.*, "A Downconversion Link for a 5G Repeater using a Passive Power Adjustment Technique and Analog Predistortion," *2020 15th European Microwave Integrated Circuits Conference (EuMIC)*, Utrecht, Netherlands, 2021, pp. 61-64.
- [III.3-6] K. -y. Lee and J. -S. Jang, "Novel method for synthesis of synchronization signal abstraction for 5G RF repeater," *2022 IEEE 16th International Conference on Application of Information and Communication Technologies (AICT)*, Washington DC, DC, USA, 2022, pp. 1-4.
- [III.3-7] H. Park, C. Lee, G. Namgung, Y. Seo and S. Kahng, "Design of 8×8 Butler Matrix Antenna for 5G Small Cell Beamforming Repeaters," *2019 8th Asia-Pacific Conference on Antennas and Propagation (APCAP)*, Incheon, Korea (South), 2019, pp. 142-143.
- [III.3-8] S. Ahmed, R. A. Antiohos and M. Faulkner, "Effects of mm-wave propagation channels on technology choices for 5G on-frequency repeaters," *2015 International Symposium on Antennas and Propagation (ISAP)*, Hobart, TAS, Australia, 2015, pp. 1-4.
- [III.3-9] X. Zhao and X. Meng, "Micro Repeater Solution for 5G Signal Coverage in High-speed Train," *2024 IEEE International Symposium on Broadband Multimedia Systems and Broadcasting (BMSB)*, Toronto, ON, Canada, 2024, pp. 1-5.
- [III.3-10] S. K. Sharma, M. Patwary, S. Chatzinotas, B. Ottersten and M. Abdel-Maguid, "Repeater for 5G wireless: A complementary contender for Spectrum Sensing intelligence," *2015 IEEE International Conference on Communications (ICC)*, London, UK, 2015, pp. 1416-1421.
- [III.3-11] R. A. Ayoubi, M. Mizmizi, D. Tagliaferri, D. D. Donno and U. Spagnolini, "Network-Controlled Repeaters vs. Reconfigurable Intelligent Surfaces for 6G mmW Coverage Extension: A Simulative Comparison," *2023 21st Mediterranean Communication and Computer Networking Conference (MedComNet)*, Island of Ponza, Italy, 2023, pp. 196-

202.

- [III.3-12] G. Leone, E. Moro, I. Filippini, A. Capone and D. D. Donno, "Towards Reliable mmWave 6G RAN: Reconfigurable Surfaces, Smart Repeaters, or Both?," *2022 20th International Symposium on Modeling and Optimization in Mobile, Ad hoc, and Wireless Networks (WiOpt)*, Torino, Italy, 2022, pp. 81-88.
- [III.3-13] H. Noh, H. Ju and J. Lee, "6G Repeaters for Non-Terrestrial Network," *2024 International Conference on Electronics, Information, and Communication (ICEIC)*, Taipei, Taiwan, 2024, pp. 1-3.
- [III.3-14] H. Yin, S. Roy and L. Cao, "Routing and Resource Allocation for IAB Multi-Hop Network in 5G Advanced," in *IEEE Transactions on Communications*, vol. 70, no. 10, pp. 6704-6717, Oct. 2022.
- [III.3-15] J. Zhang, N. Garg and T. Ratnarajah, "In-Band-Full-Duplex Integrated Sensing and Communications for IAB Networks," in *IEEE Transactions on Vehicular Technology*, vol. 71, no. 12, pp. 12782-12796, Dec. 2022.
- [III.3-16] A. Bishnu, M. Holm and T. Ratnarajah, "Performance Evaluation of Full-Duplex IAB Multi-Cell and Multi-User Network for FR2 Band," in *IEEE Access*, vol. 9, pp. 72269-72283, 2021.
- [III.3-17] J. Zhang, H. Luo, N. Garg, A. Bishnu, M. Holm and T. Ratnarajah, "Design and Analysis of Wideband In-Band-Full-Duplex FR2-IAB Networks," in *IEEE Transactions on Wireless Communications*, vol. 21, no. 6, pp. 4183-4196, June 2022.
- [III.3-18] A. H. Jazi, S. M. Razavizadeh and T. Svensson, "Integrated Access and Backhaul (IAB) in Cell-Free Massive MIMO Systems," in *IEEE Access*, vol. 11, pp. 71658-71667, 2023.
- [III.3-19] B. Lim *et al.*, "Joint association and resource allocation for multi-hop integrated access and backhaul (IAB) network," in *Journal of Communications and Networks*, vol. 25, no. 4, pp. 440-455, Aug. 2023.
- [III.3-20] P. Fiore, E. Moro, I. Filippini, A. Capone and D. D. Donno, "Boosting 5G mm-Wave IAB Reliability with Reconfigurable Intelligent Surfaces," *2022 IEEE Wireless Communications and Networking Conference (WCNC)*, Austin, TX, USA, 2022, pp. 758-763.
- [III.3-21] J. Xin, S. Xu, S. Xiong, H. Xu and H. Zhang, "A Survey on Network Controlled Repeater Technology," *2022 IEEE 8th International Conference on Computer and Communications (ICCC)*, Chengdu, China, 2022, pp. 1097-1101.
- [III.3-22] T. Azzino, A. HasanzadeZonuzi, J. Luo, N. Abedini and T. Luo, "Towards Energy- and Cost-Efficient 6G Networks," *2024 IEEE 100th Vehicular Technology Conference (VTC2024-Fall)*, Washington, DC, USA, 2024, pp. 1-7.
- [III.3-23] Z. Niu and H. Xue, "A novel portable repeater for 5G applications," *2024 IEEE International Black Sea Conference on Communications and Networking (BlackSeaCom)*, Tbilisi, Georgia, 2024, pp. 186-191.

- [III.3-24] N. Abedini and T. Luo, "Smart and Green Networks Using Repeaters and Reconfigurable Intelligent Surfaces," *2024 IEEE International Conference on Communications Workshops (ICC Workshops)*, Denver, CO, USA, 2024, pp. 1127-1133.
- [III.3-25] C. -K. Wen, L. -S. Tsai, A. Shojaeifard, P. -K. Liao, K. -K. Wong and C. -B. Chae, "Shaping a Smarter Electromagnetic Landscape: IAB, NCR, and RIS in 5G Standard and Future 6G," in *IEEE Communications Standards Magazine*, vol. 8, no. 1, pp. 72-78, March 2024.
- [III.3-26] T. -H. Shih, S. -C. Chen and S. -C. Lin, "A Low-Profile Transmitarray With Linear-To-Linear Polarization Conversion Function," *2023 IEEE International Symposium On Antennas And Propagation (ISAP)*, Kuala Lumpur, Malaysia, 2023, pp. 1-2.
- [III.3-27] K. Dong, S. Mura, M. Mizmizi, D. Tagliaferri and U. Spagnolini, "Advanced Tri-Sectoral Multi-User Millimeter-Wave Smart Repeater," *2023 IEEE International Mediterranean Conference on Communications and Networking (MeditCom)*, Dubrovnik, Croatia, 2023, pp. 205-210.
- [III.3-28] O. Haliloglu *et al.*, "Distributed MIMO Systems for 6G," *2023 Joint European Conference on Networks and Communications & 6G Summit (EuCNC/6G Summit)*, Gothenburg, Sweden, 2023, pp. 156-161.
- [III.3-29] R. Kataoka, M. Takigawa, T. Ohseki, T. Watanabe and Y. Amano, "Basic Performance Evaluation of Low Latency and High Capacity Relay Method in Millimeter-Wave Bands," *2023 IEEE Wireless Communications and Networking Conference (WCNC)*, Glasgow, United Kingdom, 2023, pp. 1-6.
- [III.3-30] T. Hasegawa, M. Konishi, Y. Ohta and A. Nagate, "An Experimental Study on Automatic Gain Control in HAPS Wireless Repeater System," *2023 IEEE Wireless Communications and Networking Conference (WCNC)*, Glasgow, United Kingdom, 2023, pp. 1-6.
- [III.3-31] K. Tokugawa *et al.*, "Design of mmW Digital Twin platform toward B5G/6G – High-Precision Measurement System and Relay Station Deployment–," *2022 IEEE 33rd Annual International Symposium on Personal, Indoor and Mobile Radio Communications (PIMRC)*, Kyoto, Japan, 2022, pp. 813-818.
- [III.3-32] R. Garg, S. Jain, P. Dania and A. Natarajan, "14.3 A 26GHz Full-Duplex Circulator Receiver with 53dB/400MHz(40dB/800MHz) Self-Interference Cancellation for mm-Wave Repeaters," *2021 IEEE International Solid-State Circuits Conference (ISSCC)*, San Francisco, CA, USA, 2021, pp. 222-224.
- [III.3-33] T. Wang and X. Wang, "DeepRP: Bottleneck Theory Guided Relay Placement for 6G Mesh Backhaul Augmentation," in *IEEE Transactions on Mobile Computing*, vol. 24, no. 3, pp. 1744-1758, March 2025.
- [III.3-34] H. R. Hashempour, G. Berardinelli, R. Adeogun and E. A. Jorswieck, "Power Efficient Cooperative Communication Within IIoT Subnetworks: Relay or RIS?," in *IEEE*

Internet of Things Journal, doi: 10.1109/IIOT.2024.3521001.

- [III.3-35] M. Luglio, C. Roseti, M. Quadrini and F. Zampognaro, "Definition of Satellite Systems Role in Integrated Access Backhaul (IAB) Architectures," *2024 International Symposium on Networks, Computers and Communications (ISNCC)*, Washington DC, DC, USA, 2024, pp. 1-6.
- [III.3-36] N. Yarkina, D. Moltchanov, A. Gaydamaka and V. Koucheryavy, "Coexistence of Multicast and Unicast Services in mmWave/sub-THz Self-Backhauled Systems: User Associations and Performance Gains," in *IEEE Transactions on Vehicular Technology*, doi: 10.1109/TVT.2024.3500880.
- [III.3-37] K. Yuasa, M. Ide, S. Kato, T. Tomura, K. Okada and A. Shirane, "5G NR Transceiver and 24GHz Wireless Power Receiver Utilizing a Low Insertion Loss Differential Output Butler Matrix for Long-Range Wireless Transmission," *2024 54th European Microwave Conference (EuMC)*, Paris, France, 2024, pp. 892-895.
- [III.3-38] L. Bisulli *et al.*, "Real-time Beamforming Testbed and Tracking Relay for mmWave Applications," *2024 IEEE 30th International Conference on Embedded and Real-Time Computing Systems and Applications (RTCSA)*, Sokcho, Korea, Republic of, 2024, pp. 114-119.
- [III.3-39] G. Maiolini Capez *et al.*, "On the Use of Mega Constellation Services in Space: Integrating LEO Platforms Into 6G Non-Terrestrial Networks," in *IEEE Journal on Selected Areas in Communications*, vol. 42, no. 12, pp. 3490-3504, Dec. 2024.
- [III.3-40] S. Kato *et al.*, "A 28GHz 5G NR Wirelessly Powered Relay Transceiver Using Rectifier-Type 4th-Order Sub-Harmonic Mixer," *2024 IEEE Symposium on VLSI Technology and Circuits (VLSI Technology and Circuits)*, Honolulu, HI, USA, 2024, pp. 1-2.
- [III.3-41] M. Ide, K. Yuasa, S. Kato, T. Tomura, K. Okada and A. Shirane, "A 256-Element Phased-Array Relay Transceiver for 5G Network Using 24-GHz Wireless Power Transfer With Discrete ICs," in *IEEE Microwave and Wireless Technology Letters*, vol. 34, no. 6, pp. 793-796, June 2024.
- [III.3-42] V. Özduran, N. Nomikos, E. Soleimani-Nasab, I. S. Ansari and P. Trakadas, "Relay-Aided Uplink NOMA Under Non-Orthogonal CCI and Imperfect SIC in 6G Networks," in *IEEE Open Journal of Vehicular Technology*, vol. 5, pp. 658-680, 2024.
- [III.3-43] G. Nagesham and S. Vappangi, "Performance of Selective DF Relay Aided Cooperative NOMA Under Imperfect SIC *," *2023 3rd International Conference on Mobile Networks and Wireless Communications (ICMNWC)*, Tumkur, India, 2023, pp. 1-8.
- [III.3-44] Y. Hwang and S. -M. Oh, "Service Procedures for On-board UEs in the 3GPP Mobile IAB Systems," *2023 14th International Conference on Information and Communication Technology Convergence (ICTC)*, Jeju Island, Korea, Republic of, 2023, pp. 1598-1600.
- [III.3-45] S. Ranjan, P. Jha, A. Karandikar and P. Chaporkar, "A Flexible IAB Architecture for

- Beyond 5G Network," in *IEEE Communications Standards Magazine*, vol. 7, no. 3, pp. 64-71, September 2023.
- [III.3-46] I. A. Bartsiokas, P. K. Gkonis, D. I. Kaklamani and I. S. Venieris, "A DL-Enabled Relay Node Placement and Selection Framework in Multicellular Networks," in *IEEE Access*, vol. 11, pp. 65153-65169, 2023.
- [III.3-47] S. Kato, K. Yuasa, M. Ide, A. Shirane and K. Okada, "A CMOS Full-Wave Switching Rectifier with Frequency Up-Down Conversion for 5G NR Wirelessly-Powered Relay Transceivers," *ESSCIRC 2022- IEEE 48th European Solid State Circuits Conference (ESSCIRC)*, Milan, Italy, 2022, pp. 345-348.
- [III.3-48] G. Y. Suk, S. -M. Kim, J. Kwak, S. Hur, E. Kim and C. -B. Chae, "Full Duplex Integrated Access and Backhaul for 5G NR: Analyses and Prototype Measurements," in *IEEE Wireless Communications*, vol. 29, no. 4, pp. 40-46, August 2022.
- [III.3-49] H. Luo, J. Wang, F. Bu, R. Ruby, K. Wu and Z. Guo, "Recent Progress of Air/Water Cross-Boundary Communications for Underwater Sensor Networks: A Review," in *IEEE Sensors Journal*, vol. 22, no. 9, pp. 8360-8382, 1 May1, 2022.
- [III.3-50] S. C. Tokgoz, S. Althunibat, S. L. Miller and K. A. Qaraqe, "Outage Analysis of Relay-Based Dual-Hop Hybrid FSO-mmWave Systems," in *IEEE Access*, vol. 10, pp. 2895-2907, 2022.
- [III.3-51] S. H. R. Naqvi, P. H. Ho and L. Peng, "5G NR mmWave indoor coverage with massive antenna system," in *Journal of Communications and Networks*, vol. 23, no. 1, pp. 1-11, Feb. 2021.
- [III.3-52] S. H. R. Naqvi and P. -H. Ho, "Achieving 5G NR mmWave Indoor Coverage Under Integrated Access Backhaul," in *IEEE Systems Journal*, vol. 15, no. 4, pp. 5429-5439, Dec. 2021.
- [III.3-53] S. K. Khan, A. Al-Hourani and K. G. Chavez, "Performance Evaluation of Amplify-and-Forward UAV Relay in Millimeter-Wave," *2020 27th International Conference on Telecommunications (ICT)*, Bali, Indonesia, 2020, pp. 1-5.
- [III.3-54] Y. J. Kim, Q. Sultan and Y. S. Cho, "Pilot Sequence Design for mmWave Cellular Systems With Relay Stations in the Presence of Blockage," in *IEEE Access*, vol. 8, pp. 80454-80467, 2020.
- [III.3-55] F. Héliot and R. Tafazolli, "Optimal Energy-Efficient Source and Relay Precoder Design for Two-Way MIMO-AF Relay Systems," in *IEEE Transactions on Green Communications and Networking*, vol. 4, no. 3, pp. 759-773, Sept. 2020.
- [III.3-56] M. Polese *et al.*, "Integrated Access and Backhaul in 5G mmWave Networks: Potential and Challenges," in *IEEE Communications Magazine*, vol. 58, no. 3, pp. 62-68, March 2020.
- [III.3-57] K. Ntontin and C. Verikoukis, "Relay-Aided Outdoor-to-Indoor Communication in Millimeter-Wave Cellular Networks," in *IEEE Systems Journal*, vol. 14, no. 2, pp. 2473-2484, June 2020.

- [III.3-58] P. Jain and A. Gupta, "Energy-Efficient Adaptive Sectorization for 5G Green Wireless Communication Systems," in *IEEE Systems Journal*, vol. 14, no. 2, pp. 2382-2391, June 2020.
- [III.3-59] E. I. s. mary and A. Rajesh, "NOMA based Co-operative Relaying under Winner II Channel (B5f) for LTE-A Network," *2019 International Conference on Vision Towards Emerging Trends in Communication and Networking (ViTECoN)*, Vellore, India, 2019, pp. 1-5.
- [III.3-60] E. Çakar, F. Kara and H. Kaya, "Error Analysis of Threshold Based Three-hop Device to Device (D2D) Communication Systems," *2019 27th Signal Processing and Communications Applications Conference (SIU)*, Sivas, Turkey, 2019, pp. 1-4.
- [III.3-61] H. Utatsu, K. Osawa, J. Mashino, S. Suyama and H. Otsuka, "Throughput Performance of Relay Backhaul Enhancement Using 3D Beamforming," *2019 International Conference on Information Networking (ICOIN)*, Kuala Lumpur, Malaysia, 2019, pp. 120-124.
- [III.3-62] X. Yan *et al.*, "The Application of Power-Domain Non-Orthogonal Multiple Access in Satellite Communication Networks," in *IEEE Access*, vol. 7, pp. 63531-63539, 2019.
- [III.3-63] S. Arzykulov, G. Nauryzbayev, T. A. Tsiftsis, B. Maham and M. Abdallah, "On the Outage of Underlay CR-NOMA Networks with Detect-and-Forward Relaying," in *IEEE Transactions on Cognitive Communications and Networking*, vol. 5, no. 3, pp. 795-804, Sept. 2019.
- [III.3-64] G. K. Xilouris, M. C. Batistatos, G. E. Athanasiadou, G. Tsoulos, H. B. Pervaiz and C. C. Zarakovitis, "UAV-Assisted 5G Network Architecture with Slicing and Virtualization," *2018 IEEE Globecom Workshops (GC Wkshps)*, Abu Dhabi, United Arab Emirates, 2018, pp. 1-7.
- [III.3-65] M. Polese, M. Giordani, A. Roy, D. Castor and M. Zorzi, "Distributed Path Selection Strategies for Integrated Access and Backhaul at mmWaves," *2018 IEEE Global Communications Conference (GLOBECOM)*, Abu Dhabi, United Arab Emirates, 2018, pp. 1-7.
- [III.3-66] X. Liu, "Secrecy Performance of a Relaying System Over Non-Identical Fading Channels," *MILCOM 2018 - 2018 IEEE Military Communications Conference (MILCOM)*, Los Angeles, CA, USA, 2018, pp. 792-797.
- [III.3-67] Y. Liu, Q. Hu and D. M. Blough, "Blockage Avoidance in Relay Paths for Roadside mmWave Backhaul Networks," *2018 IEEE 29th Annual International Symposium on Personal, Indoor and Mobile Radio Communications (PIMRC)*, Bologna, Italy, 2018, pp. 1-7.
- [III.3-68] I. Dey, Z. Zhao, M. M. Butt and N. Marchetti, "Compact Full-Duplex Amplify-and-Forward Relay Design for 5G Applications," *2018 IEEE 29th Annual International Symposium on Personal, Indoor and Mobile Radio Communications (PIMRC)*, Bologna, Italy, 2018, pp. 1-7.

- [III.3-69] M. Gapeyenko, V. Petrov, D. Moltchanov, S. Andreev, N. Himayat and Y. Koucheryavy, "Flexible and Reliable UAV-Assisted Backhaul Operation in 5G mmWave Cellular Networks," in *IEEE Journal on Selected Areas in Communications*, vol. 36, no. 11, pp. 2486-2496, Nov. 2018.
- [III.3-70] Q. Hu and D. M. Blough, "Optimizing Millimeter-Wave Backhaul Networks in Roadside Environments," *2018 IEEE International Conference on Communications (ICC)*, Kansas City, MO, USA, 2018, pp. 1-7.
- [III.3-71] T. E. A. Alharbi and D. K. C. So, "Full-Duplex Decode-and-Forward Cooperative Non-Orthogonal Multiple Access," *2018 IEEE 87th Vehicular Technology Conference (VTC Spring)*, Porto, Portugal, 2018, pp. 1-6.
- [III.3-72] Y. Shi, J. Liu, Z. M. Fadlullah and N. Kato, "Cross-Layer Data Delivery in Satellite-Aerial-Terrestrial Communication," in *IEEE Wireless Communications*, vol. 25, no. 3, pp. 138-143, JUNE 2018.
- [III.3-73] R. Jiao, L. Dai, J. Zhang, R. MacKenzie and M. Hao, "On the Performance of NOMA-Based Cooperative Relaying Systems Over Rician Fading Channels," in *IEEE Transactions on Vehicular Technology*, vol. 66, no. 12, pp. 11409-11413, Dec. 2017.
- [III.3-74] H. Ogawa, G. K. Tran, K. Sakaguchi and T. Haustein, "Traffic adaptive formation of mmWave meshed backhaul networks," *2017 IEEE International Conference on Communications Workshops (ICC Workshops)*, Paris, France, 2017, pp. 185-191.
- [III.3-75] M. Yemini, A. Zappone, E. Jorswieck and A. Leshem, "Energy Efficient Bidirectional Massive MIMO Relay Beamforming," in *IEEE Signal Processing Letters*, vol. 24, no. 7, pp. 1010-1014, July 2017.
- [III.3-76] X. Liang, Y. Wu, D. W. K. Ng, Y. Zuo, S. Jin and H. Zhu, "Outage Performance for Cooperative NOMA Transmission with an AF Relay," in *IEEE Communications Letters*, vol. 21, no. 11, pp. 2428-2431, Nov. 2017.
- [III.3-77] T. Narytnik, "The ways of creation and use of telecommunication systems in the terahertz band transport distribution 5G mobile networks," *2016 Third International Scientific-Practical Conference Problems of Infocommunications Science and Technology (PIC S&T)*, Kharkiv, Ukraine, 2016, pp. 36-39.
- [III.3-78] S. Tomasin, "MIMO Relay-Assisted Secure Uplink with Compute and Forward and Full-Duplex Devices," *2016 IEEE Globecom Workshops (GC Wkshps)*, Washington, DC, USA, 2016, pp. 1-6.
- [III.3-79] D. Wan, M. Wen, H. Yu, Y. Liu, F. Ji and F. Chen, "Non-Orthogonal Multiple Access for Dual-Hop Decode-and-Forward Relaying," *2016 IEEE Global Communications Conference (GLOBECOM)*, Washington, DC, USA, 2016, pp. 1-6.
- [III.3-80] X. Liu and X. Wang, "Outage probability and capacity analysis of the collaborative NOMA assisted relaying system in 5G," *2016 IEEE/CIC International Conference on Communications in China (ICCC)*, Chengdu, China, 2016, pp. 1-5.
- [III.3-81] A. Jaziri, R. Nasri and T. Chahed, "Congestion mitigation in 5G networks using drone

- relays," *2016 International Wireless Communications and Mobile Computing Conference (IWCMC)*, Paphos, Cyprus, 2016, pp. 233-238.
- [III.3-82] J. Ponniah and L. -L. Xie, "An achievable rate region for the two-way multiple relay channel," *2016 IEEE International Symposium on Information Theory (ISIT)*, Barcelona, Spain, 2016, pp. 1670-1674.
- [III.3-83] H. Alves, R. D. Souza and M. E. Pellenz, "Brief survey on full-duplex relaying and its applications on 5G," *2015 IEEE 20th International Workshop on Computer Aided Modelling and Design of Communication Links and Networks (CAMAD)*, Guildford, UK, 2015, pp. 17-21.
- [III.3-84] R. -A. Pitaval, O. Tirkkonen, R. Wichman, K. Pajukoski, E. Lahetkangas and E. Tirola, "Full-duplex self-backhauling for small-cell 5G networks," in *IEEE Wireless Communications*, vol. 22, no. 5, pp. 83-89, October 2015.
- [III.3-85] G. Noh, H. Chung and I. Kim, "Mobile Relay Technology for 5G," in *IEEE Wireless Communications*, vol. 27, no. 3, pp. 6-7, June 2020.
- [III.3-86] G. A. Fernandez, "A Web-Based Link Budget Tool for 5G mmWave Systems with Repeater Integration," *2023 IEEE Future Networks World Forum (FNWF)*, Baltimore, MD, USA, 2023, pp. 1-4.
- [III.3-87] S. Ke, G. Khanh Tran, Z. Li and K. Sakaguchi, "Millimeter-Wave Massive Analog Relay MU-MIMO With Blocking-Empowered User Scheduling Toward 6G," in *IEEE Open Journal of the Communications Society*, vol. 6, pp. 1-12, 2025.
- [III.3-88] G. C. M. Da Silva *et al.*, "Impact of Network Deployment on the Performance of NCR-assisted Networks," *2024 19th International Symposium on Wireless Communication Systems (ISWCS)*, Rio de Janeiro, Brazil, 2024, pp. 1-6.
- [III.3-89] M. Takigawa, R. Kataoka, I. Kanno and Y. Kishi, "Antenna Design for Robust Millimeter Wave LoS-MIMO Link in Mobile Analog Repeater Achieving Low Latency and High Capacity," *2024 IEEE 21st Consumer Communications & Networking Conference (CCNC)*, Las Vegas, NV, USA, 2024, pp. 912-917.
- [III.3-90] R. Flamini *et al.*, "Toward a Heterogeneous Smart Electromagnetic Environment for Millimeter-Wave Communications: An Industrial Viewpoint," in *IEEE Transactions on Antennas and Propagation*, vol. 70, no. 10, pp. 8898-8910, Oct. 2022.
- [III.3-91] Businesswire, "Airgain Unveils Groundbreaking Solar-Powered 5G Smart Repeater Pioneering the Future of Sustainable Connectivity," Feb. 25, 2025. [Online]. Available: <https://www.businesswire.com/news/home/20250225231962/en/>. [Accessed: Mar. 10, 2025]. Available: <https://www.airgain.com/products/airgain-lighthouse-solar/>. [Accessed: Mar. 10, 2025].

Metasurface

- [III.3-92] Y. Kato, K. Omori and A. Sanada, "D-Band Perfect Anomalous Reflectors for 6G Applications," in *IEEE Access*, vol. 9, pp. 157512-157521, 2021.

- [III.3-93] M. K. Emara, D. Kundu, K. Macdonell, L. M. Rufail and S. Gupta, "Coupled Resonator-Based Metasurface Reflector With Enhanced Magnitude and Phase Coverage," in *IEEE Transactions on Antennas and Propagation*, vol. 72, no. 1, pp. 901-914, Jan. 2024.
- [III.3-94] Z. A. P. Jibrán, M. Kalaagi, D. Seetharamdoo and C. Maye, "Multi-Channel Beam-Splitting Metasurface for Millimeter Wave Communication Systems," *2024 18th European Conference on Antennas and Propagation (EuCAP)*, Glasgow, United Kingdom, 2024, pp. 1-4.
- [III.3-95] D. Kong, T. D. Phan, J. Palosaari, J. Juuti, A. Pärssinen and P. J. Soh, "A Simplified Method for Designing Highly Efficient Reflective Metasurfaces With Wide Steering Angles," in *IEEE Antennas and Wireless Propagation Letters*, vol. 23, no. 11, pp. 3664-3668, Nov. 2024.
- [III.3-96] P. La-aiddee, P. Sangwongngam, P. Pongpaibool, D. Tancharoen, L. Wuttisittikulkij and P. Vanichchanunt, "Effects of Low-Geometrical-Precision PCB Manufacturing on mmWave Passive Metasurfaces," *2023 International Technical Conference on Circuits/Systems, Computers, and Communications (ITC-CSCC)*, Jeju, Korea, Republic of, 2023, pp. 1-6.
- [III.3-97] T. Hou, Y. Liu, Z. Song, X. Sun and Y. Chen, "MIMO-NOMA Networks Relying on Reconfigurable Intelligent Surface: A Signal Cancellation-Based Design," in *IEEE Transactions on Communications*, vol. 68, no. 11, pp. 6932-6944, Nov. 2020.
- [III.3-98] N. M. Mohammed *et al.*, "Reconfigurable intelligent surface design in phase-space," *2022 3rd URSI Atlantic and Asia Pacific Radio Science Meeting (AT-AP-RASC)*, Gran Canaria, Spain, 2022, pp. 1-4.
- [III.3-99] M. Salucci, A. Benoni, G. Oliveri, P. Rocca, B. Li and A. Massa, "A Multihop Strategy for the Planning of EM Skins in a Smart Electromagnetic Environment," in *IEEE Transactions on Antennas and Propagation*, vol. 71, no. 3, pp. 2758-2767, March 2023.
- [III.3-100] D. Kitayama, D. Kurita, K. Miyachi, Y. Kishiyama, S. Itoh and T. Tachizawa, "5G Radio Access Experiments on Coverage Expansion Using Metasurface Reflector at 28 GHz," *2019 IEEE Asia-Pacific Microwave Conference (APMC)*, Singapore, 2019, pp. 435-437.
- [III.3-101] J. S. Demetre, T. J. Smy and S. Gupta, "Static Metasurface Reflectors With Independent Magnitude and Phase Control Using Coupled Resonator Configuration," in *IEEE Transactions on Antennas and Propagation*, vol. 71, no. 4, pp. 3536-3545, April 2023.
- [III.3-102] D. T. Phan, J. Chen, M. E. Leinonen, A. Pärssinen and P. J. Soh, "Digitally Coded Reflector at 140 GHz Targeted for 6G Communications," *2023 17th European Conference on Antennas and Propagation (EuCAP)*, Florence, Italy, 2023, pp. 1-4.
- [III.3-103] S. Kosulnikov, F. S. Cuesta, X. Wang, A. Díaz-Rubio and S. Tretyakov, "Link budget estimations for millimeter-wave links via anomalous reflectors," *2023 17th*

- European Conference on Antennas and Propagation (EuCAP)*, Florence, Italy, 2023, pp. 1-3.
- [III.3-104] N. S. M. Yaziz, M. K. A. Rahim, F. Zubir and N. A. Samsuri, "A Comparison of the Bandwidth Coverage for Different Metasurface Reflector Shapes," *2023 IEEE International Symposium on Antennas and Propagation and USNC-URSI Radio Science Meeting (USNC-URSI)*, Portland, OR, USA, 2023, pp. 1423-1424.
- [III.3-105] Y. Murakami, N. Hirasawa, A. Minegishi, K. Hosokawa, I. Sudo and H. Hyakutake, "Reflection Phase Control Using a Transparent Metasurface with a Cross-Mesh Structure," *2024 IEEE International Workshop on Electromagnetics: Applications and Student Innovation Competition (iWEM)*, Taoyuan County, Taiwan, 2024, pp. 1-3.
- [III.3-106] H. Luo, Y. Wang, H. Gao, Y. Shao and H. -X. Xu, "Wide-angle Meta-reflector Using a Non-periodic Metasurface," *2024 Photonics & Electromagnetics Research Symposium (PIERS)*, Chengdu, China, 2024, pp. 1-5.
- [III.3-107] J. Budhu and A. Grbic, "Perfectly Reflecting Metasurface Reflectarrays: Mutual Coupling Modeling Between Unique Elements Through Homogenization," in *IEEE Transactions on Antennas and Propagation*, vol. 69, no. 1, pp. 122-134, Jan. 2021.
- [III.3-108] W. Khawaja, O. Ozdemir, Y. Yapici, F. Erden and I. Guvenc, "Coverage Enhancement for NLOS mmWave Links Using Passive Reflectors," in *IEEE Open Journal of the Communications Society*, vol. 1, pp. 263-281, 2020.
- [III.3-109] Z. Lu, Y. Fang, H. Yi and L. Li, "Broadband Reflectarray for Millimeter Wave Coverage Enhancement in Indoor NLOS Scenario," *2019 Cross Strait Quad-Regional Radio Science and Wireless Technology Conference (CSQRWC)*, Taiyuan, China, 2019, pp. 1-3.
- [III.3-110] E. Martinez-de-Rioja *et al.*, "Enhancement of 5G Millimeter-Wave Coverage in Indoor Scenarios by Passive Shaped-Beam Reflectarray Panels," *2022 16th European Conference on Antennas and Propagation (EuCAP)*, Madrid, Spain, 2022, pp. 1-5.
- [III.3-111] E. Martinez-de-Rioja, Á. F. Vaquero, M. Arrebola, E. Carrasco, J. A. Encinar and M. Achour, "Passive Dual-Polarized Shaped-Beam Reflectarrays to Improve Coverage in Millimeter-Wave 5G Networks," *2021 15th European Conference on Antennas and Propagation (EuCAP)*, Dusseldorf, Germany, 2021, pp. 1-5.
- [III.3-112] J. Dong, J. Zhang, X. Zhang, L. Duan, Z. Xue and X. Li, "Design of Single Layer Optically Transparent Reflectarray for 5G Outdoor and Indoor Coverage Enhancement," *2023 Cross Strait Radio Science and Wireless Technology Conference (CSRSWTC)*, Guilin, China, 2023, pp. 1-3.
- [III.3-113] R. Soroka, E. Martinez-de-Rioja, A. Arboleya and J. A. Encinar, "Design of FSS-Backed Reflectarray Cells for Coverage-Enhancing Panels with Suppressed Out-Of-Band Reflections in Millimeter-Wave 5G," *2022 16th European Conference on Antennas and Propagation (EuCAP)*, Madrid, Spain, 2022, pp. 1-5.

- [III.3-114] J. Vallejo, E. Martinez-de-Rioja and A. Arboleya, "Dual-Band Reflectarray-Based Electromagnetic Skin to Provide Millimeter-Wave Coverage in the 28/60-GHz Bands," *2024 18th European Conference on Antennas and Propagation (EuCAP)*, Glasgow, United Kingdom, 2024, pp. 1-5.
- [III.3-115] Feito-Rojo, Alejandro, et al. "Dual-Polarized Reflectarray for Coverage-Enhancing Applications in sub-THz 6G Networks." *2024 4th URSI Atlantic Radio Science Meeting (AT-RASC)*. IEEE, 2024.
- [III.3-116] H. Hashiguchi and N. Michishita, "A Derivation of Monostatic RCS of Reflectarray for Prediction of Bistatic RCS," *2023 IEEE International Symposium On Antennas And Propagation (ISAP)*, Kuala Lumpur, Malaysia, 2023, pp. 1-2.
- [III.3-117] H. Hashiguchi, N. Michishita, H. Morishita, H. Matsuno, T. Ohto and M. Nakano, "Cylindrical Near-Field Scanning of Bistatic Radar Cross Section for Reflectarray With Two-Dimensional Reflection," *2022 International Symposium on Antennas and Propagation (ISAP)*, Sydney, Australia, 2022, pp. 297-298.
- [III.3-118] T. Maruyama, T. Furuno, Y. Oda, J. Shen, N. Tran and H. Kayama, "Design of wide angle reflection reflectarray using multi-layer mushroom structure to improve propagation," *2011 XXXth URSI General Assembly and Scientific Symposium*, Istanbul, Turkey, 2011, pp. 1-4.
- [III.3-119] K. Sawairi, H. Hashiguchi and N. Michishita, "Simple Measurement Method for Reflectarray Using Monostatic-Bistatic Equivalence Theorem," *2024 IEEE International Workshop on Antenna Technology (iWAT)*, Sendai, Japan, 2024, pp. 50-51.
- [III.3-120] H. -X. Xu *et al.*, "Multifunctional Microstrip Array Combining a Linear Polarizer and Focusing Metasurface," in *IEEE Transactions on Antennas and Propagation*, vol. 64, no. 8, pp. 3676-3682, Aug. 2016.
- [III.3-121] C. Pfeiffer and A. Grbic, "Millimeter-Wave Transmitarrays for Wavefront and Polarization Control," in *IEEE Transactions on Microwave Theory and Techniques*, vol. 61, no. 12, pp. 4407-4417, Dec. 2013.
- [III.3-122] Á. F. Vaquero, M. R. Pino and M. Arrebola, "Dual-Polarized Shaped-Beam Transmitarray to Obtain a Multizone Coverage for 5G Indoor Communications," in *IEEE Antennas and Wireless Propagation Letters*, vol. 21, no. 4, pp. 730-734, April 2022.
- [III.3-123] H. Hashiguchi, N. Michishita, H. Morishita, H. Matsuno, T. Ohto and M. Nakano, "Dual Band and Dual Polarization Reflectarray Enabling Reflection to Two-dimensional Direction," *2022 IEEE International Symposium on Antennas and Propagation and USNC-URSI Radio Science Meeting (AP-S/URSI)*, Denver, CO, USA, 2022, pp. 800-801.
- [III.3-124] D. Kitayama, A. Pander, Y. Hama, and H. Takahashi, "Alignment-free twisted-split-ring metasurface on single substrate with 2π phase range for linearly polarized

- sub-terahertz wave," *Opt. Express* 31, 20769-20786, 2023.
- [III.3-125] D. Kitayama, M. Yaita, and H.-J. Song, "Laminated metamaterial flat lens at millimeter-wave frequencies," *Opt. Express* 23, 23348-23356, 2015.
- [III.3-126] A. Pander, D. Kitayama, H. Kagami, and H. Takahashi, "Multilayer-laminated optically transparent 300-GHz-band transmissive beamforming metasurface for wireless communication," *Opt. Express* 32, 24772-24786, 2024.
- [III.3-127] Zamel, H.M., Eldesouki, E.M. and Attiya A.M., "Design of anomalous reflecting metasurface for communication systems," *Sci Rep* 15, 619, 2025.
- [III.3-128] Silva, S.R., Rahman, A., de Melo Kort-Kamp, W. *et al.*, "Metasurface-based ultra-lightweight high-gain off-axis flat parabolic reflectarray for microwave beam collimation/focusing," *Sci Rep* 9, 18984, 2019.
- [III.3-129] Qu, SW., Wu, WW., Chen, BJ. *et al.*, "Controlling Dispersion Characteristics of Terahertz Metasurface," *Sci Rep* 5, 9367, 2015.
- [III.3-130] Guo, Y., Yan, L., Pan, W. *et al.*, "Scattering engineering in continuously shaped metasurface: An approach for electromagnetic illusion," *Sci Rep* 6, 30154, 2016.
- [III.3-131] C. Xue *et al.*, "Ultra-compact, broadband Huygens' metasurfaces based on induced magnetism," *Appl. Phys. Express* 12, 072005, 2019.
- [III.3-132] Zhu, R., Qiu, T., Wang, J. *et al.*, "Phase-to-pattern inverse design paradigm for fast realization of functional metasurfaces via transfer learning," *Nat Commun* 12, 2974, 2021.
- [III.3-133] Jia, Y., Qian, C., Fan, Z. *et al.*, "A knowledge-inherited learning for intelligent metasurface design and assembly," *Light Sci Appl* 12, 82, 2023.
- [III.3-134] Yang, Y., Vallecchi, A., Shamonina, E. *et al.*, "A new class of transformable kirigami metamaterials for reconfigurable electromagnetic systems," *Sci Rep* 13, 1219, 2023.

RIS/IRS

- [III.3-135] M. Maasch, M. Roig, C. Damm and R. Jakoby, "Voltage-Tunable Artificial Gradient-Index Lens Based on a Liquid Crystal Loaded Fishnet Metamaterial," in *IEEE Antennas and Wireless Propagation Letters*, vol. 13, pp. 1581-1584, 2014.
- [III.3-136] H. Matsuno *et al.*, "Development of a Dual-Polarized Direction-Variable Liquid-Crystal Meta-Surface Reflector for Intelligent Reflecting Surface," in *IEEE Access*, vol. 11, pp. 95757-95767, 2023.
- [III.3-137] D. Kitayama, Y. Hama, K. Goto, K. Miyachi, T. Motegi, and O. Kagaya, "Transparent dynamic metasurface for a visually unaffected reconfigurable intelligent surface: controlling transmission/reflection and making a window into an RF lens," *Opt. Express* 29, 29292-29307, 2021.
- [III.3-138] Kitayama, D., Pander, A. and Takahashi, H., "Analysis of Asymmetry in Active Split-Ring Resonators to Design Circulating-Current Eigenmode: Demonstration of

- Beamsteering and Focal-Length Control toward Reconfigurable Intelligent Surface,” *Sensors* 2022, 22, 681.
- [III.3-139] G. Zhang, Q. Fang, Y. Li, J. Yang, M. Hu, J. Li, G. Deng, Z. Yin, and H. Lu, "Manipulation of sub-terahertz waves using digital coding metasurfaces based on liquid crystals," *Opt. Express* 31, 9428-9436, 2023.
- [III.3-140] Silva Luis G. , Chu Z. , Xiao Pei and Cerqueira S Arismar, “A varactor-based 1024-element RIS design for mm-waves,” *Frontiers in Communications and Networks*, nol. 4, 2023, doi: 10.3389/frcmn.2023.1086011.
- [III.3-141] L. G. da Silva, P. Xiao and A. C. S., "A 2-bit Tunable Unit Cell for 6G Reconfigurable Intelligent Surface Application," *2022 16th European Conference on Antennas and Propagation (EuCAP)*, Madrid, Spain, 2022, pp. 1-5.
- [III.3-142] B. Wu, Y. Hu, Y. Tong Zhao, W. Bing Lu, and W. Zhang, "Large angle beam steering THz antenna using active frequency selective surface based on hybrid graphene-gold structure," *Opt. Express* 26, 15353-15361, 2018.
- [III.3-143] Jiang, H., Sheng, L., Luo, Y., Meng, L. and Cao W., “Design of Tunable Broadband Graphene-Based Metasurface with Amplitude-Phase Modulation,” *Materials* 2023, 16, 4633.
- [III.3-144] M. Yang *et al.*, "Dual-Stimulus Control for Ultra-Wideband and Multidimensional Modulation in Terahertz Metasurfaces Comprising Graphene and Metal Halide Perovskites,” *ACS Applied Materials & Interfaces* 2022 14 (1), 2155-2165.
- [III.3-145] H. Li *et al.*, "Wideband beam-forming metasurface with simultaneous phase and amplitude modulation,” *Optics Communications*, vol. 466, 2020, 124601.
- [III.3-146] W. Gao *et al.*, "High-Contrast Terahertz Wave Modulation by Gated Graphene Enhanced by Extraordinary Transmission through Ring Apertures,” *Nano Letters* 2014 14 (3), 1242-1248.
- [III.3-147] T. Leng, X. Huang, K. Chang, J. Chen, M. A. Abdalla and Z. Hu, "Graphene Nanoflakes Printed Flexible Meandered-Line Dipole Antenna on Paper Substrate for Low-Cost RFID and Sensing Applications," in *IEEE Antennas and Wireless Propagation Letters*, vol. 15, pp. 1565-1568, 2016.
- [III.3-148] H. Taghvaei *et al.*, "Multiwideband Terahertz Communications Via Tunable Graphene-Based Metasurfaces in 6G Networks: Graphene Enables Ultimate Multiwideband THz Wavefront Control," in *IEEE Vehicular Technology Magazine*, vol. 17, no. 2, pp. 16-25, June 2022.
- [III.3-149] E. Baladi, M. Y. Xu, N. Faria, J. Nicholls and S. V. Hum, "Dual-Band Circularly Polarized Fully Reconfigurable Reflectarray Antenna for Satellite Applications in the Ku-Band," in *IEEE Transactions on Antennas and Propagation*, vol. 69, no. 12, pp. 8387-8396, Dec. 2021.
- [III.3-150] J. An *et al.*, "Stacked Intelligent Metasurface Performs a 2D DFT in the Wave Domain for DOA Estimation," *ICC 2024 - IEEE International Conference on*

Communications, Denver, CO, USA, 2024, pp. 3445-3451.

- [III.3-151] B. Di *et al.*, "Reconfigurable Holographic Surface: A New Paradigm for Ultra-Massive MIMO," arXiv:2411.19334, 2024.
- [III.3-152] S. Zeng *et al.*, "RIS-Based IMT-2030 Testbed for MmWave Multi-Stream Ultra-Massive MIMO Communications," in *IEEE Wireless Communications*, vol. 31, no. 3, pp. 375-382, June 2024.
- [III.3-153] W. Tang *et al.*, "MIMO Transmission Through Reconfigurable Intelligent Surface: System Design, Analysis, and Implementation," in *IEEE Journal on Selected Areas in Communications*, vol. 38, no. 11, pp. 2683-2699, Nov. 2020.
- [III.3-154] Z. Wang *et al.*, "Multi-user ISAC through Stacked Intelligent Metasurfaces: New Algorithms and Experiments," arXiv:2405.01104, 2024.
- [III.3-155] 大山貴博, 川本雄一, "Intelligent Reflecting Surface (IRS)を用いた無線通信システムにおけるチャネル推定処理のオーバーヘッド削減方法," 電子情報通信学会論文誌B, Vol. J105-B, No. 3, pp.345-354, 2022.
- [III.3-156] T. Ohyama, Y. Kawamoto and N. Kato, "Intelligent Reflecting Surface (IRS) Allocation Scheduling Method Using Combinatorial Optimization by Quantum Computing," in *IEEE Transactions on Emerging Topics in Computing*, vol. 10, no. 3, pp. 1633-1644, 1 July-Sept. 2022.
- [III.3-157] T. Ohyama, Y. Kawamoto and N. Kato, "Quantum Computing Based Optimization for Intelligent Reflecting Surface (IRS)-Aided Cell-Free Network," in *IEEE Transactions on Emerging Topics in Computing*, vol. 11, no. 1, pp. 18-29, 1 Jan.-March 2023.
- [III.3-158] T. Ohyama, Y. Kawamoto and N. Kato, "Resource Allocation Optimization by Quantum Computing for Shared Use of Standalone IRS," in *IEEE Transactions on Emerging Topics in Computing*, vol. 11, no. 4, pp. 950-961, Oct.-Dec. 2023.
- [III.3-159] T. Ohyama, Y. Kawamoto and N. Kato, "Standalone Intelligent Reflecting Surface With Automatic Update of Phase-Shift Switching Schedule for Improved Communication and Localization," in *IEEE Transactions on Vehicular Technology*, vol. 73, no. 6, pp. 8503-8513, June 2024.
- [III.3-160] H. Hashida, Y. Kawamoto and N. Kato, "Adaptive Pilot Interval Optimization for Intelligent Reflecting Surface-Aided Communication Systems," in *IEEE Transactions on Vehicular Technology*, vol. 71, no. 7, pp. 7963-7966, July 2022.
- [III.3-161] R. Hibi, Y. Kawamoto and N. Kato, "Standalone-Intelligent Reflecting Surface Control Method Using Hierarchical Exploration by Beamwidth Expansion and Environment-Adaptive Codebook," in *IEEE Transactions on Vehicular Technology*, vol. 72, no. 9, pp. 11990-12000, Sept. 2023.
- [III.3-162] Y. Zhu, B. Mao and N. Kato, "On a Novel High Accuracy Positioning With Intelligent Reflecting Surface and Unscented Kalman Filter for Intelligent Transportation Systems in B5G," in *IEEE Journal on Selected Areas in*

- Communications*, vol. 42, no. 1, pp. 68-77, Jan. 2024.
- [III.3-163] H. Hashida, Y. Kawamoto and N. Kato, "Machine Learning-Based Infrastructure Sharing and Shared Operations for Intelligent Reflecting Surface-Aided Communications," in *IEEE Transactions on Cognitive Communications and Networking*, vol. 10, no. 1, pp. 198-208, Feb. 2024.
 - [III.3-164] Y. Zhu, B. Mao and N. Kato, "A Dynamic Task Scheduling Strategy for Multi-Access Edge Computing in IRS-Aided Vehicular Networks," in *IEEE Transactions on Emerging Topics in Computing*, vol. 10, no. 4, pp. 1761-1771, 1 Oct.-Dec. 2022.
 - [III.3-165] Y. Kawamoto *et al.*, "Simultaneous Multiple Connections and Increased Frequency Efficiency Using Beam Squint Approach for IRS-Based Communication," in *IEEE Transactions on Vehicular Technology*, vol. 73, no. 11, pp. 17073-17082, Nov. 2024.
 - [III.3-166] Y. Wu, B. Mao and N. Kato, "MSFL: Model-Safeguarded Federated Learning With Intelligent Reflecting Surface for Industrial Networks," in *IEEE Transactions on Network and Service Management*, 2024, doi: 10.1109/TNSM.2024.3496502.
 - [III.3-167] B. Mao, Y. Wu, J. Liu, H. Guo, J. Wang and N. Kato, "Optimizing Secrecy Rate for Federated Learning Model Aggregation With Intelligent Reflecting Surface Towards 6G Ubiquitous Intelligence," in *IEEE Transactions on Cognitive Communications and Networking*, 2024, doi: 10.1109/TCCN.2024.3454256.
 - [III.3-168] S. Xu, J. Liu, T. K. Rodrigues and N. Kato, "Robust Multiuser Beamforming for IRS-Enhanced Near-Space Downlink Communications Coexisting With Satellite System," in *IEEE Internet of Things Journal*, vol. 9, no. 16, pp. 14900-14912, 15 Aug. 2022.
 - [III.3-169] H. Hashida, Y. Kawamoto and N. Kato, "Selective Reflection Control: Distributed IRS-Aided Communication With Partial Channel State Information," in *IEEE Transactions on Vehicular Technology*, vol. 71, no. 11, pp. 11949-11958, Nov. 2022.
 - [III.3-170] H. Hashida, Y. Kawamoto, N. Kato, M. Iwabuchi and T. Murakami, "Mobility-Aware User Association Strategy for IRS-Aided mm-Wave Multibeam Transmission Towards 6G," in *IEEE Journal on Selected Areas in Communications*, vol. 40, no. 5, pp. 1667-1678, May 2022.
 - [III.3-171] Y. Zhu, Y. Kawamoto, N. Kato, K. Yano and T. Sakano, "Enhancing Indoor THz Multi-AP Joint Transmission With IRS: A Clustering and Kalman Filtering Approach for Mobile User," in *IEEE Transactions on Cognitive Communications and Networking*, 2024, doi: 10.1109/TCCN.2024.3496873.
 - [III.3-172] D. Darsena, F. Verde, I. Iudice and V. Galdi, "Design of Stacked Intelligent Metasurfaces With Reconfigurable Amplitude and Phase for Multiuser Downlink Beamforming," in *IEEE Open Journal of the Communications Society*, vol. 6, pp. 531-550, 2025.
 - [III.3-173] M. Nerini and B. Clerckx, "Physically Consistent Modeling of Stacked Intelligent Metasurfaces Implemented With Beyond Diagonal RIS," in *IEEE Communications*

Letters, vol. 28, no. 7, pp. 1693-1697, July 2024.

- [III.3-174] J. An *et al.*, "Stacked Intelligent Metasurfaces for Efficient Holographic MIMO Communications in 6G," in *IEEE Journal on Selected Areas in Communications*, vol. 41, no. 8, pp. 2380-2396, Aug. 2023.
- [III.3-175] A. Papazafeiropoulos, P. Kourtessis, S. Chatzinotas, D. I. Kaklamani and I. S. Venieris, "Near-Field Beamforming for Stacked Intelligent Metasurfaces-Assisted MIMO Networks," in *IEEE Wireless Communications Letters*, vol. 13, no. 11, pp. 3035-3039, Nov. 2024.
- [III.3-176] A. Papazafeiropoulos, J. An, P. Kourtessis, T. Ratnarajah and S. Chatzinotas, "Achievable Rate Optimization for Stacked Intelligent Metasurface-Assisted Holographic MIMO Communications," in *IEEE Transactions on Wireless Communications*, vol. 23, no. 10, pp. 13173-13186, Oct. 2024.
- [III.3-177] A. Papazafeiropoulos, P. Kourtessis, S. Chatzinotas, D. I. Kaklamani and I. S. Venieris, "Achievable Rate Optimization for Large Stacked Intelligent Metasurfaces Based on Statistical CSI," in *IEEE Wireless Communications Letters*, vol. 13, no. 9, pp. 2337-2341, Sept. 2024.
- [III.3-178] S. Li, F. Zhang, T. Mao, R. Na, Z. Wang and G. K. Karagiannidis, "Transmit Beamforming Design for ISAC With Stacked Intelligent Metasurfaces," in *IEEE Transactions on Vehicular Technology*, 2024, doi: 10.1109/TVT.2024.3517709.
- [III.3-179] Q. Li, M. El-Hajjar, C. Xu, J. An, C. Yuen and L. Hanzo, "Stacked Intelligent Metasurfaces for Holographic MIMO-Aided Cell-Free Networks," in *IEEE Transactions on Communications*, vol. 72, no. 11, pp. 7139-7151, Nov. 2024.
- [III.3-180] N. U. Hassan, J. An, M. Di Renzo, M. Debbah and C. Yuen, "Efficient Beamforming and Radiation Pattern Control Using Stacked Intelligent Metasurfaces," in *IEEE Open Journal of the Communications Society*, vol. 5, pp. 599-611, 2024.
- [III.3-181] H. Niu, J. An, A. Papazafeiropoulos, L. Gan, S. Chatzinotas and M. Debbah, "Stacked Intelligent Metasurfaces for Integrated Sensing and Communications," in *IEEE Wireless Communications Letters*, vol. 13, no. 10, pp. 2807-2811, Oct. 2024.
- [III.3-182] H. Niu, X. Lei, J. An, L. Zhang and C. Yuen, "On the Efficient Design of Stacked Intelligent Metasurfaces for Secure SISO Transmission," in *IEEE Transactions on Information Forensics and Security*, vol. 20, pp. 60-70, 2025.
- [III.3-183] J. An *et al.*, "Two-Dimensional Direction-of-Arrival Estimation Using Stacked Intelligent Metasurfaces," in *IEEE Journal on Selected Areas in Communications*, vol. 42, no. 10, pp. 2786-2802, Oct. 2024.
- [III.3-184] S. Lin, J. An, L. Gan, M. Debbah and C. Yuen, "Stacked Intelligent Metasurface Enabled LEO Satellite Communications Relying on Statistical CSI," in *IEEE Wireless Communications Letters*, vol. 13, no. 5, pp. 1295-1299, May 2024.
- [III.3-185] Y. Hu *et al.*, "Joint Beamforming and Power Allocation Design for Stacked Intelligent Metasurfaces-Aided Cell-Free Massive MIMO Systems," in *IEEE*

- Transactions on Vehicular Technology*, 2024, doi: 10.1109/TVT.2024.3499968.
- [III.3-186] C. Pei, K. Huang, L. Jin, X. Xu, Y. Zhou and Y. Guo, "Stacked Intelligent Metasurfaces Assisted Integrated-Sensing-and-Resistance Anti Jamming," in *IEEE Communications Letters*, 2024, doi: 10.1109/LCOMM.2024.3520510.
- [III.3-187] X. Yao, J. An, L. Gan, M. Di Renzo and C. Yuen, "Channel Estimation for Stacked Intelligent Metasurface-Assisted Wireless Networks," in *IEEE Wireless Communications Letters*, vol. 13, no. 5, pp. 1349-1353, May 2024.
- [III.3-188] G. Huang, J. An, Z. Yang, L. Gan, M. Bennis and M. Debbah, "Stacked Intelligent Metasurfaces for Task-Oriented Semantic Communications," in *IEEE Wireless Communications Letters*, 2024, doi: 10.1109/LWC.2024.3499970.
- [III.3-189] J. Rao *et al.*, "A Novel Reconfigurable Intelligent Surface for Wide-Angle Passive Beamforming," in *IEEE Transactions on Microwave Theory and Techniques*, vol. 70, no. 12, pp. 5427-5439, Dec. 2022.
- [III.3-190] C. Zhang *et al.*, "Millimeter-Wave Large-Angle Dual-Polarization Reconfigurable Intelligent Surface for 6G Communication Relay," in *IEEE Antennas and Wireless Propagation Letters*, vol. 23, no. 10, pp. 2900-2904, Oct. 2024.
- [III.3-191] Y. Cui, H. Sato, Y. Shibata, T. Ishinabe, H. Fujikake and Q. Chen, "A Low-Cost Structure for Reducing Reflection Loss in Intelligent Reflecting Surface of Liquid Crystal," in *IEEE Antennas and Wireless Propagation Letters*, vol. 22, no. 12, pp. 3027-3031, Dec. 2023.
- [III.3-192] L. Dai *et al.*, "Reconfigurable Intelligent Surface-Based Wireless Communications: Antenna Design, Prototyping, and Experimental Results," in *IEEE Access*, vol. 8, pp. 45913-45923, 2020.
- [III.3-193] Q. Hu, H. Yang, X. Zeng and X. Y. Zhang, "Wideband Reconfigurable Intelligent Surface Using Dual-Resonance Element," in *IEEE Antennas and Wireless Propagation Letters*, vol. 22, no. 10, pp. 2422-2426, Oct. 2023.
- [III.3-194] Y. Chen *et al.*, "Design of 2-Bit Single Linearly Polarized Reconfigurable Intelligent Surface for Single-Beam/Multibeam Scanning," in *IEEE Antennas and Wireless Propagation Letters*, vol. 23, no. 8, pp. 2366-2370, Aug. 2024.
- [III.3-195] L. Zhu *et al.*, "Dual Linearly Polarized 2-bit Programmable Metasurface With High Cross-Polarization Discrimination," in *IEEE Transactions on Antennas and Propagation*, vol. 72, no. 2, pp. 1510-1520, Feb. 2024.
- [III.3-196] B. J. Xiang, X. Dai and K. -M. Luk, "A Wideband Low-Cost Reconfigurable Reflectarray Antenna With 1-Bit Resolution," in *IEEE Transactions on Antennas and Propagation*, vol. 70, no. 9, pp. 7439-7447, Sept. 2022.
- [III.3-197] B. G. Kashyap, P. C. Theofanopoulos, Y. Cui and G. C. Trichopoulos, "Mitigating Quantization Lobes in mmWave Low-Bit Reconfigurable Reflective Surfaces," in *IEEE Open Journal of Antennas and Propagation*, vol. 1, pp. 604-614, 2020.
- [III.3-198] J. Tian, S. Li, C. He, M. Premaratne, W. Zhu and J. Zhou, "Ultra-Broadband and

- Multi-Polarized Electrically Reconfigurable Reflectarray Antenna," in *IEEE Transactions on Antennas and Propagation*, 2024, doi: 10.1109/TAP.2024.3486014.
- [III.3-199] Q. J. Lim, C. Ross, A. Ghosh, F. W. Vook, G. Gradoni and Z. Peng, "Quantum-Assisted Combinatorial Optimization for Reconfigurable Intelligent Surfaces in Smart Electromagnetic Environments," in *IEEE Transactions on Antennas and Propagation*, vol. 72, no. 1, pp. 147-159, Jan. 2024.
- [III.3-200] B. Narottama and S. Aïssa, "Quantum Machine Learning for Performance Optimization of RIS-Assisted Communications: Framework Design and Application to Energy Efficiency Maximization of Systems With RSMA," in *IEEE Transactions on Wireless Communications*, vol. 23, no. 10, pp. 12830-12843, Oct. 2024.
- [III.3-201] C. Ross, G. Gradoni, Q. J. Lim and Z. Peng, "Engineering Reflective Metasurfaces With Ising Hamiltonian and Quantum Annealing," in *IEEE Transactions on Antennas and Propagation*, vol. 70, no. 4, pp. 2841-2854, April 2022.
- [III.3-202] A. Taneja and S. Rani, "Quantum-Enabled Intelligent Resource Control for Reliable Communication Support in Internet-of-Vehicles," in *IEEE Transactions on Consumer Electronics*, vol. 70, no. 3, pp. 5545-5552, Aug. 2024.
- [III.3-203] E. Colella, L. Bastianelli, V. M. Primiani, Z. Peng, F. Moglie and G. Gradoni, "Quantum Optimization of Reconfigurable Intelligent Surfaces for Mitigating Multipath Fading in Wireless Networks," in *IEEE Journal on Multiscale and Multiphysics Computational Techniques*, vol. 9, pp. 403-414, 2024.
- [III.3-204] X. Zhao, J. Schalch, J. Zhang, H. R. Seren, G. Duan, R. D. Averitt, and X. Zhang, "Electromechanically tunable metasurface transmission waveplate at terahertz frequencies," *Optica* 5, 303-310, 2018.
- [III.3-205] Manjappa, M., Pitchappa, P., Singh, N. *et al.*, "Reconfigurable MEMS Fano metasurfaces with multiple-input-output states for logic operations at terahertz frequencies," *Nat Commun* 9, 4056, 2018.
- [III.3-206] L. Cong, P. Pitchappa, N. Wang and R. Singh, "Electrically Programmable Terahertz Diatomic Metamolecules for Chiral Optical Control," *Research*, 2019, doi: [10.34133/2019/7084251](https://doi.org/10.34133/2019/7084251).
- [III.3-207] F. Hu *et al.*, "A dynamically tunable terahertz metamaterial absorber based on an electrostatic MEMS actuator and electrical dipole resonator array," *Journal of Micromechanics and Microengineering*, Vol. 26, No. 2, 2016.
- [III.3-208] A. Araghi *et al.*, "Reconfigurable Intelligent Surface (RIS) in the Sub-6 GHz Band: Design, Implementation, and Real-World Demonstration," in *IEEE Access*, vol. 10, pp. 2646-2655, 2022.
- [III.3-209] H. Lin *et al.*, "A dual-band reconfigurable intelligent metasurface with beam steering," *J. Phys. D: Appl. Phys.* **55** 245002, 2022.
- [III.3-210] H. Xu *et al.*, "Aberration-free and functionality-switchable meta-lenses based on tunable metasurfaces," *Appl. Phys. Lett.* 109, 193506, 2016.

- [III.3-211] R. João Ricardo *et al.*, “Metamaterial-Inspired Flat Beamsteering Antenna for 5G Base Stations at 3.6 GHz,” *Sensors* **21**, no. 23, 2021.
- [III.3-212] Taravati, S., Eleftheriades, G.V. Full-duplex reflective beamsteering metasurface featuring magnetless nonreciprocal amplification. *Nat Commun* **12**, 4414, 2021.
- [III.3-213] Venkatesh, S., Lu, X., Saeidi, H. *et al.*, “A high-speed programmable and scalable terahertz holographic metasurface based on tiled CMOS chips,” *Nat Electron* **3**, 785–793, 2020.
- [III.3-214] N. Kari *et al.*, “An electrically driven terahertz metamaterial diffractive modulator with more than 20 dB of dynamic range,” *Appl. Phys. Lett.* **104**, 091115, 2014.
- [III.3-215] Chen, HT., Padilla, W., Cich, M. *et al.*, “A metamaterial solid-state terahertz phase modulator,” *Nature Photon* **3**, 148–151, 2009.
- [III.3-216] M. Zheng Chen *et al.*, “Accurate and broadband manipulations of harmonic amplitudes and phases to reach 256 QAM millimeter-wave wireless communications by time-domain digital coding metasurface,” *National Science Review*, Volume 9, Issue 1, January 2022.
- [III.3-217] J. -B. Gros, V. Popov, M. A. Odit, V. Lenets and G. Lerosey, "A Reconfigurable Intelligent Surface at mmWave Based on a Binary Phase Tunable Metasurface," in *IEEE Open Journal of the Communications Society*, vol. 2, pp. 1055-1064, 2021.
- [III.3-218] S. Pramanik, S. C. Bakshi, C. Koley, D. Mitra, A. Monti and F. Bilotti, "Active Metasurface-Based Reconfigurable Polarization Converter With Multiple and Simultaneous Functionalities," in *IEEE Antennas and Wireless Propagation Letters*, vol. 22, no. 3, pp. 522-526, March 2023.
- [III.3-219] M. Jiang *et al.*, "Electrically Triggered VO₂ Reconfigurable Metasurface for Amplitude and Phase Modulation of Terahertz Wave," in *Journal of Lightwave Technology*, vol. 39, no. 11, pp. 3488-3494, June1, 2021.
- [III.3-220] D. Tang *et al.*, “Programmable VO₂ metasurface for terahertz wave beam steering,” *iScience* Volume 25, Issue 8, 19 August, 2022.
- [III.3-221] A. Barom *et al.*, “Millimeter Wave Reconfigurable Metasurface Intelligent Reflecting Surface Based on Piezoelectric Crystal for 5th and 6th Generation of Wireless Communication,” *Communications and Network*, **14**, 109-118, 2022.
- [III.3-222] Katare, K.K., Biswas, A. & Akhtar, M.J. “Near-field phase modulation using a semicircular radially gradient metasurface for beam steering of an RF antenna,” *J Comput Electron* **18**, 671–679, 2019.
- [III.3-223] Hong, Qiao Ru, *et al.* "Programmable amplitude-coding metasurface with multifrequency modulations." *Advanced Intelligent Systems* **3.8**, 2021.
- [III.3-224] Xinyun Song, Weixu Yang, Kai Qu, Xudong Bai, Ke Chen, Yijun Feng, and Weiren Zhu, "Switchable metasurface for nearly perfect reflection, transmission, and absorption using PIN diodes," *Opt. Express* **29**, 29320-29328, 2021.
- [III.3-225] M. Yoo *et al.*, “Active metasurface for controlling reflection and absorption

- properties,” *Appl. Phys. Express* **7** 112204, 2014.
- [III.3-226] Mehdi Kiani, Ali Momeni, Majid Tayarani, and Can Ding, "Spatial wave control using a self-biased nonlinear metasurface at microwave frequencies," *Opt. Express* **28**, 35128-35142, 2020.
- [III.3-227] W. Li *et al.*, "PIN tuned phase-gradient-metasurface transmitarray for beam steering application," *2016 11th International Symposium on Antennas, Propagation and EM Theory (ISAPE)*, Guilin, China, 2016, pp. 276-278.
- [III.3-228] Li, L., Jun Cui, T., Ji, W. *et al.*, "Electromagnetic reprogrammable coding-metasurface holograms,” *Nat Commun* **8**, 197, 2017.
- [III.3-229] Lee, S., Choi, M., Kim, TT. *et al.*, "Switching terahertz waves with gate-controlled active graphene metamaterials,” *Nature Mater* **11**, 936–941, 2012.

III.4. Overall trend

Figure III.4-1 illustrates trends in the number of publications on repeater, metasurface, and RIS/IRS. The database used to generate this figure consists of journals and conference papers published in IEEE Xplore from 2010 to 2024, with the number of publications containing the following keywords in their titles.

- repeater: repeater, relay
- metasurface: meta-surface, metasurface, meta surface
- RIS/IRS: RIS, IRS, reconfigurable intelligent surface, intelligent reflecting surface

As shown in this figure, the number of publications on repeaters has decreased since peaking in 2012. A considerable amount of research and development has been conducted on repeater technologies. Currently, they are defined as NCR and IAB in 3GPP standardization, marking their transition from the R&D phase to the commercialization phase. On the other hand, the number of publications on metasurface and RIS/IRS has been increasing year by year, confirming that these are emerging technologies. In particular, the number of publications on RIS/IRS has seen a sharp rise since 2018, with an increase rate approximately twice that of metasurface. In addition, the trend in the number of papers published by RIS and IRS is shown in Figure III.4-2. As can be seen from this figure, the number of papers published by RIS is greater. Since RIS/IRS includes metasurface technology, it is rapidly becoming a new research field.

Figure III.4-3 is a visualization of the keywords related to metasurface, RIS/IRS, and repeater, based on the analysis results from the Text Mining Tool (<https://textmining.userlocal.jp/>). The publication papers used for aggregation are the same as those extracted in Figure III.4-1, and the keywords registered for each paper in IEEE Xplore were compiled. During the aggregation process, synonymous terms were unified where possible. The font size represents the frequency of occurrence. Common to all figures, the font size of general words related to wireless communication, such as “communication” and analytical words such as “analysis” or “optimization” is larger. Words that are smaller than these general terms represent the specific features of each technology. There are more words related to higher-layer topics, such as “repeater”, “system”, and “evaluation”. For metasurface, they are related to the usage methods, such as “Radar” or technical terms like antenna characteristics and wave properties. RIS/IRS shows a broader distribution of terms, ranging from system-level concepts to component technologies. Additionally, the smaller words are more specific, indicating the relevance of technical terms and their interconnections.

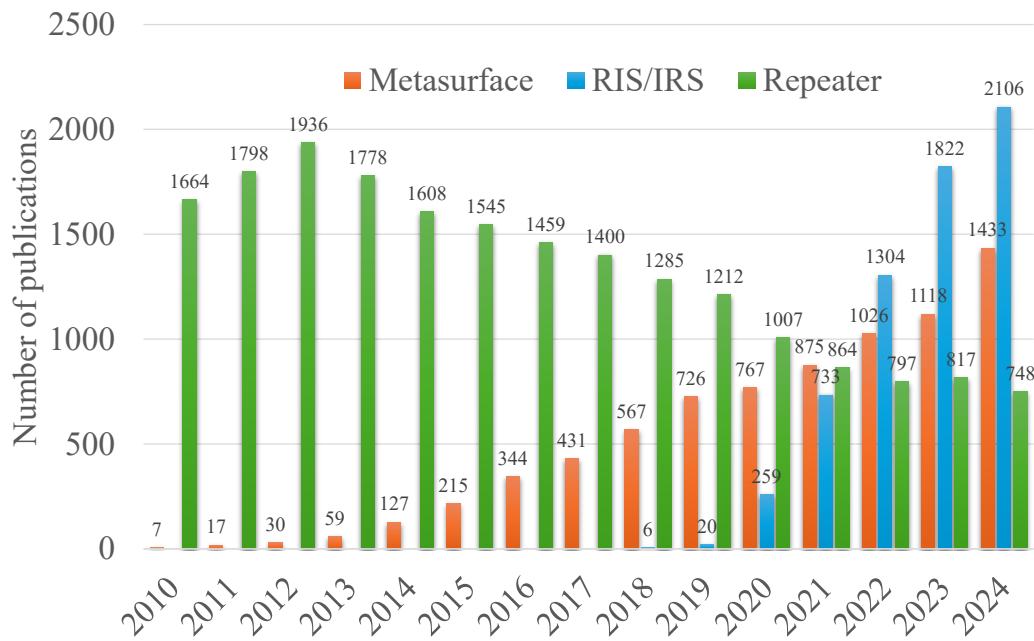


Fig. III.4-1. Trends in the number of publications in IEEE Xplore.

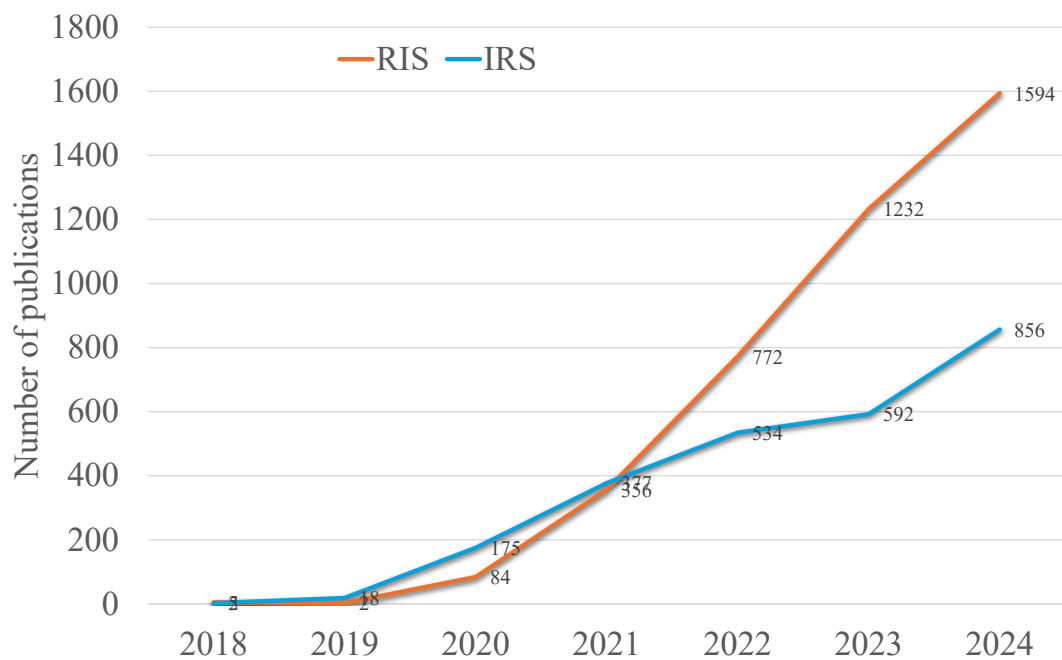


Fig. III.4-2. RIS/IRS trends in the number of publications in IEEE Xplore.

III.5. Technology trend on repeater

Overview of Repeater Technology

Repeater-related technologies such as NR Repeater [III.5-1], NCR (Network-controlled Repeater) [III.5-2], IAB (Integrated Access and Backhaul) [III.5-3], [III.5-4], [III.5-5], and Wireless Access and Backhaul (WAB) [III.5-6], [III.5-7] have been standardized or are in the process of being standardized by 3GPP.

NR Repeater is a repeater equipped with an AF relay function that amplifies and forwards received signals without performing modulation and demodulation of packets. The RF requirements were standardized in Rel-17. It is designed to operate in the FR1 (0.41-7.125 GHz band) and FR2-1 (24.25-52.6 GHz band) frequency ranges. Repeater classes have been introduced to support various deployment scenarios such as macro cells, micro cells, and pico cells. NR Repeater minimizes delay caused by signal processing and can be realized with a simple hardware configuration, but at the same time, the effects of noise and interference from the external environment are directly propagated.

NCR is a repeater equipped with not only an AF relay function but also the ability to receive and process control information from the network side. It was standardized in Rel-18. Like the NR Repeater, it amplifies and forwards received signals. By using control information from the network (such as beamforming and TDD configuration), it is possible to reduce unnecessary noise amplification and improve spatial directivity for transmission and reception.

IAB is a backhaul relay technology equipped with a DF relay function that performs signal processing such as demodulation, decoding, and error correction on received signals, and then re-encodes and modulates them for forwarding. IAB nodes have gNB-DU and UE functions, enabling multi-hop wireless backhaul. The backhaul is conducted via the L2 BAP (Backhaul Adaptation Protocol). It was standardized in Rel-16 and further expanded in Rel-17/Rel-18. It allows for flexible and extremely dense network deployment through wireless backhaul. The ability to remove noise, interference, and distortion that occur during transmission improves signal quality. However, there is a possibility of processing delays, increased complexity in implementation and operation, and higher costs.

WAB is a backhaul relay technology equipped with a DF relay. Unlike IAB nodes, it possesses gNB functions including gNB-CU and UE functions, and the backhaul is conducted via PDU Session. The existing 5G mobility management procedures can be applied to local services and backhaul that were challenging with IAB. Use cases include relaying between ground stations and passenger terminals with vehicles equipped with WAB functionality, backhaul via NTN, Multi-access Edge Computing and local services, and backhaul for local gNBs in public safety or disaster recovery. It is being standardized in Rel-19.

Commercialization Trends

As mentioned in III.5.1, the standardization of various items related to repeater technology is progressing, and it is transitioning from the research and development stage to the practical application

stage. We conducted a survey on the commercialization status of repeaters and summarized the findings in Table. III.5-1.

Most of the devices that have been commercialized are NR Repeaters. Repeaters conforming to Rel-17 NR Repeater standards [III.5-21] are also beginning to appear. In addition to AF relay functions, they are differentiating themselves by adding unique features such as installation on windows [III.5-12] and automatic area construction [III.5-16]. Although NCRs are few in number, examples of commercialization have emerged this year [III.5-23]. IAB is in the field test stage.

Table. III.5-1 Repeater Field Test and Commercialization

Reference	Status	Category	Frequency	Use-case	Feature
[III.5-8]	Commercialization	NR Repeater	28GHz 2Band BandWidth:400MHz	Indoor/Outdoor	
[III.5-9]	Commercialization	NR Repeater	27.5-28.35GHz BandWidth850MHz	-	
[III.5-10]	Commercialization	NR Repeater	3.5GHz	Indoor/Outdoor	Time Division Duplex (TDD) Synchronization detection
[III.5-11]	Commercialization	NR Repeater	26.5-29.5 GHz or 37-40GHz	Indoor/Outdoor	
[III.5-12]	Commercialization	NR Repeater	27.5-28.35 GHz or 37.6-40GHz	Indoor/Outdoor	On the window
[III.5-13]	Commercialization	NR Repeater	26.5-29.5 GHz 27.5-28.35GHz BandWidth:1GHz	Indoor/Outdoor	
[III.5-14]	Commercialization	NR Repeater	700MHz 850MHz 17700-2100MHz 1900MHz	IoT device: ATM, Kiosk, Vehicle, Security application	
[III.5-15]	Commercialization	NR Repeater	3.3-3.8GHz 4.4-5.0GHz	Indoor/Outdoor	-
[III.5-16]	Field Test	NR Repeater	28GHz	Outdoor	Autonomous Area Formation Optimizing Relay Routes
[III.5-17]	Commercialization	NR Repeater	3.7-3.98GHz Bandwidth:20-100MHz	Indoor/Outdoor	
[III.5-18]	Commercialization	NR Repeater	Sub6/28GHz	-	-
[III.5-19]	Commercialization	NR Repeater	Quadband: 2G, 3G, 4G, 5G-NR FDD, NB-IoT	Indoor	-
[III.5-20]	Commercialization	NR Repeater	3.3-3.8GHz 3.3-4.2GHz	Indoor	-
[III.5-21]	Commercialization	NR Repeater	3.5GHz Bandwidth: 100MHz	Indoor	Compliant with the upcoming 3GPP Release 17 NR repeater standard
[III.5-22]	Commercialization	NR Repeater	3.7-3.84GHz 3.7-3.98GHz	-	-
[III.5-23]	Commercialization	NCR	Sub6	Outdoor	Solar-powered, grid-independent operation
[III.5-24]	Field Test	NCR	28GHz	Moving Vehicle	Cloud AI control rapid beam/gNB switching
[III.5-25]	Proof of concept	IAB	mm Wave	Disaster recovery Other critical situations	-
[III.5-26]	Field Test	IAB	Backhaul Link: 39GHz Access Link: 39GHz	Tall buildings Isolated islands Mountain regions	-
[III.5-27]	Field Test	IAB	mm Wave	-	Multi-hop
[III.5-28]	Field Test	IAB	Backhaul Link: mm Wave Access Link: Sub6	-	-

Research Trends

To understand research trends, we investigated repeater-related literature published since 2010 in IEEE Xplore. Fig. III.5-1 shows a graph of papers by technical field. The categories are divided into AF relay, DF relay, IAB, and NCR. The technology category with the most papers is IAB, followed

by AF. IAB considers various layers, not only hardware [III.3-32] but also network [III.3-14], mobile relay [III.3-44], and coexistence with RIS [III.3-12] [III.3-20]. AF is exploring new use cases such as Simultaneous Wireless Information and Power Transfer (SWIPT) [III.3-41], HAPS [III.3-30], LEO [III.3-39], and UAV [III.3-53].

Fig. III.5-2 is a frequency-based graph. The categories are classified as 'up to 24 GHz' like Sub6, '24 to 100 GHz' like millimeter waves, and 'Above 100 GHz' like terahertz and optical. Most of the research falls under '24 to 100 GHz' related to millimeter waves. Research using terahertz and optical frequencies is also gradually increasing, such as studies applying sub-terahertz to IAB backhaul [III.3-33] and dual-hop hybrid systems with optical and millimeter waves [III.3-50].

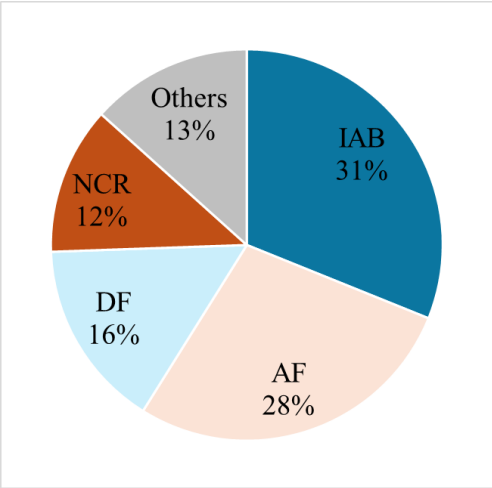


Fig. III.5-1. Percentage of papers by technical category

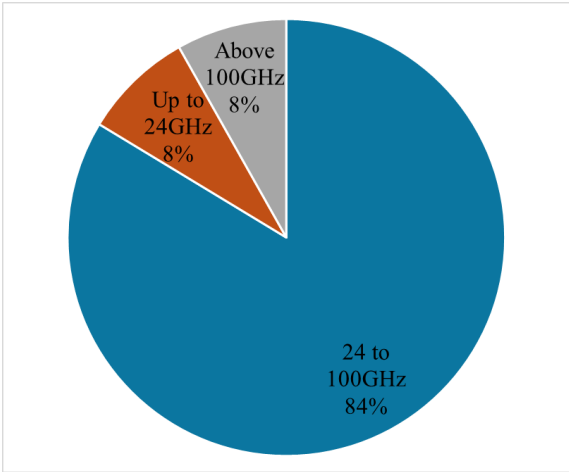


Fig. III.5-2. Percentage of papers by frequency category

REFERENCE

- [III.5-1] 3GPP, "Work Item Description: NR Repeaters," 3GPP TSG RAN Meeting #94e RP-213514, Dec. 2021. [Online]. Available: <https://portal.3gpp.org/desktopmodules/WorkItem/WorkItemDetails.aspx?workitemId=900070>
- [III.5-2] 3GPP, "Work Item Description: NR Network-controlled Repeaters," 3GPP TSG RAN Meeting #102 RP-232886, Dec. 2023. [Online]. Available: <https://portal.3gpp.org/desktopmodules/WorkItem/WorkItemDetails.aspx?workitemId=970079>
- [III.5-3] 3GPP, "Work Item Description: Integrated access and backhaul for NR," 3GPP TSG RAN meeting #91e RP-210442, Mar. 2021. [Online]. Available: <https://portal.3gpp.org/desktopmodules/WorkItem/WorkItemDetails.aspx?workitemId=820070>
- [III.5-4] 3GPP, "Work Item Description: Enhancements to Integrated Access and Backhaul for NR," 3GPP TSG RAN Meeting #94e RP-213668, Dec. 2021. [Online]. Available: <https://portal.3gpp.org/desktopmodules/WorkItem/WorkItemDetails.aspx?workitemId=860050>
- [III.5-5] 3GPP, "Work Item Description: Mobile IAB (Integrated Access and Backhaul) for NR," 3GPP TSG RAN Meeting #103 RP-240104, Mar. 2024. [Online]. Available: <https://portal.3gpp.org/desktopmodules/WorkItem/WorkItemDetails.aspx?workitemId=941009>
- [III.5-6] Qualcomm Incorporated, Xiaomi, "Rel-19 Views on Additional Topology Enhancements," 3GPP TSG RAN Meeting #102 RP-233021, Dec. 2023. [Online]. Available: https://www.3gpp.org/ftp/tsg_ran/TSG_RAN/TSGR_102/Docs
- [III.5-7] 3GPP, "Work Item Description: Study on additional topological enhancements for NR," 3GPP TSG RAN Meeting #104 RP-241264, Jun. 2024. [Online]. Available: <https://portal.3gpp.org/desktopmodules/WorkItem/WorkItemDetails.aspx?workitemId=1020082>
- [III.5-8] FRTEK, "PrimAer," FRTEK. [Online]. Available: https://www.frttek.co.kr/en/m/board/board.php?bo_table=wireless&cate=RF&idx=102 [Accessed: 2025-03-10].
- [III.5-9] TJ innovation, "mmWave OTA repeater SDS 28G-V," TJ innovation. [Online]. Available: http://www.tj-innovation.com/en/bbs/board.php?bo_table=test_en/ [Accessed: 2025-03-10].
- [III.5-10] SOLiD, "Press-releases: SOLiD is Key to SK Telecom 5G In-Building Award Winning Solution," SOLiD. [Online]. Available: <https://solid.com/us/solid-is-key-to-sk-telecom-5g-in-building-award-winning-solution/> [Accessed: 2025-03-10].
- [III.5-11] PIVOTAL COMMWARE, "Pivot 5G," PIVOTAL COMMWARE. [Online]. Available: <https://pivotalcommware.com/pivot-5g/> [Accessed: 2025-03-10].
- [III.5-12] PIVOTAL COMMWARE, "Echo 5G," PIVOTAL COMMWARE. [Online]. Available: <https://pivotalcommware.com/echo-5g/> [Accessed: 2025-03-10].
- [III.5-13] WILSON CONNECTIVITY, "Wilson Network 257," WILSON CONNECTIVITY. [Online]. Available: https://www.wilsonpro.com/products/network_257/ [Accessed: 2025-03-10].
- [III.5-14] WILSON CONNECTIVITY, "IoT 5-Band," WILSON CONNECTIVITY. [Online]. Available: <https://www.wilsonpro.com/products/wilsonpro-iot-5-band> [Accessed: 2025-03-10].
- [III.5-15] MORELINK, "5G ICS Repeater | Product," MORELINK. [Online]. Available: <https://morelinktek.com.tw/product/ics-repeater/> [Accessed: 2025-03-10].

- [III.5-16] KDDI, “KDDI and Kyocera Succeeded in Developing Wireless Relay Technology That Dramatically Expands Millimeter-Wave Coverage,” KDDI. [Online]. Available: https://newsroom.kddi.com/english/news/detail/kddi_nr-403_3675.html [Accessed: 2025-03-10].
- [III.5-17] Advanced RF Technologies, “SDRX Series,” Advanced RF Technologies. [Online]. Available: <https://www.adrftech.com/sdrxseries> [Accessed: 2025-03-10].
- [III.5-18] DDK, “Local 5G (Private 5G) Repeater,” DDK. [Online]. Available: <https://denkikogyo.co.jp/en/elec/product/mobile/15g/> [Accessed: 2025-03-10].
- [III.5-19] ZYXEL, “MagicOffice Repeater,” ZYXEL. [Online]. Available: <https://www.zyxel.com/global/en/products/in-building-coverage/quad-band-repeater-magicoffice-repeater> [Accessed: 2025-03-10].
- [III.5-20] Comba, “Comba Launches New Generation of Repeaters to Enhance Indoor Connectivity,” Comba. [Online]. Available: <https://www.comba-telecom.com/en> [Accessed: 2025-03-10].
- [III.5-21] Nextivity, “Nextivity Solves In-Building 5G Connectivity Challenges with Release of CEL-FI GO G51 Self-Configuring 5G NR Repeater,” Nextivity. [Online]. Available: <https://nextivityinc.com/press-release/nextivity-solves-in-building-5g-connectivity-challenges-with-release-of-cel-fi-go-g51-self-configuring-5g-nr-repeater/> [Accessed: 2025-03-10].
- [III.5-22] SureCall, “5G C-Band Signal Boosters for Large Buildings,” SureCall. [Online]. Available: <https://surecall.com/enterprise/c-band-signal-boosters/> [Accessed: 2025-03-10].
- [III.5-23] Airgain, “Airgain Lighthouse Solar Smart Network-Controlled Repeater (NCR),” Airgain. [Online]. Available: <https://www.airgain.com/products/airgain-lighthouse-solar/> [Accessed: 2025-03-10].
- [III.5-24] Movandi, “Landmark Movandi 5G mmWave Mobile Test Achieves 19X Industry Average Download Speeds,” Movandi. [Online]. Available: <https://movandi.com/landmark-movandi-5g-mmwave-mobile-test-achieves-19x-industry-average-download-speeds/> [Accessed: 2025-03-10].
- [III.5-25] Verizon, “Deploying the 5G Ultra Wideband Network just got a little easier,” Verizon. [Online]. Available: <https://www.verizon.com/about/news/deploying-5g-ultra-wideband-network-easier/> [Accessed: 2025-03-10].
- [III.5-26] NTT DOCOMO, “NTT DOCOMO and Huawei Prove IAB's Value in 5G Test Using 39 GHz Band,” NTT DOCOMO. [Online]. Available: https://www.docomo.ne.jp/english/info/media_center/pr/2018/0522_00.html [Accessed: 2025-03-10].
- [III.5-27] Verana Networks, “Verana Networks announces field trial agreement with Verizon for its ground-breaking 5G mmWave IAB solution,” Verana Networks. [Online]. Available: <https://verananetworks.com/verana-networks-announces-field-trial-agreement-with-verizon-for-its-ground-breaking-5g-mmwave-iab-solution/> [Accessed: 2025-03-10].
- [III.5-28] Kyocera, “Kyocera Corporation and SoftBank Corp. Succeeded in Demonstration of Backhaul System Utilizing 5G Millimeter-Wave,” Kyocera. [Online]. Available: <https://global.kyocera.com/newsroom/news/2022/000591.html> [Accessed: 2025-03-10].

III.6. Technology trend on metasurface

In this section, we summarize the technical trends based on 41 papers that have been published since 2015 and are searchable on IEEE Xplore, and have been cited, concerning “metasurfaces (static)” as defined in the technical category. Reflective and Refractive panels using static metasurfaces are positioned as a cost-effective method of expanding coverage because they do not require power supply or maintenance.

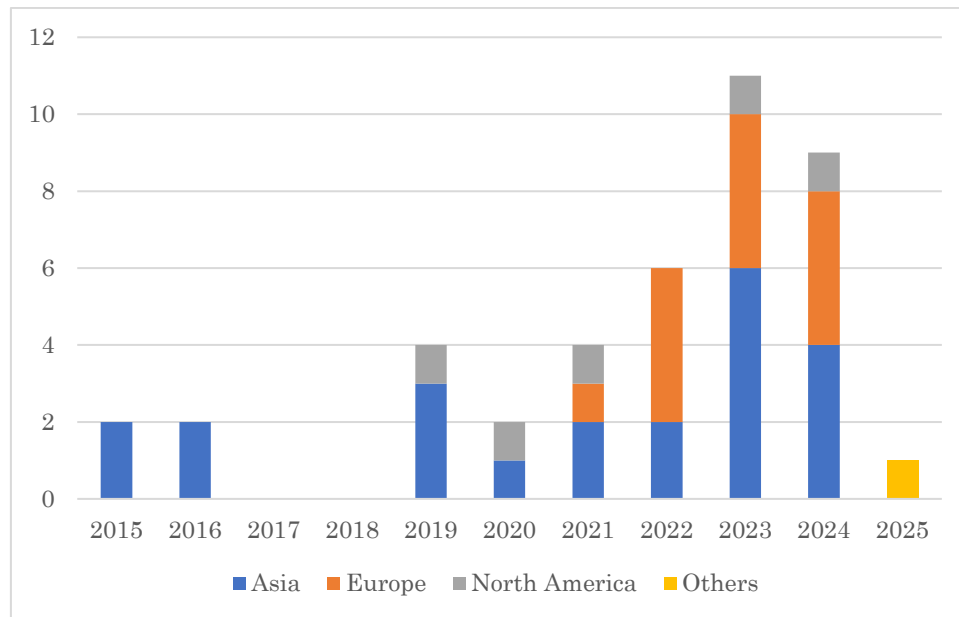


Fig. III.6-1. Number of papers per year and breakdown by region

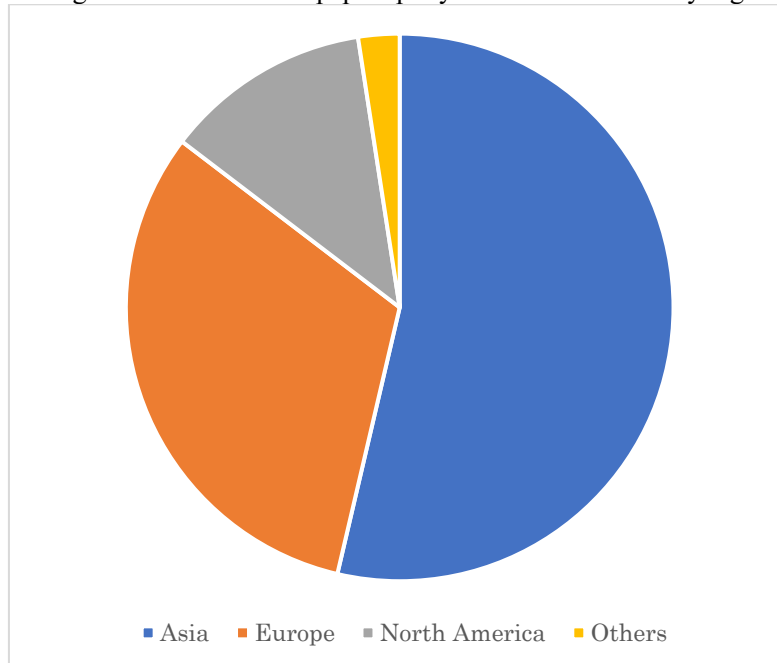


Fig. III.6-2: regional publication ratio in 2015-2025

Figure III.6-1 shows the number of papers published each year, classified by region as Asia, Europe, North America, and other. Overall, the number of papers published from Europe has increased since 2020. In terms of research content trends, before 2020, there were mainly studies on design guidelines for reflective properties using meta-patterns, and from the 2020s onwards, there have been papers that experimentally verify the effectiveness of coverage expansion. In recent years, there has been an increase in studies on improving design efficiency, including the use of AI. The frequency applied is mainly 28 GHz, and many papers have chosen practical frequencies as research topics when FR2 is developed.

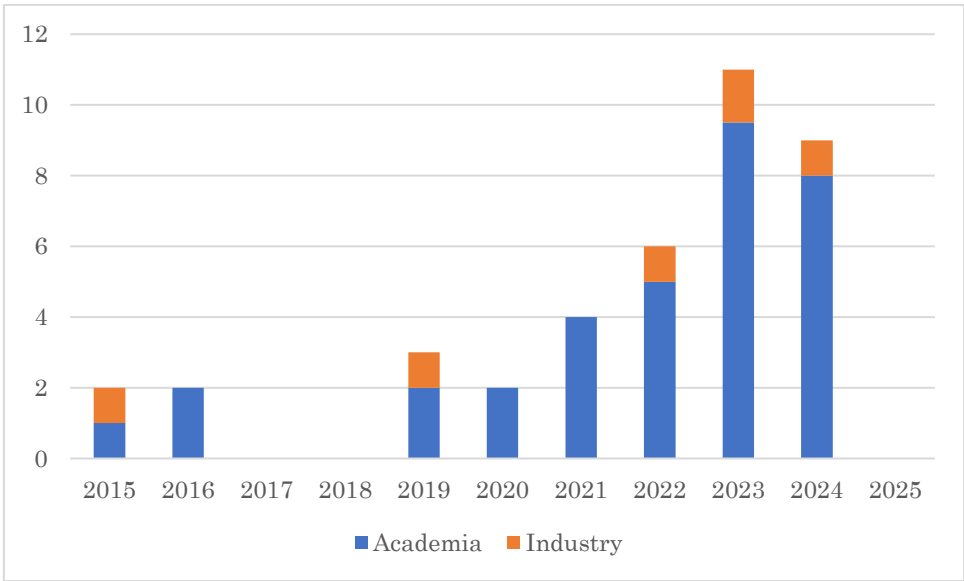


Fig. III.6-3. number of papers per year and breakdown by issuing organization

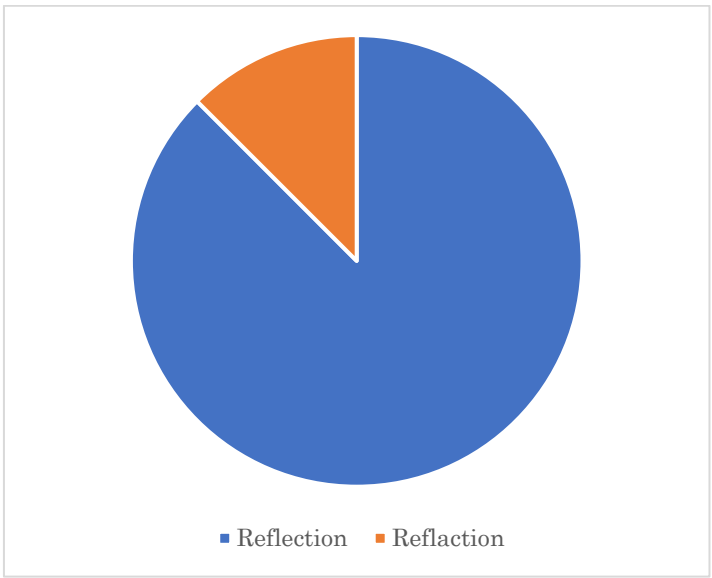


Fig. III.6-4. technical category ratio in 2015-2025

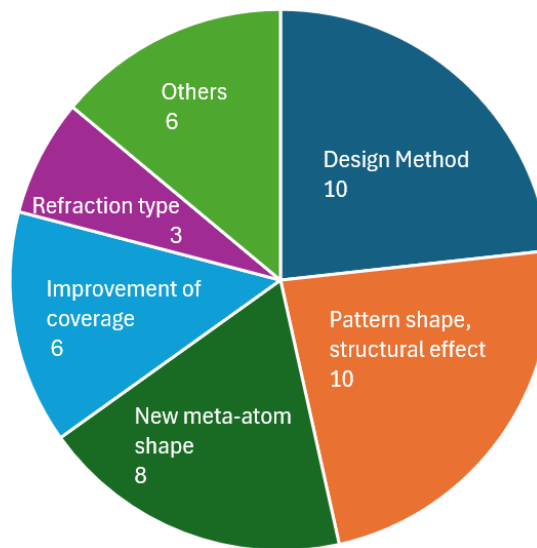
The results of the regional breakdown of the number of papers published during the survey period shown in Figure III.6-2 show that more than half of the reports came from the Asian region (53%), followed by Europe (31%) and North America (12%).

Figure III.6-3 shows the transition in activities of companies, universities and public institutions by year of publication. While the majority of activities are still in the embryonic stage of research at universities and public institutions, recent reports from companies are beginning to include practical perspectives, and there are signs of commercialization of materials that expand coverage in transmission and reflection modes using metasurfaces.

Figure III.6-4 shows the results of classifying the technology categories that achieve improved coverage using metasurfaces into transmission mode and reflection mode. Here, the classification is based on the handling of radio waves. The research in each mode includes specific materials that are characterized by being transparent in the visible light range, which reflects the needs of use cases.

Trends in research

Figure III.6-5 shows the number of papers for each main topic. The extracted papers were classified into the following categories: design methods, influence of pattern shape and structure, proposals for new meta-atom shapes, demonstration of coverage improvement, refraction types, and others. The following sections describe the characteristics of each category.



III.6-5. Area of Research Work on Static Metasurfaces for Coverage Improvement

Research on design methods for static metasurfaces

In addition to proposals for simplifying the design of metasurfaces for practical use, such as the design of high-efficiency abnormal reflection metasurfaces (PARM) with wide steering angles using a simplified method that does not rely on impedance matching [III.3-189] and the design of digitally coded reflectors [III.3-196], there are also proposals that provide a physical-based modeling framework for engineering complex propagation environments, there are also reports that evaluate the impact of geometric accuracy when using conventional PCB manufacturing methods on the performance of reflectors [III.3-192]. As computational design methods, there are reports that use

genetic algorithms [III.3-221], deep learning [III.3-227], and inverse design methods based on transfer learning [III.3-226].

The effect of pattern shape and structure on reflectance performance

An example comparing the reflectance performance and bandwidth coverage of four types of shape: circular, octagonal, hexagonal, and square [III.3-198], a comparison of flat plate reflectors, cylindrical reflectors, and spherical reflectors [III.3-202], an example using a unit cell combining segmented ring resonators (SRR) and dipole ring resonators (DRR) [III.3-187], one that uses a multi-channel beam-splitting metasurface [III.3-188], and one that uses a dual-polarized reflector array cell [III.3-205, III.3-207, III.3-208, III.3-209].

Proposal of a new meta-atom shape

A report on the design strategy of a non-periodic metallic reflector in the microwave region, which can have a reflection angle at a different incident angle [III.3-200], a report on the introduction of a square ring and four arrows to achieve a wide reflection phase range to improve the millimeter wave communication coverage in a non-line-of-sight (NLoS) scenario in a room [III.3-203], and a report on the proposal of a multi-layered mushroom reflector array that achieves a wide angle of reflection (AOR) at an ultra-high frequency to improve the multi-input multi-output (MIMO) capacity in a line-of-sight environment a multilayer mushroom reflector array that achieves a wide angle of reflection (AOR) at very high frequencies has been proposed [III.3-212]. In order to realize industrial products, it has been reported that the alignment-free characteristics of the constituent layers can be obtained by using a split-ring resonator (SRR) configuration, which facilitates production and mounting [III.3-217, III.3-218, III.3-219].

Demonstration of improved coverage

Several efforts to improve millimeter wave (mmWave) coverage in 5G and 6G communication systems have been reported as solutions to overcome the high path loss and blocking in the millimeter wave band. New approaches have been proposed to achieve highly efficient beamforming to improve indoor, outdoor, and indoor/outdoor coverage.

In an actual urban environment, measurements were taken over a range of 35 meters, and there were significant effects confirmed by actual measurements, such as an example where the beam reference signal received power (BRSRP) improved by about 15 dB and downlink throughput improved by 100% [III.3-194]. There is an example of using multi-hop (MH) cascaded reflection to improve the EM coverage of base station antennas in complex urban environments [III.3-193].

In order to achieve highly efficient communication in next-generation networks, it has been proposed that, in addition to improving coverage by enhancing signals, unnecessary signals should be canceled using static RISs [III.3-191].

Information on the materials that make up the metasurface (static)

Examples of polymer substrates being used as the substrate material for the metasurface can be seen, as low relative permittivity and low loss tangent are suitable for use in the millimeter wave band. Cyclo-olefin polymer (COP) [III.3-186], Megtron-7 substrate [III.3-189], FR-4 [III.3-198], RT Duroid 5880 [III.3-209], etc. are used, and the thickness is 100 to 500 micrometers depending on the frequency used for the metasurface. In the case of optically transparent metasurfaces, there are some cases where the material is not specified, but it is thought that glass plates or transparent resin films are used. Patterned copper is often used as the metal that makes up the metasurface on the substrate surface [III.3-186, III.3-189, III.3-198, III.3-209]. In some cases, a land plane is formed on the back surface, and in other cases, FSS is formed to allow radio waves to pass through, but in these cases, copper is also often used. There are also cases where flat reflectors, cylindrical reflectors, and spherical reflectors made of aluminum have been used experimentally [III.3-202].

III.7. Technology trend on RIS/IRS

Hardware Point of View

The main study items of RIS/IRS technology from the hardware point of view are the design of the unit cell structure and a dynamization method to electrically control the scattering properties of the cells (Fig. III.7-1). Based on the used materials, unit cells can be categorized into two groups: those composed of metal patterning and those composed of dielectrics. The study of dielectric cells has been predominantly focused on the visible to infrared wavelength range, owing to their capacity for low-loss phase design. The fabrication of dielectric cells in the radio frequency band presents a significant challenge, as the required thickness of the cell scales proportionally to the wavelength. Consequently, the majority of RIS/IRS unit cells reported in the radio band are fabricated by metal patterning. In addition to ease of fabrication, another advantage of metal-based cells is that they can easily adapt dynamic functions in combination with active components or functional materials. The design of the unit cell structure with an additional role as a bias line for the control signal enables modification of the properties of the active component or the functional material, and control of the scattering characteristics of the cell.

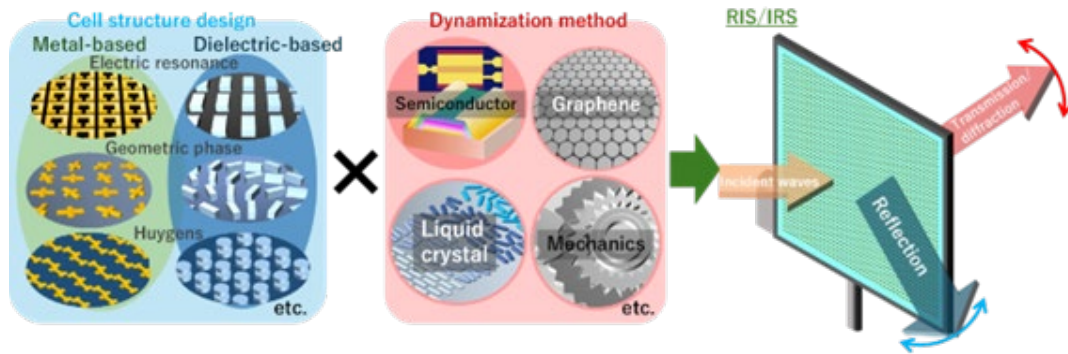


Fig. III.7-1. Conceptual diagram of RIS/IRS's main study items from an RF hardware perspective.

Frequency Point of View

A variety of dynamization methods have been reported, including semiconductor devices, graphene, liquid crystals (LC), phase-change materials (PCM), and micro-electromechanical systems (MEMS). The trend of RIS/IRS operating frequencies for each of the aforementioned dynamization methods is shown in Fig. III.7-2. Semiconductor-based RIS/IRS using PIN/Schottky diodes or transistors can be categorized into two primary types: one in which discrete components are additionally mounted in cells and the other in which the components are integrated in the cell using a semiconductor substrate. The discrete type is used below the millimeter-wave band, and the integrated type is used above the sub-terahertz band. These RIS/IRS devices are capable of operating at speeds of nanoseconds or less and have the potential for a variety of wireless applications. The other dynamization methods using graphene, LC, PCM, and MEMS have been reported in the wide frequency range from 10 GHz to 1 THz. Graphene-based RIS/IRS has been demonstrated to possess the capability for high-speed modulation in the order of nanoseconds or less and is being actively studied especially in the THz-

band where semiconductor devices cannot operate in such high frequencies. Graphene, a two-dimensional material with a few atomic layers, has the potential to make the RIS/IRS on flexible substrates, and the development of manufacturing technology for industrial applications is expected. LC-based RIS/IRS, which dynamically controls the scattering properties through the orientation of LC molecules, has a major advantage for practical applications since large-scale production technology has been already established for LC displays (LCDs). Despite the response time being generally in the order of milliseconds, which is slower than other methods, it is considered sufficiently applicable to use cases where the control of scattering characteristics requires following the motion of a walking person or a moving vehicle. PCM, in which external stimuli such as thermal and optical excitations induce a change in crystal structure, which in turn changes material properties such as electrical conductivity, has also been actively investigated. The response time of PCM varies considerably depending on the way of external stimulation. For instance, PCM-based RIS/IRS with optical excitation demonstrates a response time of less than a nanosecond. MEMS-based RIS/IRS, where the control signal causes a change in the physical structure of the cell, can achieve a large modulation depth. Their response speed is strongly correlated with the weight of the moving parts, and since unit cell size is generally negatively correlated with frequency, they can achieve response speeds comparable to other methods in some high-frequency bands.

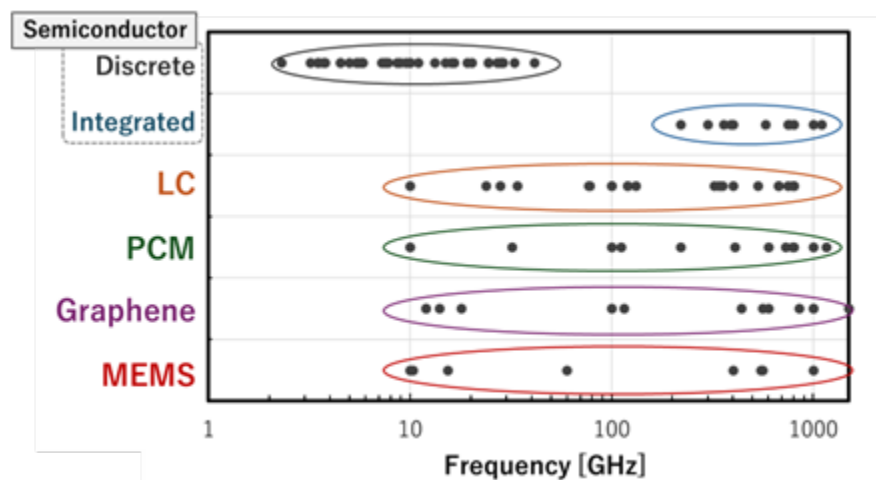


Fig. III.7-2. Reported RIS/IRS with various dynamization methods on their operation frequencies.

As mentioned above, a variety of dynamization methods are available for RIS/IRS devices, but the most appropriate method is considered to depend on a specific use case. In addition to the response time, cost/size is another important aspect. For example, if the RIS/IRS is used for beamforming together with a transmitter or receiver, an RIS/IRS size of several times the wavelength is sufficient. Conversely, if the use case requires installation in a propagation channel far from the transmitter/receiver, size of the RIS/IRS of several tens to several hundred times the wavelength is necessary.

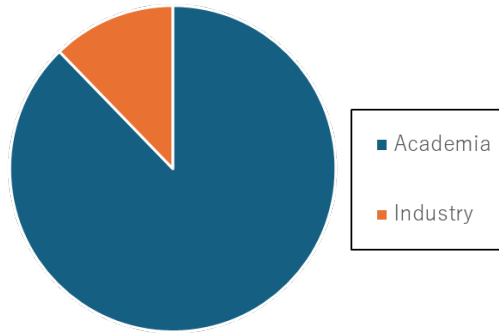


Fig. III.7-3. Ratio of institutions publishing papers on RIS/IRS.

Fig. III.7-3 shows a breakdown of institutions (universities or industries) that have published papers on RIS/IRS based on the survey in section III-7.3. For RIS/IRS, as with metasurface (static), the majority of reports (over 80%) originate from universities. However, there has been a gradual increase in the number of reports from industries over the past few years, and it is expected that this trend will continue as RIS/IRS approaches practical application.

Future Use Case (Reconfigurable Intelligent Surfaces for Beam Manipulation)

Reconfigurable Intelligent Surfaces (RIS) enhance wireless communication by enabling beamforming and beam shaping, significantly improving spectral efficiency, particularly in multi-user MIMO, ultra-massive MIMO, and millimeter-wave (mmWave) networks. RIS plays a crucial role in ultra-massive MIMO by providing a passive, energy-efficient alternative to active beamforming. By reducing reliance on power-intensive RF chains, RIS enables precise phase and amplitude adjustments to dynamically steer, focus, or split beams. This enhances spectral efficiency and extends coverage, particularly in dense urban and indoor environments where high-frequency signals suffer from severe path loss.

A recent study highlighted advancements in RIS-based wireless communication, with a focus on antenna design, prototyping, and experimental validation. This research presents practical implementations and performance evaluations of RIS, confirming its benefits in real-world scenarios. It provides valuable insights into RIS architectures, hardware configurations, and optimization techniques that improve spectral efficiency and network reliability [III.7-1]. Additionally, recent experiments in IMT-2030 testbeds have demonstrated that RIS-assisted beamforming significantly enhances signal strength, mitigates interference, and improves spectral efficiency in mmWave MIMO networks [III.7-2].

Beyond traditional phase-control methods, RIS technology has evolved to support independent amplitude and phase control, offering greater flexibility for adaptive beam manipulation. Unlike conventional RIS designs that primarily adjust phase shifts, this approach simultaneously optimizes wave amplitude, enhancing signal robustness and transmission efficiency [III.7-3]. Experimental validations confirm that RIS with independent amplitude-phase control improves beamforming precision and wavefront engineering.

Despite these advantages, practical implementation challenges remain. The reconfiguration speed of RIS is limited by current hardware technologies, particularly in programmable metasurfaces, where tuning elements such as PIN diodes and varactors are constrained by switching speed and resolution limitations. Additionally, acquiring accurate channel state information (CSI) is essential for optimal beam manipulation.

Further explanations can be found in [III.3-105], [III.3-110], [III.3-117], [III.3-119], [III.3-121], [III.3-124], [III.3-145], [III.3-146], [III.3-149], [III.3-150], [III.3-151], [III.3-153], [III.3-157], and [III.3-168].

REFERENCE

- [III.7-1] L. Dai et al., "Reconfigurable Intelligent Surface-Based Wireless Communications: Antenna Design, Prototyping, and Experimental Results," in *IEEE Access*, vol. 8, pp. 45913-45923, 2020.
- [III.7-2] S. Zeng et al., "RIS-Based IMT-2030 Testbed for MmWave Multi-Stream Ultra-Massive MIMO Communications," in *IEEE Wireless Communications*, vol. 31, no. 3, pp. 375-382, June 2024.
- [III.7-3] J. C. Liang, L. Zhang, Z. W. Cheng, P. Zhang, and T. J. Cui, "Flexible Beam Manipulations by Reconfigurable Intelligent Surface With Independent Control of Amplitude and Phase," *Frontiers in Materials*, vol. 9, p. 946163, 2022.
- [III.7-4] M. Di Renzo, "State of the Art on Stacked Intelligent Metasurfaces: Communication, Sensing and Computing in the Wave Domain," *arXiv preprint arXiv:2411.19687*, 2024.
- [III.7-5] J. Zhao, Y. Liu, and X. Yang, "Stacked Intelligent Metasurface Performs a 2D DFT in the Wave Domain for DOA Estimation," *IEEE Transactions on Antennas and Propagation*, vol. 71, no. 4, pp. 3561-3572, Apr. 2023.
- [III.7-6] S. Tan, X. Wu, and Y. Zhang, "Multi-user ISAC through Stacked Intelligent Metasurfaces: New Algorithms and Experiments," *IEEE Transactions on Signal Processing*, vol. 71, no. 6, pp. 5123-5137, June 2023.

IV. Standardization survey

With the rapid increase in mobile data traffic, fueled by the expansion of smart devices, interactive services, and intelligent applications, carrier frequencies are moving to higher bands [IV-1]. Among these, millimeter-wave (mmWave) frequencies, a component of the New Radio (NR) spectrum used in 5G, span from 24.25 GHz to 52.6 GHz as defined by the Third Generation Partnership Project (3GPP) as Frequency Range 2 (FR2). While mmWave offers quicker data transmission and reduced latency compared to the Sub-7 GHz frequencies (FR1), which range from 0.410 to 7.125 GHz, it faces challenges such as limited coverage due to significant propagation losses and the directness of radio waves [IV-2]- [IV-4]. Despite these limitations, mmWave is essential for managing increasing data volumes, and the mid-range frequencies between Sub-6 and mmWave (FR3) are gaining interest for future 6G technologies. To improve the reliability and reach of mmWave communication, relay systems in distributed environments have become a focal point recently. These systems, which include integrated access backhaul (IAB) [IV-5], reconfigurable intelligent surface (RIS) / intelligent reflecting surface (IRS) [IV-6], and network-controlled repeater (NCR) [IV-7], enhance coverage and deployment flexibility without requiring fiber connections, thus reducing costs as shown in Fig. IV-1. Each system varies in its approach: IAB employs a decode-and-forward mechanism, processing signals at higher layers; RIS/IRS uses a passive approach to reflect signals without amplification; and NCR amplifies and forwards signals using analog beamforming techniques, enhancing direct communication between the base station and devices without decoding the information. These developments in relay technology are crucial for expanding the effective deployment and functionality of mmWave networks.

Fig. IV-1 Concept of relay systems' contribution for the coverage extension.

IV.1. Network Controlled Repeater (NCR)

The discussion of repeaters in 3GPP has been introduced as commercial services from 2G to 4G generations. In the context of 5G NR (New Radio), discussions about repeaters began with Release 17, targeting both FR1 (sub-6 GHz band) and FR2 (millimeter wave band) [IV-8]. Subsequently, in Release 18 (2022), technical standards were formulated in RAN1 about NCR shown in Fig. IV.1-1 [IV-9], with a particular focus on the necessity of the control plane. Key topics included beam steering,

TDD (Time Division Duplex), and power management (ON/OFF). Those functions and basic feature of NCR has been started discussion in Release 19 38.806 [IV-10]. Meanwhile, WAB (Wireless Access and Backhaul) was introduced, including the core network, marking further technological advancements [IV-11] [IV-12].

Fig IV.1-1. Concept of NCR Architecture in 3GPP Release 18.

Based on the above discussions, the key technologies in management of NCR are discussed as follows.

- **Side Control Information (SCI):** This is crucial for configuring and managing NCRs, allowing the network to control the repeater operation more effectively, reducing unwanted noise amplification, and improving signal directivity, especially beneficial in FR2 which includes millimeter-wave frequencies.
- **Beam Management:** Essential for managing the directionality of signals in high-frequency deployments. Beam management helps in configuring transmit and receive paths dynamically based on user equipment mobility and changing channel conditions. This is particularly important for NCRs to adapt to FR2's beamforming requirements.
- **Timing and TDD Control:** Involves managing TDD configurations to align with network demands. Proper TDD control ensures that NCRs correctly manage the timing for downlink and uplink transmissions, maintaining network efficiency and reducing latency.
- **ON-OFF Control:** This functionality allows the network to turn the NCRs on or off as needed, which is crucial for minimizing interference when the repeater's assistance is not required. It also aids in improving the energy efficiency of the network by turning off the repeater when not in use.

These technologies highlight the evolution of repeater functions from simple signal boosting to complex network elements managed and controlled by network signals, enhancing overall network performance and reliability in Beyond 5G and 6G.

IV.2. Integrated Access and Backhaul (IAB)

IAB (Integrated Access Backhaul) is a technology aimed at integrating wireless access and backhaul to enable efficient data communication. This technology is particularly effective in areas where new infrastructure is needed or where there is a desire to reduce communication costs. The basic architecture of IAB is shown in Fig. IV.2-1.

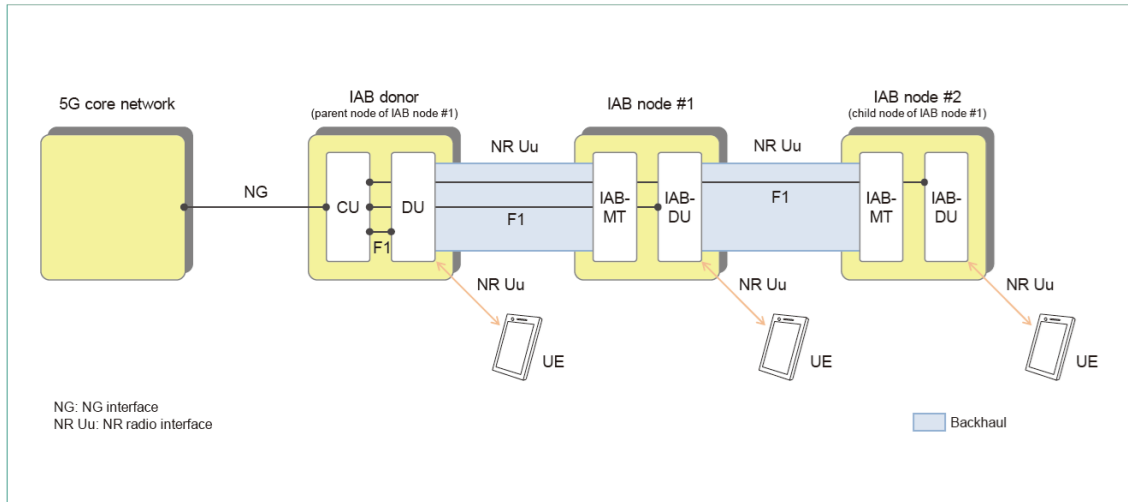


Fig. IV.2-1 Basic IAB architecture [IV-13]

The standardization trends of IAB have been promoted by 3GPP across Releases 16, 17, and 18. In addition, the following descriptions are defined by the 3GPP [IV-14]-[IV-19].

Release 16:

The basic architecture of IAB was introduced, and specifications aimed at the integration of wireless access and backhaul were established. In particular, the importance of end-to-end connectivity from user equipment (UE) to the core network and resource management was emphasized.

Release 17:

The functionality of multi-hop communication was expanded, and new types of IAB nodes were introduced. Additionally, the management of QoS was enhanced, and improvements in automated resource management capabilities were achieved, leading to more efficient communication.

Release 18:

Currently under development, this specification is advancing the integration of AI and automation technologies, with expectations for increased efficiency in network management. Furthermore, improvements in energy efficiency and enhanced security features are key themes, and the adaptation to a variety of new use cases is also anticipated.

In Release 16, IAB aims to optimize data communication between remote radio nodes (RANs) and the core network as an architecture that integrates wireless access and backhaul. Applications are considered particularly for areas where new infrastructure cannot be built or where rapid deployment is required. IAB nodes integrate wireless access and backhaul functions and support various types of wireless interfaces. Nodes are connected via standardized wireless interfaces, enabling efficient data transmission. IAB is especially useful for rapid network deployment in densely populated urban areas and remote regions, allowing for flexible responses to temporary increases in demand, such as in events or construction sites.

In Release 17, the definition of new types of IAB nodes was included, allowing for more flexible connections between different types of IAB nodes. The functionality of multi-hop communication, which allows data to be transmitted through multiple nodes, was also enhanced, thereby expanding the range of communication. Enhancements in architecture, advanced management features, and security requirements are being developed, positioning them as crucial elements in next-generation communication infrastructure. This is expected to enable network deployment suited to a variety of use cases.

IAB is anticipated to provide cost reduction and installation flexibility in network deployment, particularly in urban and remote areas, and it is believed that the concept will continue to evolve in future generations of communication technologies, including 6G and beyond.

IV.3. RIS/IRS

The use of RIS has been discussed in several standards development organizations (SDOs) such as 3GPP, ITU-R, ESTI and IEEE 802.11 Working Group (WG). In particular, ETSI launched a dedicated group to discuss the standardization of RIS [IV-20], and it released several group specifications (GS) [IV-6, IV-21, IV-22]. Activities of these SDOs about RIS are as follows.

Activities in 3GPP

3GPP Rel.-18 workshop was held in June 2021. In this workshop, some companies proposed including RIS as a SI in 3GPP for Rel-18. However, the proposal was not approved for Rel-18 because RIS seemed premature technology [IV-23].

Activities in ETSI

Industry Specification Group (ISG) on Reconfigurable Intelligent Surfaces (RIS) launched in September 2021 [IV-20] to coordinate pre-standardization research efforts into RIS technology across various EU collaborative projects. This group published the following documents.

- ETSI GR RIS 001 V1.1.1 (2023-04) Reconfigurable Intelligent Surfaces (RIS); Use Cases, Deployment Scenarios and Requirements [IV-21]
 - ✧ Updated to ETSI GR RIS 001 V1.2.1 (2025-02)

- ETSI GR RIS 003 V1.1.1 (2023-06) Reconfigurable Intelligent Surfaces (RIS); Communication Models, Channel Models, Channel Estimation and Evaluation Methodology [IV-22]
 - ✧ Updated to ETSI GR RIS 003 V1.2.1 (2025-02)
- ETSI GR RIS 002 V1.1.1 (2023-08) Reconfigurable Intelligent Surfaces (RIS); Technological challenges, architecture and impact on standardization [IV-6]

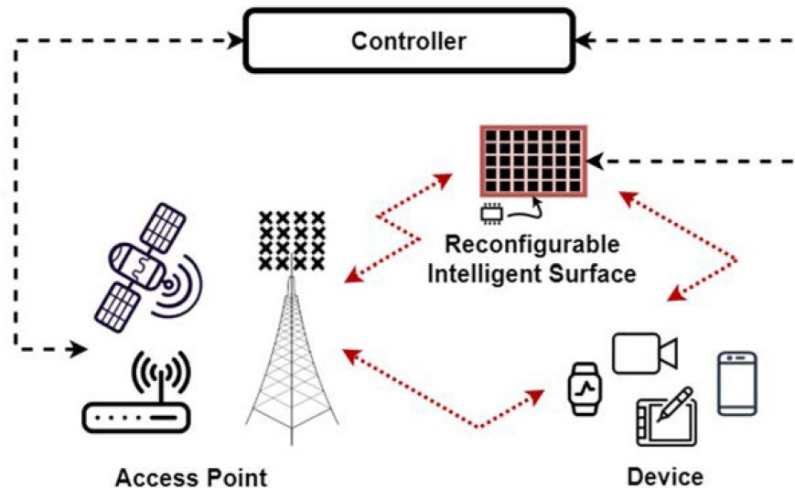


Fig. IV.3-1 Example of deployment scenario of RIS considered in ESTI [IV-6].

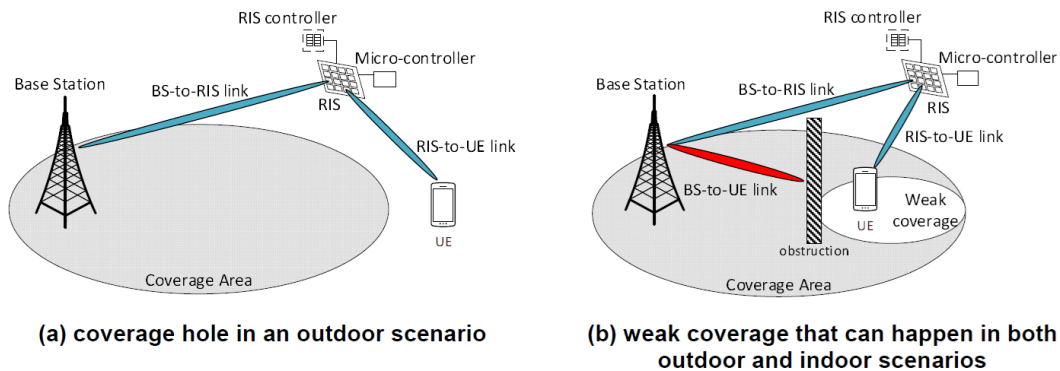


Fig. IV.3-2 Example of scenario of RIS-integrated network for coverage enhancement [IV-6].

ETSI GR RIS 001 gives a definition of RIS and categorizes its use cases into 8 factors (coverage enhancement, spectral efficiency, beam management, physical layer security, localization accuracy, sensing capabilities, energy efficiency, and link management). ETSI GR RIS 001 also shows several key deployment scenarios of RIS and its requirements.

ETSI GR RIS 002 summarizes deployment scenarios of RIS from several viewpoints such as controlling type, capability aspect, complexity aspect, and regulation aspects. ETSI GR RIS 002 also describes technological aspects of RIS entity, architecture of RIS-integrated network, and radio and

physical layer aspect of RIS-integrated network. Figs. IV.3-1 and IV.3-2 show examples of deployment scenarios of RIS and RIS-integrated network [IV-6].

ETSI GR RIS 003 describes RIS models, mathematical channel models, channel estimation, key performance indicators and evaluation methodology. to specify derived requirements and to identify technology challenge [IV-22].

Activities in ITU-R

ITU-R published Report ITU-R M.2516-0 (11/2022) “Future technology trends of terrestrial International Mobile Telecommunications systems towards 2030 and beyond.” In Section 6.4.1 of this Report, RIS is introduced as one of technologies to enhance radio interface of IMT systems.

ITU-R also published Recommendation ITU-R M.2160-0 (11/2023) “Framework and overall objectives of the future development of IMT for 2030 and beyond.” In this Recommendation, RIS is introduced as one of the potential technologies that would improve performance and overcome challenges in traditional beam-space antenna array beamforming. In addition, it is described that further study on RIS is needed to overcome major challenges of operating in bands above 92 GHz such as limited transmission power, the obstructed propagation environment due to high propagation losses and blockage.

Activities in IEEE 802.11 WG

Several presentations about the use of RIS in IEEE 802.11 wireless LAN were made in Wireless Next Generation Standing Committee (WNG SC), in which new topics to be standardized are discussed. However, further discussion to form a specific group to discuss the use of RIS has not been made because “what should be determine in the IEEE 802.11 standard to utilizes RIS” is not clarified.

- Salah Eddine Zegrar, Liza Afeef Omar Shehab El Din, Hüseyin Arslan, and Başak Özbakış, “EHT via Reconfigurable Surfaces,” doc.: IEEE 802.11-20/1720r1 (2020-11).
- Ryutaro Ohmoto and Hiroki Hagiwara, “Proposal on intelligent radio path control technique to improve SNR and resolve the radio shadow zone in millimeter wave band system,” doc.: IEEE 802.11-24/1554r1 (2024-11).

For future standardization of wireless communication networks incorporating RIS/IRS:

For developing specifications of specific wireless communication networks incorporating RIS/IRS, several topics will be discussed in detail. Possible discussion topics are as follows.

- Use cases of RIS/IRS: Does RIS/IRS need to change its beam direction according to the position or movement of UE(s). (Is tracking of UE(s) necessary?)
- Configurations of RIS/IRS: Do we need to specify the number, size and arrangement of RIS/IRS elements?
- How to indicate the beam shape: Do we indicate the weight of each RIS/IRS element or codebook index of RIS weights?

IV.4. Summary

The current statuses of standardization on NCR, IAB, and RIS/IRS in several points are summarized in Table IV.4-1. There are several points to be studied further for these technologies in terms of standardization in the future [IV-24].

Table IV.4-1. Summary of standardization status on NCR, IAB, and RIS/IRS.

	NCR	IAB	RIS/IRS
Use Case / Deployment Scenario	Discussed [IV-7] [IV-9]	Supported [IV-14]	Discussed [IV-6, IV-21]
Channel Model	Discussed [IV-25]	Discussed [IV-25]	Discussed [IV-11]
Control/Signaling	Discussed [IV-7] [IV-9]	Supported [IV-16]	Discussed [IV-6]
Interference Management	Not Yet	Not yet	Not yet

REFERENCE

- [IV-1] W. Jiang, B. Han, M. A. Habibi, and H. D. Schotten, "The road towards 6g: A comprehensive survey," IEEE Open Journal of the Communications Society, vol. 2, pp. 334–366, 2021.
- [IV-2] 3GPP TS 38.101-2 V18.7.0, "NR; User Equipment (UE) radio transmission and reception; Part 2: Range 2 Standalone," September 2024
- [IV-3] 3GPP TS 38.101-1 V18.7.0, "NR; User Equipment (UE) radio transmission and reception; Part 1: Range 1 Standalone," October 2024.
- [IV-4] D. Shakya, M. Ying, T. S. Rappaport, H. Poddar, P. Ma, Y. Wang, and I. Al-Wazani, "Comprehensive fr1(c) and fr3 lower and upper mid-band propagation and material penetration loss measurements and channel models in indoor environment for 5g and 6G," IEEE Open Journal of the Communications Society, vol. 5, pp. 5192–5218, 2024.
- [IV-5] 3GPP TR 38.874 V16.0.0, "NR; study on integrated access and backhaul," January 2019.
- [IV-6] ETSI GR RIS 002 V1.1.1, "Reconfigurable Intelligent Surfaces (RIS); technological challenges, architecture and impact on standardization," August 2023.
- [IV-7] 3GPP TR 38.867 V18.0.0, "Study on NR network-controlled repeaters," September 2022.
- [IV-8] 3GPP TR38.830 V17.0.0, "Study on NR coverage enhancements," Dec. 2020.
- [IV-9] 3GPP TR 38.867 V1.0.0, "Study on NR Network-Controlled Repeater," September 2022.
- [IV-10] 3GPP, "NR Repeater Radio Transmission and Reception," 3rd Generation Partnership Project (3GPP), TS 38.806, Mar. 2025, v. 19.0.0.
- [IV-11] Qualcomm Incorporated, Xiaomi, "Rel-19 Views on Additional Topology Enhancements," 3GPP TSG RAN Meeting #102 RP-233021, Dec. 2023. [Online]. Available: https://www.3gpp.org/ftp/tsg_ran/TSG_RAN/TSGR_102/Docs
- [IV-12] 3GPP, "Work Item Description: Study on additional topological enhancements for NR," 3GPP TSG RAN Meeting #104 RP-241264, Jun. 2024. [Online]. Available: <https://portal.3gpp.org/desktopmodules/WorkItem/WorkItemDetails.aspx?workitemId=1020082>

- [IV-13] Y. Matsumura, S. Kumagai, T. Min, and K. Harada, "5G Advanced Technologies for Mobile Broadband," NTT Docomo Technology Journal, vol. 22, no. 3, Jan. 2021.
- [IV-14] 3GPP TS 38.300, "NR; NR and NG-RAN Overall description: Stage 2," Dec. 2024.
- [IV-15] 3GPP TS 38.401, "NG-RAN; Architecture description," Dec. 2024.
- [IV-16] 3GPP TS 38.174, "NR; Integrated Access and Backhaul (IAB) radio transmission and reception," Dec. 2024.
- [IV-17] 3GPP TR 38.809, "NR; Background for integrated access and backhaul radio transmission and reception (Rel-16)," March 2022.
- [IV-18] 3GPP TR 38.874, "NR; Study on integrated access and backhaul FS_NR_IAB (Rel-16)," Dec. 2018.
- [IV-19] 3GPP TR 22.839, "Study on vehicle-mounted relays; stage 1 (release 18)," Dec. 2021.
- [IV-20] Industry Specification Group (ISG) on Reconfigurable Intelligent Surfaces (RIS), <https://www.etsi.org/committee/1966-ris> (accessed on February 25, 2025).
- [IV-21] ETSI GR RIS 001, "Reconfigurable Intelligent Surfaces (RIS); Use Cases, Deployment Scenarios and Requirements," V1.1.1, April 2023.
- [IV-22] ETSI GR RIS 003, "Reconfigurable Intelligent Surfaces (RIS); Communication Models, Channel Models, Channel Estimation and Evaluation Methodology," V1.1.1, June 2023.
- [IV-23] Chao-Kai Wen, Lung-Sheng Tsai, Arman Shojaeifard, Pei-Kai Liao, Kai-Kit Wong, and Chan-Byoung Chae, "Shaping a Smarter Electromagnetic Landscape: IAB, NCR, and RIS in 5G Standard and Future 6G," IEEE Communications Standards Magazine, vol. 8, issue 1, pp. 72-78, March 2024. DOI:10.1109/MCOMSTD.0008.2300036
- [IV-24] 3GPP, "Study on channel model for frequencies from 0.5 to 100 GHz," 3rd Generation Partnership Project (3GPP), TR 38.901, Mar. 2022, v.17.1.0. [Online]. Available: <http://www.3gpp.org/DynaReport/38901.htm> (visited on 03/31/2022).
- [IV-25] 3GPP, "Study on channel model for frequencies from 0.5 to 100 GHz," 3rd Generation Partnership Project (3GPP), TR 38.901, Mar. 2022, v.17.0.0. [Online]. Available: <http://www.3gpp.org/DynaReport/38901.htm> (visited on 09/26/2017).

V. Recent activities in Japan

This chapter introduces individual R&D activities related to repeater, metasurface and RIS/IRS in Japan. The chapter is divided into two big sections i.e. Section V.1 and Section V.2 respectively presenting R&D activities related to repeater, followed by metasurface and RIS/IRS. In Section V.1, there are two big groups of technologies i.e. Group A discussing technologies related to AF relay (NCR) and Group B discussing other relay technologies. Similarly, Section V.2 is furthermore categorized into two big groups of technologies i.e. Group C discussing technologies related to metasurface (static) and Group D discussing technologies related to RIS/IRS.

GROUP A – AF Relay (NCR)

Group A presents contributions from Science Tokyo for the development of massive analogy relay technologies at mmWave band and a field evaluation system at the campus. DKK introduces the developed phased array antenna technology for 6G analog repeater system. KDDI Research presents the latest research results on low latency relay technology to extend millimeter wave area.

GROUP B – Other Relay Technologies

Panasonic System Networks R&D Lab. presents the wireless transport technology for Xhaul.

GROUP C – Metasurface (Static)

Group C presents the analysis of using transmissive metasurfaces at mmWave band (DOCOMO, NTT), the development of optically transparent dual-band meta-surface reflector (KDDI Research), metasurface technologies for controlling radio waves in specific directions (Kyocera), a social implementation technology for passive reflector that support the Sub6 band and above (DNP), and the development of a transparent & flexible metasurface reflector film (SEKISUI CHEMICAL).

GROUP D – RIS/IRS (Programmable)

Group D presents an efficient beam searching in hybrid intelligent reflecting/refracting surfaces aided mmWave 6G network (Tohoku Univ., Kyocera), relay-related technologies in new radio network topology (NTT, DOCOMO), beamforming-based IRS control method for sub-THz communications in indoor office environments (Hokkaido Univ.), a beam squint-aware frequency resource allocation method for IRS-aided communication (Tohoku Univ., NTT), prototype and evaluation of IRS for 60 GHz band (PSNRD, Tohoku Univ.), experimental evaluation of impact of IRS at 60 GHz band against radio channel at Sub-6 GHz band (ATR, Tohoku Univ.), performance evaluation of RIS-empowered 6G system (DOCOMO), development and field trial of liquid crystal RIS (KDDI), multishape radio and its experimental studies using OAM, Airy, and Bessel beams in Sub-THz Bands (NTT).

V.1. Repeater

GROUP A -- AF relay (NCR)

- V.1.1 Field evaluation of mmWave relays in various topologies (Science Tokyo)
- V.1.2 mmWave massive analogy relay MIMO (Science Tokyo)
- V.1.3 mmWave massive analogy relay MU-MIMO with resource and user scheduling (Science Tokyo)
- V.1.4 Phased array antenna technology for 6G analog repeater system (DKK)
- V.1.5 Research on low latency relay technology to extend millimeter wave area (KDDI Research)

V.1.1. Field evaluation of mmWave relays in various topologies

Naoya Okubo, Kei Sakaguchi, Gia Khanh Tran
Institute of Science Tokyo

Abstract — In the early stage of consideration of millimeter-wave (mmWave) introduction into 5G, it was envisioned as a localized deployment in hotspots using small cells, rather than a broad area deployment. As of 2024, the deployment of mmWave 5G in the United States is indeed focused on hotspots such as stadiums, and it has been successful as a premium plan for business. However, in Japan, the broad deployment of 5G is mandatory and a unique business model for mmWave 5G has not been established. Against this background, analog repeaters have recently gained attention as a low-cost solution for mmWave coverage expansion. In this paper, we present a mmWave repeater-based coverage extension experiments conducted at Ookayama Campus of Institute of Science Tokyo (Science Tokyo)¹.

1. Introduction

In the early stage of consideration of millimeter-wave (mmWave) introduction into 5G, it was envisioned as a localized deployment in hotspots using small cells, rather than a broad area deployment [V.1.1-1]. As of 2024, the deployment of mmWave 5G in the United States is indeed focused on hotspots such as stadiums, and it has been successful as a premium plan for business. However, in Japan, the broad deployment of 5G, including mmWave, is mandatory and a unique business model for mmWave 5G has not been established. Therefore, the key to business is how to expand the coverage of mmWave 5G at low cost. In line with this trend. Against this background, analog repeaters, which have beamforming capabilities in addition to amplification functions, have recently attracted attention as a low-cost effective solution for mmWave coverage expansion. In this paper, we present the coverage extension experiment using mmWave 5G repeaters conducted at Ookayama Campus of Institute of Science Tokyo (Science Tokyo) [V.1.1-2].

2. 5G environment at the Ookayama Campus of Science Tokyo

In this section, we introduce a private 5G testbed at the Ookayama Campus of Science Tokyo. This testbed is built in an NSA (Non-Stand Alone) configuration, where multiple Sub6/mmWave base stations (BSs) are deployed within the coverage area of the LTE base station serving as the anchor link [V.1.1-3]. Authorized user equipment (UE) can connect to this environment, and in this experiment, a mmWave-compatible smartphone was used [V.1.1-4]. As for the repeater used in the experiments, it consists of two units: the Donor Unit (DU) and the Service Unit (SU) [V.1.1-5]. The DU

¹ Tokyo Institute of Technology (Tokyo Tech) changed its name to Institute of Science Tokyo (Science Tokyo) in October 2024.

communicates with the BS while the SU communicates with the user equipment (UE). The DU and the SU are connected via a fiber optic cable.

Table V.1.1-1 Device Specifications.

Base station		Repeater		Smartphone	
Operating Frequency	n257 (27.0-27.4 GHz)	Operating Frequency	27.0 – 27.4 GHz	OS	Android 10
Carrier Aggregation	4 CC × 100 MHz	Max. EIRP	41 dBm	Chipset	Snapdrag on 765G 5G
Max. EIRP	51 dBm /400 MHz	MIMO support	2x2 MIMO	Supported Modulation Schemes	QPSK, 16QAM, 64QAM
SCS	120 kHz	System Gain	≤ 105 dB	MIMO support (DL)	2x2 MIMO

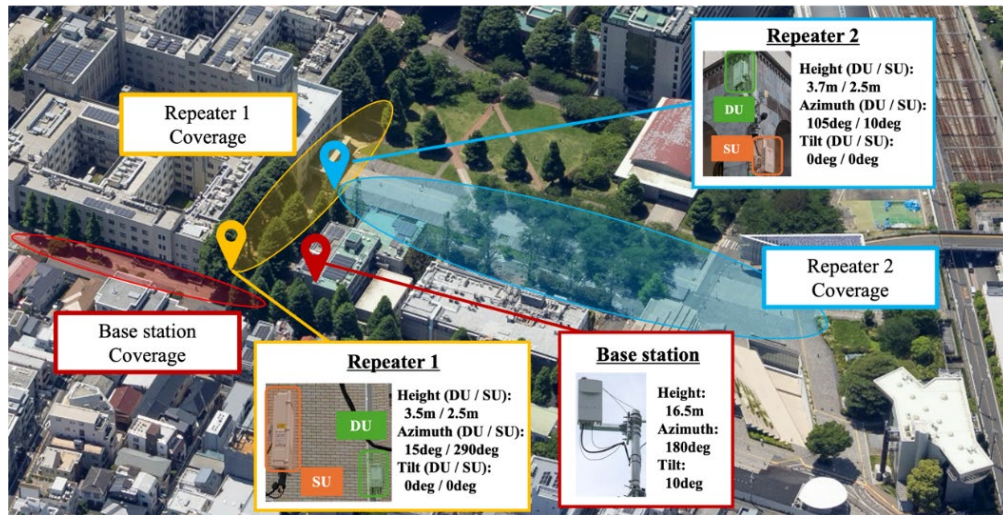


Fig. V.1.1-1 Network Deployment of 5G mmWave Base Station and Repeater at Ookayama Campus of Science Tokyo.

Fig. V.1.1-1 shows the locations of the mmWave BS and repeaters used in the experiment as colored-pins, and the coverage of them as colored-circles. For the repeater 1, the DU connect to the BS while the SU provides coverage for the yellow-colored area. Additionally, for Repeater 2, the DU connects to the SU of Repeater 1 and the SU provides coverage for the blue-colored area. In this way, we introduced a multi-hop architecture to wirelessly relay signals between Repeater 1 and Repeater 2. The summary of specifications and system configuration diagram of the BS, repeater, and smartphone used in this experiment are shown in Table V.1.1-1 and Fig. V.1.1-2, respectively.

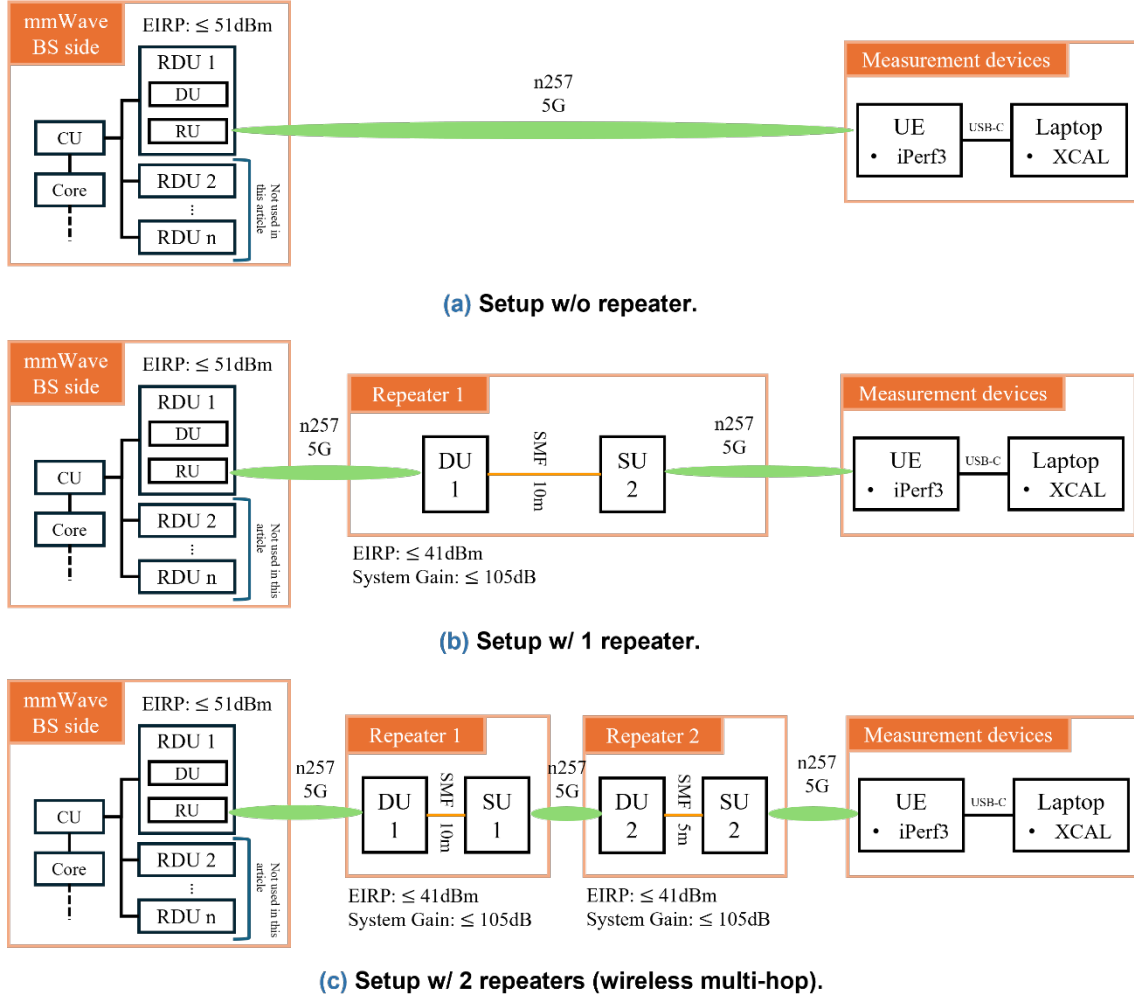


Fig. V.1.1-2 System Configuration Diagram for Experiments.

3. Experiments & Results

Fig. V.1.1-3 shows the experimental results of coverage extension using mmWave repeaters. As shown in Fig. V.1.1-3 (a), in the east-west orientation, there was almost no coverage without repeaters due to the straight-line propagation of mmWave. However, as shown in (b), by introducing one repeater (Repeater 1) and directing the SU to the west, a stable throughput of over 1 Gbps in downlink was achieved, with a peak throughput of approximately 1.8 Gbps. On the other hand, coverage did not extend to the north due to the blocking effects of buildings and trees and the beam width of the device.

Here, the advantage of introducing multiple repeaters come into play. As shown in Fig. V.1.1-3 (c), by introducing a second repeater, an area achieving a downlink throughput of about 1 Gbps was newly formed extending nearly 100 meters to the north. Although the wireless multi-hop with analog repeaters amplifies not only the desired signal but also noise, i.e., degrading the SINR (Signal to Interference plus Noise Ratio), a high throughput of about 1 Gbps was still achieved. From these

results, it can be said that the effectiveness of deploying multiple mmWave analog repeaters in a wireless multi-hop configuration is demonstrated.

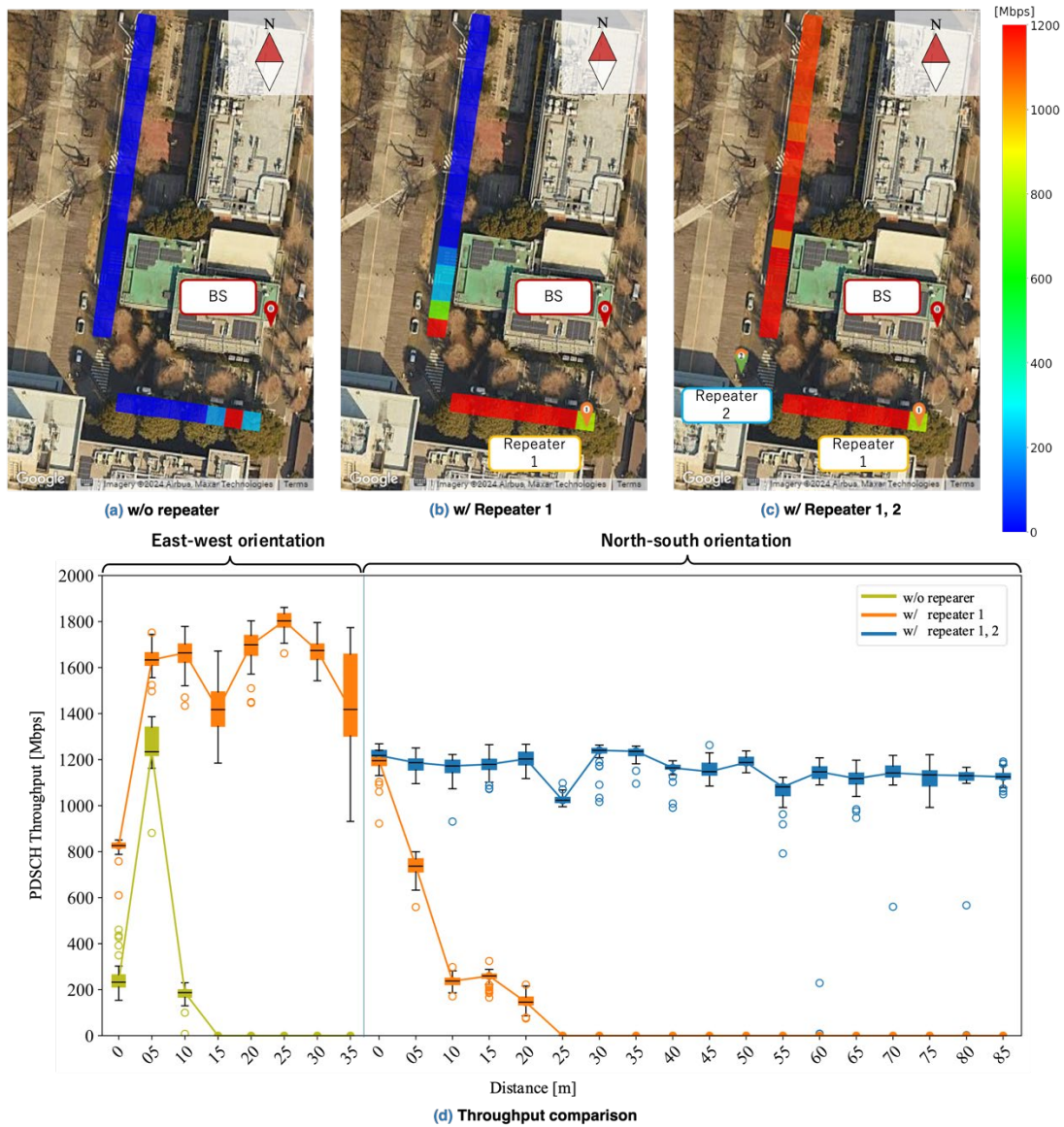


Fig. V.1.1-3 Measurement Results of Physical Layer Throughput (PDSCH Throughput) in Downlink. (The heatmap shows the median of 1-minute measurements taken every 5 meters.)

4. Conclusion

In this paper, we presented a 5G mmWave repeater-based coverage extension experiments conducted at the Ookayama Campus of Science Tokyo. It has been demonstrated that repeaters enable to effectively provide high-speed communications exceeding 1 Gbps in downlink, even in locations that were previously NLOS. As shown in this paper, repeater is a useful tool for significantly expanding mmWave coverage as long as power and deployment locations can be secured, and they are expected to become a key technology for low-cost mmWave area expansion.

REFERENCE

[V.1.1-1] K. Sakaguchi et al., “Millimeter-Wave Evolution for 5G Cellular Networks,” *IEICE Trans. Commun.*, vol. E98-B, no. 3, pp. 388-402, Mar. 2015.

[V.1.1-2] N. Okubo, K. Tokugawa, J. Nakazato, S. Ke, Y. Chen, G. K. Tran, K. Sakaguchi, M. Kuchitsu, T. Itagaki, “Field Evaluation of 5G mmWave Relays in Various Topologies: NLOS Coverage Enhancement and Tolerance against Blockage,” *IEEE Access*. **[Under Review]**

[V.1.1-3] J. Nakazato, Z. Li, K. Maruta, K. Kubota, T. Yu, G. K. Tran, K. Sakaguchi, S. Masuko, “MEC/Cloud Orchestrator to Facilitate Private/Local Beyond 5G with MEC and Proof-of-Concept Implementation,” *Sensors*, 2022.

[V.1.1-4] Rakuten Mobile, “Rakuten Mobile Releases New Original 5G Smartphone: Rakuten BIG s.” [Online]. Available: https://corp.mobile.rakuten.co.jp/english/news/press/2021/0419_02/

[V.1.1-5] FRTek, “PrimAer.” [Online]. Available: https://www.frtex.com/jp/board/board.php?bo_table=wireless&cate=RF&idx=102

V.1.2. mmWave massive analog relay MIMO

Kei Sakaguchi

Institute of Science Tokyo

Takumi Yoneda, Masashi Iwabuchi, Tomoki Murakami

NTT Access Network Service Systems Laboratories

Abstract—In this paper, we consider the use of massive analog Relay Stations/Repeaters (RSs) to relay the transmission signals. By relaying the signals with a large number of RSs, an artificial Multiple-Input Multiple-Output (MIMO) propagation environment can be formed, which enables mmWave MIMO communications to the NLOS environment. We describe a theoretical study of a massive relay MIMO system and extend it to include multi-hop relays. Simulations are conducted, and the numerical results show that the proposed system achieves high data rates even in a grid-like urban environment.

1. Introduction

In mmWave bands, due to the propagation loss, the influence of reflected paths and diffracted paths is small and the direct path is dominant. As a result, the number of streams tends to be small in Single-User (SU) Multiple-Input Multiple-Output (MIMO) [V.1.2-1]. We focus on distributed Amplifier-and-Forward (AF) relays to solve the above-mentioned issues. Since the AF method only amplifies signals, delay is almost negligible. Moreover, its cost, size, and power consumption of nodes are relatively small, so that it is suitable to install a large number of AF nodes.

There have been several studies on AF relay methods for mmWave communications. The performance of mmWave communications with a full-duplex AF relay was investigated in [V.1.2-2] by considering the effect of beam width and self-interference. In [V.1.2-3], the basic characteristics of mmWave MIMO communications with multiple AF relays were evaluated under a fixed topology, and it shows potential of the method. When applying the AF relay to mmWave mobile communications, adaptive beam-forming is required to improve communication quality. The conventional AF relay only performs amplification and frequency conversion but adaptive beam-forming has not been considered. Moreover, relay-node selection from massive relay nodes is also important in the case of mobile communications.

In this paper, we propose an mmWave massive analog relay MIMO system for mobile communications by extending the authors' previous work in [V.1.2-4]. A large number of dynamically controllable AF Relay Stations (RSs) are deployed to relay signals for NLOS User Equipment (UE). Adaptive beam-forming in each RS is assumed. A dynamic RS selection algorithm based on UE location is introduced to generate an artificial multipath channel to improve capacity of mmWave MIMO communications. The RSs should have a function of adaptive beam switching for dynamic RS selection and a function of beam tracking to follow the UE's mobility. We start from the formulation in single-hop relay, and then extend it to multi-hop relays to improve mmWave capacity. The full search of optimized route for multi-hop relays requires a huge computational cost for beam selection

due to the massive number of RSs. Hence, a fast-routing algorithm is introduced in this paper to maximize channel capacity. Numerical evaluations are conducted to verify the effectiveness of the proposed massive analog relay MIMO system.

2. mmWave Massive Analog Relay MIMO

2.1 System Model

Fig. V.1.2-1 shows the system architecture consisting of one source (BS), one destination (UE), and a massive number of RSs. Because of the compact size, low cost, and low power consumption of analog RSs, it is feasible to massively and non-invasively deploy them in the target environments to enhance or enable mmWave communications.

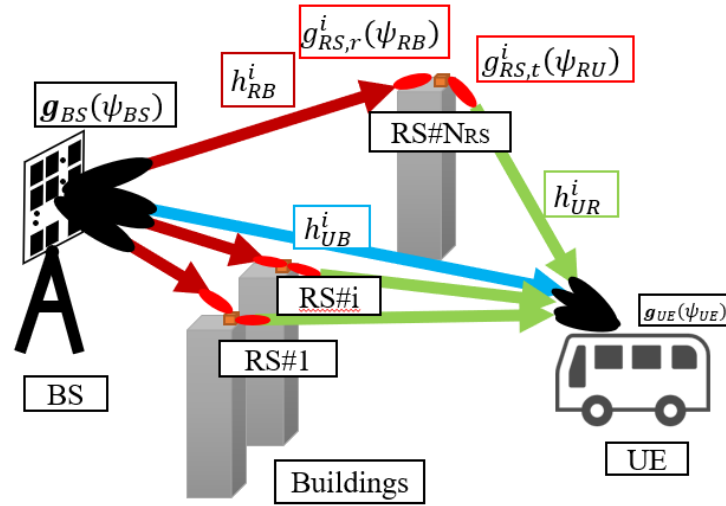


Fig.V.1.2-1 System model for mmWave massive relay MIMO

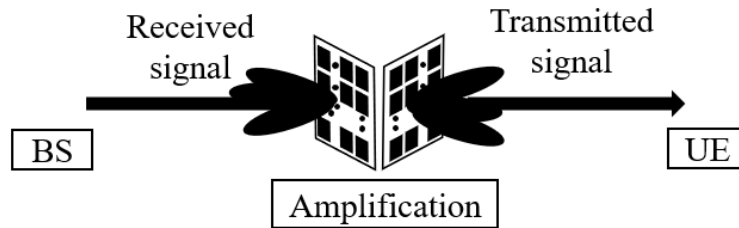


Fig. V.1.2-2 mmWave analog relay with beamforming

Fig. V.1.2-2 illustrates the architecture of an analog RS. An analog RS node has two sides, of which one is the receiving side and the other is the transmitting side. As shown in the figure, both sides are assumed to be able to perform high-performance dynamic beam control. The analog RS is supposed to be an AF RS that can amplify the received signal and transmit it without latency.

3. Expansion to Multi-Hop

3.1 System Model

In this section, as shown in Fig. V.1.2-3, the proposed system is extended from a single-hop to multi-hop relay system, in which the artificial MIMO channels are actively generated by multi-hop AF RSs, to further cover the area where the mmWave communications are not possible even if the signals have been relayed for single hop.

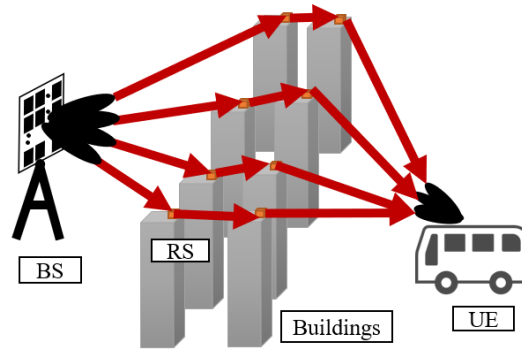


Fig. V.1.2-3 System model for mmWave massive multi-hop relay MIMO

3.2 Beam Selection Algorithm Based on Routing

In order to maximize channel capacity, the optimized routes and corresponding beams of RSs need to be derived through full-search, which traverses all the combinations of the beam selections in the BS and RSs. However, the full-search algorithm inevitably results in an enormous and unaffordable computational cost. Since the position of the UE could change time by time, the routes and beams need to be recalculated instantaneously according to the new UE position to guarantee the mmWave communication. Therefore, it is neither practical nor feasible to use the full-search method for fast moving UEs such as vehicles.

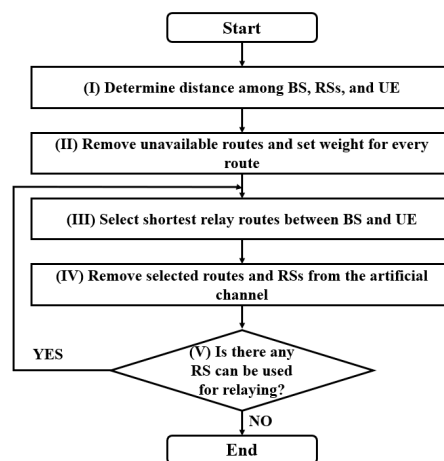


Fig. V.1.2-4 Routing algorithm

To complete the selection of beams in real time, we propose an algorithm to determine relay routes and corresponding beams of RSs sequentially by finding the shortest paths. Fig. V.1.2-4 shows the

proposed routing algorithm for the massive multi-hop relay MIMO system. It is assumed that the BS knows all RS locations in advance and can obtain UE location in real time. The BS finds routes based on the proposed algorithm and specifies the relay beam indices. It is assumed that an RS is used only for a single route since the signal multiplexing capability is not considered for RSs in this paper. Blockage between RSs and the UE by moving objects, such as vehicle, is ignored.

4. Numerical Analysis

4.1 Simulation Model

System performances in two layouts are evaluated: In 1-D model, RSs are arranged linearly at equal intervals (30 m), and totally 64 RSs are deployed as shown in Fig. V.1.2-5 (a). In 2-D model, RSs are deployed at four corners on tops of buildings, and totally 64 RSs are deployed in 16 buildings in a gridded layout. 12 of the 16 buildings are 20m height, which are marked as blue buildings in Fig. V.1.2-5 (b), and the rest are 30 m height. The UE, which is assumed to be a vehicle, moves among buildings. The heights of the BS and UE are 35 m and 3 m, respectively.

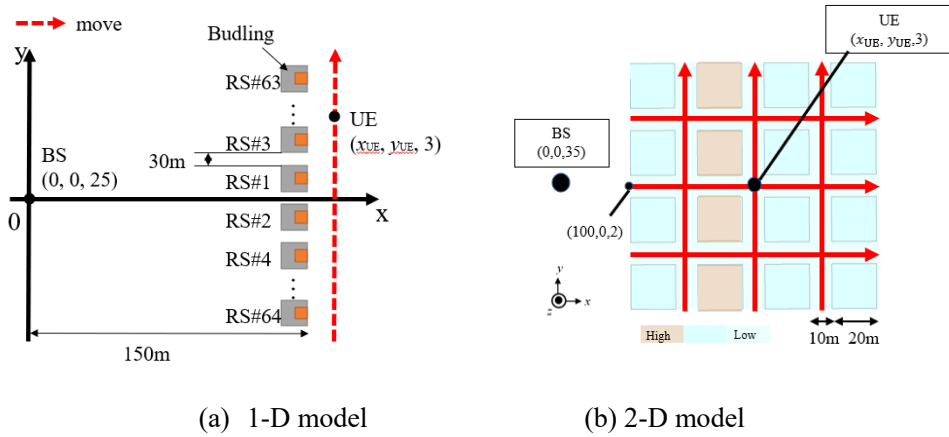


Fig. V.1.2-5 Simulation model

4.2 Simulation Result

For the 1-D model, Fig. V.1.2-6 (a) shows channel capacity plotted every 15 m when the UE moves. In the conventional method (w/o RS), in most UE positions, mmWave communications are not possible due to the blockage effects of buildings. However, in the proposed method, channel capacities of about 5Gbps or more is obtained regardless of UE position. At positions where channel capacity was able to be obtained by LOS path, i.e., $y_{UE} = -30, 0, 30$ m, further increase on channel capacity can be obtained. Fig. V.1.2-6 (b) shows dependency of channel capacity on the available number of RSs. To evaluate capacities with a different number of RSs, RSs are turned on in order from #1 to #64 as shown in Fig. V.1.2-5 (a). Evaluations are done at three different UE positions $y_{UE} = 0, 150, 360$ m. As the number of RSs is increased, channel capacity increases, whereas when a certain number of RSs are used, there is no more significant improvement of channel capacity. From different UE positions,

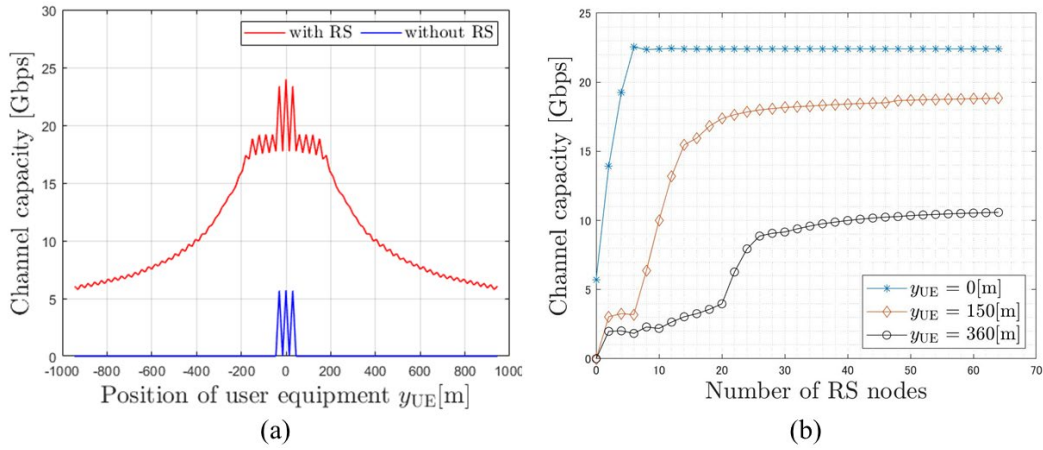


Fig. V.1.2-6 Simulation result of 1-D model

it can be understood that significant improvements of channel capacity are contributed by RSs closer to the UE. It indicates the effectiveness of dynamic RS selection to improve channel capacity, and remaining RSs can be turned off to save power consumption.

For the 2-D model, system performance of multi-hop massive relay MIMO for mmWave communications is evaluated in the grid environment. Fig. V.1.2-7 shows the Cumulative Distribution Function (CDF) of channel capacities for cases of multi-hop, single-hop, and w/o hop. Channel capacity is calculated every 5 m in a gridded arrangement shown in Fig. V.1.2-5 (b). Results show that without RSs, channel capacity is 0Gbps, namely mmWave communications are not available in around 80% of the area in the environment. On the other hand, by hopping with RSs, channel capacity is greatly improved and 100% coverage is available. Compared with the single-hop case, the multi-hop case can further improve channel capacity of about 12 Gbps with about 10% cumulative probability.

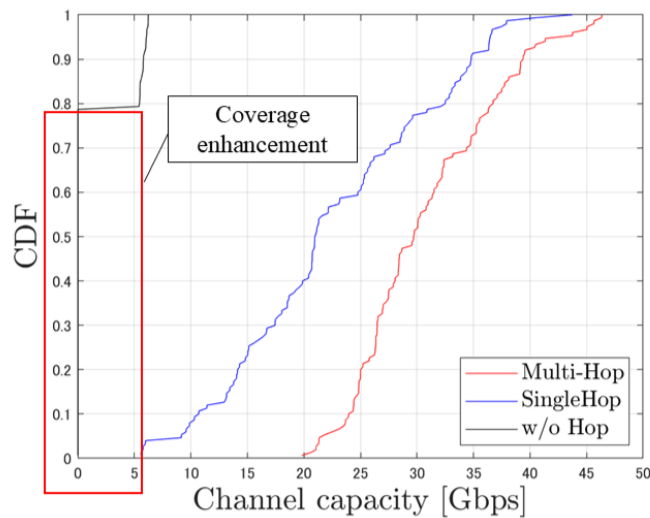


Fig. V.1.2-7 Simulation result of 2-D model

More importantly, the steepness of the curve of the multi-hop case also indicates that it does not only improve channel capacity but also provides stable mmWave communications regardless of locations.

5. Conclusion

In this paper, we proposed a massive analog relay MIMO system for mmWave communications to generate an artificial multipath environment for the UE by using a massive number of RSs. In the proposed system, the mmWave MIMO transmission is enabled, and the channel capacity is greatly improved. Besides, it also makes the mmWave communications in the NLOS environment possible. A practical and feasible routing algorithm for deriving multi-hop routes using massive RSs was also proposed. Moreover, a comprehensive system performance analysis was conducted for verification. The results confirm that the proposed multi-hop system can dramatically improve system performance, further improve channel capacity compared to the single-hop and w/o hop systems, and provide high capacity mmWave communications everywhere in the simulation environment.

REFERENCE

- [V.1.2-1] S. Sun, T. S. Rappaport, R. W. Heath, A. Nix, and S. Rangan, "MIMO for millimeter-wave wireless communications: beamforming, spatial multiplexing, both?", *IEEE Commun. Mag.*, vol. 52, issue 12, Dec. 2014.
- [V.1.2-2] G. Yang and M. Xiao, "Performance Analysis of Millimeter-Wave Relaying: Impacts of Beamwidth and Self-Interference", *IEEE Trans. Commun.*, vol. 66, issue 2, Feb. 2018.
- [V.1.2-3] H. Abbas and K. Hamdi, "Millimeter Wave Communications over Relay Networks", *IEEE WCNC*, Apr. 2018.
- [V.1.2-4] Y. Sugihara and K. Sakaguchi, "mmWave massive analog relay MIMO for improvement of channel capacity", *IEEE WCNCW*, Apr. 2020.

V.1.3. mmWave massive analog relay MU-MIMO with resource and user scheduling

Suwen Ke, Gia Khanh Tran, Zongdian Li, Kei Sakaguchi

Institute of Science Tokyo

Abstract —The utilization of millimeter wave (mmWave) in 5G represents a milestone in cellular networks by greatly enhancing communication capacity. However, the limited coverage and susceptibility to blockage of current mmWave services pose challenges. To solve this dilemma, in 6G, relay technologies, such as analog repeaters and reconfigurable intelligent surfaces (RIS), need to be effectively used to enhance the coverage and capacity of existing mmWave stations. In this paper, we introduce a mmWave massive relay system, consisting of massive analog relay stations to construct artificial channels for mobile users. To enhance the performance of mmWave multi-user multiple-input and multiple-output (MU-MIMO), we propose a user scheduling method that actively exploits the blocking environment to reduce interference and optimize the system capacity. Numerical analysis and simulations are conducted to validate the proposed system and methods.

1. Introduction

Towards the vision of beyond 5G and 6G-enabled super smart society, there is an increasing demand for new technologies that require communication systems with higher data rate and larger capacity performance, such as vehicle to everything (V2X) and extended reality (XR) [V.1.3-1]. To empower that, the utilization of millimeter wave (mmWave) and massive multiple-input and multiple-output (massive MIMO) has become a recent trend for high-capacity communications. However, there are still some pressing issues to be addressed such as mmWave's limited coverage. Moreover, the severe path loss leads to the sparsity of reflected waves that can reach the user. Therefore, it is difficult to leverage multi-path gains in mmWave massive MIMO [V.1.3-2].

To address those problems, deploying relay nodes was proposed and recognized as an efficient method to extend mmWave coverage [V.1.3-3]. The reconfigurable intelligent surface (RIS), also known as the intelligent reflecting surface (IRS), is one example of relay nodes. It can efficiently reflect and control signal transmission angles at a low energy cost [V.1.3-4]. However, its communication range remains limited [V.1.3-5]. As another example, RF repeaters have been used in past-generation communication systems. They are capable of amplifying and forwarding received signals, but limited in accurate beamforming.

Recently, the concept of network controlled repeater (NCR) has been discussed in the third generation partnership project (3GPP) Rel-18 [V.1.3-6]. The NCR represents a type of relay station that can amplify and forward signals with side control information, such as beamforming information. By unseizing NCR, a mmWave analog relay MIMO system was initially introduced to extend coverage and enhance spatial multiplexing gains artificially through a large number of relay stations with multi-hop configurations [V.1.3-7]. However, these studies primarily focused on single-user scenarios. Building on this, in this paper, we proposed a multi-user mmWave analog relay MIMO

system with a user scheduling method that takes advantage of the blocking environment to further improve the system capacity and ensure the fairness of each user's capacity performance.

2. System Model

2.2 Analog Relay Station

We propose to use amplify-and-forward (AF) relay with beamforming capabilities, which can directly forward the amplified signal, in this system. Unlike the decode-and-forward (DF) relay, although the AF relay amplifies noise along with the signal, it reduces latency [V.1.3-8]. Furthermore, similar to RIS, the analog relay station can perform beam steering for both the BS and UE sides [V.1.3-9], enhancing the BS's coverage and constructing an artificial channel for the MIMO system through amplification.

2.2 mmWave Multi-user Massive Relay MIMO with User Scheduling

Fig. V.1.3-1 shows the system model for the MU-MIMO communication system with user scheduling. This setup features a BS equipped with mmWave massive antenna, a large number of AF relay stations (RS), and multiple UE. Different from applying MU-MIMO with random grouping of UEs in the area, we propose a user scheduling method to divide UEs with less inter-user interference into different groups to improve resource utilization. The different colors denote UEs in different

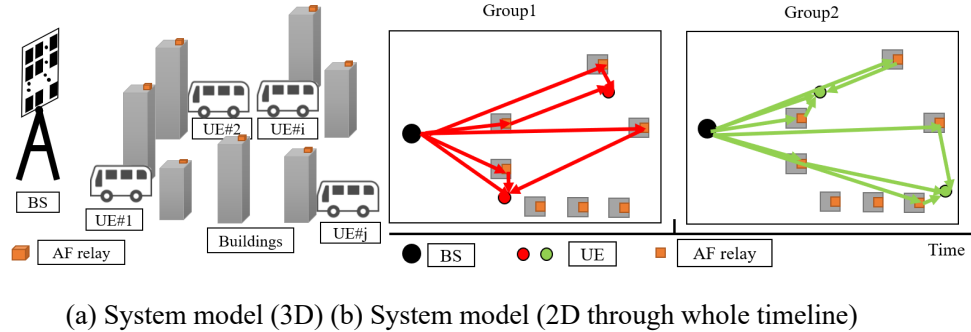


Fig. V.1.3-1 System model of multi-user massive relay MIMO with user scheduling

groups using different time slots. In the same group, we will simultaneously transmit and receive data from multiple UEs by using spatial multiplexing techniques among multiple antennas at the same time and frequency resources. Moreover, we propose a distance-based RS allocation method and a Round-Robin beam selection algorithm to efficiently distribute resources among UEs in the same group, further enhancing the system's overall channel capacity.

3. Resource Allocation and User Scheduling

It is more complicated to handle the multi-user scenario compared to the single-user case in terms of resource allocation, including RSs and antenna beams, especially in an environment with a large number of UEs. We elucidate strategies and algorithms pertaining to resource allocation and user scheduling in this paper.

3.1 Relay allocation

To implement the analog relay MU-MIMO system, the first step involves determining the antenna directivities of each RSs on the UE side. There are two types of overlapping RSs, as Fig. V.1.3-2 shows, which cause interference, thereby deteriorating channel capacity.

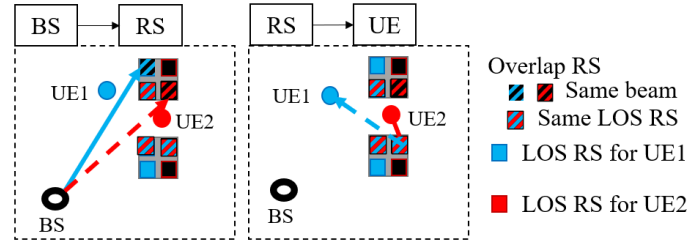


Fig. V.1.3-2 Two types of overlapping relay station

For the first type, the overlapping from UE's viewpoint, one RS can only generate one beam to one UE. Therefore, in order to make a performance balance among UEs, the UE who is assigned fewer RSs has the higher priority to select RSs (distance-based) when allocating the overlapping LOS RSs. The second type of overlapping is from the BS's viewpoint, due to the proximity of their assigned RSs, some of the RSs may have to exploit the same beam from the BS, which causes significant interference. We will elaborate on how to handle the beam selection problem in such a case in 3.2.

3.2 Beam selection

To ensure fairness among UEs, we employ the Round-Robin beam selection method to select beams for UEs one by one. It can provide a fair and efficient selection process to maximize UE capacity without significantly increasing computational complexity, as well as ensure the number of beams allocated to different UEs remains nearly equal. Instead of aiming for a global optimal solution of the system capacity, the Round-Robin approach seeks to find a locally optimal solution for each UE in each iteration.

3.3 User scheduling

In a multi-user scenario, user scheduling plays a crucial role. By implementing user scheduling, we can avoid allocating UEs with significant inter-user interference into the same communication resource group. To achieve optimal user scheduling, one option is to perform an exhaustive search to traverse all possible options and calculate their channel capacities for comparisons. This approach has the highest accuracy but it is intractable.

To address this challenge, we propose a blocking-empowered user scheduling method by comparing the number of overlapping LOS RSs. It can group UEs based on their positions, locations of RSs, and map of the environment to maximize the minimum capacity by making the locally optimal choice at each stage. Physically, such a worst scenario happens when the MU-MIMO UEs need to share the

same spatial resources via overlapping RSs such that spatial multiplexing cannot be expected due to inter-beam interferences. In our proposed user scheduling method, which is called the minimize maximum interference (min-max) method, it attempts to maximize the lowest rate UE group by identifying possible combinations of UEs that causes such low rate, and avoid the grouping of such worst scenarios.

4. Numerical Simulation

4.1 Simulation Configuration

Simulation model of massive relay MIMO is shown in Fig. V.1.3-3. We simulated a hotspot distribution model to evaluate the system performance. In hotspot model, 50 percent of UEs are distributed in the red hotspot area around the center crossroad, and the others are distributed in the remaining pink distribution area.

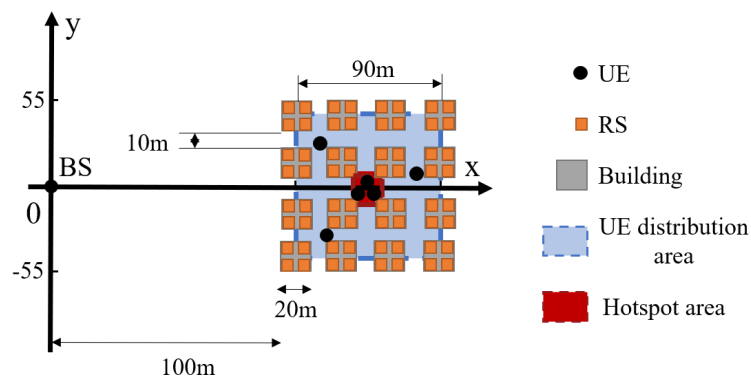


Fig. V.1.3-3 Simulation model of multi-user massive relay MIMO with user scheduling

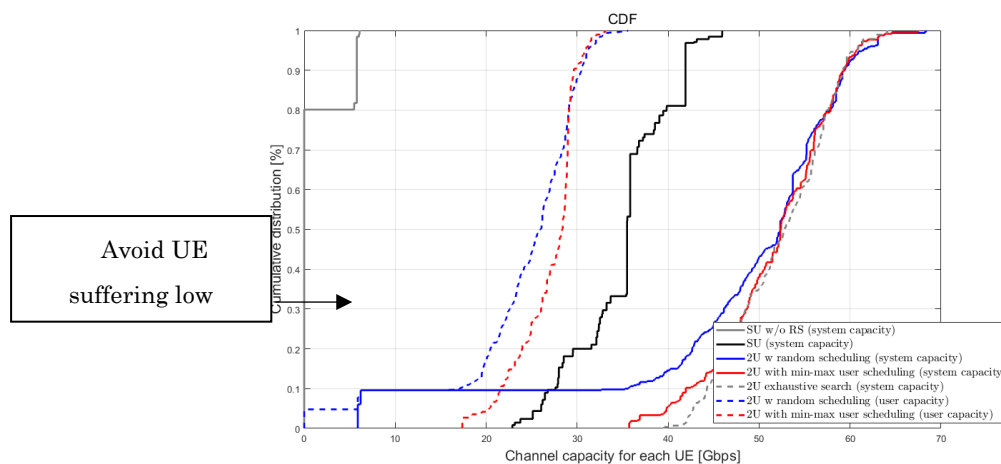


Fig. V.1.3-4 Comparison of CDF of channel capacity for multi-user massive relay MIMO in hotspot model

4.2 Simulation Result

We consider a hotspot model with more densely populated UE environments introduced in Fig. V.1.3-3. Here, we generate 12 UEs randomly in the hotspot area and 12 UEs in the remained distribution area. Similarly, each 2 UEs are selected in one UE group. This process repeats 40 times in simulation, and we calculate the capacity for each UE. Figure V.1.3-4 shows the CDF of the capacity by using single-user with and without RSs, multi-user with random user scheduling, proposed min-max user scheduling and exhaustive search. From this figure, 5% of UEs experience a channel capacity of 0 Gbps in the case of random user scheduling. However, with the min-max method user scheduling, the channel capacity of the lowest-performing UE is increased to over 15 Gbps. Considering scenarios with a large number of UEs in practical applications, especially in situations where UEs gather at the hotspot, user scheduling becomes a more important approach for enhancing fairness and avoiding some UEs with extremely low capacity.

5. Conclusion

In this paper, we extended the mmWave massive analog relay MIMO system from supporting the single user to supporting multi-user, as a more realistic and complete NCR system for 6G. We presented the relevant mechanisms and algorithms for this system and verified it with numerical simulation. The results indicate that RSs can effectively expand coverage area, and user scheduling can significantly enhance system capacity, especially in areas with high user density in MU-MIMO system.

REFERENCE

- [V.1.3-1] K. Sakaguchi, T. Haustein, S. Barbarossa, E. C. Strinati, A. Clemente, G. Destino, A. Pärssinen, I. Kim, H. Chung, J. Kim, W. Keusgen, R. J. Weiler, K. Takinami, E. Ceci, A. Sadri, L. Xian, A. Maltsev, G. K. Tran, H. Ogawa, K. Mahler and R. W. Heath Jr. "Where, when, and how mmWave is used in 5G and beyond," in *IEICE Transactions on Electronics*, vol.100, no.10, pp.790-808, Oct. 2017.
- [V.1.3-2] S. Sun, T. S. Rappaport, R. W. Heath, A. Nix, and S. Rangan, "Mimo for millimeter wave wireless communications: Beamforming, spatial multiplexing, or both?," in *IEEE Communications Magazine*, vol. 52, no. 12, pp. 110–121, Dec. 2014.
- [V.1.3-3] J. N. Laneman, D. N. Tse, and G. W. Wornell, "Cooperative diversity in wireless networks: Efficient protocols and outage behavior," in *IEEE Transactions on Information theory*, vol. 50, no. 12, pp. 3062–3080, Nov. 2004.
- [V.1.3-4] C. Huang, A. Zappone, G. C. Alexandropoulos, M. Debbah, and C. Yuen, "Reconfigurable intelligent surfaces for energy efficiency in wireless communication," in *IEEE transactions on wireless communications*, vol. 18, no. 8, pp. 4157–4170, Jun. 2019.
- [V.1.3-5] J. Zhao, "A survey of intelligent reflecting surfaces (irss): Towards 6g wireless communication networks," in *arXiv preprint arXiv:1907.04789*, 2019.
- [V.1.3-6] X. Lin, "An overview of 5g advanced evolution in 3gpp release 18," in *IEEE Communications Standards Magazine*, vol. 6, no. 3, pp. 77–83, Oct. 2022.

[V.1.3-7] K. Sakaguchi, T. Yoneda, M. Iwabuchi, and T. Murakami, “Mmwave massive analog relay mimo,” in *ITU J. Future Evol. Technol*, vol. 2, pp. 43–55, Sep. 2021.

[V.1.3-8] G. Yang and M. Xiao, “Performance analysis of millimeter-wave relaying: Impacts of beamwidth and self-interference,” in *IEEE Transactions on Communications*, vol. 66, no. 2, pp. 589–600, Oct. 2017.

[V.1.3-9] R. A. Ayoubi, M. Mizmizi, D. Tagliaferri, D. De Donno, and U. Spagnolini, “Network controlled repeaters vs. reconfigurable intelligent surfaces for 6g mmw coverage extension,” in *arXiv preprint arXiv:2211.08033*, 2022.

V.1.4. Phased array antenna technology for 6G analog repeater system

Keisuke Sato
DKK Co., Ltd.

Abstract — A proposed mmWAVE repeater consists of a donor unit and a service unit, installed without interference. Both units include a compact phased array antenna and an up/down converter, implemented on a multilayer PCB. To support 2x2 MIMO, each unit has two phased array antennas (4x4=16 elements) with orthogonal polarization planes. The phased array antenna can be rotated in the body of unit for different polarization planes, reducing costs. The MIMO signals are converted mmWAVE frequency to different intermediate frequencies by Up/Down converter, allowing communication over a single coaxial cable, contributing to miniaturization. The phased array can realize a high-gain beam for donor unit connects to fixed-position base stations, and a wide-angle beam for service unit connects to mobile stations, accommodating various environments and mobility.

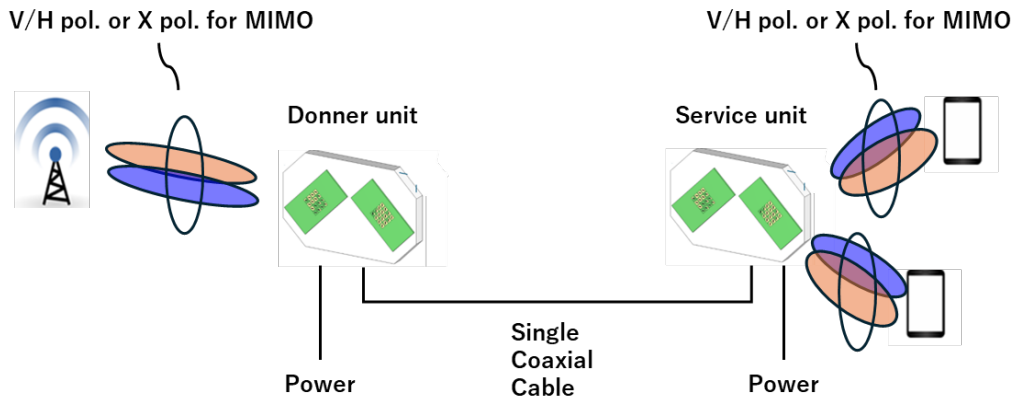
1. Introduction

A repeater system has been investigated to compensated increased path loss and straightness in 5G mmWAVE band. To install, the repeater system structure is compact as much as possible. This report introduces a compact phased array antenna system and a up/down converter configuration to realize a compact 5G analog repeater [V.1.4-1] [V.1.4-2].

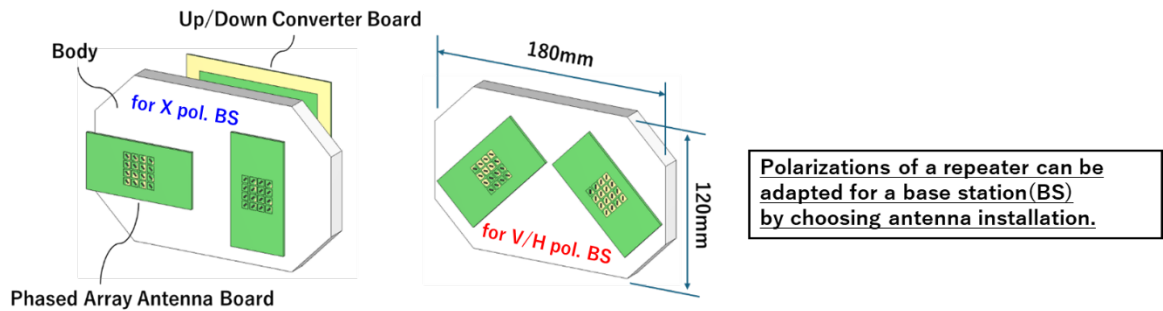
2. Phased Array Antenna for mmWAVE Repeater System

Fig. V.1.4-1 shows the concept of a small analog repeater. The repeater consists of a donor unit and service unit. The donor unit and the service unit are installed without interference with each other. Fig. V.1.4-2 shows the prototype structure. Table V.1.4-1 shows the repeater performance achieved with this concept. Both the donor and service unit of the repeater consist of a phased array antenna and an up/down converter, in which the beamforming IC (BFIC) and antenna are implemented on a multilayer printed circuit board (PCB). To support 2x2 MIMO in the millimeter wave band, two phased array antennas are installed in one unit (donor or service unit) with orthogonal polarization planes. The phased array antenna has a relatively small configuration of 4x4=16 elements. The purpose of this configuration is to reduce the heat dissipation area by reducing the output power. The antenna is connected to the up/down converter by a coaxial connector located at the center of the backside of the antenna. The antenna board can be rotated around the connector to connect to the chassis, enabling V/H polarization and $\pm 45^\circ$ polarization with the same component. This configuration enables support for different polarization planes of base stations, at a relatively low cost. The up/down converter has two local signal sources. It converts the mmWAVE frequency f_{RF} from the two phased array antennas for MIMO into different intermediate frequency bands f_{IF1} and f_{IF2} by multiplying the local signals f_{LO1} and f_{LO2} . By using different intermediate frequencies, the two signals required for MIMO can be communicated between the donor and service over a single coaxial cable, contributing to the miniaturization of the repeater system.

Fig. V.1.4-3 shows the beamforming characteristics. The beam patterns shown in these figures can be realized by changing only the exciting phase of each array element. In other words, these beam patterns always maximize amplifier gain in the phased array antenna. For the donor unit, a high-gain beam with wide-angle steering is preferred for connection to a fixed-position Base station (BS). For service units connected to Mobile Station (MS), a wide-angle beam with a beam width of about 80° was designed because the wide beam may be appropriate depending on the number of MSs, their mobility, and the environment around MSs.



(a) Configuration of proposed small repeater system.



(b) Phased array antenna system for proposed repeater system.

Fig. V.1.4-1 Concept of compact analog repeater system.

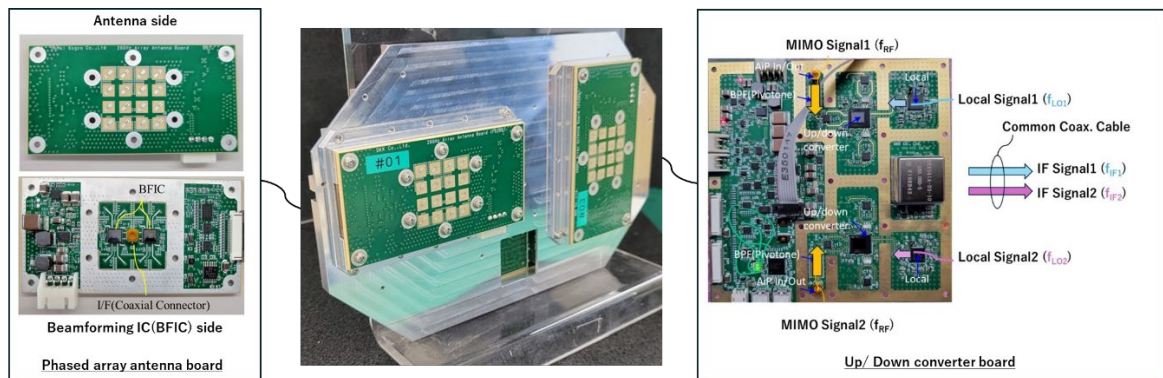


Fig. V.1.4-2 Prototype of phased array antenna system.

Table V.1.4-1 Specification of the repeater system.

Frequency Band	28GHz(N257) Bandwidth: 400MHz
Polarization	Dual pol. (V/H pol. or X pol)
EIRP (max.)	+36 dBm
System Gain	70 dB

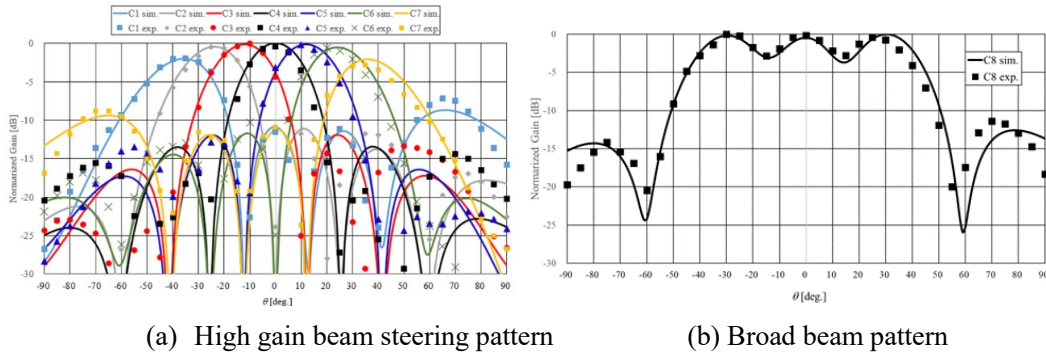


Fig. V.1.4-3 Beamforming performance.

3. Conclusion

This report presents the compact phased array antenna and the up/down converter to realize the compact analog repeater system. This compact repeater system can be changed its polarization due to changes in proposed phased array antennas deployment. Two MIMO signals from/to orthogonal polarization antenna can be passed thorough in one common coaxial cable between the donner and the service unit can be passed through by using the proposed up/down converter.

References

- [V.1.4-1] 3GPP TS38.300 V18.0.0:NR; NR and NG-RAN Overall Description; Stage2,” Dec. 2023.
- [V.1.4-2] K. SATO, “Millimeter Wave Base Station Antenna for 5G Mobile Communication,”IEICE Technical Report, Technical Committee on Antenna and Propagation, AP2024-9, May 2024.

V.1.5. Research on low latency relay technology to extend millimeter wave area

Ryochi Kataoka, Masahiro Takigawa, Issei Kanno, Takahiro Hayashi

KDDI Research Inc.

Abstract— In order to realize use cases being considered for 5G and beyond, such as teleoperation and AI utilization, high-capacity and low-latency communications for both the uplink and downlink are becoming increasingly important. To efficiently extend the coverage of millimeter-wave service area, the use of repeater that have beamforming capability for both access and backhaul link, such as network-controlled repeater (NCR), has been considered. This paper introduces our developed repeater with such the beamforming capability that extends the coverage efficiently while maintaining high-capacity and low-latency characteristics of 5G-NR in millimeter-wave, and ensuring flexibility of installation or mobility.

1. Introduction

Millimeter wave bands are being used in 5G to achieve high speed and high capacity. However, it currently does not provide sufficient coverage from a cost perspective, and repeaters that expand the area at low cost are attracting attention and being considered for deployment [V.1.5-1]. In order to extend coverage even more effectively, 3GPP standardized Network-Controlled Repeater (NCR), which provides beamforming capability for each of the backhaul and access links [V.1.5-2]. Here, when the links before and after relaying are in the same frequency band, self-interference occurs due to the wraparound within the repeater. To sufficiently suppress self-interference, it is necessary to ensure isolation between antennas and to operate an interference cancellation function using digital signal processing. However, in order to ensure isolation between antennas, restrictions are placed on the location and direction of antenna installation, and the processing delay is increased by operating the interference cancellation function. In this paper, we introduce a repeater configuration that efficiently extends coverage and ensures flexibility in installation and mobility while maintaining the high capacity and low latency characteristics of 5G-NR at millimeter waves.

2. Proposed low-latency relay method

We have been studying low latency relay communication technology in the high frequency band for extending the millimeter wave area for Beyond 5G / 6G [V.1.5-3]. First, we introduce a relaying method that converts frequency-multiplexed signals into spatial-multiplexed signals during relaying in order to realize low latency and high capacity relaying communications. Fig. V.1.5-1 shows an image of the proposed AF relaying method. In the proposed relaying method, the proposed relaying method achieves higher capacity by frequency multiplexing in the link where the UE communicates with a small number of antennas. In the link where multiple antennas are available between the repeater (RS) and the BS, spatial multiplexing is used to achieve high capacity while suppressing the increase in resource usage. At this time, the frequency bands between the UE and RS and between RS and BS are changed to suppress the generation of self-interference. Furthermore, by lowering the

frequency band between the RS and BS, where resource usage is low, from that between the UE and RS, it is possible to extend the distance more than when relaying in the same frequency band. For low latency relaying, analog circuits are used during the relaying process to convert between frequency-multiplexed and space-multiplexed signals without modulation and demodulation, while maintaining the number of multiplexes.

Fig. V.1.5-2 shows the circuit configuration in the RS for converting four multiplexes using the proposed method. If the conversion is in one direction, such as from frequency multiplexing to spatial multiplexing, it is possible to configure a relatively simple circuit as shown in the figure. Here, $f_{c(UE-RS)}$ is the frequency between UE and RS and $BW_{(UE-RS)}$ is the bandwidth, and the center frequency and bandwidth for n multiplexes on the frequency axis are $f_{c(UE-RS)}(1) \sim f_{c(UE-RS)}(n)$ and $BW_{(UE-RS)}(1) = BW_{(UE-RS)}(2) = \dots = BW_{(UE-RS)}(n)$, respectively. Also, the frequency between RS and BS is $f_{c(RS-BS)}$ and the bandwidth is $BW_{(RS-BS)} = BW_{(UE-RS)}(n)$. As shown in Fig. V.1.5-2, at RS, the frequency-multiplexed received signal is branched into n pieces at the divider. Here, $n = 4$ in Fig. V.1.5-2, and the received signal is distributed into 4 parts. Next, the signals are amplified by a low noise amplifier (LNA) and separated for each CC (component carrier) with a BPF (Band-pass filter). Then, it is converted to a common transmit frequency $f_{c(RS-BS)}$ and transmitted from each antenna after amplified by a PA (power amplifier).

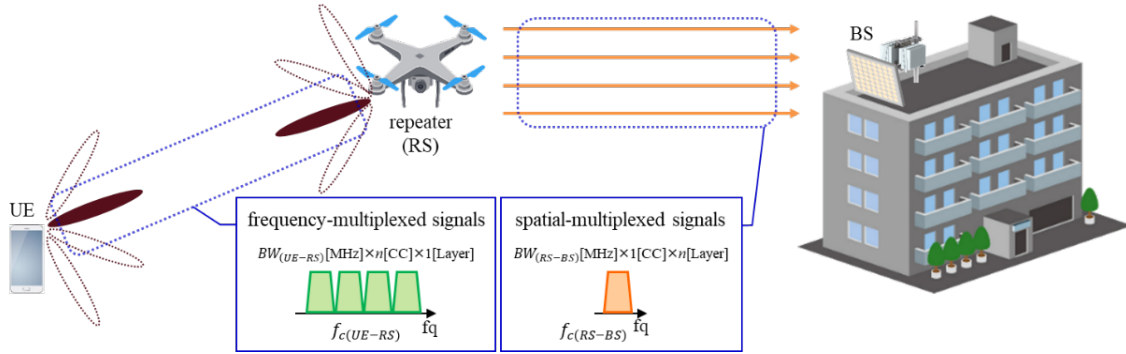


Fig. V.1.5-1. Proposed AF relaying method.

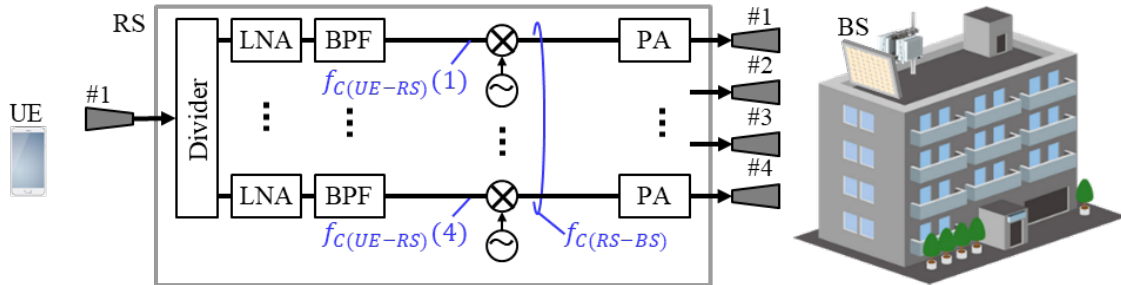


Fig. V.1.5-2. Circuit configuration of the proposed method.

3. Prototype analog repeater



Fig. V.1.5-3. Prototype repeater.



Fig. V.1.5-4. Prototype relay circuit.

Fig. V.1.5-3, 4. show the prototype repeater and relay circuits, respectively. In Fig. V.1.5-3, the 39 GHz band BF (beam forming) antenna is mounted on a tripod, and the 28 GHz band BF antenna is mounted on an orange jig. The 28 GHz band spatial multiplexing is assumed to be based on LoS-MIMO [V.1.5-4], and the layout in the figure is a square arrangement with the element spacing approximately equal horizontally and vertically. In the square LoS-MIMO configuration, the characteristics are maximized by setting the appropriate element spacing for the transmission/reception distance, but it is known that the characteristics drop off sharply when the transmission/reception distance changes. Therefore, in this study, a non-square antenna arrangement that is robust to variations in the transmit/receive distance is also considered [V.1.5-5]. In the relay circuit shown in Fig. V.1.5-4., the signal is down-converted to the 1.75 GHz band and passed through

a SAW filter with a passband width of 100 MHz twice to separate adjacent signals on the frequency axis. Here, we measured the group delay in the prototype relay circuit using network analyzer and confirmed that the group delay was about 0.25 [μ s] at maximum within the signal bandwidth. This is shorter than the NCP (normal cyclic prefix) length of 0.59 [μ s] for SCS (sub carrier spacings) 120 kHz, and it is expected that communication will be completed within the same slot even during relay.

4. Experimental evaluation

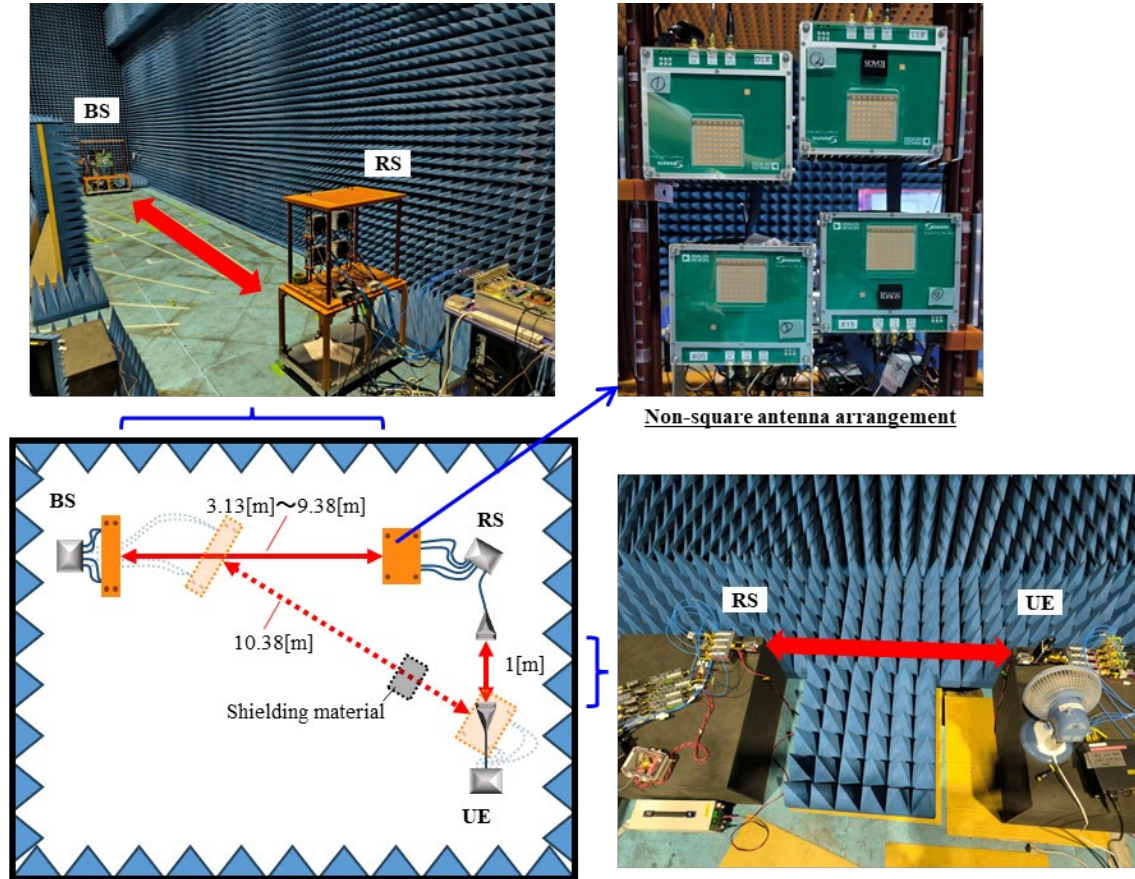


Fig. V.1.5-5. Experiments in a radio anechoic chamber and non-square configuration.

Fig. V.1.5-5. shows the experimental environment in a radio anechoic chamber using the prototype device. The evaluation is conducted assuming cell edge, and the transmission power is adjusted to a level that enables direct 5G communication with SISO and MCS index 0. Polarization-based spatial multiplexing (polarization MIMO) is not used in both the 5G-envisioned communication and the proposed relay communication. Since the probability of NLoS increases with distance from the base station, we simulated a situation in which there is a barrier between the base station and the terminal during 5G-enabled communication as the cell edge environment. In the experiment, a wooden box with the same height as the antenna was set up as a shielding. The distance between the base station and the repeater is based on 9.38 m, which is the longest distance between the base station and the repeater. When the distance is shortened, the transmission power is adjusted according to the calculated propagation loss, so that the same level of received power is achieved. Here, for the 39 GHz

band between the UE and RS, a horn antenna is used instead of the BF antenna shown in Fig. V.1.5-3.

Fig. V.1.5-6. shows the evaluation results. In Fig. V.1.5-6, it can be seen that the communication speed has improved on average compared to direct communication, although the throughput characteristics vary depending on the distance because the evaluation was not performed in an ideal non-square configuration due to the size of the prototype BF antenna and the fixture limitations.

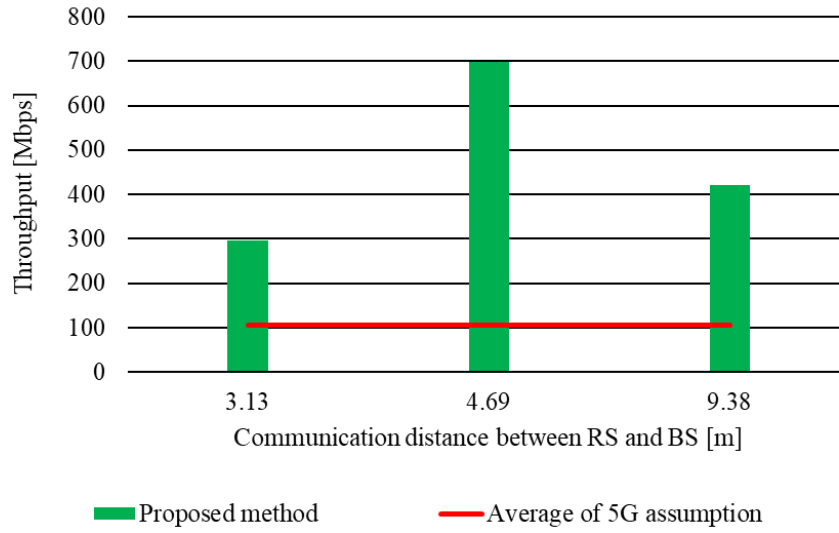


Fig. V.1.5-6. Throughput evaluation.

5. Conclusion

In this paper, we introduced a repeater configuration that efficiently extends coverage and ensures flexibility in installation and mobility while maintaining the high capacity and low latency characteristics of 5G-NR at millimeter waves. In the proposed configuration, frequency conversion is performed before and after relaying to prevent self-interference, and LoS-MIMO with a non-square configuration robust to distance is used because the communication distance between the base station and the repeater changes as the repeater moves. Experimental evaluation in an anechoic chamber using a prototype confirmed that the communication speed is improved over direct communication. In addition, outdoor proof-of-concept experiments are also currently underway. This repeater configuration is expected to save space and reduce the size of the repeater because it can be configured with only analog circuits while maintaining flexibility in antenna installation. Therefore, the repeater can be used not only for fixed repeater installations, but also for temporary area construction and mobile repeaters installed in vehicles.

Acknowledgement

This research is supported by the Ministry of Internal Affairs and Communications in Japan (JPJ000254).

REFERENCE

- [V.1.5-1] KDDI Press Release, “KDDI and Kyocera Succeeded in Developing Wireless Relay Technology That Dramatically Expands Millimeter-Wave Coverage,” Jan. 2025. [Online]. Available: https://newsroom.kddi.com/english/news/detail/kddi_nr-403_3675.html
- [V.1.5-2] 3GPP TS 38.300, V18.4.0, “Technical Specification Group Radio Access Network; NR; NR and NG-RAN Overall Description; Stage 2,” Dec. 2024.
- [V.1.5-3] R. Kataoka, M. Takigawa, T. Ohseki, T. Watanabe and Y. Amano, "Basic Performance Evaluation of Low Latency and High Capacity Relay Method in Millimeter-Wave Bands," 2023 IEEE Wireless Communications and Networking Conference (WCNC), Glasgow, United Kingdom, 2023, pp. 1-6, doi: 10.1109/WCNC55385.2023.10118819.
- [V.1.5-4] M. Takigawa, R. Kataoka, I. Kanno and Y. Kishi, "Antenna Design for Robust Millimeter Wave LoS-MIMO Link in Mobile Analog Repeater Achieving Low Latency and High Capacity," 2024 IEEE 21st Consumer Communications & Networking Conference (CCNC), Las Vegas, NV, USA, 2024, pp. 912-917, doi: 10.1109/CCNC51664.2024.10454777.
- [V.1.5-5] K. Nishimori, et. al., “On the Transmission Method for Short-Range MIMO Communication,” IEEE Trans. Vehicular Tech., 2011.

GROUP B -- Other relay technologies

V.1.6 Wireless transport technology for Xhaul (PSNRD)

V.1.6. Wireless transport technology for Xhaul

Hiroaki Asano

Panasonic System Networks R&D Lab.

Takeshi Yasunaga

Panasonic Connect

Abstract— This paper provides an overview of wireless transport technology for Xhaul and describes the points that unlicensed bands are expected to be actively used in 6G networks. Next, we describe the developed wireless transport equipment using 60 GHz unlicensed bands and future trends. And, for mobility platforms using 60GHz, the developed technology that uses millimeter wave radar with machine learning to predict wireless quality to avoid blocking and achieve seamless handover and RAT change is also described. These technologies are expected to expand to wireless transport technology for Xhaul.

1. Introduction

In 5G networks, configuration in which CUs, DUs, and RUs are prepared according to RAN function split option 2 and option 7-2 and are connected via backhaul, midhaul, and fronthaul are often used. In addition to large capacity, flexibility, scalability, power saving, low cost, reliability, security, and integrated management are required for RAN, and is being put into practical use for 5G [V.1.6-1]. For 6G networks, RAN functional splitting, virtualization and various functions have been considered according to requirements [V.1.6-2]. Support for NTN will be required, and traffic per user will further increase, user density will also increase, and higher frequency bands will be used for access networks. With the study of cell-free technology or distributed MIMO, it is necessary to place many antennas close to terminals. It is also required that antennas will be mounted on UAVs, HAPSs or LEO/GEOs, and it can be used in areas where conventional service coverage is difficult, and it is also desirable to support moving cells such as vehicles or high-speed trains. In these cases, wireless transport technology for Xhaul will become more important. Fig. V.1.6-1 -shows RAN architecture with Xhaul.

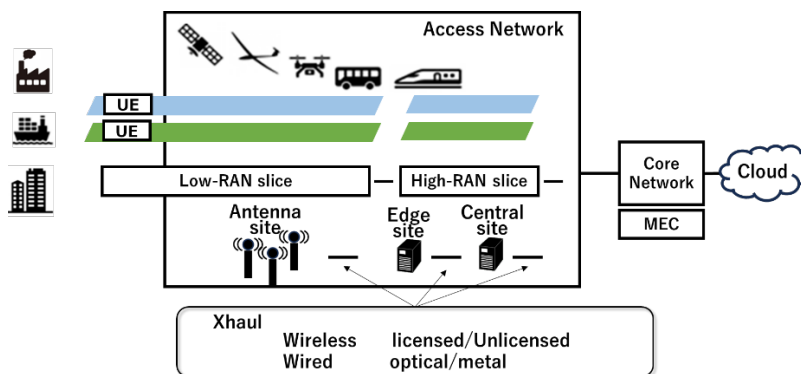


Fig. V.1.6-1 RAN architecture and Xhaul technology.

Regarding wireless, it is desirable to actively utilize unlicensed bands in addition to licensed bands. Discussions regarding frequency allocation in licensed bands will continue, in addition to this, effective use of unlicensed bands will enable the early realization of 6G networks.

When using an unlicensed band, sufficient management is required to prevent unexpected interference when sharing it with other users. The RAN is required to comprehensively manage the operational status of Xhaul, including the use of unlicensed bands, and to realize efficient operation of the entire network.

2. Unlicensed Band Technology for Wireless Transport

In 6G networks, it is expected that unlicensed bands will be used for wireless transport for Xhaul. Here, the IEEE802.11ad [V.1.6-3] compliant wireless equipment and the system technology that uses the unlicensed 60GHz band, which has the potential to be used for wireless transport for Xhaul, are described.

2.1. 60GHz Wireless Transport Equipment (IEEE802.11ad)

We have developed the 60GHz band wireless transmission equipment that was compliant with IEEE802.11ad. The equipment has the beamforming function using the 32-element antenna and autonomously selects the optimal beam for communication between an AP and STAs within a $\pm 60^\circ$ range. Devices equipped with lens antennas are also prepared.

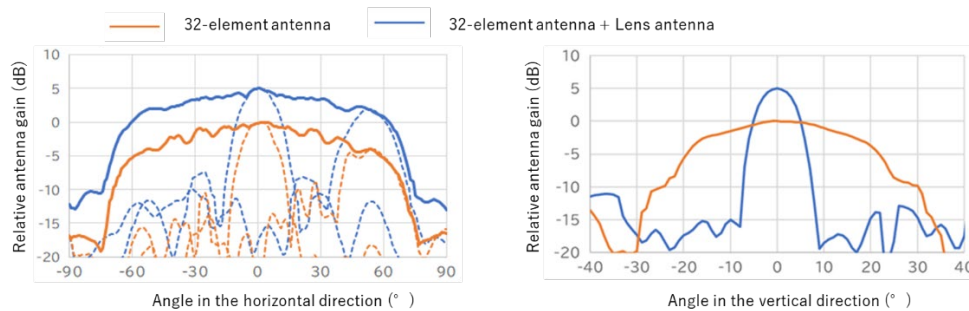
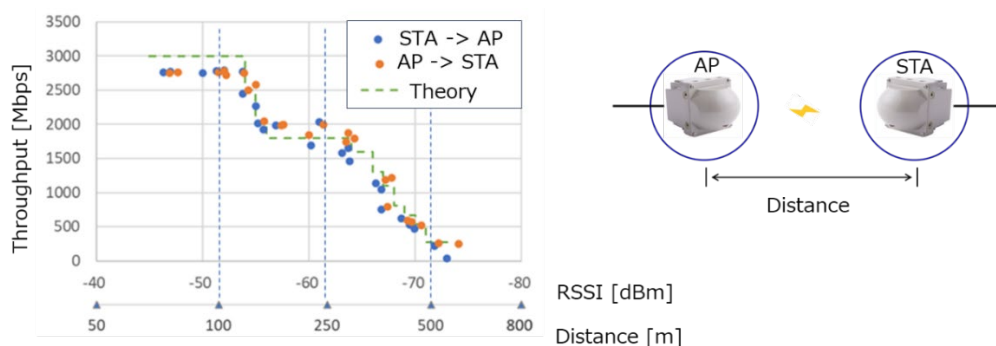


Fig. V.1.6-2 The horizontal and vertical antenna gain with/without the lens antenna.

Lens antennas ensure antenna gain by narrowing the beam width in the vertical direction and enable long-distance transmission. The horizontal and vertical antenna gains with and without the lens antenna are shown in Fig. V.1.6-2. -By using the lens antenna, the beam is narrowed in the vertical direction, and beamforming remains unchanged in the horizontal direction. Fig. V.1.6-3 -shows the results of evaluating the transmission throughput at the IP layer with respect to the distance/wireless quality between the AP and the STA. The equipment implements up to MCS12, and the theoretical value at the IP layer for each MCS value is also shown in dotted lines. The evaluation result shows that communication is possible at over 2.5Gbps up to about 120m, and transmission speeds of about

1Gbps can be obtained up to about 300m. This is the result of evaluation using devices equipped with lens antennas.



-Fig. V.1.6-3 The transmission evaluation results of the wireless transport device

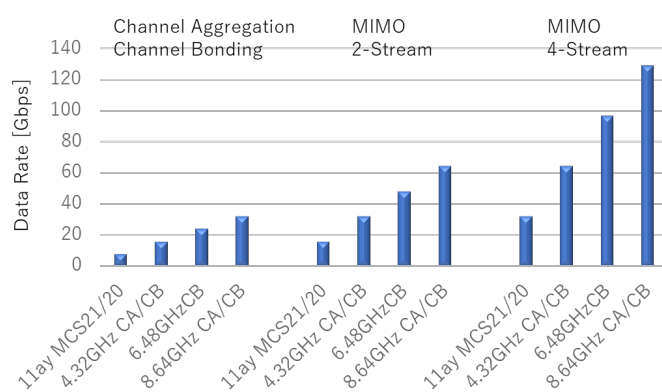


Fig. V.1.6-4 Data rates at PHY layer specified in IEEE802.11ay

- Fig. V.1.6-4 shows the transmission rate at PHY layer specified by IEEE802.11ay [V.1.6-4], which was specified further advancement of IEEE802.11ad. In Japan, up to four channels are available at 2.16GHz per channel from 57GHz to 66GHz. In IEEE802.11ay, when using four channels simultaneously with channel aggregation or channel bonding, the maximum transmission speeds on the physical layer are 64.7Gb/s with 2-Stream MIMO and 129.4Gb/s with 4-Stream MIMO. It has plenty of potential to support increased capacity for 6G networks.

2.2. Wireless Transport for Mobility Platform

Millimeter wave transmission is required to be utilized for mobility platforms to achieve large capacity, for example, to support moving cells. Millimeter-wave transmission is highly susceptible to shielding due to its linearity, so techniques to predict and avoid shielding are needed. To solve this problem, we have developed the technology to predict wireless quality using millimeter wave radar and machine learning. Fig. V.1.6-5 -shows the developed millimeter wave transport system for mobility platform using 5G-GWs. The 5G-GW was equipped with the AP and the STA of 60 GHz W-LAN (Wireless LAN) for multi-hop backhaul, and the AP to provide the 60 GHz W-LAN access

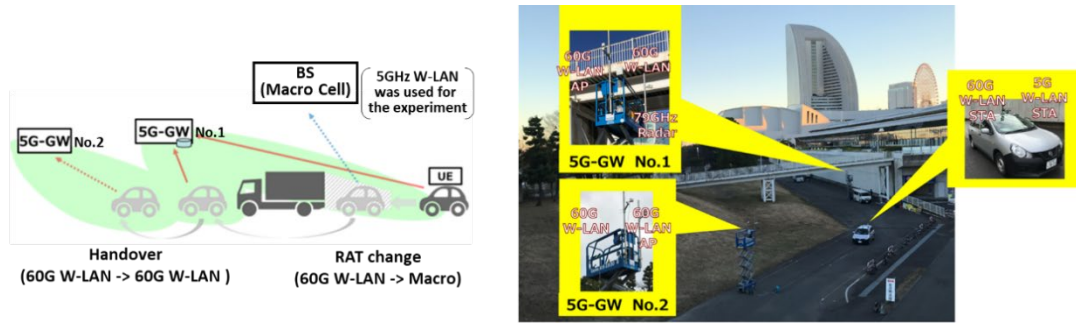


Fig. V.1.6-7 The evaluation system

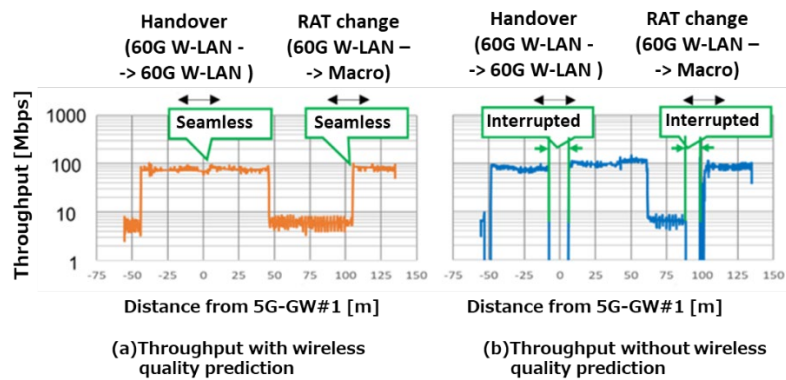


Fig. V.1.6-8 The results of the throughput with/without wireless quality prediction

3. Conclusion

In this paper, we explained the importance of wireless transport technology for Xhaul and the direction in which unlicensed bands will be used in 6G networks. And the developed unlicensed 60 GHz W-LAN equipment which is compliant to IEEE802.11ad and its application to a mobility platform that can avoid blocking and realize seamless RAT change and handover by using millimeter wave sensors with machine learning to predict radio quality were described. These technologies are expected to expand to wireless transport technology for Xhaul.

Acknowledgements

Some part of this paper was supported by “Research and development project for expansion of radio spectrum resources” of MIC, Japan. (JPJ000254)

REFERENCE

- [V.1.6-1] Y. Yoshida, "Mobile Xhaul Evolution: Enabling Tools for a Flexible 5G Xhaul Network," OFC, 2018
- [V.1.6-2] N. Aihara, et. al., "A User-Centric RAN Architecture using Cell Free massive-MIMO for 6G System," 2021 IEICE Society conference BS-3-9, Sep. 2021.
- [V.1.6-3] IEEE, "802.11ad-2012 – IEEE standard for local and metropolitan area networks – Part 11: Wireless LAN Medium Access Control (MAC) and Physical Layer (PHY) Specifications Amendment 3: Enhancements for Very High Throughput in the 60 GHz Band," Dec. 2012
- [V.1.6-4] IEEE, "802.11ay-2021 - IEEE Standard for Information Technology--Telecommunications and Information Exchange between Systems Local and Metropolitan Area Networks--Specific Requirements Part 11: Wireless LAN Medium Access Control (MAC) and Physical Layer (PHY) Specifications Amendment 2: Enhanced Throughput for Operation in License-exempt Bands above 45 GHz," Jul. 2021.
- [V.1.6-5] H.Asano, et al., "High power efficiency millimeter-wave network with communication quality prediction technology," IEEE VTS 17th APWCS, 2021.
- [V.1.6-6] M.Uesugi, et al., "Proof of Concept of Optimum Radio Access Technology Selection Scheme with Radars for Millimeter-Wave Networks," IEICE Trans. Commun., vol. E106-B, No.9, 2023.

V.2. Metasurface and RIS/IRS

GROUP C -- Metasurface (static)

- V.2.1 Analysis of using transmissive metasurfaces toward 5G evolution and 6G (DOCOMO, NTT)
- V.2.2 Development of optically transparent dual-band meta-surface reflector (KDDI Research)
- V.2.3 Metasurface technologies for controlling radio waves in specific directions (Kyocera)
- V.2.4. Social implementation technology for passive reflector that support the Sub6 band and above, and the results of verification (DNP)
- V.2.5 Transparent & flexible metasurface reflector film (SEKISUI CHEMICAL)
- V.2.6 Reconfigurable metasurface reflector with multi sheets/sliding sheets (DKK)

V.2.1. Analysis of using transmissive metasurfaces toward 5G evolution and 6G

Kenta Goto, Satoshi Suyama

NTT DOCOMO, INC.

Daisuke Kitayama, Adam Pander

NTT Device Technology Labs., NTT Corporation.

Abstract— Toward further enhancement of 5G and 6G, metasurface and reconfigurable intelligent surface (RIS) have been attracting much attention thanks to cost-effective and energy-efficient features. Experimental trials have been conducted to verify their effectiveness. In consideration of a legacy deployment, it is difficult to create a coverage area at the foot of a building in millimeter-wave (mmW) bands. Thus, for mmW coverage enhancement, we propose a novel solution that combines multiple transmissive metasurfaces (TMSs) with beamforming (BF) in a base station (BS). To verify the effectiveness of our proposed solution, experimental trials using a 28 GHz-band 5G BS and a user equipment were conducted. The BF function selectively aims the beam at one of five TMSs, and then TMS re-directs the radio wave to the foot area. This paper introduces an overview of the trials and shows downlink throughput measured in the trials. In addition, toward 6G, novel design methodology of TMSs for sub-terahertz band and its effectiveness are introduced.

1. Introduction

In order to meet various use cases for further enhancement of 5G (5G Evolution) and 6G, a future radio access network that can flexibly realize a variety of higher requirements is expected to be required. In recent years, a technical concept called New Radio Network Topology (NRNT) has been proposed to improve performances of radio access technologies (RATs) by increasing the number of line-of-sight (LOS) paths between multiple base station (BS) antennas (replacements) and a target user equipment (UE) and providing more room for path selection [V.2.1-1].

Elemental technologies for NRNT are metasurface and reconfigurable intelligent surface (RIS). Metasurface, an artificially engineered material, is comprised of a set of periodically arranged wavelength-order-sized unit cells and is a passive device. RIS is capable of adaptively manipulating incoming radio waves by using external stimuli and is an active device. It can improve various radio access performances, and thanks to cost effective and energy efficient features, a great deal of studies have been reported in recent years [V.2.1-2], [V.2.1-6].

In the case of service area deployment in outdoor, it is difficult to create a coverage area at the foot of a building, when a base station (BS) is installed on the rooftop of the same building. High frequency bands such as millimeter-wave (mmW) band have significant distance attenuation and linearity, and this technical issue becomes more pronounced as the frequency is higher. To solve this problem, the authors propose a new solution that combines a beamforming (BF) function in BS with multiple

transmissive metasurfaces (TMSs). In order to demonstrate the effectiveness of the proposed solution, 28 GHz-band experimental trials were conducted from October to November 2022 [V.2.1-6]. A 28 GHz-band 5G non-stand-alone (NSA) BS and a UE were used. BS with the BF function was deployed inside the building of DOCOMO R&D Center, and five TMSs were attached to a glass window in front of BS. This paper shows transmission performances measured by mmW experimental equipment of 5G BS and UE. Through the experimental trials, it is cleared the proposed solution can expand a mmW coverage area at the foot of the building in an indoor to outdoor scenario. Moreover, for sub-terahertz band toward 6G, we introduce our design methodology that is twisted metasurface structure and a backside polarization layer and experimentally confirm the effectiveness of this approach. The proposed structure is robust against interlayer alignment errors.

2. 28 GHz-Band 5G Experimental Trials Using Transmissive Metasurface

The authors have proposed a novel cost-effective massive MIMO (mMIMO) transmitter architecture exploiting RIS for 6G in the high frequency bands, which is called RIS-aided mMIMO [V.2.1-7]. In RIS-aided mMIMO, a small-size phased array antenna performs the first BF, and then multiple transmissive RISs carry out the second BF to adaptively control the beam generated by the first BF. For example, the RIS-aided mMIMO using above 2-step BF procedure generates a pencil beam for long-distance transmission or orthogonalizes spatially multiplexed MIMO streams to achieve extremely high capacity for 6G. However, it is not easy to apply the proposed RIS-aided architecture to a current experimental equipment of BS. Thus, in order to evaluate the potential of the RIS-aided architecture by an experimental trial, a simplified architecture that combines the first BF procedure with multiple passive TMSs is proposed in this paper. The BF function in BS directs the beam to the multiple TMSs, allowing the radio waves through TMSs to reach UEs which are located at the foot of the building. TMSs are designed to re-direct the incident waves to the downward direction. Especially in the high frequency bands, it is inherently difficult to directly deliver the radio waves to the foot area. In addition, detailed characteristics of each TMS can designed individually, and the BF function selects the best TMS among the multiple ones based on the maximum received power criterion, when the number of beams is one (single-beam transmission) and the distance between BS and TMSs is not so long. Of course, the number of the selected TMSs strongly depends on the number of beams in BS and the distance. To demonstrate the effectiveness of the simplified architecture with BF and TMSs, the mmW experimental trials were conducted from October to November 2022 at the DOCOMO R&D Center in Kanagawa Prefecture, Japan. Fig. V.2.1-1 shows the configuration of the experimental trials. A 5G NSA BS and a commercially available UE were used as the experimental equipment in the trials. BS was deployed inside the building of the DOCOMO R&D center with the BS antenna facing horizontally parallel to the ground surface without antenna tilt, and five TMSs were attached horizontally based on the intersection of a glass window in front of BS and the extension of the central axis of the BS antenna. The distance between BS and the window glass (TMSs) is set to 0.9 m and the BS antenna height is approximately 20 m. A trolley with UE was moved at a speed of approximately 5 km/h within the premises of the DOCOMO R&D center including the foot of the building and on the

sidewalk, near the building. UE measured DL throughput. In the trials, to reduce an influence of the human shielding caused by the measurer, the trolley was always pulled in the direction away from BS. UE was oriented to match the direction of the person moving the trolley, assuming that a person was operating a smartphone. UE was also adjusted to be almost 1.2 m high by using a styrene foam, and a laptop personal computer was connected to UE for the measurement. Main specifications of the BS equipment are summarized below. The center frequency and the system bandwidth are set to 27.65 GHz, and 300 MHz, respectively. The BS antenna is mMIMO having 512 antenna elements in total, 256 elements per polarization, and it has analog BF function. It can transmit up to two streams for the MIMO spatial multiplexing. Note that the center frequency and the system bandwidth in LTE are 2667.5 MHz, and 5 MHz, respectively.

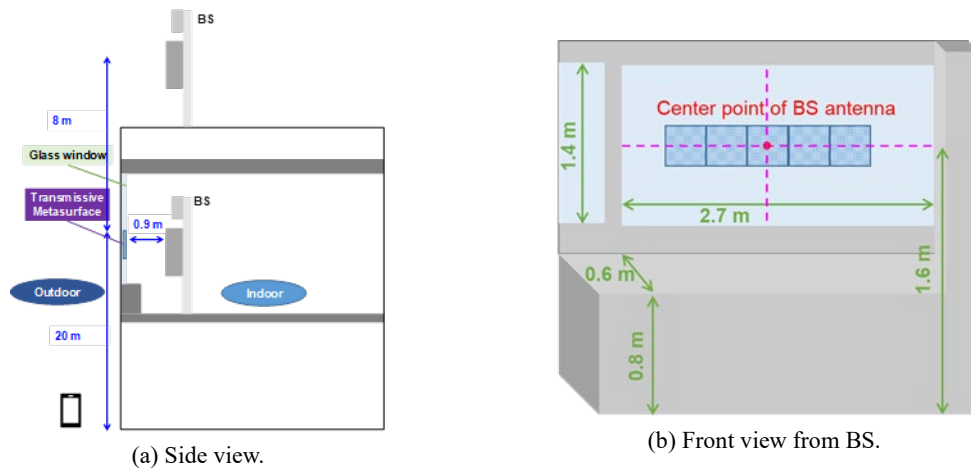


Fig. V.2.1-1. Experimental environment.

3. Experimental Results

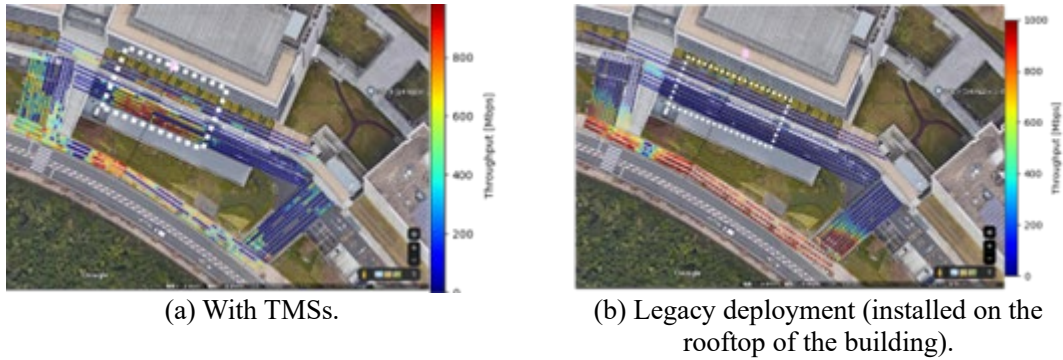


Fig. V.2.1-2. Heatmap of DL throughput.

Let us show some experimental results measured in mmW experimental trials exploiting five TMSs. The heat maps of the DL throughput are shown in Fig. V.2.1-2. The white box in Fig. V.2.1-2 is a target area that can be expected to be improved based on the design of TMSs and is in NLOS environments. Fig. V.2.1-2 (a) show that approximately 1 Gbps maximum DL throughput can be achieved in the target area and that the DL throughput drastically increases thanks to TMSs, compared to the result of legacy deployment shown in Fig. V.2.1-2 (b) which describes the DL throughput when BS was deployed on the rooftop of the building which is almost 28 m high. Since the trial was conducted

on different dates, January 2023, the trees around the measurement area were cut down, and thus the blocking effect of the trees must be reduced. In addition, BS performances were improved by updating the software installed into BS. However, from Fig. V.2.1-2 (b), it can be seen that the measured DL throughput is only a few Mbps at the foot of the building, and that it is difficult to create 28 GHz-band coverage area at the foot of the building. Therefore, the combination of the BF function in BS and multiple TMSs is considered to be a great effective solution toward realizing the mmW coverage enhancement.

4. TMSs for sub-terahertz band toward 6G

As described in the previous sections, TMS is effective in optimizing millimeter-wave coverage. It can be inferred that sub-terahertz band, which are being considered for use in 6G systems, will face the same coverage challenges as millimeter-wave band. TMS becomes even more important in 6G systems because the higher the frequency, the greater the impact of TMS on the wireless environment for the same aperture size. In the previous sections, the propagation direction was determined based on the transmission intensity profile. However, to improve the aperture efficiency, it is better to determine the propagation direction based on the phase profile.

Huygens metasurfaces are promising to make transmission phase profiles with low loss because they allow for phase design in the range of 2π while still matching the free-space wave impedance. Some works have reported the implementation of this approach with two metal layers on a single substrate [V.2.1-8]. However, a Huygens metasurface uses both electric and magnetic resonance simultaneously to obtain the desired impedance, which requires high alignment precision between the layers. Static-type TMSs applied to window glass or walls should be inexpensive and easy to fabricate from industrial perspective.

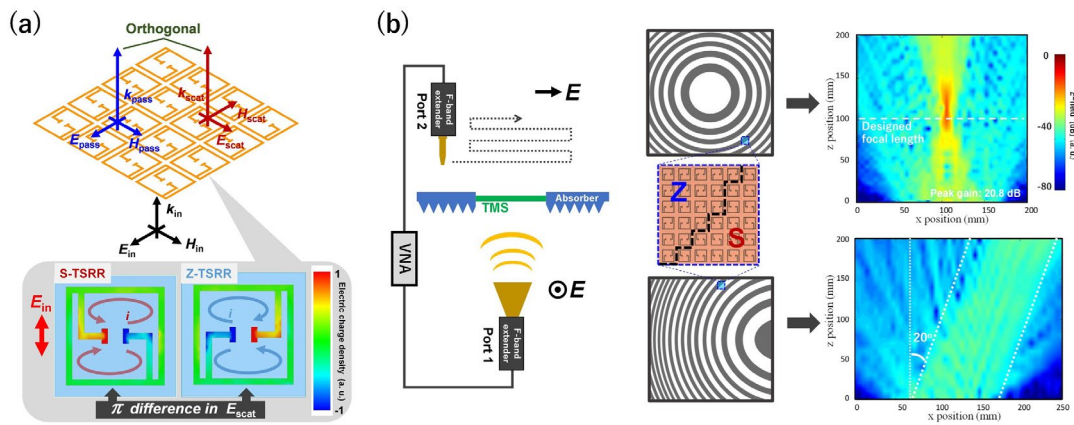


Fig. V.2.1-3 (a) Geometry of the twisted metasurface and simulated electric charges excited by incident waves. (b) Zone patterns for the twist direction and measured E-field distributions [V.2.1-7].

In [V.2.1-9], twisted metasurface structure and a backside polarization layer are used to efficiently make a transmission phase profiles by using scattered waves of polarization orthogonal to the incident waves as transmitted waves (Fig. V.2.1-3 (a)). A 1-bit $0/\pi$ phase profile can be made with low loss of

less than 1 dB by simply changing the twist direction of the structure, enabling a focusing and deflection function at 110 GHz as shown in Fig. V.2.1-3 (b). This structure is robust to interlayer alignment errors because the scattering phase is independently determined only in the metasurface layer, while the polarizer is used only to improve the efficiency, which is an advantage from a fabrication point of view.

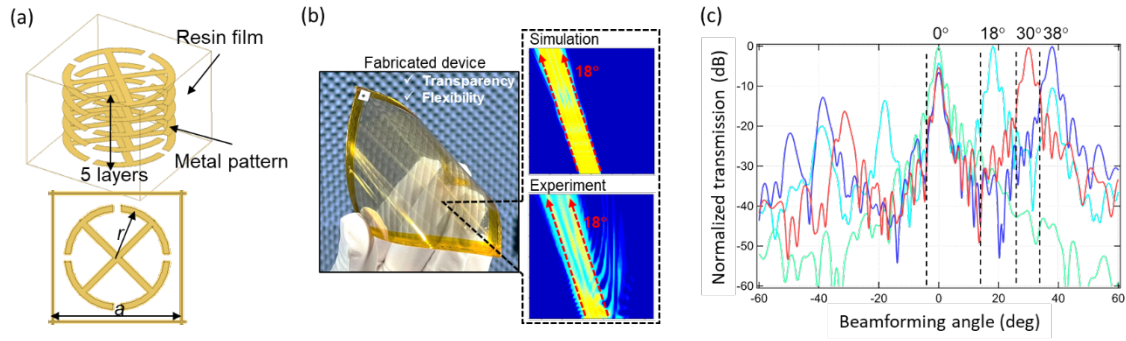


Fig. V.2.1-4. (a) Multilayer metamaterial cell for 2π controllability. (b) Fabricated gradient metasurface and beamforming results for 18 degrees beam deflection. (c) Far-field results for gradient metasurfaces with beamforming angles of 0° , 18° , 30° , and 38° .

Steering angle ($^\circ$)	0	18	30	38
Phase step ($^\circ$ /cell)	0	45	72	90
Symbol rate (Gbaud)	25	21	20	18
Data rate (Gb/s)	100	84	80	72
Constellation: Mod. 16QAM				

Fig V.2.1-5. Results of the data transmission evaluation through transmission-type beamforming metasurfaces at 300 GHz band.

Another approach to designing metasurface devices in sub-terahertz frequencies is multilayer structures that obtain full phase control by implementing multiple layers of the same metamaterial shape. By changing the size of features in metamaterial cells, a single layer can provide up to $\pi/2$ phase change range; thus, it is necessary to stack multiple layers to extend this range to full 2π transmission phase control. A full controllable phase range can be used to design any type of metasurface device, in particular, gradient phase metasurfaces were explored in [V.2.1-10] [V.2.1-11] at the 300 GHz band, as shown in Fig. V.2.1-4 (a). Gradient metasurface beamforming devices use discretized transmission phase step profiles generated by adjacently arranging metamaterial cells exhibiting different

transmission phases next to each other, enabling the deflection of the incident beam into a predesigned direction (Fig V.2.1-4 (c)). Although the fabrication of multilayer structures poses some difficulties, these structures are less sensitive to fabrication errors and provide very high efficiency in the control of beam propagation, together with the wide bandwidth necessary for large data transmission rates. Also, due to the self-standing structure of the device and materials used in the fabrication, devices in [V.2.1-9] exhibit high optical transparency and flexibility (Fig V.2.1-4 (b)). To prove the usability and efficiency of metasurface beamforming technology in sub-THz, data transmission rates, and constellation patterns were measured and are shown in Fig. V.2.1-5. For beamforming angles between 0 and 38 degrees, the data transmission rates from above 100 Gbps to 72 Gbps were recorded over a 25-cm link distance, respectively, using the 16QAM modulation. These are the highest data rates obtained for any beamforming technique in this frequency band, confirming the very large potential of this technology in the future development of 6G systems with controllable propagation paths.

REFERENCE

- [V.2.1-1] NTT DOCOMO, INC., “White paper: 5G Evolution and 6G (version 5.0),” Jan. 2023. [Online]. Available: https://www.nttdocomo.co.jp/english/binary/pdf/corporate/technology/whitepaper_6g/DOCOMO_6G_White_PaperEN_v5.0.pdf
- [V.2.1-2] M. D. Renzo, M. Debbah, D.-T. Phan-Huy, A. Zappone, M.- S. Alouini, C. Yuen, V. Sciancalepore, G. C. Alexandropoulos, J. Hoydis, H. Gacanin, J. d. Rosny, A. Bounceur, G. Lerosey, and M. Fink, “Smart radio environments empowered by reconfigurable AI meta-surfaces: an idea whose time has come,” *EURASIP J. Wireless Commun. and Netw.*, vol. 2019, no. 1, pp. 1-20, Dec. 2019.
- [V.2.1-3] Q. Wu and R. Zhang, “Towards smart and reconfigurable environment: Intelligent reflecting surface aided wireless network,” *IEEE Commun. Mag.*, vol. 58, no. 1, pp. 106-112, Jan. 2020.
- [V.2.1-4] K. Goto, S. Suyama, T. Yamada, K. Arai, O. Kagaya, “Experimental Trials with Combination of Multiple Transmissive Metasurfaces and Beamforming for mmW Coverage Enhancement,” in *Proc. IEEE 98th Veh. Technol. Conf. (VTC-Fall)*, pp. 1-5, Oct. 2023
- [V.2.1-5] Daisuke Kitayama, Yuto Hama, Kenta Goto, Kensuke Miyachi, Takeshi Motegi, and Osamu Kagaya, "Transparent dynamic metasurface for a visually unaffected reconfigurable intelligent surface: controlling transmission/reflection and making a window into an RF lens," *Opt. Express* 29, 29292-29307 (2021)
- [V.2.1-6] NTT DOCOMO Press Release,6 “DOCOMO conducts world's first trial of transmissive metasurface on window to deliver indoor radio waves to outdoor foot of building,” Jan. 2023. [Online]. Available: https://www.docomo.ne.jp/english/info/media_center/pr/2023/0130_02.html
- [V.2.1-7] X. Hou, X. Li, X. Wang, L. Chen, and S. Suyama, “Some observations and thoughts about reconfigurable intelligent surface application for 5G Evolution and 6G,” *ZTE commun.*, vol. 20, no. 1, pp. 14-20, Mar. 2022.

- [V.2.1-8] V. G. Ataloglou, M. Chen, M. Kim, and G. V. Eleftheriades, "Microwave Huygens' Metasurfaces: Fundamentals and Applications," *IEEE J. Microwaves* 1(1), 374–388 (2021).
- [V.2.1-9] D. Kitayama, A. Pander, Y. Hama, and H. Takahashi, "Alignment-free twisted-split-ring metasurface on single substrate with 2π phase range for linearly polarized sub-terahertz wave," *Opt. Express* 31, 20769-20786 (2023)
- [V.2.1-10] A. Pander, D. Kitayama, H. Kagami, and H. Takahashi, "Multilayer-laminated optically transparent 300-GHz-band transmissive beamforming metasurface for wireless communication", *Opt. Exp.* 32(14). 24772–24786, 2024.
- [V.2.1-11] A. Pander, H. Kagami, H. Hamada, D. Kitayama and H. Takahashi, "Over 70 Gb/s data transmission rate with 300-GHz-band transmission-type beamforming metasurface for beyond-5G wireless communication," 2024 Eighteenth International Congress on Artificial Materials for Novel Wave Phenomena (Metamaterials), Chania, Greece, 2024, pp. 1-4, doi: 10.1109/Metamaterials62190.2024.10703329.

V.2.2. Optically transparent dual-band meta-surface reflector

Hiromi Matsuno, Takuya Ohto and Takahiro Hayashi

KDDI Research Inc.

Abstract— A metasurface reflector, which directs reflected signals to an intended direction, has the potential to provide a low-cost and low-power option for signal coverage enhancement. This paper describes the development and characterization of metasurface reflectors based on an optically transparent dual-band metasurface reflector.

1. Introduction

Demands for mobile communication systems have been increasing year by year. More frequency bandwidth is needed to provide such communication quality. In fifth-generation mobile communication systems (5G), the use of millimeter-wave bands, where wide bandwidth is available, has started. It is expected to be increased toward beyond 5G and 6G to accommodate continuously growing data traffic of mobile communication systems [V.2.2-1], [V.2.2-2].

To utilize the millimeter-wave bands in mobile communication systems, the use of reflectors, which can reduce coverage holes is also anticipated. However, the size of the reflector may need to be increased to enhance the reflection power, which can disturb the landscape. In addition, the number of reflectors may increase as the frequency bands expand. They increase the deployment constraints of reflectors.

In this section, the implementation and measurement of an optically transparent dual-band metasurface reflector are introduced. The optically transparent feature alleviates the deployment constraint of metasurface reflectors by minimizing landscape disturbance. The dual-band capability also reduces the number of reflectors required.

2. Unit Cell Design

This section describes the dual-band metasurface reflector [V.2.2-3]. Fig. V.2.2-1 (a) and (b) show a photograph of the reflector and a schematic of its unit cell, respectively. The reflector is designed for each 28 GHz band and the 39 GHz band. The former band has already been assigned, and the latter band is expected to be assigned to Japan. The unit cell comprises one cross element for the 28 GHz band and four patch elements for the 39 GHz band. The reflector also comprises three layers. Each cross element and patch element is designed on the top and middle layers of the reflector, respectively, with a common ground plane designed on the bottom layer. Each layer comprises an optically transparent conductor sheet and is spaced with an optically transparent resin. For reflector design, a supercell structure with a periodically designed reflection phase. Because the ratio of the wavelengths of 28 and 39 GHz is approximately 4:3, the reflection phases of 28 GHz and 39 GHz are designed every $90 (=360/4)^\circ$ and $120 (360/3)^\circ$, respectively. For this development, the reflector is designed to reflect the signal from 0° to 45° .

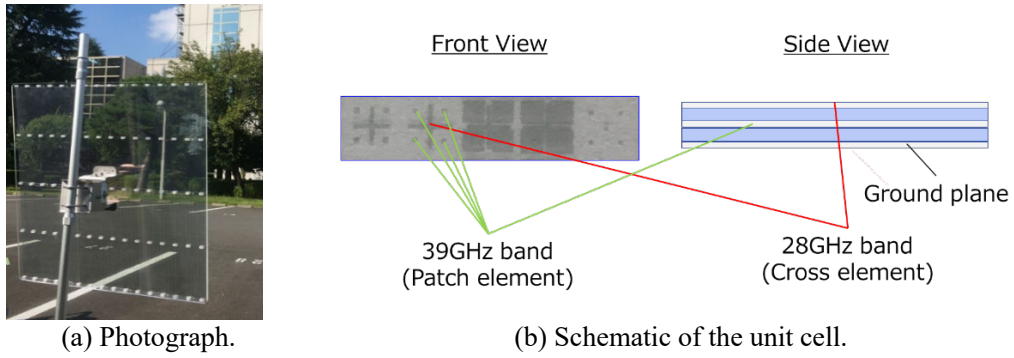


Fig. V.2.2-1 Optically Transparent Dual-Band Metasurface Reflector.

3. Field test

Field test was conducted with the developed reflector. Fig. V.2.2-2 shows the reference signal received power (RSRP) with and without the reflector at 28 GHz and 39 GHz. In the measurement, a reflector with a size of 790 mm \times 810 mm is used. As the figure shows, the RSRP of approximately 10 dB was improved in the designed direction (45°) in each 28 GHz and 39 GHz by the reflector.

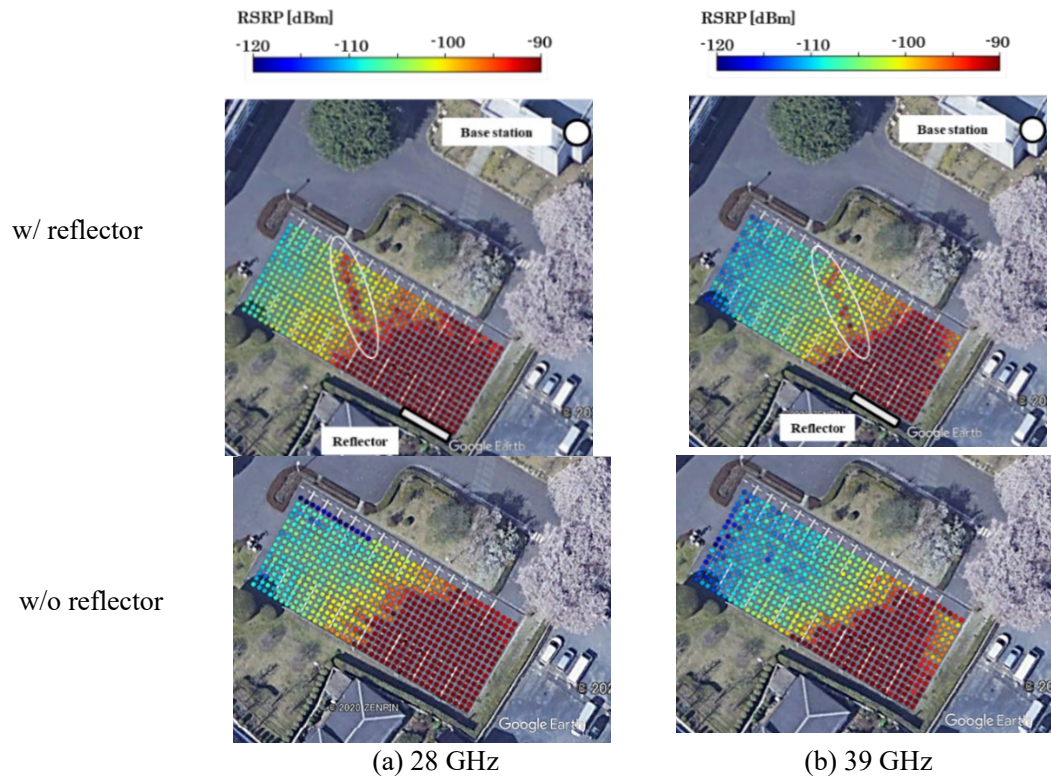


Fig. V.2.2-2 The results of field test.

4. Conclusion

This section describes the implementation and measurement results of previously developed metasurface reflectors. To efficiently reflect signals towards intended users, it is essential to mitigate hardware limitations associated with such reflectors.

REFERENCE

[V.2.2-1] ITU-R, “Studies on Frequency-related Matters for International Mobile Telecommunications Identification Including Possible Additional Applications to Mobile Service on Primary Basis Portion(s) of Frequency Range between 24.25 and 86 GHz for the Future Development of Internal Telecommunication for 2020 and Beyond,” 2015.

[V.2.2-2] KDDI, Beyond 5G/6G White Paper ver.2.0.1, Oct. 2021.

https://www.kddiresearch.jp/tech/whitepaper_b5g_6g/

[V.2.2-3] C. O. Nguyen, et al., “Dual Band and Dual Polarized Reflect Array Using Cross Dipole and Patch Elements,” in *Proc. of ISAP2020*, pp.821-822, 2021.

V.2.3. Metasurface technologies for controlling radio waves in specific directions

Masamichi Yonehara, Nobuki Hiramatsu, Hiromichi Yoshikawa, Takuya Hotaka
KYOCERA Corporation

Abstract—There are many experimental reports on reflection-type metasurfaces, but fewer on transmission-type metasurfaces compared to reflection-type metasurfaces. Additionally, there are few reports of experiments conducted under the same conditions for both reflection-type metasurfaces and transmission-type metasurfaces. Therefore, in this paper, reflection-type metasurfaces and transmission-type metasurfaces capable of forming arbitrary wavefronts through layered structures are proposed, and it is demonstrated through outdoor received power measurements that the proposed metasurfaces are effective for area expansion in non-line-of-sight (NLOS) environments.

1. Introduction

In the fifth-generation mobile communication system (5G), the 28 GHz band is allocated. This frequency band has a higher directivity of radio waves compared to traditional mobile communication systems and is less prone to diffraction, making coverage holes more likely to occur. To solve this issue, numerous reflection-type metasurfaces have been proposed [V.2.3-1] [V.2.3-3]. Regarding transmission-type metasurfaces, a review paper published in 2021 details their fundamental theories and applications [V.2.3-4]. Many applications have been proposed for transmission-type metasurfaces, including a transmission-type metasurface that can control directivity by being placed directly above a patch antenna [V.2.3-5]. This structure consists of a single resonator, making a 360° phase change fundamentally difficult. Pfeiffer et al. proposed Huygens' metasurfaces composed of sheet reactance layers and split-ring resonator layers, achieving a 360° phase change, though multiple substrates are needed to enlarge the aperture size [V.2.3-6]. Additionally, metasurfaces capable of dual-beam refraction by controlling the phase of unit cells have been proposed, showing remarkable advancements in metasurface elements [V.2.3-7]. However, there is no clear design theory for these unit cell structures, and their transmission characteristics are shown as results of optimizing structural parameters. Focusing on experimental validation of the effectiveness of metasurfaces, there are currently fewer reports on verifying the effectiveness of area expansion compared to reports on metasurface structures. For transmission-type metasurfaces, there are fewer reports compared to reflection-type metasurfaces, and few instances where both reflection-type metasurfaces and transmission-type metasurfaces have been tested under the same conditions.

Therefore, this report introduces a transmission-type metasurface designed using circuit synthesis theory, a design theory for microwave bandpass filters, and also introduce a reflection-type metasurface. The application of filter theory to design unit cells makes it possible to guarantee the transmission characteristics of transmission-type metasurfaces in advance. Additionally, outdoor experiments demonstrate that the proposed metasurfaces are effective in improving received power in NLOS environments.

2. Metasurfaces

This section describes structures and characteristics of metasurfaces. The proposed transmission-type metasurface unit cell structure is designed based on the circuit synthesis theory of microwave bandpass filters. In designs using the ABCD matrix, the final transmission characteristics are determined as a result of optimizing structural parameters, but by using microwave filter theory to design unit cells, it is possible to guarantee transmission characteristics in advance. Since the design method and design examples are described in detail in [V.2.3-8], this report introduces the designed elements. Fig. V.2.3-1 shows a typical configuration example and its characteristics of the unit cell. The unit cell is composed of a multilayer printed circuit board with four resonators and a conductor layer that controls coupling coefficient between the resonators. It is also designed to have a four-fold rotational symmetry structure and operates for two orthogonal linear polarizations. The characteristics of the unit cell are calculated using an electromagnetic field simulator based on the finite element method. Fig. V.2.3-2 shows the radiation field characteristics of the transmission-type metasurface arranged with unit elements. The radiation field is calculated using a physical optics approximation, and the obtained results are normalized to the maximum value. The size of the transmission-type metasurface is 300 mm \times 300 mm. The refraction angle is designed to be 60 degrees, and the phase is adjusted to form a wide beam. The beam width obtained as a result of the design is 11.7 degrees. As for the unit cell of the reflection-type metasurface, it can be easily realized by replacing the conductor layer that adjusts the coupling between the second and third resonators in the transmission-type metasurface unit cell with a ground plate. With this change, the number of resonators is two degrees, and the conductor layer for coupling coefficient adjustment is one layer. Fig. V.2.3-3 shows a typical configuration example and its characteristics of the reflection-type metasurface unit cell. Fig. V.2.3-4 shows the normalized radiation field characteristics of the reflection-type metasurface arranged with unit cells. The size of the reflection-type metasurface is also 300 mm \times 300 mm, similar to the transmission-type metasurface. The reflection-type metasurface is designed with a reflection angle of 45 degrees and the phase distribution is adjusted to form a wide beam, similar to the transmission-type metasurface. The beam width obtained as a result of the design is 8.3 degrees.

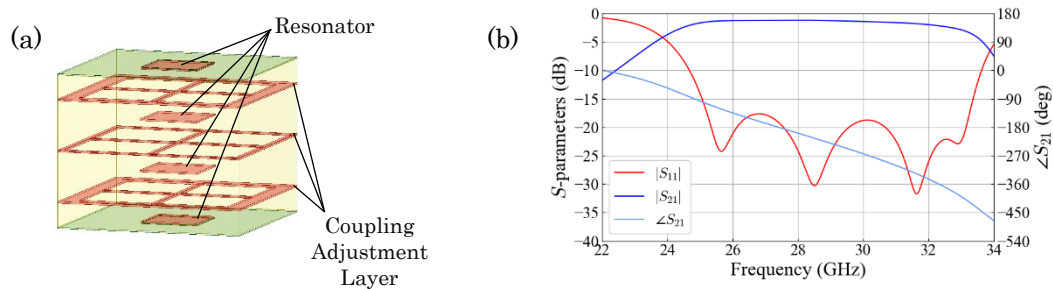


Fig. V.2.3-1. Typical element of transmission-type metasurface.
(a) perspective view. (b) Scattering parameters characteristics.

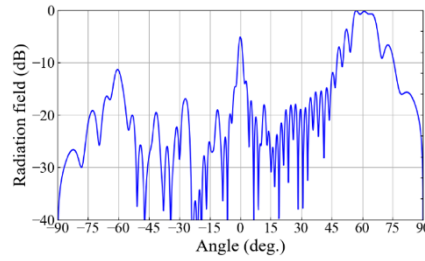


Fig. V.2.3-2. Radiation field characteristic of transmission-type metasurface.

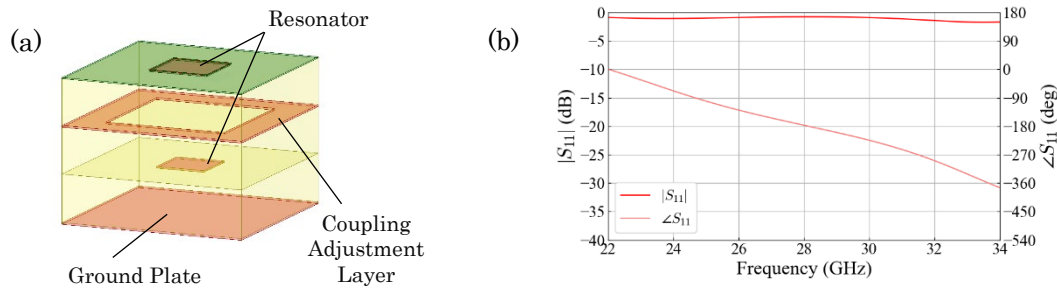


Fig. V.2.3-3. Typical element of reflection-type metasurface.
(a) perspective view. (b) Reflection coefficients characteristics.

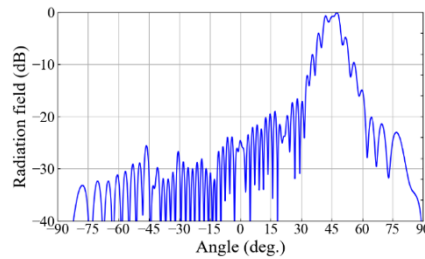


Fig. V.2.3-4. Radiation field characteristic of reflection-type metasurface.

3. Experiments

In this section, the effectiveness of the reflection-type metasurface and transmission-type metasurface designed in the previous section is verified through outdoor received power measurements. The measurements are conducted in Asahi City, Chiba Prefecture, Japan. Fig. V.2.3-5 shows a photograph of the measurement area. The measurement area is in a NLOS environment relative to the transmitting station.

Fig. V.2.3-6 shows the appearance of each metasurface used for measurement. When the measurement, the metasurfaces are in a housing case with an angle adjustment mechanism, and fine adjustments of the angle are made as necessary when installing each metasurface. The enclosure not only has an angle adjustment function but also features weather resistance.

The results of the received power distribution in the measurement area with and without these metasurfaces are shown in Fig. V.2.3-7 and Fig. V.2.3-8. Since the measurement area is a NLOS environment, the received power is significantly lower under the condition without metasurfaces as shown in Fig. V.2.3-7 (b) and Fig. V.2.3-8 (b), compared to the vicinity of the LOS area. On the other hand, as shown in Fig. V.2.3-7 (c) and Fig. V.2.3-8 (c), the installation of metasurfaces improves the

received power in the desired irradiation area. The effect is up to 23 dB for transmission-type metasurface and up to 18 dB for reflection-type metasurface. Both are sufficient improvements in received power, but under the current conditions, the transmission-type metasurface had a higher improvement effect. The reason is considered to be the difference in propagation loss due to the path difference to the receiving point and the difference in aperture size of each metasurface relative to the Fresnel zone determined by the positional relationship of Tx, Rx, and a metasurface.



Fig. V.2.3-5. Photographs of experimental environment.

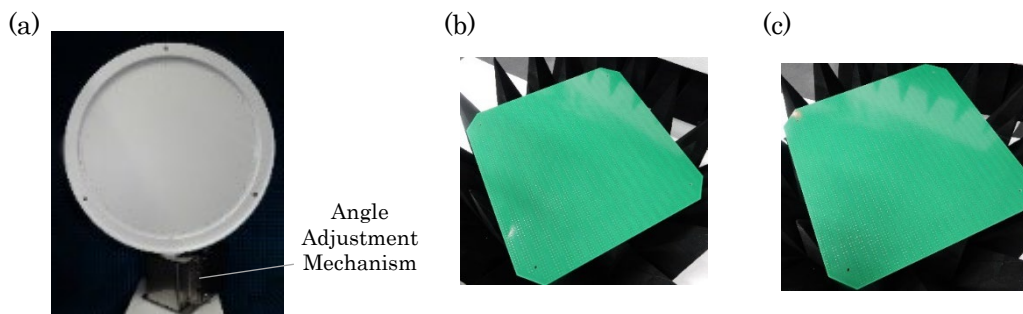


Fig. V.2.3-6. Metasurface prototypes.

(a) Housing case. (b) transmission-type metasurface. (c) reflection-type metasurface.

4. Conclusion

This report introduced structures and characteristics of unit cells for transmission-type metasurface designed based on filter theory, as well as reflection-type metasurface designed based on transmission-type metasurface. It was demonstrated that the transmission-type metasurface and reflection-type metasurface constructed using the designed unit cells form wide beams in the desired design directions. Finally, outdoor measurements in the same environment showed that both transmission-type metasurface and reflection-type metasurface are effective for area expansion. Under the current conditions, the transmission-type metasurface had a higher improvement effect, but the reflection-type metasurface also had sufficient improvement effects, making it important to use them flexibly. These metasurfaces are a promising option for area expansion as they are low-cost and require no power.

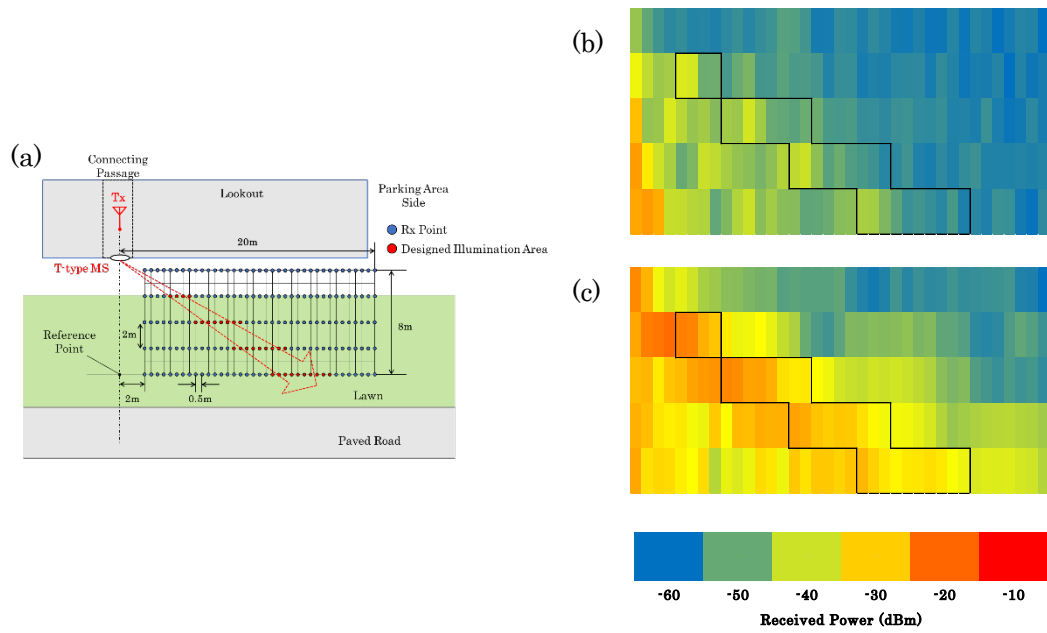


Fig. V.2.3-7. Experimental environment and results of field test.

(a) Top view (b) Without transmission-type metasurface. (c) With transmission-type metasurface.

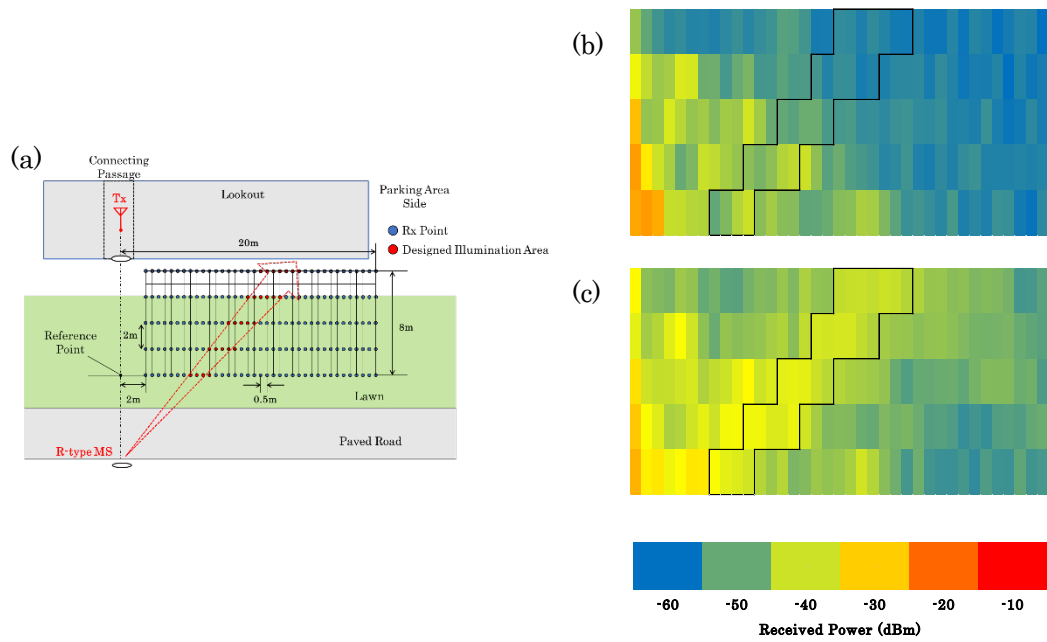


Fig. V.2.3-8. Experimental environment and results of field test.

(a) Top view (b) Without reflection-type metasurface. (c) With reflection-type metasurface.

REFERENCE

- [V.2.3-1] E. Martinez-De-Rioja, Á. F. Vaquero, M. Arrebola, E. Carrasco, J. A. Encinar, and M. Achour, "Passive dual-polarized shaped-beam reflectarrays to improve coverage in millimeter-wave 5G networks," *Proc. 15th Eur. Conf. Antennas Propag. (EuCAP)*, pp. 1-5, 2021.
- [V.2.3-2] L. Wang, H. Hagiwara, Y. Rikuta, and T. Kobayashi, "Optically transparent dual-polarized reflectarray with independently controllable beam for 5G communication systems," *IEICE Commun. Exp.*, vol. 10, no. 10, pp. 798-802, July 2021.
- [V.2.3-3] S. Costanzo, F. Venneri, A. Borgia, and G. D. Massa, "Dual-Band Dual-Linear Polarization Reflectarray for mmWaves/5G Applications," *IEEE Access*, vol. 8, pp. 78183-78192, April 2020.
- [V.2.3-4] V.G. Ataloglou, M. Chen, M. Kim, and G.V. Eleftheriades, "Microwave Huygens' metasurfaces: fundamentals and applications," *IEEE J. Microwaves*, vol.1, no.1, pp.374–388, 2021.
- [V.2.3-5] H. Nakano, S. Mitsui and J. Yamauchi, "Tilted-Beam High Gain Antenna System Composed of a Patch Antenna and Periodically Arrayed Loops," *IEEE Trans. Antennas Propag.*, vol. 62, no. 6, pp. 2917–2925, June 2014.
- [V.2.3-6] C. Pfeiffer and A. Grbic, "Metamaterial Huygens' surfaces: Tailoring wave fronts with reflectionless sheets," *Phys. Rev. Lett.*, vol. 110, no.19, 2013.
- [V.2.3-7] R.Y. Wu, L. Bao, L.W. Wu, and T. Cui, "Broadband transmission– type 1-bit coding metasurface for electromagnetic beam forming and scanning," *Sci. China-Phys. Mech. Astron.*, vol.63, no.8, 2020.
- [V.2.3-8] H. Yoshikawa, N. Hiramatsu, M. Yonehara, and H. Nakano, "A design method of transmission-type metasurfaces using circuit synthesis theory of microwave bandpass filters," *IEICE Trans. Elect.*, vol.E106–C, no.11, Nov. 2023 (Invited).

V.2.4. Social implementation technology for passive reflector that support the Sub6 band and above, and the results of verification

Yuichi Miyazaki, Atsuo Nakamura, Yusuke Isawa, Kenro Hirata
Dai Nippon Printing Co., Ltd.

Abstract—In this paper, we will present typical social implementation issues and countermeasures, using the passive metasurface reflector (Reflectarray) we are developing as an example, and report on the results of demonstration tests. Verification at millimeter wave frequencies confirmed improvements through beamforming and multi-step reflection via the reflector. In addition, verification at Sub6 frequencies showed that it was possible to expand the area from the first floor indoors to the third floor indoors via the outdoors, making it possible to wirelessly relay video in areas outside the coverage area.

1. Introduction

We have been focusing on and developing passive, static-type metasurface reflectors (Reflectarray: RA) that do not require power supply work, do not incur running costs, and can be installed with simple installation work. In order to implement RA in society, we have come to understand that there are various points to consider, not just the reflectance performance, and we have already reported on the development status based on these points [V.2.4-1], but we will outline them again here.

2. Issues in the social implementation of RA and approaches to solving these issues

Here, we will explain some examples of social implementation issues (concerns) that we have identified through customer interviews and other means, as well as the status of our development in response to these issues.

2.1. Adjusting the reflected beam profile

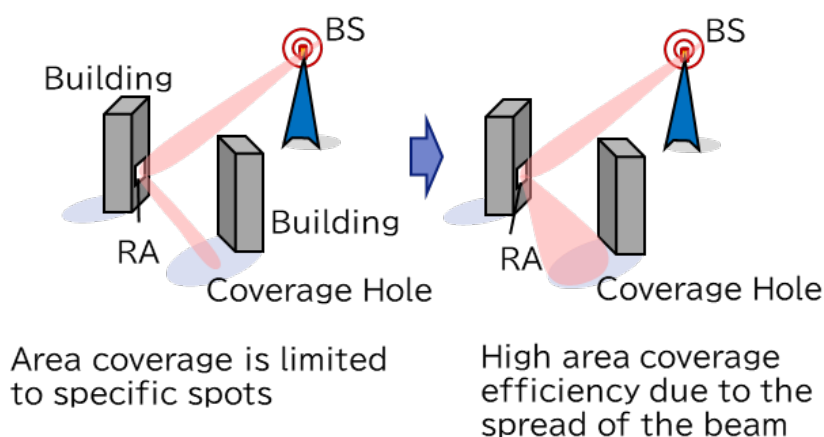


Fig. V.2.4-1: The need to widen reflected waves

In terms of social implementation, there are situations where “coverage holes cannot be efficiently covered unless the reflected wave is intentionally broadened (Fig. V.2.4-1)” and “the base station is located close to the RA, and the incident wave is not a plane wave”. Considering these situations, the RA we have developed is characterized by the fact that each combination of incident and reflected directions is set for each virtual division of the reflective surface. Furthermore, by making the division finer, it is possible to accommodate not only plane waves but also spherical waves incident on the surface, and it is also possible to expand the reflected waves to the desired shape. RA designed in this way can also be used when the relative position between the base station and RA does not meet the far-field conditions. In addition, the way the reflected wave is spread can be freely set in the horizontal and vertical directions, so efficient area coverage can be achieved according to the situation.

2.2. Increasing the size of the RA to ensure the required reflected power and support Sub6

From the perspective of social implementation, it is necessary to determine the size of the RA by working backwards from the power that needs to be delivered in order to deliver the required strength of radio waves to the coverage hole. In addition, the size of the RA designed for Sub6 is larger than that of the RA designed for millimeter waves when the radar cross-section is the equivalent of that of the RA designed for millimeter waves. When designing a large-size RA to ensure the necessary reflected power, we use a method of designing a large-size single piece of RA instead of a method of designing multiple RAs that are designed as single pieces and then lined up to make a large size. The reason for this is to achieve the function explained in section V.2.4.2.1, but it also has the effect of providing a stable link budget regardless of the position of the terminal within the reflective area.

2.3. Application to areas outside the line of sight

If there is no line of sight between the base station and the RA, or between the RA and the coverage hole, the expected effect will not be achieved. As a countermeasure, it is possible to deliver radio waves by using multiple RAs and reflecting them multiple times, but in this case, it is important to set the reflected beam profile while considering the radio wave propagation route, and to design the size of the RA while considering the propagation and reflection loss in the multiple reflections.

3. Confirming the actual effectiveness of the developed RA

Table V.2.4-1: Specifications of the RAs used for verifications

Design Items	RA#1	RA#2	RA#3
Target frequency [GHz]	28	28	4.8
Schematic of reflection design			
BRCS [dBsm](boresight)	31.2	17.4	24.4
Reflection loss [dB] (Estimated)	3	3	2

To confirm the effectiveness of the millimeter wave band RA and Sub6 band RA that we designed, we conducted effectiveness verification at the “Local 5G Open Lab” [V.2.4-2], a local 5G verification environment jointly established by NTT East and the University of Tokyo, and at the “ANRITSU 5G LAB” [V.2.4-3] owned by ANRITSU CORPORATION. The specifications of the RAs used for verifications are shown in Table V.2.4-1.

3.1. Verification of RA for millimeter waves in the Local 5G Open Lab

We installed one RA in the 28 [GHz] base station installed indoors and checked whether the communication situation in the emergency staircase area at the back of the elevator hall improved. To measure the reception status and throughput, we used ANRITSU CORPORATION's spectrum analyzer (Field Master Pro MS2090A), area tester (ML8780A), and FCNT LIMITED's local 5G-compatible smart device (FMP181L).

As shown in Fig. V.2.4-2, after the RA#1 was installed, the received power in the emergency staircase area improved by more than 10 [dB], and improvements were also observed in the uplink and downlink throughput.

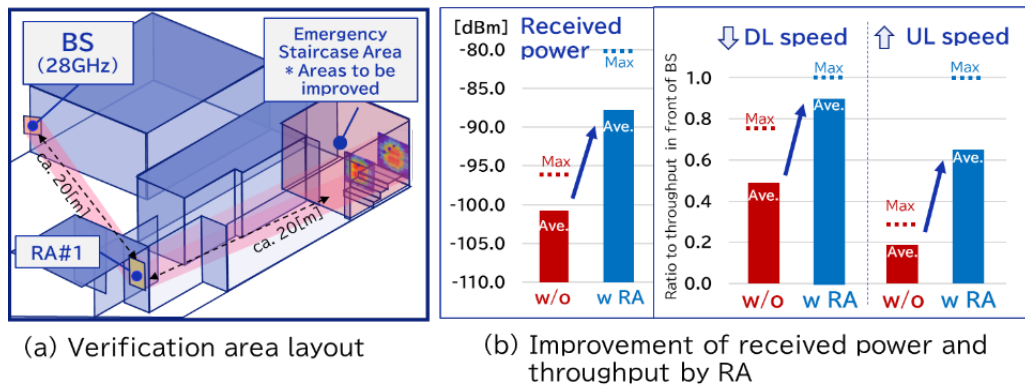


Fig. V.2.4-2: The improvement effect of installing RA#1

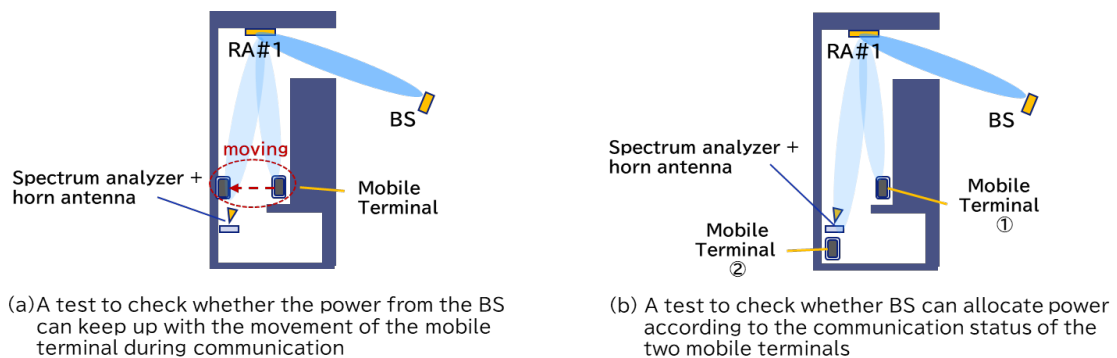


Fig. V.2.4-3: Beamforming test via RA

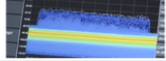
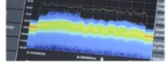
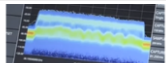
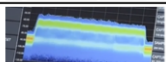
Here, we conducted a test to confirm the behavior of beamforming within the communication area formed by the RA#1.

In the test shown in Fig. V.2.4-3(a), it was observed that the signal density reaching the horn antenna from the RA increased as the terminal in communication approached the horn antenna. In the test

shown in Fig. V.2.4-3(b), it was confirmed that the signal density reaching the direction of terminal (2) from the RA#1 changed depending on the communication status of each of the two terminals, as shown in Table V.2.4-2.

These results show that the base station performing beamforming was able to recognize the terminal beyond the RA#1 and communicate with the two terminals separately. As a result, this RA#1 does not interfere with beamforming to the terminal, and it is expected to be applied as part of the propagation path in MIMO.

Table V.2.4-2: Communication status of the two terminals and changes in the signal received by terminal (2) from RA in the test shown in Fig. V.2.4-3(b)

	Mobile Terminal②	Mobile Terminal①	Received spectrum *)	Notes
1	w/o connection			
2	w/o connection	Connect (DL)		A horn antenna receives part of the communication signal that reaches terminal ①.
3	Connect (DL)	Connect (DL)		As terminal ② starts communicating, the number of signals going to terminal ② increases in time division.
4	Connect (DL)	Connect (UL)		The number of signals heading towards terminal ② increases further (waveform becomes more dense).

*) Signal received from the RA direction by the horn antenna in front of mobile terminal ②

Next, we will show the results of an experiment in which the communication status of a coverage hole that could not be improved by a single RA was improved by combining two RAs in series.

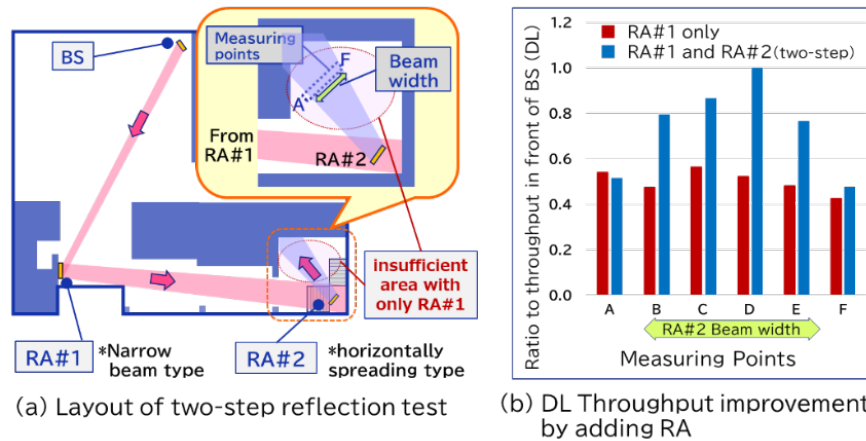


Fig. V.2.4-4: Verification of improved communication conditions by arranging two RA units in series

As shown in Fig. V.2.4-4(a), the back of the emergency staircase area is a place where the reflected wave of RA#1 is blocked. Therefore, as shown in Fig. V.2.4-4(b), for DL throughput at measurement points A-F, simply installing RA#1 only resulted in a value close to the DL throughput before RA#1 installation shown in Fig. V.2.4-2(b). Therefore, when an additional RA#2 was installed to spread the reflected wave horizontally, it was confirmed that the throughput improved between measurement points B and E. Although the graph in Fig. V.2.4-4(b) only shows DL Throughput, UL also improved in the same way, confirming the effectiveness of multi-step reflections.

3.2. RA verification for the Sub6 band at ANRITSU 5G LAB

We used an RA installed in an outdoor parking lot to verify whether it would be possible to improve the communication conditions in the indoor area on the third floor by reflecting radio waves from a 4.8 GHz base station installed at the back of the first floor of the building towards the 3rd-floor windows [V.2.4-4]. An image of the verification is shown in Fig. V.2.4-5. For this verification, we used RA#3 (Table V.2.4-1), which was designed to match the verification environment, and fixed it to the lamp post by the parking lot. We used ANRITSU CORPORATION's area tester (ML8780A) and KYOCERA Corporation's 5G-compatible device (KSG-C-100A) to measure received power and throughput.

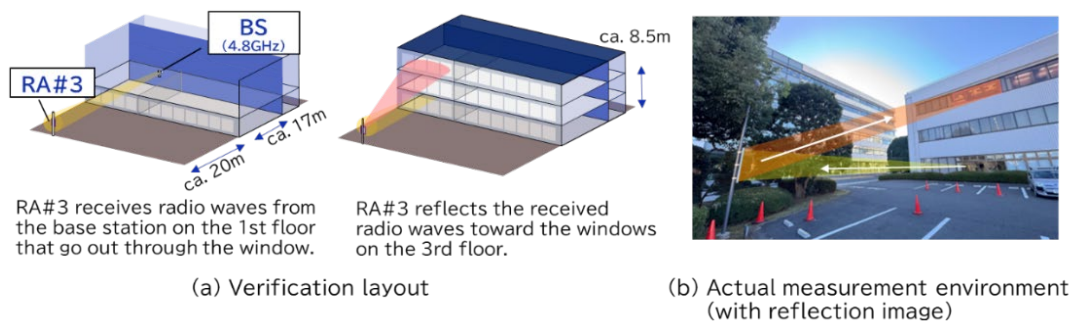


Fig. V.2.4-5: Layout of the verification and appearance of the verification environment

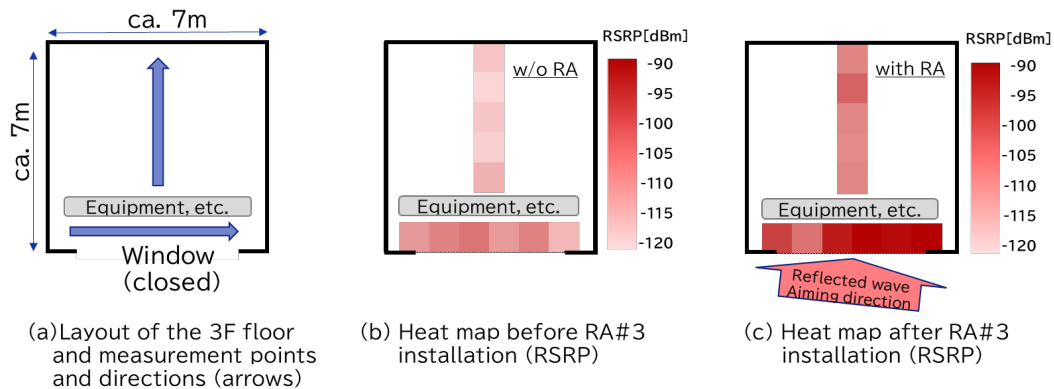


Fig. V.2.4-6: RSRP change on 3F floor before and after RA#3 installation in parking lot

Before the RA#3 was installed, the indoor area on the 3rd floor was unable to communicate with the base station, and the measured value of the received power from the 1st floor base station was RSRP -71.3 [dBm] at the planned RA#3 installation location, with the 1st floor window closed.

In designing the RA#3 to be used, it was necessary to decide on the specifications, and first, considering the ease of adjusting the installation angle, the incident and reflected directions of the RA were set so that when the RA's reflective surface faced directly at the building wall (= parallel to the edge of the parking lot), the reflected wave would reach the 3rd floor window. Next, we need to decide on the target value for the received power that reaches the window on the third floor, and in this verification, we have set it at RSRP -95 [dBm].

Fig. V.2.4-6 shows the change in received power on the 3rd floor before and after the installation of the RA#3. The target area was a room of approximately 7 [m] square with the windows closed, and RSRP measurements were taken at a height of 1.1 [m] above the floor in two directions: one along the windows and the other away from the windows (Fig. V.2.4-6(a)). The heat map after the installation of the RA#3 showed an average improvement of 12.3 [dB] and a maximum improvement of 25.1 [dB] compared to before the installation of the RA#3. The improvement tended to be stronger near the windows, but even in places further away from the windows, an average improvement of 9.4 [dB] and a maximum improvement of 15.4 [dB] was measured (Fig. V.2.4-6(b)(c)).

In addition, Fig. V.2.4-7 shows the results of measuring the UL/DL throughput at each point before and after the RA#3 was installed. Before the RA#3 was installed, it was not possible to communicate with the base station (Fig. V.2.4-7(a)), but after the RA#3 was installed, it became possible to measure the throughput for both UL and DL, and in the area where communication was possible, UL throughput averaged 5.4 [Mbps] (with a maximum of 10 [Mbps]), and DL throughput averaged 99.1 [Mbps] (with a maximum of 150 [Mbps]), confirming that radio waves from the base station reached the 3rd floor, and that radio waves from the terminal also reached the base station via the RA#3.

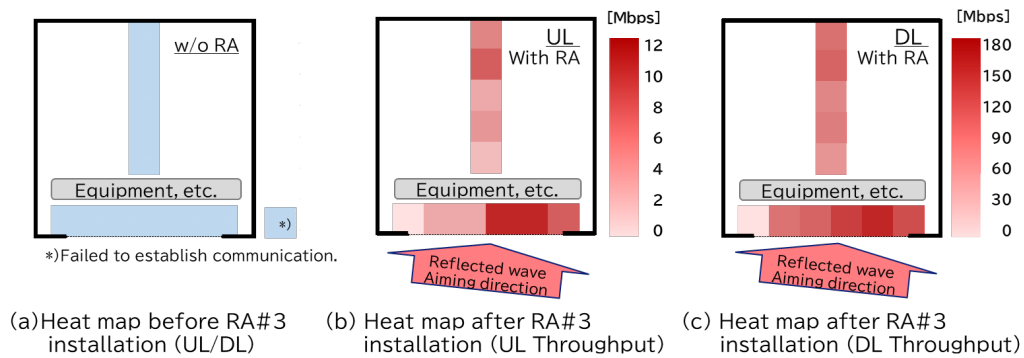


Fig. V.2.4-7: UL/DL throughput change on 3F floor before and after RA#3 installation in parking lot

Based on these results, we conducted a test of video wireless relay via the RA#3 between the 3rd and 1st floors. The schematic diagram of this test is shown in Fig. V.2.4-8. We confirmed that video could be relayed in Full-HD quality in a configuration where video data captured by the camera on the 3rd floor was sent to the BTS on the 1st floor via the RA#3, and the video data returned from the BTS was displayed on the monitor on the 3rd floor.

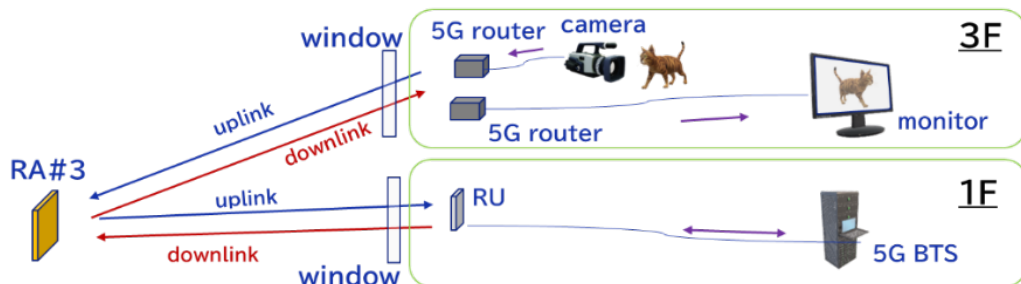


Fig. V.2.4-8: Schematic of video relay via RA#3

4. Conclusion

In this paper, we have reported on the issues involved in the social implementation of RA, the concept for solving these issues in passive and static RA, and the results of RA verification tests that were carried out based on this concept. In addition, we have reported on the results of verification tests carried out in the Sub6 band, which is currently becoming more widely used, and we believe that we have gained some knowledge that will help to promote the early adoption of RA.

It is assumed that high-frequency bands will continue to be used in 6G, and the problem of radio wave coverage will become more apparent, but we expect that the RA with consideration for social implementation that we are developing will be effective as a means of solving problems even after 5G.

Acknowledgements

We would like to express our gratitude to NTT East LOCAL 5G OPEN LAB for providing the verification environment for the millimeter wave verification tests, and to ANRITSU CORPORATION, KOZO KEIKAKU ENGINEERING Inc., and AK Radio Design Inc. for providing the verification environment and cooperating with the measurement and analysis for the Sub6 verification tests.

REFERENCE

- [V.2.4-1] Y. Miyazaki, “Development of Reflectarray (RA) for 5G communication and its social implementation.”, IEICE General Conference, Hiroshima, Japan, 2024, BCI-1-03.
- [V.2.4-2] NTT East Corporation, “LOCAL 5G OPEN LAB”, <https://business.ntt-east.co.jp/solution/local5g/openlab/>, (accessed Feb. 2025).
- [V.2.4-3] ANRITSU CORPORATION, “ANRITSU 5G LAB”, <https://www.anritsu.com/ja-jp/test-measurement/technologies/5g-lab>, (accessed Feb. 2025).
- [V.2.4-4] Y. Miyazaki, “Development of Reflectarray for Sub6 band and a validation case study”, IEICE Technical Report RCS2024-274,SR2024-110,SRW2024-65(2025-03).

V.2.5. Transparent & flexible metasurface reflector film

Masatoshi Sano, Shinjiro Fukuyama
SEKISUI CHEMICAL CO., LTD.

Abstract — This paper introduces the characteristics of a transparent reflective film that can be applied to a wide range of frequencies. We compared the reflective properties of the film when it is flat and when it is bent into a convex shape, utilizing the film's flexibility, with those of a metal plate. Measurements and simulations at 28 GHz, 39 GHz, and 120 GHz confirmed that the reflective film has reflective properties equivalent to those of a metal plate, and that when bent into a convex shape, the change in received power with respect to the angle becomes flat.

1. INTRODUCTION

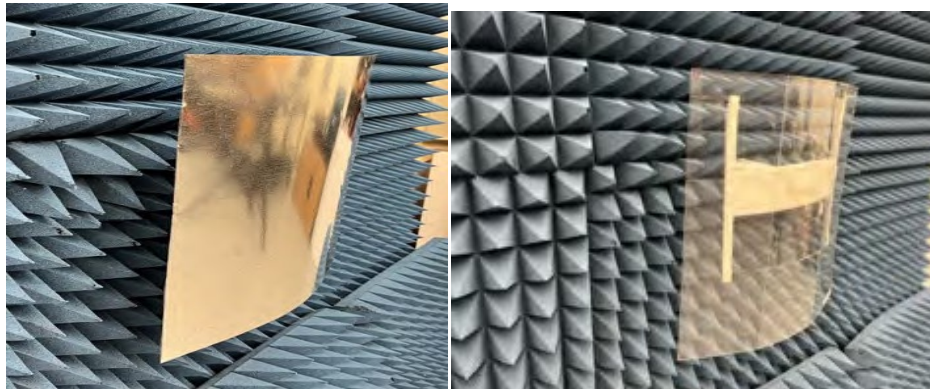
One of the foremost challenges in a millimeter wave (mmWave) and sub-THz network, is its ability to close a link with good coverage capabilities. This requires a line-of sight (LOS) or at least a strong first-order reflected non-LOS (NLOS) path to form a stable link for radio communications. The availability of a NLOS link depends on the reflection profile of a scattered, the material, and the frequency of operation. A conventional approach to providing a stable NLOS link is by the deployment of multiple access points or active repeaters [V.2.5-1] and relays. A recent study published that environment can be made a controllable factor which will re-engineer electromagnetic waves. These controllable environments have the potential to be less prone to disruptions in wireless networks, by steering towards desirable directions, having safe zones and extending radio coverage [V.2.5-2].

Strategical placements of reflectors in an indoor environment were studied using analytical derivations. The results showed the coverage dependency on the location, placement of the reflectors and their sizes [V.2.5-3]. Other solutions proposed to this problem are to increase the transmit power or deploy highly sensitive receivers. Due to practical limitations on increasing transmit power by regulatory bodies and the cost ineffectiveness of highly sensitive receivers, one of the most convenient alternatives to this is the use of passive reflectors. The deployment of passive reflectors with good reflection characteristics can be used to our advantage to replace the multiple access points and repeaters. Earlier simulation and measurement studies, such as [V.2.5-4] have shown that objects such as metal act as a perfect reflector, enabling strong reflections for directional NLOS communication. Thus, the deployment of the passive metallic reflectors can create a favorable propagation environment by introducing new multipath components (MPCs) in the channel and increasing the overall spatial diversity of the MPCs. Metals, however, have a dramatic influence on appearance especially the indoor environment spoiling the landscape.

In places where the deployment of metal reflectors is not reasonable, transparent reflectors take over and serve the purpose. These reflectors offer a sustainable, easy-to-deploy alternative without altering the appearance of the surface to increase the network coverage. Penetration properties of these transparent reflectors in an indoor and an open-door environment was studied in our past work [V.2.5-5]. The experiment result showed better reflection performance, improvement in coverage by

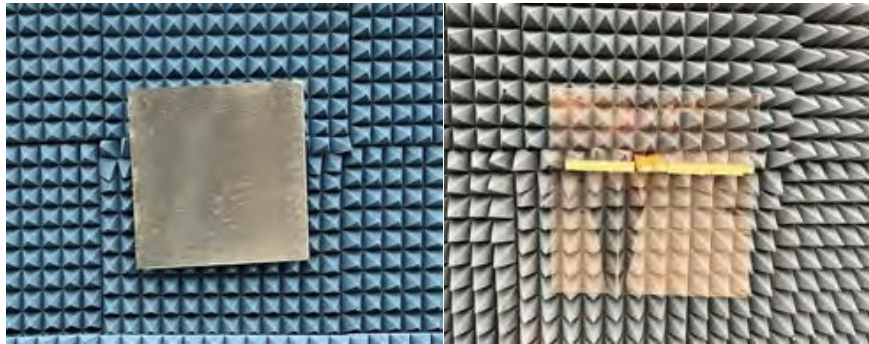
preserving the radio waves within the environment in presence of passive transparent reflectors. Amongst the different kinds of reconfigurable intelligent surfaces (RISs) being researched currently [V.2.5-6], our film under test is electromagnetic based (EM) based RIS. The film withholds the capacity to preserve the impinging radio waves and passively reflect the first-order derivative for enhancing the network coverage. These reflectors, as tested in [V.2.5-5] provide a strong NLOS link in a wireless network and have a penetration loss comparable to metal. Hence, this film might be an economical and sustainable alternative to conventional methods of increasing the signal strength. The conventional methods are undoubtedly effective, but are subjected to higher infrastructure and deployment costs. Another distinctive advantage of this film, is its nonplanar structure and free-form conformity that leads to easy deployment, re-usable and high durability. These transparent reflectors can be deployed on any structure without altering the appearance of the surface it is mounted on. They reflect all the incident rays enabling them to reach shielded, dense areas eliminating any blind spots.

In this work, we characterize the propagation characteristics using the passive transparent reflector in a controlled indoor environment. We conducted our experiments in an intelligent radio environment, motivated by the high importance of a controllable environment to improve signal coverage. In Fig. V.2.5-2, a panel made of broadband pyramidal absorbers is shown which is used to eliminate the other second-order reflections. The reflector is placed in between the panel along the elevation axes of the transmitter and receiver radio heads. The diffusion characteristics of the film enables a wide frequency coverage useful for 5G and 6G communications and will play an important role in enhancing achieving the 1000x capacity out of a channel. The main usage of the passive transparent reflector is to make at least one strong first-order non-LOS (NLOS) reflection path to complete a link, in a wireless network. The flat and curved shape reflectors used in the measurement setup are shown in Fig. V.2.5-1.



(a) Convex metal reflector.

(b) Convex transparent reflector.



(c) Flat metal reflector.

(d) Flat transparent reflector.

Fig. V.2.5-1: Flat and curved passive reflectors 16"x16".

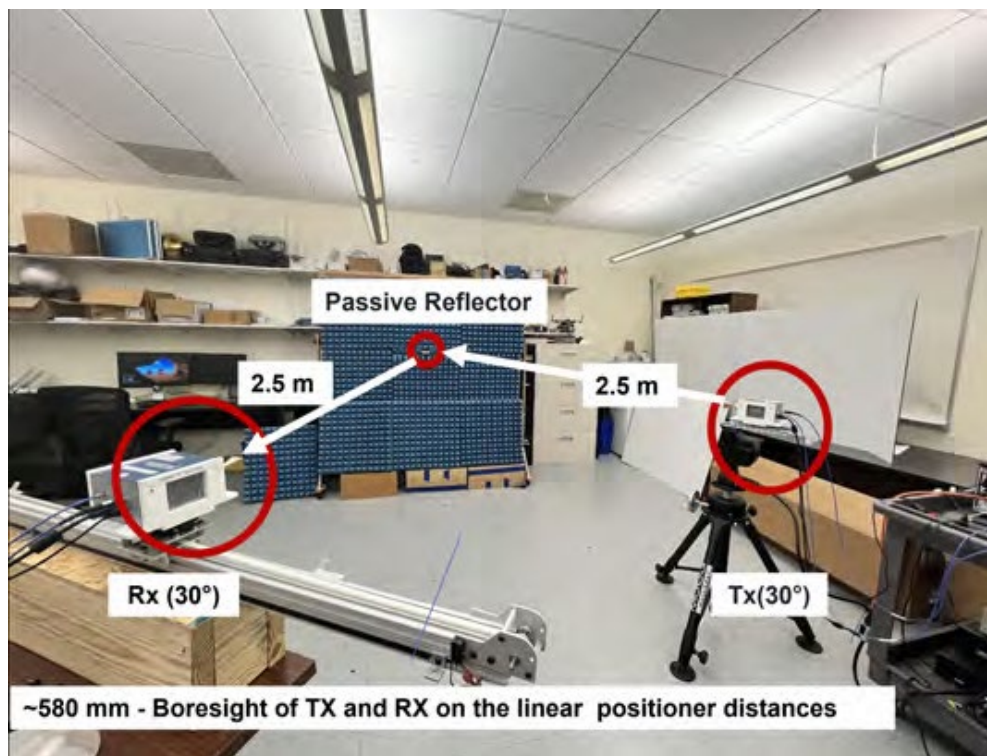


Fig. V.2.5-2: Measurement setup for evaluating reflector characteristics using a channel sounder that operates at multiple mmWave and sub-THz frequencies.

Frequency (GHz)	28	39	120
IF (GHz)	10.56	10.56	12.6
Bandwidth (GHz)	1.5	1.5	1.5
Transmitted power (dBm)	-10	-10	10
TX antenna gain (dBi)	17	20	21
RX antenna gain (dBi)	17	20	21

TABLE V.2.5-1: Measurement parameters.

2. MEASUREMENT AND SIMULATION RESULTS

In this section, measurement results for the metal and Sekisui transparent reflectors are provided. The ray-based simulation results for metal reflectors are also compared with the measurement results. After conducting the measurements using channel sounder equipment, we processed the data points obtained in Matlab and averaged them across all multipath reflections in the NLOS environment.

A. Measurement Results Analysis

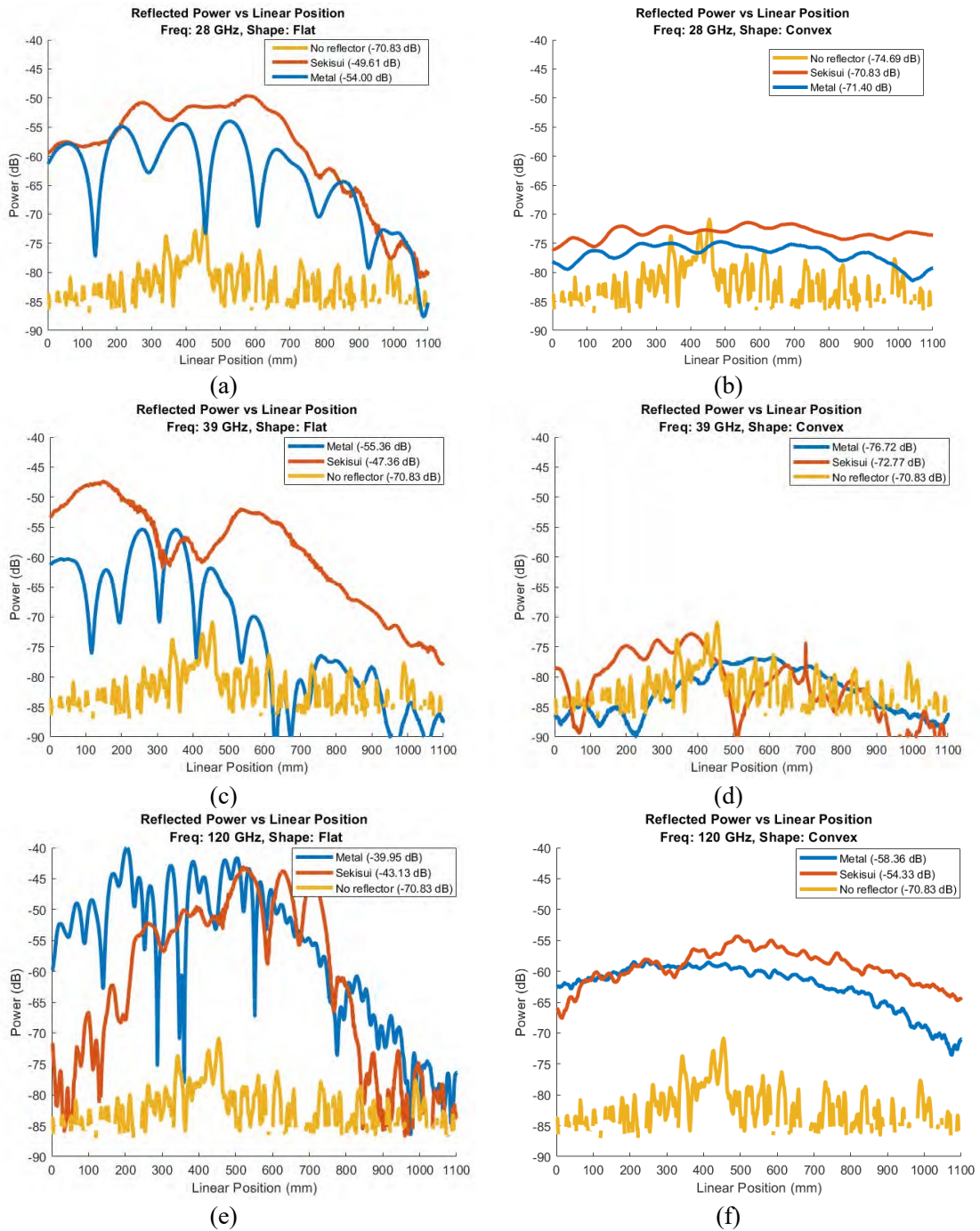
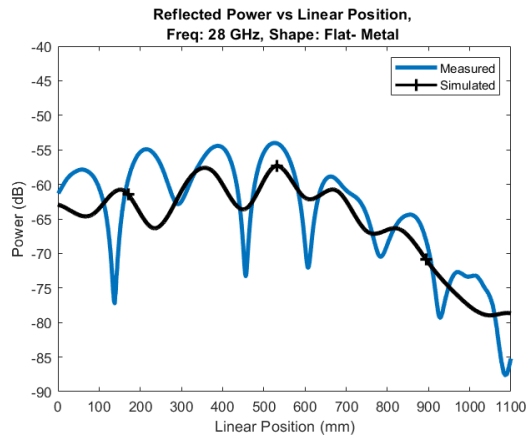
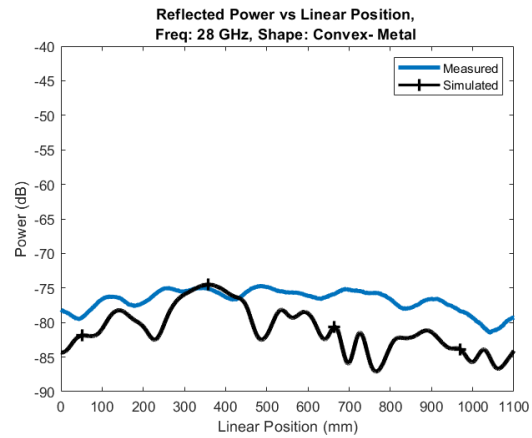


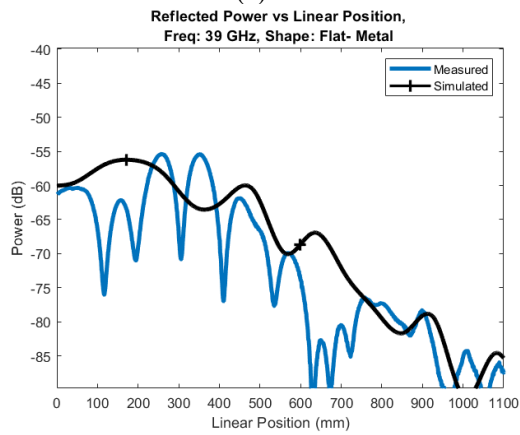
Fig. V.2.5-3: Flat and curved reflector propagation measurements at three different frequency bands.



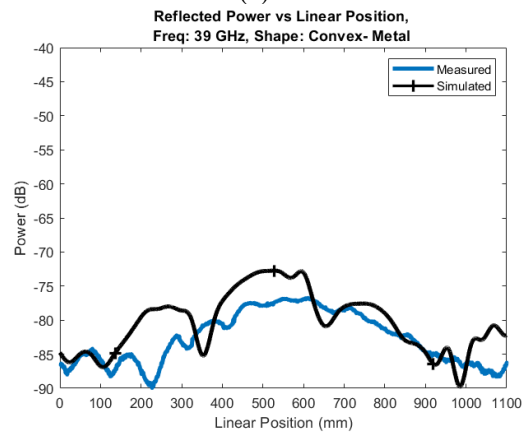
(a)



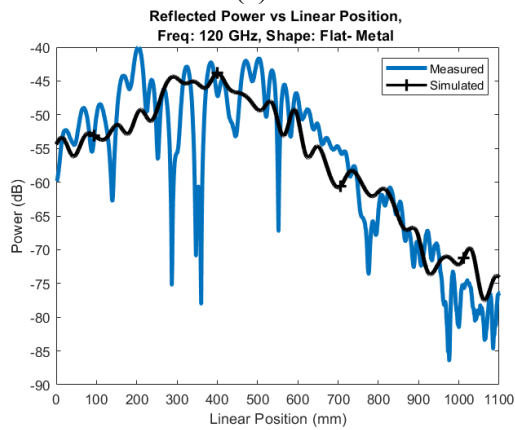
(a)



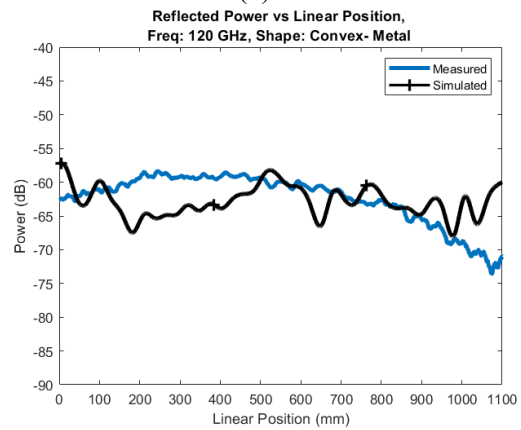
(b)



(b)



(c)



(c)

Fig. V.2.5-4: Comparison of simulation and measurement results
(reflector type: flat - metal reflector)

Fig. V.2.5-5: Comparison of simulation and measurement results
(reflector type: convex - metal reflector)

Fig. V.2.5-3 presents the reflected power versus linear position using the metal and Sekisui transparent reflector (TR). We compared the flat and curved results for maximum power received in three different scenarios namely; using metal, Sekisui TR and no reflector. The received power at 28 GHz using no reflector is -70.83 dB, metal is -54 dB and Sekisui transparent reflector is -49.61 dB. The plot shows that the Sekisui reflector outperforms the metal reflector by 1 dB in its reflection

capacity and the curve represents a smoother distribution compared to metal. In the case of metal we see, large varying fringing dips which is absent in the case of Sekisui TR. Using the curved reflector (convex), we see that reflected power distribution is now more uniformly flat reduced by nearly 20 dB. The max. reflected power we received using Sekisui transparent reflector is -70.83 dB and using metal is -71.40 dB. There's less than a 1 dB difference in the power received between the metal and Sekisui TR. The fringing properties also seem diminished in the case of convex reflectors.

Fig. V.2.5-3(c) and (d) illustrate the reflectivity properties at 39 GHz, which indicate that we get 8 dB enhanced power using Sekisui flat TR and 4 dB enhanced power using Sekisui curved reflector compared to metal. Similarly, Fig. V.2.5-3(e) and (f) denote the reflected power at 120 GHz, which follows the same trend of enhanced reflectivity properties using curved Sekisui reflectors. The curved Sekisui reflector indicates a 4dB of increase in power received compared to metal. However, there's a slight deviation in the above trend in the case of flat reflectors where Sekisui TR has 3 dB less power received than metal.

B. Comparison of Ray Tracing and Measurement Results

The simulations of the ray-based analytical model are also carried out in Matlab. The geometry, size of the reflector, transmit power, and antenna radiation pattern from the measurements are used for the simulation setup. The simulation results for the flat metal reflector of size 0.44 m×0.44 m at 28 GHz, 39 GHz, and 120 GHz are provided in Fig. V.2.5-4. The fluctuations in the received power observed are due to constructive and destructive interference of rays from different facets. The number of facets used in simulations for 28 GHz and 39 GHz is 36, whereas for the 120 GHz the number of facets is 256. A large number of facets helps to capture small power fluctuations at 120 GHz as observed during the measurements.

From Fig. V.2.5-4 it can be observed that the width of approximately half cycles due to constructive and destructive interference decreases with increasing frequency, also observed during the measurements. Furthermore, as expected, the received power is highest near the RX position where the incident and reflected ray angles are the same. It is observed the received power decreases as we move towards the RHS of the linear RX positioner. The decrease is due to an increase in the azimuth angle of the rays from the main reflection position that is 30° on the LHS from the center. The large angle of the rays in the azimuth plane results in small antenna gain and hence reduced received power (see (1)). The decrease is not significant on the LHS of the linear positioner because the reflected energy is mainly distributed at an angle of 30° towards the LHS. Overall, the simulation results for flat reflector closely agree to measurement results.

The simulation results for the convex metal reflector of size 0.44 m×0.44 m at 28 GHz, 39 GHz, and 120 GHz are provided in Fig. V.2.5-5. Compared to the flat reflector, the received power in Fig. V.2.5-5 does not change significantly on the RHS of the linear positioner. The small reduction of the received power on the RHS of the linear positioner compared to the flat reflector is due to uniform divergence of rays in the azimuth plane. Furthermore, the overall received power is smaller compared to the flat reflector. The reduced received power for the convex reflector compared to the flat reflector is due to

the higher attenuation of rays for the convex reflector. Similar to the flat reflector, fluctuations in the received power observed are due to constructive and destructive interference of the rays. The rays from curved azimuth plane at different height sections contribute to the constructive and destructive interference.

3. CONCLUDING REMARKS

In this work, we perform a comprehensive coverage analysis on the basis of extensive radio propagation experiments in an indoor NLOS environment at mmWave and sub-THz frequencies. Channel measurements are performed using passive metallic and transparent reflectors of different shapes and sizes to enhance the received power. The results reveal that flat transparent reflectors give better coverage in the NLOS region than metal reflectors, and convex reflector distributes the received power uniformly over the distance covered. The highest received power using Sekisui's transparent reflectors is nearly -40 dBm (flat reflector), -54 dBm (convex-shaped) at 120 GHz. The measurement findings for metal reflectors were contrasted with ray tracing simulations replicated with the same environment, which correlate closely to our measured results. The findings also suggest that aside from the path loss in the first order of propagation when energy spreads into the far field, THz channels are comparable to current mmWave wireless propagation channels. At 120 GHz, the transparent reflector's performance is at its peak, indicating that these reflectors may be utilized to improve wave guiding at greater sub-THz frequencies. We have fewer reflections in LOS-directed channels at these frequencies due to narrower beam antennas on both ends of the link.

REFERENCE

- [V.2.5-1] O. Ozdemir, F. Erden, I. Guvenc, T. Yekan, and T. Zarian, "28 GHz mmwave channel measurements: A comparison of horn and phased array antennas and coverage enhancement using passive and active repeaters," in Proc. IEEE SoutheastCon, Raleigh, NC, Mar. 2020, pp. 1–9.
- [V.2.5-2] C. Liaskos, S. Nie, A. Tsioliaridou, A. Pitsillides, S. Ioannidis, and I. Akyildiz, "A new wireless communication paradigm through softwarecontrolled metasurfaces," IEEE Communications Magazine, vol. 56, no. 9, pp. 162–169, 2018.
- [V.2.5-3] S. J. Maeng, C. K. Anjinappa, and Guvenc, "Coverage probability analysis of passive reflectors in indoor environments," IEEE Communications Letters, vol. 26, no. 10, pp. 2287–2291, 2022.
- [V.2.5-4] W. Khawaja, O. Ozdemir, Y. Yapici, F. Erden, and I. Guvenc, "Coverage enhancement for NLOS mmWave links using passive reflectors," IEEE Open J. Commun. Soc., vol. 1, pp. 263–281, 2020.
- [V.2.5-5] C. K. Anjinappa, A. P. Ganesh, O. Ozdemir, K. Ridenour, W. Khawaja, I. Guvenc, H. Nomoto, and Y. Ide, "Indoor propagation measurements with transparent reflectors at 28/39/120/144 ghz," in 2022 IEEE International Conference on Communications Workshops (ICC Workshops). IEEE, 2022, pp. 1118–1123.

[V.2.5-6] M. Di Renzo, A. Zappone, M. Debbah, M.-S. Alouini, C. Yuen, J. de Rosny, and S. Tretyakov, “Smart radio environments empowered by reconfigurable intelligent surfaces: How it works, state of research, and the road ahead,” *IEEE Journal on Selected Areas in Communications*, vol. 38, no. 11, pp. 2450–2525, 2020.

[V.2.5-7] “NI, mmWave transceiver system.” Date accessed: 01-26-2022. [Online]. Available: <http://www.ni.com/sdr/mmwave>

[V.2.5-8] K. Du, O. Ozdemir, F. Erden, and I. Guvenc, “Sub-terahertz and mmwave penetration loss measurements for indoor environments,” in *Proc. IEEE Int. Conf. Commun. (ICC) Workshops*, Montreal, QC, Canada, Jun. 2021, pp. 1–6.

[V.2.5-9] “Arrick robotics, xy linear positioners.” Date accessed: 06-11-22. [Online]. Available: <https://arrickrobotics.com/linear.html>

V.2.6. Reconfigurable metasurface reflector with multi sheets/sliding sheets

Keisuke Sato
DKK Co., Ltd.

Abstract — This paper focuses on passive Metasurface reflectors that can control reflected waves without requiring a power supply. Specifically, it introduces multi sheets and sliding sheets reflector. The sliding sheets reflector is based on Huygens' principle, with a cell structure that allows horizontal reflection angle adjustments by sliding sub-reflectors vertically. This changes the horizontal phase gradient and reflection angle. The Multi sheets reflector combines multiple reflectors with different reflection angles to achieve a wide beam. This report concludes these reflector technologies can meet future demands for millimeter wave communications.

1. Introduction

Metasurface reflectors have been investigated for enhancing communication area in low cost. Generally, the passive Metasurface performance is fixed due to their artificial periodic pattern structure [V.2.6-1]. This report focuses on passive Metasurface Reflectors that can control reflected waves without requiring a power supply. Specifically, we introduce two types of Metasurface Reflectors: multi sheets and sliding sheets.

2. Passive Metasurface Reflector for mmWave Band

2.1. Metasurface Reflector with Sliding Sheets

A characteristic of passive Metasurface Reflectors is that the incident and reflection angles are fixed by the grating period d of the supercell, and the reflection characteristics change when the reflector is used at an angle different from the design angle [V.2.6-2]. When used at angles other than the designed angle, the reflection characteristics change, leading to a lack of flexibility in improving received power. This limitation becomes particularly problematic in operating environments, where the installation location may restrict the ability to optimize received power in the coverage area. To solve these issues, we propose a sliding Metasurface Reflector that enables fine adjustments to the reflection angle even after installation. This approach enhances flexibility and makes it possible to improve the received power in the coverage area, even under installation constraints.

Fig. V.2.6-1 shows the concept of the prototype sliding Metasurface Reflector, while Table 2.6-1 presents specification of this Metasurface Reflector. The Metasurface Reflector is designed based on Huygens' principle [V.2.6-3]. Fig. V.2.6-1 (c) depicts the cell structure, which is periodically arrayed in both vertical and horizontal directions, along with the relative phase distribution of each unit cell. When the incident angle is fixed, the horizontal reflection angle can be adjusted by sliding each segmented sub-Metasurface Reflector vertically by an appropriate amount. This adjustment function can change the horizontal phase gradient, thereby altering the reflection angle. Fig. V.2.6-1 (d) demonstrates the sliding amounts for each sub-Metasurface. Because the phase distribution is periodic

and repeats every 2π , the sliding amount for each sub-Metasurface can be limited to within a periodic length d .

Table 2.6-1 Specification of Metasurface Reflector with Sliding Sheets

Frequency Band	28GHz (N257)
Polarization	Dual pol. (V/H pol.)
Design of Incident Angle	Azimuth = 0° Elevation = 20°
Design of Reflection Angle	Azimuth = 45° Elevation = 0°
Size of Metasurface Reflector	$187.56 \times 192.08 \text{ mm}$
PCB	FR4($t=1.0$, $\epsilon_r=4.5$)

Fig. V.2.6-2 shows the electromagnetic field analysis and the measured angular characteristics of the Radar Cross Section (RCS). Table V.2.6-2 summarizes the angles corresponding to the RCS peak values shown in Fig. V.2.6-2.

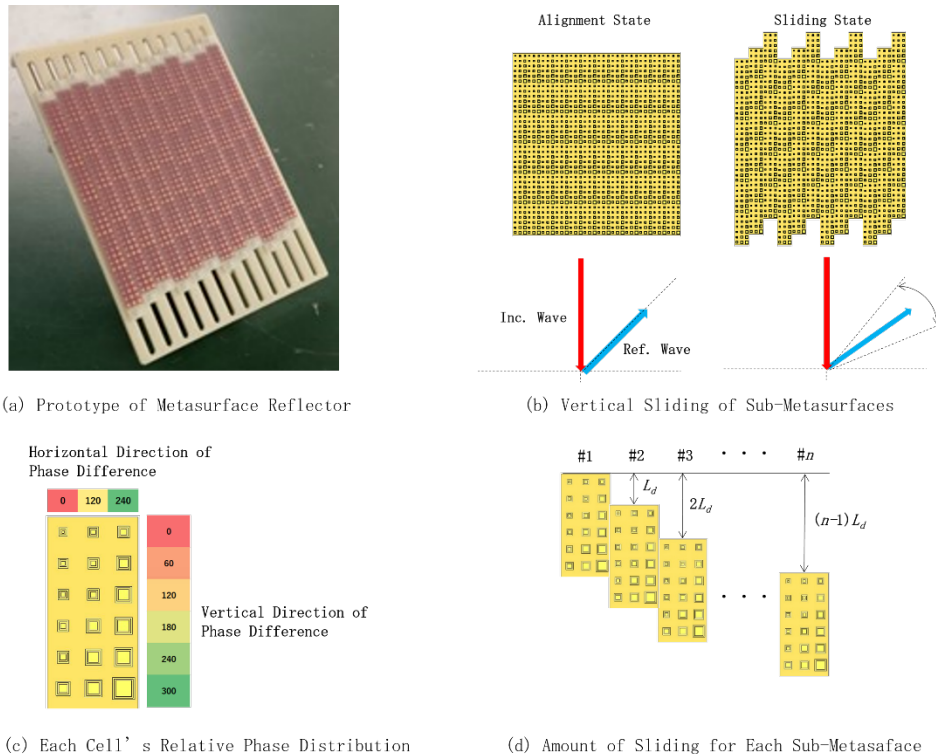


Fig. V.2.6-1 Concept of Metasurface Reflector with Sliding Sheets

When comparing the results, it is observed that at shallow angles (Fig. V.2.6-1(a), Fig. V.2.6-1 (c)), the reflection angles align well with the desired values. However, at deep angles (Fig. V.2.6-1 (b), Fig. V.2.6-1 (d)), unnecessary modes may appear in the peak direction. As the amount of sliding increases, characteristic degradation occurs due to phase discontinuities between sub-Metasurfaces and coupling effects caused by surface waves. Despite these limitations, the system allows for fine-tuning of the

reflection angle after installation, provided the amount of sliding is appropriately managed to maintain optimal performance.

Table V.2.6-2 Reflection Angle for Vertical Sliding (Peak Direction)

Amount of Sliding L_d	Variable to Shallow Angle		Variable to Deep Angle	
	Simulation (Fig. 2(a))	Measurement (Fig. 2(c))	Simulation (Fig. 2(b))	Measurement (Fig. 2(d))
w/o slide	41.7°	41.6°	41.7°	41.6°
2 mm	38.5°	38.2°	45.0°	45.0°
4 mm	35.5°	35.0°	48.5°	49.0°
6 mm	32.6°	32.0°	52.2°	53.0°
8 mm	29.7°	29.2°	56.4°	57.2°
10 mm	27.0°	26.4°	60.9°	61.6°
12 mm	24.3°	23.6°	65.9°	68.0°
15.63 mm (Half Length of Period)	19.6°	21.0°	19.6°	21.0°

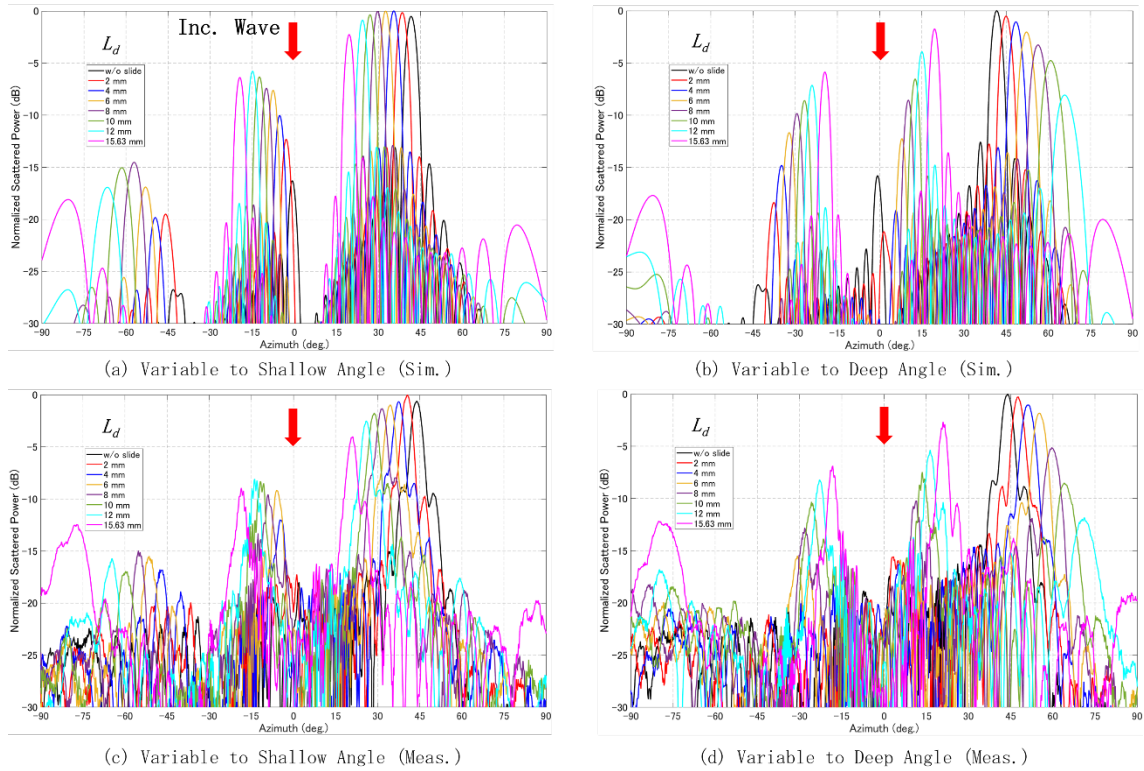


Fig.V.2.6-2 RCS pattern of Metasurface Reflector with Sliding Sheets

2.2. Realize wide reflection beam by Multi-sheet Metasurface Reflector

In previous section, we described a reflector that changes the relationship between the incident and reflection angles by sliding the Metasurface Reflector element [V.2.6-4]. On the other hand, when using millimeter waves for mobile communications, a wide coverage area is required. In order to compensate for the large propagation loss in the millimeter wave band, high-gain antennas are used. But the coverage is limited due to the narrow beam width [V.2.6-5]. Therefore, this Multi-Sheet

Metasurface Reflector [V.2.6-6] takes advantage of the fact that by combining multiple reflectors with different reflection angles, the synthesized reflection pattern has a wide beam.

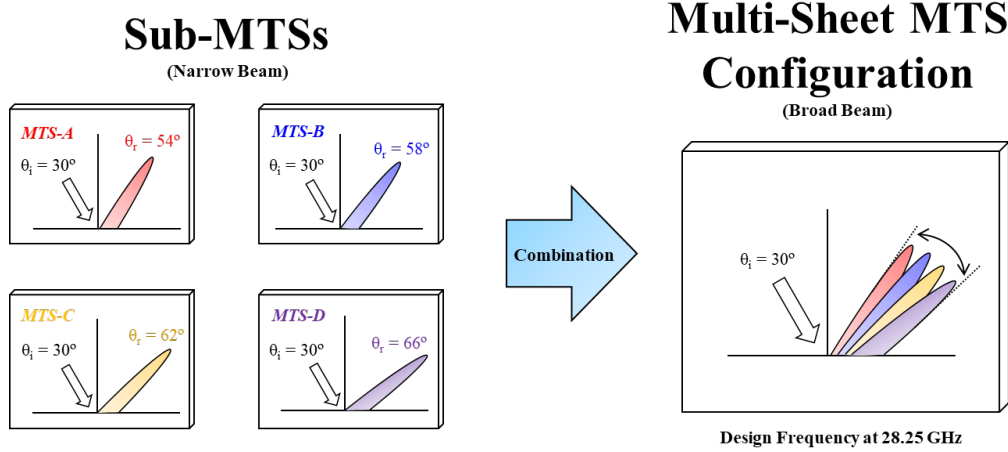


Fig. V.2.6-3 Concept of Multi-Sheet Metasurface Reflector

In the example below, the incident direction θ_i is 30° and the reflection direction θ_r is 60° . In order to widen the beam width in the reflection direction, four types of reflectors with reflection angles θ_A to θ_D were designed. Each has a different reflection angle and dimensions [V.2.6-7], as shown in Table 2.6-1. Different reflection angles can be achieved by changing the phase rotation period by setting the number of reflective elements that make up the reflector and the reflection phase. A wide-angle reflection directivity can be obtained by arranging these four reflectors with different reflection angles side by side.

The analysis results from the electromagnetic field simulation are shown in Fig. V.2.6-5. The incident plane wave is reflected according to the set angle of each reflector, and the synthesis directivity is spread horizontal plane.

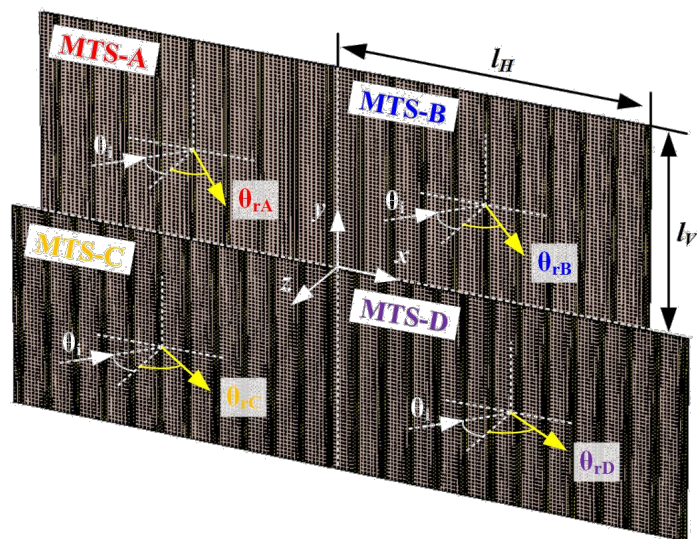


Fig. V.2.6-4 Configuration of Multi-Sheet Metasurface Reflector

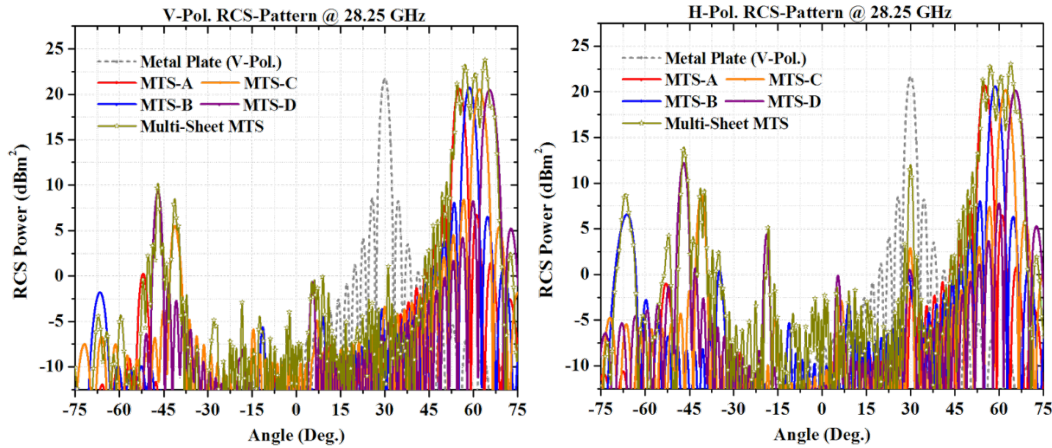


Fig.V.2.6-5 Simulation Result RCS scattering pattern of Multi-Sheet Metasurface Reflector

For the actual measurement evaluation, outdoor propagation experiments were conducted using an experimental station. A 90° NLOS environment was prepared, and the reflector was installed between the base station and the measurement area. To confirm the spread of power after reflection, RSRP measurements were performed using an area scan, and evaluation was performed using received power mapping and CDF. For comparison, measurements were also performed using a metal reflector that reflects normally, and when no reflector was installed. Horn antennas were used for both the transmitting (Tx) and receiving (Rx) antennas for the measurements to reduce the effects of multipath.

The measurement results are shown in the circles in Fig. V.2.6-6. Points shown in red indicate low RSRP, and points shown in green indicate high RSRP. The received power is high around the Metasurface Reflector installation point because direct waves come from the Tx antenna. On the other hand, when a metal plate was installed, an improvement in received power was seen on the center line from the metal reflector, but no improvement was seen outside. In measurements using Multi-sheet Metasurface Reflector, the points shown in yellow made up most of the measurement area, confirming that received power had improved over a wide area.

The cumulative distribution function (CDF) of various measurement results is shown in Fig. V.2.6-7. From these results, the degree of improvement in RSRP is large when using a multi-sheet reflector.

3. Conclusion

In this paper, we have described two types of Metasurface Reflectors that can contribute to expanding the coverage area in mmWave band. These can use without power supply and can be installed anywhere. We propose this as one of the technologies that can meet the future demand for millimeter wave communications.

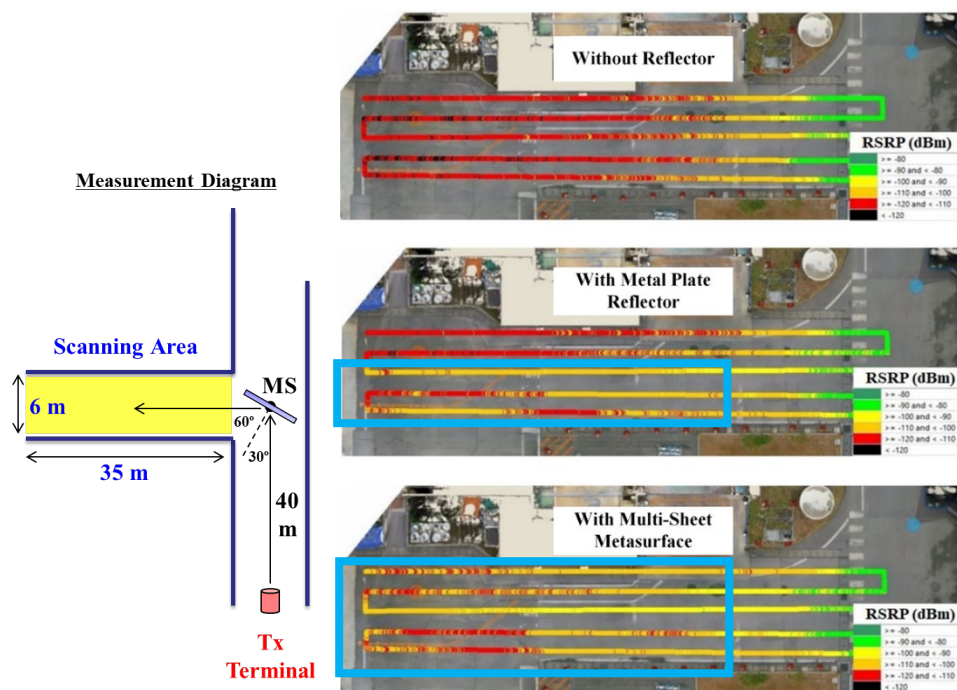


Fig. V.2.6-6 Coverage Area Measurement each type of Reflector

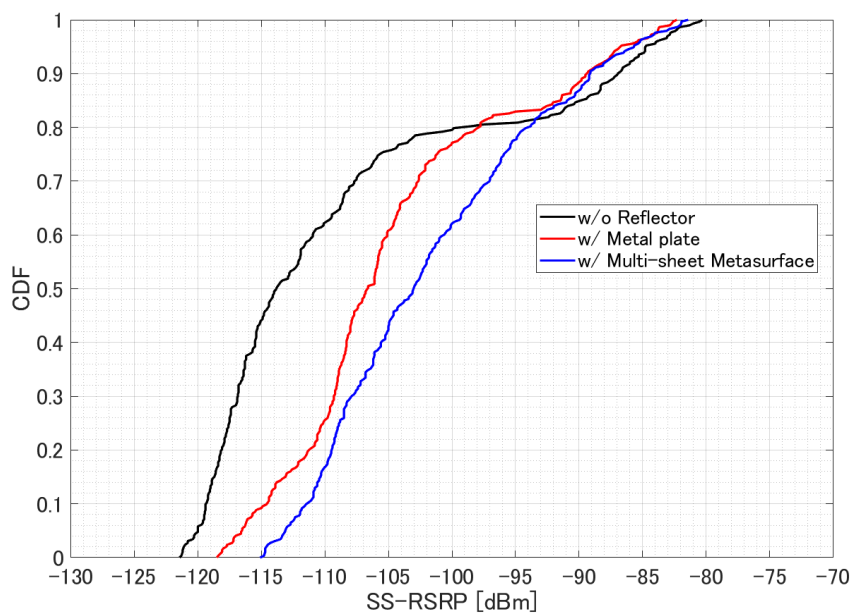


Fig.V.2.6-7 Received Power (RSRP) Improvement Effect Inside the Measurement Area

REFERENCE

- [V.2.6-1] A. Díaz-Rubio, V. S. Asadchy, A. Elsakka, and S. A. Tretyakov, "From the generalized reflection law to the realization of perfect anomalous reflectors." *Science advances* 3.8, 2017.
- [V.2.6-2] W. Khawaja, O. Ozdemir, Y. Yapici, F. Erden, and I. Guvenc, "Coverage Enhancement for NLOS mmWave Links Using Passive Reflector," *IEEE Open Journal of the Communications Society*, vol. 1, pp. 263-281, Jan. 2020.
- [V.2.6-3] A. M. H. Wong, and G. V. Eleftheriades. "Perfect Anomalous Reflection with a Bipartite Huygens' Metasurface." *PHYSICAL REVIEW X Phys Rev X* 8, 2018.
- [V.2.6-4] N. Yu, P. Genevet, M. A. Kats, F. Aieta, J.-P. Tetienne, F. Capasso, and Z. Gaburro, "Light Propagation with Phase Discontinuities: Generalized Laws of Reflection and Refraction," *Science*, vol. 334, Iss. 6054, pp. 333-337, Oct. 2011.
- [V.2.6-5] T. Hongnara, Y. Shirasawa, T.Sasaki, K.Sasaki, K.Sato, I. Oshima., "Dual-polarized broad-beam reflective metasurface based on multi-sheet configuration for local 5G application at 28.25 GHz." 2021 15th European Conference on Antennas and Propagation (EuCAP). IEEE, 2021.
- [V.2.6-6] T. Hongnara, T. Sasaki, K. Sasaki, K. Sato, I. Oshima, N. Michishita, H. Nakabayashi, and K. Cho, "Dual-Polarized Reflective Metasurface Based on Cross-Shaped Resonator for 5G Wireless Communication Systems at 28 GHz," in *Proc. 2019 Int. Symp. Ant. Propag. (ISAP)*, X'ian, China, 2019.
- [V.2.6-7] C. A. Balanis, *Aperture Antenna, in Antenna Theory Analysis and Design*, John Wiley & Son, 2005.

GROUP D -- RIS/IRS (programmable)

- V.2.7 An efficient beam searching in hybrid intelligent reflecting/refracting surfaces (IRS)-aided mmWave 6G network (Tohoku Univ., Kyocera)
- V.2.8 Relay-related technologies in new radio network topology (NTT, DOCOMO)
- V.2.9 Beamforming-based IRS control for Sub-Terahertz-band communications in indoor office environments (Hokkaido Univ.)
- V.2.10 Beam squint-aware frequency resource allocation for IRS-aided communication (Tohoku Univ., NTT)
- V.2.11 Prototype and evaluation of intelligent reflecting surface for 60 GHz band (PSNRD, Tohoku Univ.)
- V.2.12 Experimental evaluation of impact of intelligent reflecting surface for 60 GHz band on radio channel in Sub-6 GHz band (ATR, Tohoku Univ.)
- V.2.13 Performance evaluation of RIS-empowered 6G system by system-level and link-level simulations (DOCOMO)
- V.2.14 Liquid crystal RIS : development and field trial (KDDI)
- V.2.15 Multishape radio and its experimental studies using OAM, Airy, and Bessel beams in Sub-THz bands: RIS perspective on beam manipulation (NTT)

V.2.7. An efficient beam searching in hybrid intelligent reflecting/refracting surfaces (IRS)-aided mmWave 6G network

Shikhar Verma, Yuichi Kawamoto, Nei Kato

Tohoku University

Takahiro Saiwai, Masamichi Yonehara

KYOCERA Corporation

Abstract— Hybrid Intelligent Reflective/Refractive Surfaces (HIRS) are devices that can reflect or refract radio waves in any direction by adjusting their elements and are expected to solve indoor and outdoor coverage challenges in high frequency bands. This paper investigates a hierarchical beam-sweeping (HBS) approach tailored for HIRS-assisted millimeter-wave networks, aiming to pinpoint user locations with reduced overhead.

1. Introduction

Most of the studies related to IRS-assisted wireless communications assume that the IRS can reflect only one side, which limits the coverage of users located on the same side of the IRS [V.2.7-1], [V.2.7-2], [V.2.7-3]. Limiting their applicability in scenarios requires bidirectional coverage, such as indoor-outdoor environments. To address this limitation, Hybrid Intelligent Reflecting/Refracting Surfaces (HIRS) have emerged as a compelling solution. As shown in Fig. V.2.7-1, HIRS combines reflective and refractive techniques to serve users on both sides of the surface, thereby offering enhanced versatility and coverage [V.2.7-4], [V.2.7-5].

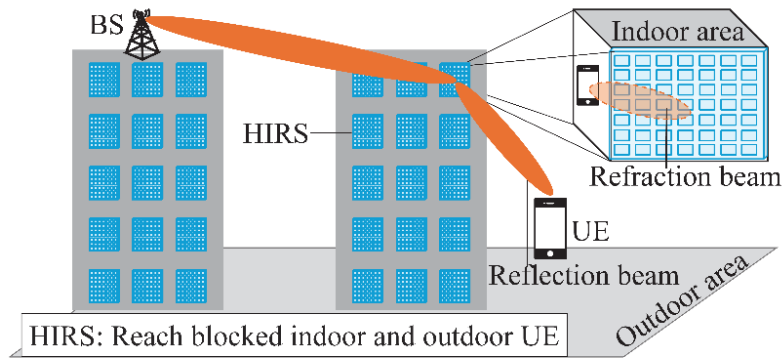


Fig. V.2.7-1. Consider scenario of HIRS-aided mmWave 6G network

HIRS has great potential, it needs to search for users in both reflective and refracting areas, and it may not be possible to search for users within the allowable beam search time. In this paper, we consider hierarchical beam sweeping (HBS) for HIRS-aided millimeter wave networks, aiming to detect all users within the beam search time.

2. System model

First, we explain HIRS- aided HBS and then explain the challenges of HBS.

2.1. HBS HIRS-aided HBS

Initially, base stations (gNBs) conduct a coarse search by emitting Synchronization Signal Block (SSB) frames with wider beams, as shown in Fig. V.2.7-2. In an IRS-assisted system, users directly communicate with gNBs receive these wider beams, while the IRS reflects beams for users not in direct contact. The IRS accomplishes this by mirroring the beam across its coverage area, maintaining the same width but redirecting it as instructed by the gNB. As outlined in [V.2.7-6], the IRS utilizes a beam expansion method to create different beam widths using phase shifts of IRS elements.

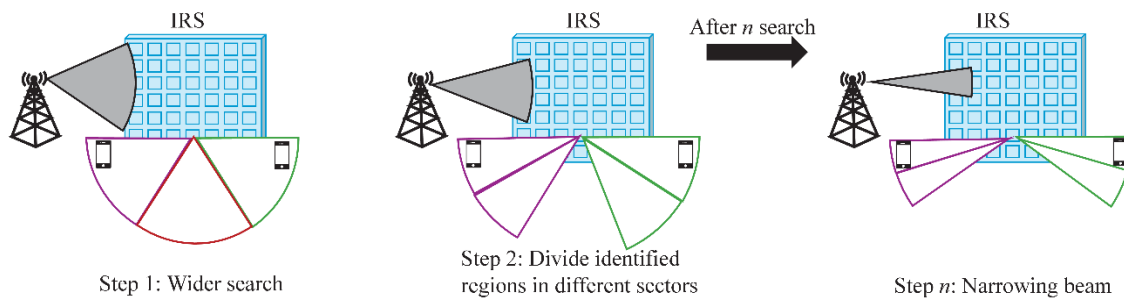


Fig. V.2.7-2. HBS method using IRS

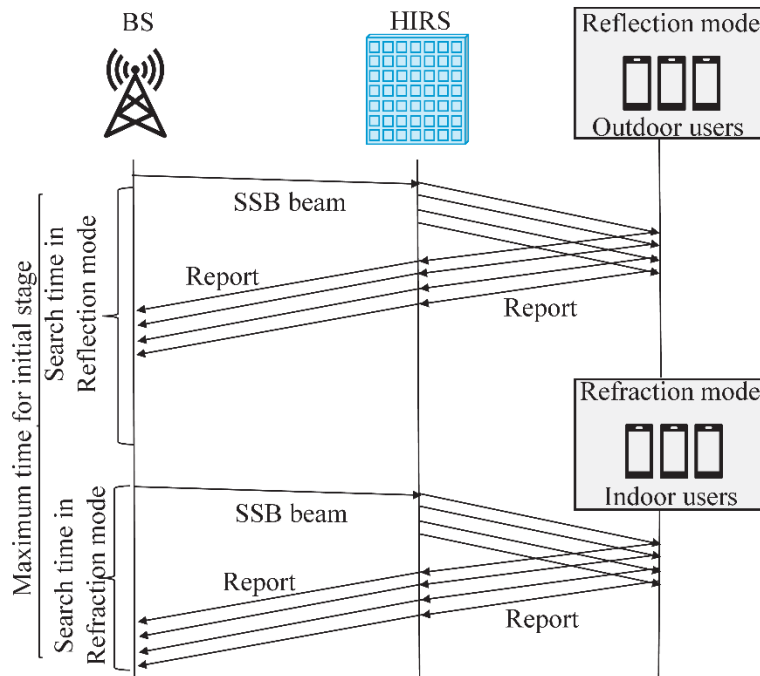


Fig. V.2.7-3. Process of the initial stage of HBS in HIRS

Similarly, HBS can be adapted for HIRS systems. However, the beam searching process is performed one mode at a time, focusing on either reflection or refraction. The gNBs initiates beam search by

sending a beam, and the HIRS reflects or refracts it to each incident SSB frame over a broader area. The outdoor or indoor space is divided into various angular subareas as per gNB's instructions, and the phase shift of HIRS is adjusted to achieve an angular beam width for each subarea using the beam expansion method. UEs monitor all SSB beams from different directions facilitated by HIRS and select the beam with the strongest signal strength. Subsequently, the UE transmits a PRACH to the location associated with a specific SSB beam ID through HIRS to the gNB. The detailed process of the initial step of HBS using HIRS is depicted in Fig. V.2.7-3. After the initial exploration, the base station undertakes a beam refinement process where HIRS reflects or refracts the beam refinement signals in different directions, generating narrower beam widths. The HIRS operates in one mode at a time, transitioning to another mode after completing beam searching in the current mode. The HBS method is employed to reduce beam searching time by segmenting the search space into distinct levels or stages, rather than exhaustively exploring all possible beam directions.

2.2. HBS problem

Due to the base station sending multiple SSB frames to users, including one to the HIRS, a challenge arises in communicating with all users under the IRS coverage. This can result in unequal search times between direct BS-UEs and BS-IRS-UEs, potentially leading to insufficient time to search users within IRS coverage and total beam search time. Moreover, the HBS method is typically lengthy owing to having numerous coarse steps starting with broader beam widths at the lowest detectable SNR, gradually narrowing down with increasing SNR. Despite dividing the search time between BS-UEs and BS-IRS-UEs, the lengthy hierarchical approach may not adequately explore both areas of HIRS, comprising different user densities and coverage areas.

In this paper, we propose commence the beam search at the initial stage with a beam width close to the optimal beam pairs of UEs, ensuring maximum SNR at the initial stage to avoid several steps of having lower SNR.

3. Proposed approach

The indoor and outdoor optimal beam width (W_{in}, W_{out}) that maximizes the total SNR (SNR_{total}) of all indoor and outdoor UEs within the HIRS coverage is calculated. However, since the number of UEs (N_{in}, N_{out}) is unknown before the beam search stage, it is estimated to use past communication data. The SNR (SNR_{in}, SNR_{out}) depends on the beam width-dependent transmission gain from HIRS and the distance from HIRS. For the distance from HIRS, the maximum distance (r_{in}, r_{out}) indoors and outdoors is used based on past UE location information.

The beam search time is the sum of the indoor (BST_{in}) and outdoor (BST_{out}) beam sweep times (BST) and must be less than or equal to the beam sweep time given in the SSB frame. In addition, the beam range ($-\alpha$ to α) is limited by the HIRS hardware limitations. Furthermore, the SNR ($SIN_{edge}^i, SOUT_{edge}^j$) of indoor beam i and outdoor beam j received at the edges of the indoor and outdoor areas must exceed a threshold (S_{th}).

The objective function and constraints defined above are shown below.

$$\begin{aligned}
& \text{Maximize: } E[SNR_{total}] \\
& = \frac{E[SNR_{in}(W_{in}) \times N_{in} + E[SNR_{out}](W_{out}) \times N_{out}]}{N_{total}}
\end{aligned}$$

Subject to:

Constraint 1: $BST = BST_{in}(W_{in}) + BST_{out}(W_{out})$

Constraint 2: $-\alpha \leq \phi_{in}^i, \phi_{out}^j \leq \alpha$

Constraint 3: $SINR_{edge}^i(W_{in}, r_{in}), SOUT_{edge}^j(W_{out}, r_{out}) \geq S_{th}$
where $i \in (1, NB_{in}), j \in (1, NB_{out})$

By optimizing the above objective function, we can obtain the optimal indoor and outdoor beamwidths that maximize the total SNR of all indoor and outdoor UEs within the HIRS coverage. For a detailed description of the optimization method, refer to [V.2.7-7].

4. Performance analysis

In this section, we perform simulations to demonstrate the effectiveness of the proposed approach.

4.1. Parameter settings

Table 1 provides detailed parameter settings for simulating our proposed initial step of HBS using HIRS. Users are uniformly and randomly distributed within the indoor and outdoor coverage area. Based on these settings, we run the simulations 1000 times to find the total average SNR.

TABLE V.2.7-1. Parameter Settings

Parameter	Value
Maximum beam sweep time	1.473 ms
Each beam sweep time	0.0357 ms
Range of W_{in} , W_{out}	1° to 120°
Range of ϕ_{out} and ϕ_{in} (α)	-60° to 60°
Number of IRS elements	6400
IRS element spacing	wavelength/2
Transmission power from BS	35 dBm
Noise	-90.96 dBm
Carrier frequency	28 GHz
Total number of users	30
Number of indoor users	5 to 25
Number of outdoor users	5 to 25
Indoor area size	40 m to 150 m (gap: 10 m)
Outdoor area size	30 m to 150 m (gap: 10 m)
SNR threshold (SSB minimum SNR level) [V.1.7-8]	-8.47 dB
Base station-HIRS distance	100m
Number of simulations	1000

4.2. Simulation results

We compare the proposed approach with an approach where maximum beam search time is equally allocated between indoor and outdoor areas.

We vary the outdoor area size from 50 to 150m with a gap of 10m, while the indoor area size remains constant at 50m, and both indoor and outdoor user counts are set to 15. The comparison results are

depicted in Fig. V.2.7-4, where it is evident that the proposed approach consistently provides higher total average SNR compared to the comparison approach. In Fig. V.2.7-5, we analyze the proposed approach and the comparison approach for varying numbers of indoor and outdoor users, with fixed indoor and outdoor area sizes set to 100m. Across different user counts, our proposed approach consistently yields higher total average SNR compared to the comparison approach.

These analyses underscore the adaptability of the proposed approach to dynamic changes in the indoor and outdoor environment, ensuring optimal beam widths to maximize the total average SNR within the maximum beam search time.

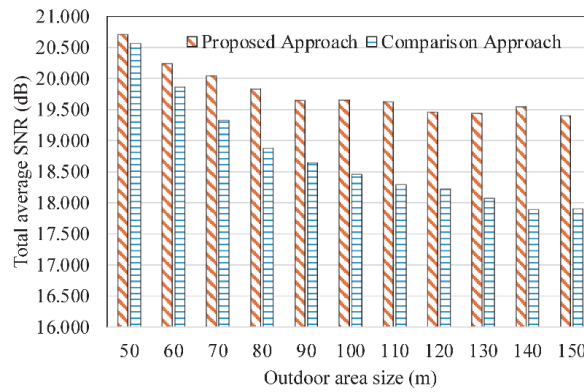


Fig. V.2.7-4. Analysis of proposed and comparison approach with varying outdoor area sizes (50m to 150m) and fixed indoor area size of 50m, with 15 indoor and 15 outdoor users.

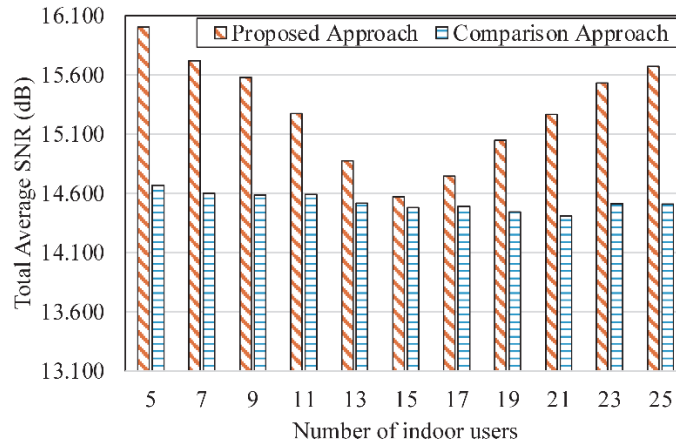


Fig. V.2.7-5. Analysis of the proposed and comparison approach, with varying numbers of indoor users, and fixed area sizes of 100m.

5. Conclusion

This paper investigates a hierarchical beam-sweeping (HBS) approach tailored for HIRS-assisted millimeter-wave networks, aiming to pinpoint user locations with reduced overhead. We proposed a method to ensure high SNR for all users within the maximum allowed beam search time. Recognizing

the dynamic nature of indoor and outdoor environments, we introduce a novel method to optimize beam width allocation based on the environment at the start of the beam searching process. We validate the effectiveness of our approach through numerous simulations.

REFERENCE

- [V.2.7-1] Y. Pan, K. Wang, C. Pan, H. Zhu and J. Wang, "Sum-Rate Maximization for Intelligent Reflecting Surface Assisted Terahertz Communications," in *IEEE Transactions on Vehicular Technology*, vol. 71, no. 3, pp. 3320-3325, March 2022.
- [V.2.7-2] A. Sirojuddin, D. D. Putra and W. -J. Huang, "Low-Complexity Sum-Capacity Maximization for Intelligent Reflecting Surface-Aided MIMO Systems," in *IEEE Wireless Communications Letters*, vol. 11, no. 7, pp. 1354-1358, July 2022.
- [V.2.7-3] D. Badheka, J. Sapis, S. R. Khosravirad and H. Viswanathan, "Accurate Modeling of Intelligent Reflecting Surface for Communication Systems," in *IEEE Transactions on Wireless Communications*, vol. 22, no. 9, pp. 5871-5883, Sept. 2023.
- [V.2.7-4] H. Zhang et al., "Intelligent Omni-Surfaces for Full-Dimensional Wireless Communications: Principles, Technology, and Implementation," in *IEEE Communications Magazine*, vol. 60, no. 2, pp. 39-45, February 2022.
- [V.2.7-5] S. Zeng et al., "Reconfigurable Intelligent Surfaces in 6G: Reflective, Transmissive, or Both?," in *IEEE Communications Letters*, vol. 25, no. 6, pp. 2063-2067, June 2021.
- [V.2.7-6] R. Hibi, Y. Kawamoto and N. Kato, "Standalone-Intelligent Reflecting Surface Control Method Using Hierarchical Exploration by Beamwidth Expansion and Environment-Adaptive Codebook," in *IEEE Transactions on Vehicular Technology*, vol. 72, no. 9, pp. 11990-12000, Sept. 2023.
- [V.2.7-7] S. Verma, Y. Kawamoto, N. Kato, T. Saiwai and M. Yonehara, "An Efficient Beam Searching in Hybrid Intelligent Reflecting/Refracting Surfaces (IRS)-Aided mmWave 6G Network," in *IEEE Transactions on Vehicular Technology*, vol. 73, no. 12, pp. 19299-19312, Dec. 2024, doi: 10.1109/TVT.2024.3450914.
- [V.2.7-8] 3GPP TSG RAN WG1 #103, e-Meeting, October 26th – November 13th, 2020, Agenda item: 8.8.1.2, Source: Nokia, Nokia Shanghai Bell, Title: Baseline coverage evaluation of UL and DL channels – FR2, Document: R1-2008702.

V.2.8. Relay-related technologies in new radio network topology

Daisuke Murayama, Riku Ohmiya, Tomoki Murakami

NTT Corporation

Kenta Goto, Satoshi Suyama

NTT DOCOMO, INC.

Abstract— The New radio network topology (NRNT) in beyond fifth-generation (B5G) mobile network is a crucial concept for the efficient utilization of high-frequency bands, including millimeter and terahertz waves. To realize NRNT, additional technical studies and experimental evaluations are essential, particularly concerning the integration of relay nodes, including reconfigurable intelligent surface (RIS). This paper presents two experimental results conducted in indoor environments. The first experiment examines the reception power improvement achieved by developing RIS. The second experimental assess the environmental resistance resulting from the application of network topology control, which includes the integration of relay nodes.

1. Introduction

As a technological concept transitioning from Beyond 5G to 6G, the NRNT has been proposed. This concept aims to enhance radio access performance and reduce power consumption by increasing links between Transmission Reception Points (TRP), such as base station (BS) antennas, mobile terminals (MT), and relay nodes, including RIS [V.2.8-1]-[V.2.8-4]. Additionally, traditional wireless network topologies designed on a single-cell basis are evolving into a novel configuration where large and small cells are superimposed. The NRNT brings several advantages, including expanded coverage and line-of-sight (LOS) areas, improved resistance to shielding, capacity expansion through increased multiple input multiple output (MIMO) space multiplexing, and more.

In real-world environments, the topology dynamically changes based on factors such as the environment, situation, and service demand. Therefore, control systems must exhibit adaptability to temporal fluctuations. This paper introduces relay-related technologies currently under research and development. Furthermore, we present experimental demonstrations showcasing the reception power improvement achieved by implementing RIS and the resistance to environmental changes achieved through network topology control in indoor environments, contributing to the realization of the NRNT concept.

2. Experimental Evaluation of Received Power Improvement Effect

This section introduces angular profile experiments using a 28 GHz band channel sounder and presents their results to elucidate the improvement effect on reception power when RIS are installed in indoor environments. Figure V.2.8-1 depicts the layout of the experimental environment at the NTT

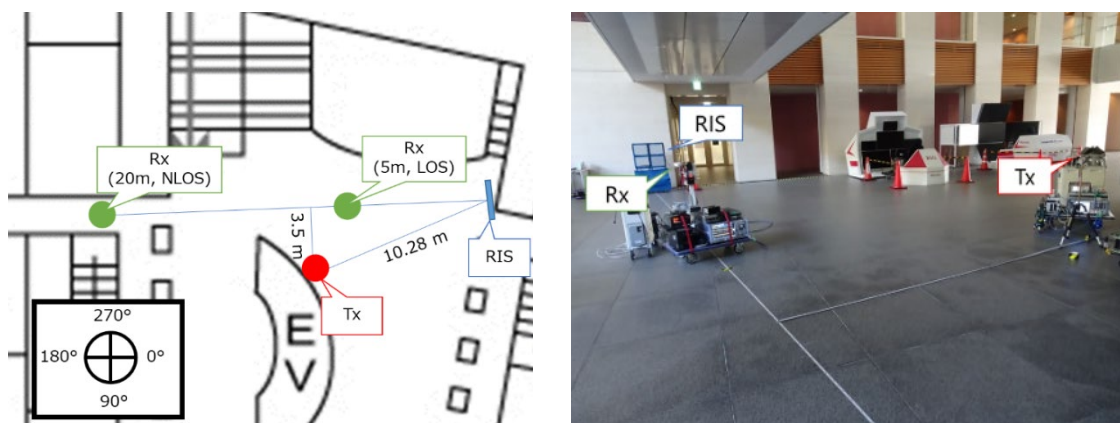


Fig. V.2.8-1 Experimental environment

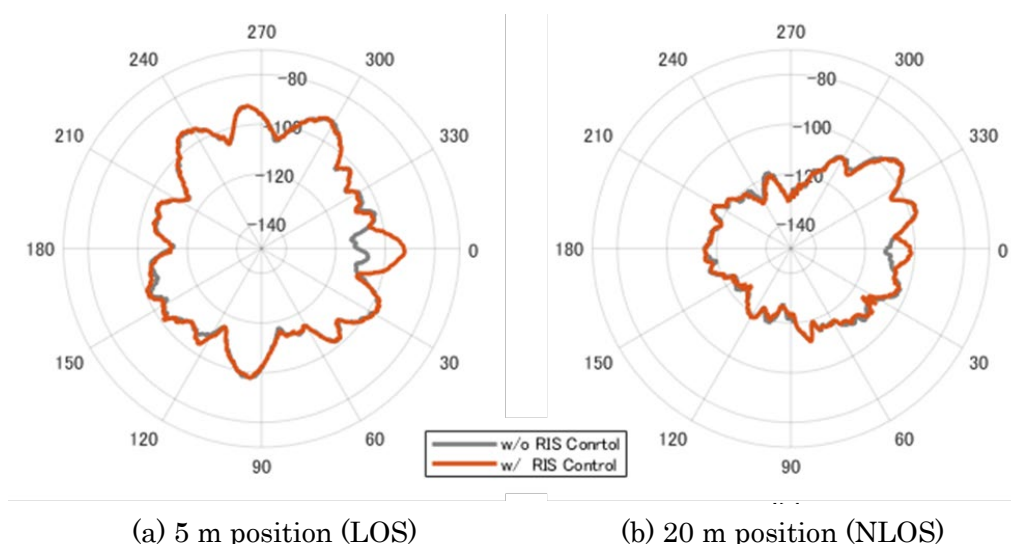


Fig. V.2.8-2 Angle profiles

DOCOMO R&D Center and includes a photograph for reference. In this setup, the positions of the transmitter and RIS were fixed, while the receiver was installed in LOS and non-LOS (NLOS) conditions. The distance from the RIS to the receiver was set at 5 m and 20 m, respectively. We conducted measurements of angular profiles at each receiver position with the RIS configured to reflect signals in the receiver's direction. The measurement specifications are detailed in Table V.2.8-1.

Figure V.2.8-2 illustrates the measured angular profile in the environment. In the LOS condition, RIS control substantially enhanced the reception power at the receiver by approximately 20 dB. Similarly, in the NLOS environment, RIS control led to an improvement of around 11 dB in the reception power at the receiving station. Consequently, even in a multipath indoor propagation environment, significant enhancement in reception power can be achieved by dynamically adjusting the RIS based on the receiver's position. Furthermore, since RIS control has the potential to contribute to the expansion of area coverage, promising practical applications can be anticipated in the future.

Table. V.2.8-1. Experimental specifications

Center frequency	27.6 GHz
Bandwidth	200 MHz
Transmit power	37 dBm (5 W)
Transmit antenna (gain)	Omni (3.5 dBi)
Receive antenna (beam width, gain)	Horn (10 deg., 24.6 dBi)
Height of transmitter	1 m
Height of receiver	1 m
Height of RIS	1 m

3. Experimental Evaluation of Fast Design and Control Techniques for Wireless Network Including Relay Nodes

NRNT networks that use multiple relay nodes have many candidates for available relay node locations and directions. A huge amount of calculation is required to automatically derive an area design that combines multiple relay nodes. For this reason, it was difficult to realize control that updates the network topology as the environment changes. Therefore, we devised a method to derive the sub-optimal placement independently for each cluster using a clustering method based on unsupervised machine learning. This method avoids the explosion in the number of placement combinations to be evaluated and enables fast derivation of network design. The procedure is shown below.

- (1) Search for base station placement(s) that maximize the number of evaluation points that satisfy the required quality at the base station only, without considering the placements of relay nodes.
- (2) Using the base station placement derived in (1), eliminate from the candidates relay node(s) placement(s) that do not result in reception quality higher than the threshold value.
- (3) Cluster the evaluation points for which the required quality was not satisfied by the base station placement derived in (1) with the same number of relay nodes to be used, using the kmeans++ method.
- (4) Search for the relay node placements that maximize the number of evaluation points that satisfy the required quality independently for each cluster calculated in (3).
- (5) If the ratio of evaluation points satisfying the overall required quality is above the threshold value, the process is terminated, and if it is below the threshold value, the process is re-derived by increasing the number of relay nodes by one.

An area quality evaluation was conducted in a shielded room at NTT Yokosuka R&D Center by creating an environment with a lot of shielding that was simulated as an indoor logistics warehouse through experiments. We assumed an environmental change from two rows of $1.24 \text{ m} \times 6.75 \text{ m} \times 2.5 \text{ m}$ shields to four rows in an $11.8 \text{ m} \times 21.8 \text{ m} \times 2.6 \text{ m}$ shielded room. This area was covered by a local 5G base station in the 28 GHz band connected to a WiGig AP in the 60 GHz band as a regenerative relay station. Figure V.2.8-3 shows the network configuration and Fig. V.2.8-4 shows the measurement scenery. Figure V.2.8-5 (a)-(d) show color maps of the measured throughput at each evaluation point. Before the environmental change, the configuration without any repeaters in (a)

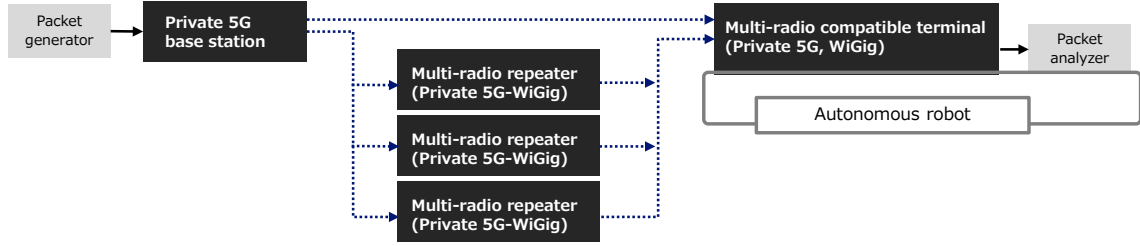


Fig. V.2.8-3 Network Configuration



Fig. V.2.8-4 Measurement scenery

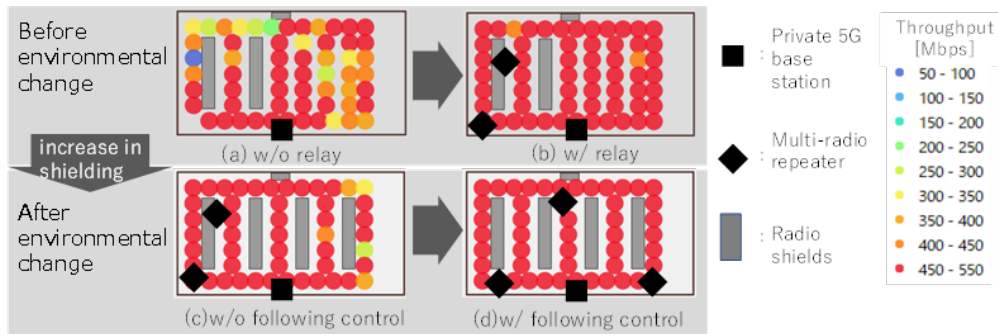


Fig. V.2.8-5 Experimental results (throughput maps)

could not cover the entire area with high quality, but the quality of the entire area could be improved by using a relay station as shown in (b). After the environmental change, the quality of some areas decreased without the control (redesign) in (c), but with the control (redesign) in (d) using this algorithm, the quality of all areas was maintained. The computation time was reduced to about $1/5.5 \times 10^{-8}$ under the present experimental conditions (896 candidate base station locations and 1776 candidate relay station locations), compared to the method that compares and evaluates all combinations. The above shows that the proposed algorithm can maintain high area quality while updating the area design to follow changes in the environment.

4. Conclusion

We presented experiments aimed at assessing the impact of RIS on enhancing received power and evaluating tolerance to environmental changes through network topology control, crucial aspects for the realization of NRNT. In the RIS evaluation experiment, we demonstrated the dynamic alteration of the indoor propagation environment through effective RIS control. Additionally, in the network topology control experiments, we illustrated that a highly flexible network topology can facilitate rapid design derivation and control. Integrating these technologies, we aim to actualize NRNT-based networks during the 5G Evolution era.

REFERENCE

- [V.2.8-1] NTT DOCOMO INC., “White Paper 5G Evolution and 6G (Version 5.0),” 2023.
https://www.docomo.ne.jp/english/corporate/technology/whitepaper_6g/.
- [V.2.8-2] S. Suyama, M. Iwabuchi and T. Yamada, “New Radio Network Topology for 5G Evolution and 6G,” Journal of IEICE, vol.106, No.9, pp.808-815, Sep. 2023.
- [V.2.8-3] NTT Corporation, NTT DOCOMO INC., “NTT and NTT DOCOMO Trial First Use of User-tracking Metasurface Reflector for Extreme Mobile Coverage in Current 5G and Coming 6G Era Will enable high-speed millimeter-wave communications indoors,”
<https://group.ntt/en/newsrelease/2021/11/12/211112b.html>
- [V.2.8-4] I. Masashi, et al. "Intelligent radio-wave design: Distributed intelligent reflecting surface with direction-based control for millimeter-wave communications," IEICE Proceedings Series 63, IA2-2, 2020.

V.2.9. Beamforming-based IRS control for Sub-Terahertz-band communications in indoor office environments

Yasutaka Ogawa, Toshihiko Nishimura, Takeo Ohgane

Hokkaido University

Satoshi Suyama

NTT DOCOMO, INC.

Abstract—Using a sub-Terahertz band, we can achieve extreme high-speed communications required by Beyond 5G/6G systems. For transmission to user equipment (UE) behind an obstacle, we can employ intelligent reflecting surfaces (IRSs). According to propagation measurements in the band, we have only a few multipath components in indoor office environments. This leads to an IRS control method based on beamforming because the number of radio waves outside the optimum main beam is very small, and power that is not used for transmission from the IRS to UE is little. We apply beams generated by a Butler matrix or a DFT matrix. Simulation results show that the proposed method reveals good performance.

1. Introduction

A sub-Terahertz (THz) band is expected to play a great role in Beyond 5G/6G systems to achieve extreme high-data-rate communications. Radio waves in a sub-THz band are, however, hard to propagate behind an obstacle due to large diffraction losses. Intelligent reflecting surfaces (IRSs) can solve the propagation problem. In this paper, we investigate IRS control based on beamforming. An IRS has a set of beams. A base station (BS) sends pilot symbols, and for a different pilot, the IRS changes the beam. User equipment (UE) measures the received power for each beam, and informs the BS of the beam that provides the largest received power. The BS controls the IRS so that it can use the optimum beam providing the maximum power at the UE. This method does not need either channel state information or phase optimization. It is easy to determine the phases of the IRS. However, the

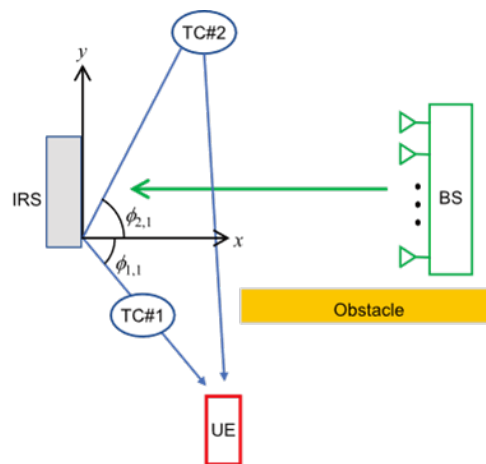


Fig. V.2.9-1. An IRS-assisted wireless network (Top view).

performance depends on environments where it is deployed. When we have only a few multipath

components in the environment, the method will work very well because the number of multipath components outside the optimum main beam is small, and power that is not used for transmission from the IRS to UE is little. According to [V.2.9-1], the total number of observed multipaths at 140 GHz is small in office environments. It is expected that the IRS based on beamforming works well in sub-THz bands. In this paper, we evaluate the performance using the sub-THz-band channel model proposed in [V.2.9-2].

2. Beamforming-Based IRS Control

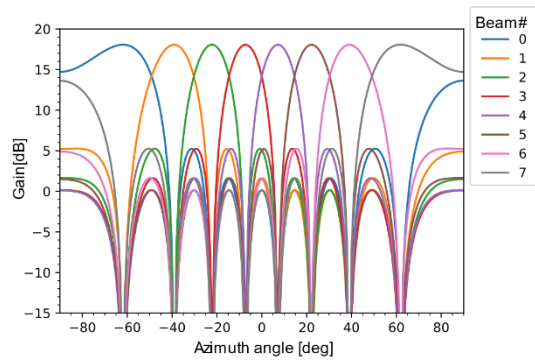
This section clarifies IRS control based on beamforming treated in this paper. Figure V.2.9-1 depicts the top view of a system model discussed here. Note that its multipath environment is an example. In the figure, we have two time clusters (TCs) and one subpath per TC. We express azimuth angle as φ . The direct path from the BS is blocked by an obstacle, and the UE is in a non-line-of-sight environment. The IRS reflects the incident radio waves toward the UE that has a single antenna. The IRS consists of $Q \times Q$ reflecting elements with half-wavelength spacing, where Q is a power of 2.

We have four sets of beams, and call them codebooks in this paper. The codebooks are defined as follows:

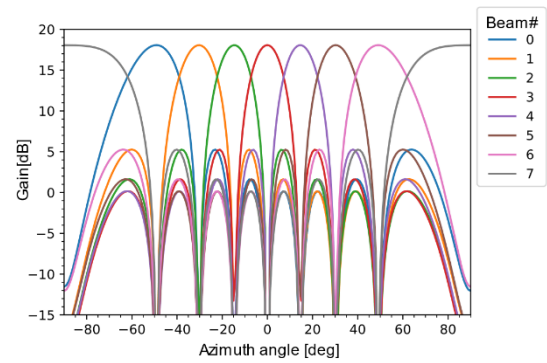
1. Codebook BB consisting of Q^2 beams formed by phases of a Butler matrix for both the azimuth and the elevation directions
2. Codebook DB consisting of Q^2 beams formed by phases of a DFT matrix for the azimuth direction and phases of a Butler matrix for the elevation direction
3. Codebook BD consisting of Q^2 beams formed by phases of a Butler matrix for the azimuth direction and phases of a DFT matrix for the elevation direction
4. Codebook DD consisting of Q^2 beams formed by phases of a DFT matrix for both the azimuth and the elevation directions

The reason why we use the four codebooks will be clarified later. It should be noted that we do not have either Butler matrix circuits or DFT matrix circuits. Phases realized by those circuits are given to phase-shift devices.

The beam patterns in the azimuth domain are shown in エラー! 参照元が見つかりません。 for codebooks BB and DB, where $Q = 8$ and elevation angle -7.2° . Since we have 64 elements, the maximum gain is 18 dB. Note that we assume that each IRS element works as an isotropic antenna with 0 dBi gain. From the figures, we see that the gain at angles where two beams cross each other is about 14 dB. This means that if we use a single codebook, we have about 4 dB degradation in the worst case. Furthermore, it is seen that beams of one codebook have the maximum gain around angles where beams of the other codebook have the lowest value, and that beams of both codebooks help each other. The degradation is reduced to about 1 dB. This is the reason why we use both the Butler matrix and DFT matrix codebooks. We have stated the azimuth case so far, but the situation is the same also for the elevation. Thus, we have BB, DB, BD, and DD in all. The four codebooks improve



(a) Codebook BB.



(a) Codebook DB.

Fig. V.2.9-2 Beam patterns in the azimuth domain for codebooks BB and DB.

$Q = 8$ and elevation angle -7.2° .

the performance comparing with the single codebook BB. In the next section, it will be shown that the performance of the four codebooks is much better than that of the single codebook BB.

Now, we explain the IRS control in more detail. The BS sends pilot symbols. Each symbol has L equal-amplitude components at equal frequency intervals in a communication band. We choose the beam that maximizes the received power. The reason why we use multiple frequency points is because we want to choose the beam that maximizes the received power in frequency-selective fading environments due to multipath delay.

Table V.2.9-1. Simulation parameters.

Frequency range [GHz]	140 ~141
Number of IRS elements, $Q \times Q$	8×8
Number of frequency points in each pilot symbol, L	11
Number of trials	1000

3. Simulations

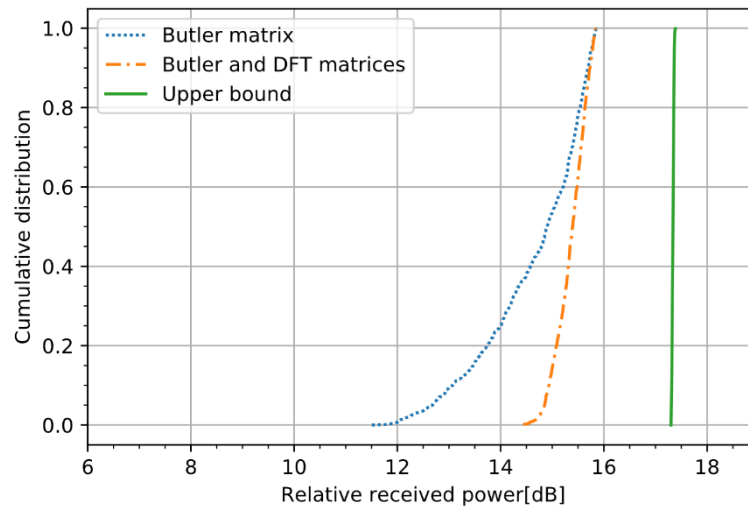


Fig. V.2.9-3 Cumulative distributions of relative received power for 3-path case

We evaluated the performance of the IRS based mainly on the channel model proposed in [V.2.9-2]. The main simulation parameters are listed in Table V.2.9-1. We examined two cases of multipath propagation, where the number of multipath components is 3 and 6. Refer to [V.2.9-1] for detail simulation parameters.

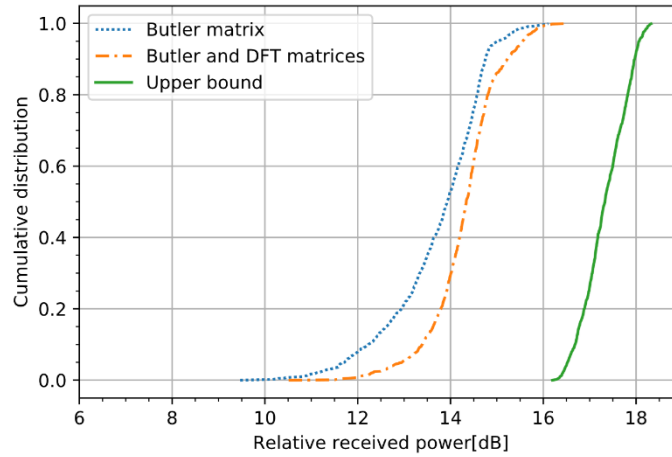


Fig. V.2.9-4 Cumulative distributions of relative received power for 6-path case

Now, we present simulation results. We conducted 1000 trials changing the azimuth angles of departure, elevation angles of departure, and multipath phases. Figure V.2.9-3 and V.2.9-4 show the cumulative distributions of relative received power for 3-path and 6-path cases, respectively. The legends are defined as follows:

“Butler and DFT matrices” is the distribution for the beamforming method using the four codebooks proposed in the previous section.

“Butler matrix” is that using the single codebook BB.

“Upper bound” is the distribution of received power in a case where we could optimize the IRS phases for all the L frequency points.

We see from these figures that the performance of 3-path scenario (fewer-multipath case) is better than that of 6-path one (more-multipath case). The reason for this has been stated in Section 1. For the 3-path case, the degradations of the proposed four-codebook method from the upper bound are only 1.98 dB and 2.56 dB at the cumulative distributions of 50 % and 5 %, respectively. We think that those degradations are small. Even when we have as many as 6 multipath components, the degradations are less than 4 dB. From these results, we can say that the proposed method is useful for IRS control in sub-THz bands.

4. Conclusion

IRSs enable to realize communications overcoming the propagation problem in sub-THz bands. Since the number of multipath components is small in the band, we have proposed the IRS control based on beamforming that is realized by phases of a Butler or DFT matrix. This method can avoid difficult channel estimation and phase optimization problems. Simulation results have shown that it reveals good performance in the sense that the received power is not so lower than the upper bound value.

REFERENCE

- [V.2.9-1] Y. Ogawa, S. Tadokoro, S. Suyama, M. Iwabuchi, T. Nishimura, T. Sato, J. Hagiwara, and T. Ohgane, “Smart radio environments with intelligent reflecting surfaces for 6G sub-Terahertz-band communications,” *IEICE Trans. Commun.*, vol. E106-B, no. 9, pp. 737–747, Sept. 2023.
- [V.2.9-2] S. Ju, Y. Xing, O. Kanhere, and T. S. Rappaport, “Millimeter wave and sub-Terahertz spatial statistical channel model for an indoor office building,” *IEEE J. Sel. Areas Commun.*, vol. 39, no. 6, pp. 1561–1575, June 2021.

V.2.10. Beam squint-aware frequency resource allocation for IRS-aided communication

Hiroaki Hashida, Ei Tanaka, Yuichi Kawamoto,

Tohoku University

Masashi Iwabuchi, Riku Omiya, Yoghitha Ramamoorthi, Tomoki Murakami,

NTT Corporation

Abstract—An intelligent reflecting surface (IRS) is a device that reflects radio waves in any direction by setting the phase shift of the reflecting elements. This is expected to solve the problems of high-frequency band communications, such as vulnerability to obstacles, and realize super-multiplex connections in the high-frequency band. Considering the reflective elements of the IRS can only be time-division controlled and can support only one user per time slot, it is highly likely that a large number of resource blocks will be allocated to a single user to perform communication. However, in such a scenario, the frequency efficiency is reduced because of the effect of the beam squint. In this paper, we demonstrate the effectiveness of a method proposed to increase the frequency efficiency by optimizing the reflection direction through resource allocation and IRS phase control.

1. Introduction

To support sixth generation (6G) ultra-high-speed and high-capacity communications, attention has been focused on high-frequency bands capable of utilizing a wide frequency range. However, high-frequency bands are more susceptible to diffraction and blockage by obstacles than low-frequency bands. Intelligent reflective surfaces (IRS) offer a plausible solution to this problem [V.2.10-1]. IRS is a device that integrates a large number of reflective elements in a planar fashion, each of which is capable of controlling the amplitude and phase of the incident signal. By incorporating IRS into the network and intelligently controlling the reflections, problems in the high-frequency band can be effectively solved [V.2.10-2]–[V.2.10-4]. By their nature, IRS can only perform time-division control and generally support only one user per time slot. Therefore, when multiple users are supported by the IRS, the communication request of one user should be satisfied in a small number of timeslots; therefore, a large resource block (RB) is allocated to one user for communication. However, in such a scenario, the frequency efficiency is reduced because of the beam squint effect [V.2.10-5] [V.2.10-

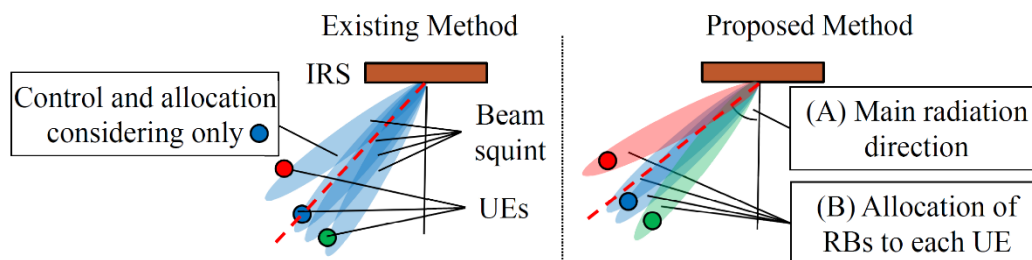


Fig. V.2.10-1. Illustrative representation of existing method and proposed method.

6]. In this paper, we propose an IRS control and frequency allocation scheme that effectively uses a beam squint to maximize the frequency efficiency of the IRS.

2. What is Beam Squint?

Beam squint refers to a phenomenon in which the direction of reflection of an IRS changes based on its frequency of incidence. The misalignment of the reflection direction caused by the beam squint is expressed by (1).

$$\sin\theta = \left(1 - \frac{f_c}{f}\right)\sin\theta_{in} + \frac{f_c}{f}\sin\theta_c \quad (1)$$

where f_c and θ_c denote the center frequency and its reflection direction, respectively, θ_{in} denotes the angle of the radio wave incident on the IRS, and f , θ denotes the frequency incident on the IRS and its reflection direction.

3. Control Parameters of Proposed Method

We propose an IRS control and frequency allocation scheme for multiple user equipments (UEs) that makes effective use of a beam squint to maximize the frequency efficiency of the IRS. Therefore, the proposed method is effective for communicating with multiple UEs. From (1), the direction of reflection θ at a given frequency f depends on the variables θ_c and f (θ_{in} is a constant that indicates the angle of incidence from the base station (BS) to the IRS). Specifically, as shown in Fig. , the direction in which reflection control should be applied needs to be considered as well as which RBs should be assigned to UEs based on the misalignment of the reflection directions for each RB. The existing method allocates all available RBs to one UE, and the main radiation direction is perfectly directed to the UE. In other words, by optimizing the following two parameters, the beam squint can be effectively utilized and the frequency efficiency of communication through the IRS can be maximized. The two parameters are as follows: (A) the main radiation direction controlled by the phase of the IRS and (B) the allocation of RBs to UEs. (A) changed θ_c in (1). For (B), f changes based on which RB and UE is assigned determines the angle of presence θ_{UE} of the UEs and the direction of reflection θ of the assigned RB. (When $\theta_{UE} = \theta$, the IRS has the maximum gain for the UE.) The proposed method determines (A) and (B) to maximize (capacity of all UEs)/(bandwidth) in an environment with multiple UEs. In this study, (A) is treated as a discrete value with 0.1-degree

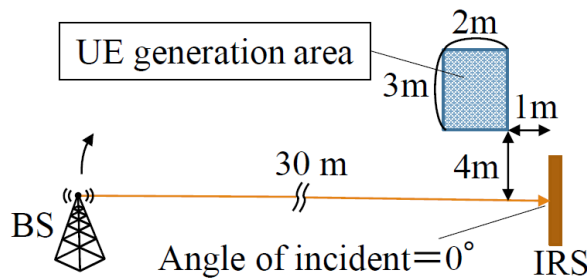


Figure V.2.10-2. Simulation environment.

increments, and both (A) and (B) are determined by brute force to demonstrate the upper performance limit of the proposed method.

4. Performance Evaluation

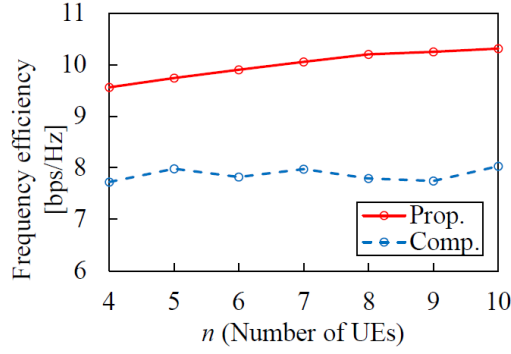


Fig. V.2.10-3. Frequency efficiency per number of UEs

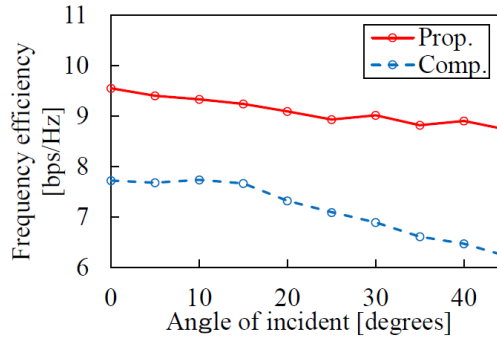


Fig. V.2.10-4. Frequency efficiency with respect to angle of incident

4.1. Environment

In this evaluation, the environment shown in Fig. V.2.10-2 was verified. n UEs were generated in the UE generation area in a uniform distribution. Ten RBs were randomly selected from 268 RBs available at 28 GHz. The available RBs were randomly selected from 10 of the 268 RBs available for communication in the 28 GHz. It was assumed that the direct waves reaching the UEs from the BS were completely blocked by obstacles, as shown in Fig. V.2.10-2. The antenna gains of the BS and UE were set to 0 dBi because the performance of the BS and UE antennas was not relevant in this simulation. We verify the effectiveness of the proposed method by comparing it with the existing method of IRS time-division communication. Specifically, the available RBs were randomly selected from 10 of the 268 RBs assigned to the UE closest to the IRS, and the main radiation direction of the IRS was set to the direction of the UE's presence. The evaluation index indicates the frequency efficiency [bit per sec (bps)/Hz] of the communication for n UEs. In this study, the heights of BS, IRS, and UEs were assumed to be equal, and only the direct path between BS and IRS and the direct path between the IRS and UEs are considered without considering the path reflected from the ground or obstacles.

4.2. Results

The results of the simulation evaluation of the environment described in the previous section are presented in Figs. V.2.10-3 and V.2.10-4. Figure V.2.10-3 shows the results when the number of UEs n is varied. Figure V.2.10-4 shows the results when the BS is moved upward in Fig. V.2.10-2, and the angle of the radio wave incident on the IRS is varied from 0° . Each plot represents the average of 100 simulations. This is because randomness exists in the generation of UEs and the available RBs. First, Fig. V.2.10-3 shows that the proposed method becomes more dominant as the number of UEs n increases. This is because as the number of UEs increases, the probability of the existence of UEs that can gain more by beam squinting increases. Fig. V.2.10-4 shows that when the angle of incidence of the radio wave incident from the BS to the IRS changes and the IRS controls the reflection to an angle farther from the specular reflection, the proposed method shows stable performance, whereas the performance of the comparative method deteriorates. This is because as shown in (1), the comparative method is more susceptible to the negative effects of the beam squint, because the beam shift from one RB to the other increases as the angle of incidence changes.

5. Conclusion

Beam squint negatively affects existing IRS control methods. In this paper, by optimizing the IRS reflection direction control and resource allocation, a beam squint was effectively utilized to increase the frequency efficiency of IRS-based communications. It was demonstrated that the proposed method is more effective in environments with dense UEs and high beam squint.

REFERENCE

- [V.2.10-1] M. Agiwal, A. Roy, and N. Saxena, "Next generation 5G wireless networks: A comprehensive survey," *IEEE Commun. Surveys Tuts*, vol. 18, no. 3, pp. 1617-1655, 3rd Quart. 2016.
- [V.2.10-2] R. Hibi, Y. Kawamoto and N. Kato, "Standalone-Intelligent Reflecting Surface Control Method Using Hierarchical Exploration by Beamwidth Expansion and Environment-Adaptive Codebook," *IEEE Transactions on Vehicular Technology*, vol. 69, no. 5, pp. 3313-3351, May 2021.
- [V.2.10-3] H. Hashida, Y. Kawamoto, and N. Kato, "Intelligent reflecting surface placement optimization in air-ground communication networks toward 6G," *IEEE Wireless Communications*, vol. 72, no. 9, pp. 11990-12000, Sept. 2023.
- [V.2.10-4] Y. Liang et al., "Large Intelligent Surface/Antennas (LISA): making reflective radios smart," *Journal of Communications and Information Networks*, vol. 4, no. 2, pp. 40-50, June 2019.
- [V.2.10-5] E. Tanaka, Y. Kawamoto, N. Kato, M. Iwabuchi, R. Ohmiya, and T. Murakami, "Exploiting Reflection Direction Variation for Phase Control in Multiple Simultaneous IRS Links," *2023 IEEE 97th Vehicular Technology Conference*, Florence, Italy, 2023.
- [V.2.10-6] E. Tanaka, Y. Kawamoto, N. Kato, M. Iwabuchi, Y. Ramamoorthi, T. Murakami, "Frequency Resource Allocation for IRS-aided Communication using Beam Squint Approach," *2024 IEEE 21th Consumer Communications & Networking Conference (CCNC 2024)*, Las Vegas, NV, USA, Jan. 2024.

V.2.11. Prototype and evaluation of intelligent reflecting surface for 60 GHz band

Hiroyuki Uno, Hiroyuki Uejima, Hirofumi Kosaka, Ken Katsurashima

Panasonic System Networks R&D Lab. Co., Ltd.

Ryuhei Hibi, Yuichi Kawamoto

Tohoku University

Abstract— Intelligent Reflecting Surface (IRS) is gaining recognition as a new technology component to realize B5G/6G. It enables to manipulate the phase shift of the incident wave, thereby providing control over the propagation of electromagnetic waves. This paper outlines a prototype IRS for 60 GHz band, the analyzed results by the electromagnetic simulation, and the results of characterization experiments developed by this research group.

1. Introduction

Commercial services for the 5th generation mobile communication system (5G) have been launched in Japan since 2020, and B5G/6G, the next generation mobile communication system, is currently being considered toward the further advancement of communication services [V.2.11-1]. For B5G/6G, the use of millimeter wave bands and sub-terahertz bands, which are higher than microwave bands and quasi-millimeter wave bands used in 5G, is being considered to achieve further high-speed and high-capacity communications. These high-frequency bands have the feature that strong rectilinear propagation and large propagation loss have less chance of going around to the back of shielding objects such as buildings compared as microwave bands used in conventional mobile communication systems, and thus the communication range becomes significantly narrow. Therefore, this problem is a major issue to be considered for achieving the realization of the future B5G/6G.

As one of the methods to solve such problems, the utilization of intelligent reflecting surface (IRS) has garnered interest, and its research and development have been actively carried out [V.2.11-2]-[V.2.11-4]. The IRS is a reflector consisting of a planar array of microscopic structures called meta-surface. By changing the reflective properties of each unit-cell forming the meta-surface, the direction of reflection of radio waves incident on the IRS can be controlled in the desired direction. The IRS enables radio waves from base stations to reach users while avoiding shielding, thereby contributing to the expansion of areas where a good communication environment can be provided.

Various IRSs using switching devices, liquid crystals, and so on have been proposed [V.2.11-5] [V.2.11-6], however, there are few research examples corresponded to millimeter wave bands. In this paper, we introduce the design and results of the characterization experiment of the prototype IRS using the 60 GHz band, which our research group has developed based on various studies [V.2.11-7]. The choice of 60 GHz band was determined by the operating frequency of the radio equipment used for wireless communication tests and is also intended to verify the applicability to millimeter waves and sub-terahertz waves that will be used in future B5G/6G.

The rest of this paper is organized as follows. The design of the prototype IRS and the results of reflection characteristics using electromagnetic (EM) simulation are introduced in Section 2. Section 3 shows the experimental results. Finally, we offer our conclusion in Section 4.

2. Design and Simulation of Prototype IRS

2.1. Configuration

Fig. V.2.11-1 shows the overall configuration of the prototype IRS. Our designed IRS consists of the IRS board and the electrical control board. In Fig. V.2.11-1, the meta-surface formed by 6,400 unit-cells is equivalent to the phase control block of the IRS board. A unit-cell is composed of reflective element and PIN diode, and the ON/OFF state of each PIN diode is controlled by the MCU block in the electrical control board. By optimizing the ON/OFF control of PIN diodes, the direction of reflection of radio waves incident on the IRS board can be controlled.

2.2. EM Simulation Model

The EM simulation model of the IRS board is shown in Fig. V.2.11-2. The IRS board is composed of numerous unit-cells that arranged in reticular pattern on the +Z side plane of the dielectric substrate as shown in Fig. V.2.11-2 (a) and can control the reflection direction by adequately setting the reflection phase of each unit-cell. The EM simulation is performed with 256 elements due to work station performance. Figure V.2.11-2 (b) illustrates the unit-cell that composed of linearly polarized

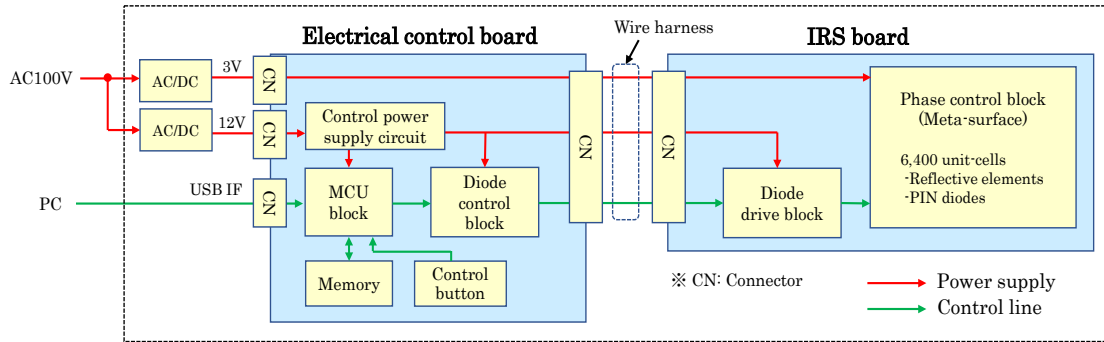


Fig. V.2.11-1 Overall configuration of prototype IRS.

reflective element with side length of L_p and height of T_l , dielectric substrate, stub via, choke stub, and PIN diode. The dielectric substrate is used R-5775 (Panasonic), and its relative permittivity (ϵ_r) and loss tangent ($\tan \delta$) are set to 3.55 and 0.005 respectively in the simulation. The length of stub via is determined to optimize the reflection phase and the choke stub is formed to prevent the RF signal of 60 GHz from entering the control bias line. The PIN diode, which is used MA4AGFCP910 from M/A-COM, is changed ON state or OFF state by supplying a DC bias (V_d) and a control voltage (V_c), thereby be able to switch the reflection phase of the unit cell to either 0 degree or 180 degrees.

2.3. EM Simulation Results

2.3.1. Reflection Phase of Unit-cell

Figure V.2.11-3 shows the simulation model and results for the reflection phase of unit-cell. Figure V.2.11-3 (a) is the simulation model of the reflection phase, and Fig. V.2.11-3 (b) is the simulated reflection phase as a function of frequency. This simulation uses CST studio suite's the finite element method (FEM), with the lateral boundaries of the unit-cell set as periodic boundary condition. The PIN diode is modeled as lumped parameter elements and its equivalent circuit for 60 GHz band is extracted from S-parameters. The ON state is modeled as a series of $R = 5.2 \text{ } \square\square$ resistors and $L = 0.8 \text{ nH}$ inductors, whereas the OFF state is modeled as a series of $C = 0.105 \text{ pF}$ capacitors and $R = 3 \text{ } \square$ resistors. Moreover, the side length L_p and the height Tl of patch element is set to 1.17 mm and 0.3

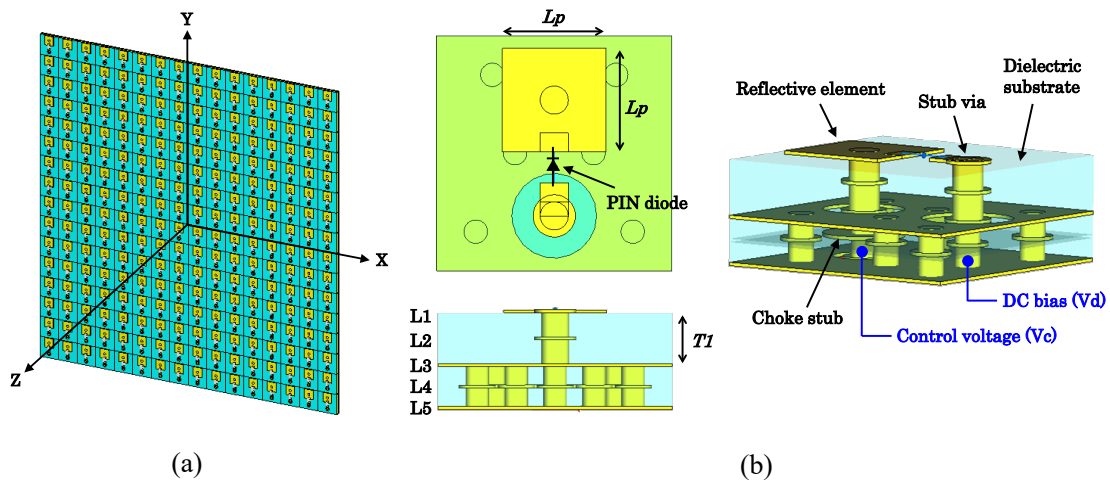


Fig. V.2.11-2 EM simulation model of IRS board.

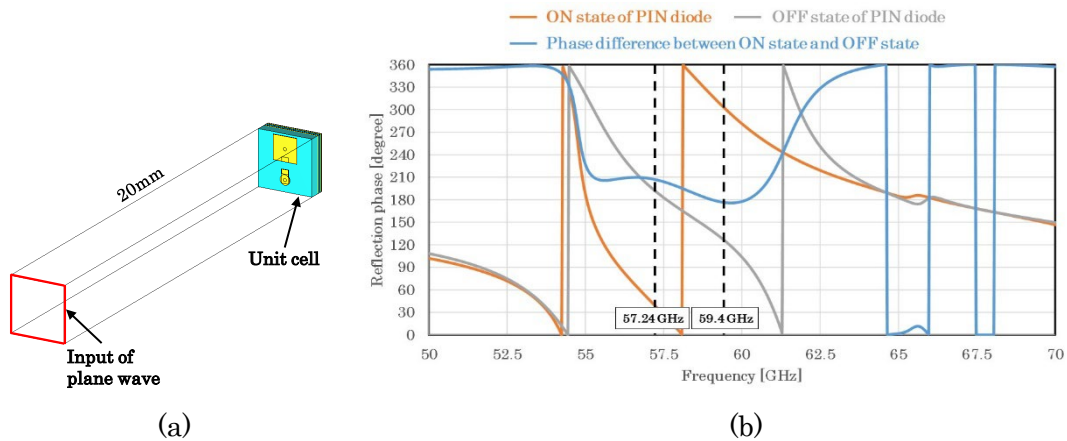


Fig. V.2.11-3. Simulation model and results for reflection phase of unit-cell.

mm, respectively.

As shown in Fig. V.2.11-3 (b), it can be seen that the phase difference between the ON state and OFF state is adjusted to approximately 180 degrees for an operating frequency (57.24 - 59.4 GHz) of wireless communication tests.

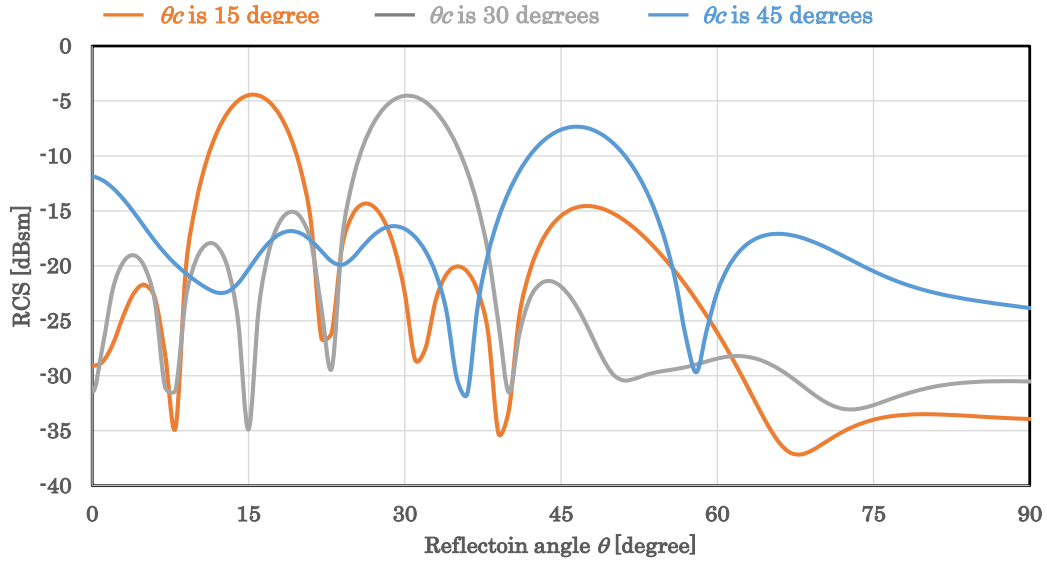


Fig. V.2.11-4 Simulated far-field patterns of reflected wave at 58.32 GHz.

2.3.2. Reflection Characteristics of IRS Board

This chapter presents the simulation results of the reflection characteristics for the IRS board shown in Fig. V.2.11-2. In this simulation, the far-field pattern of radar cross section (RCS) is analyzed when the Y-axis linearly polarized plane wave is incident from the +Z direction and each PIN diode is adjusted as shown in Fig. V.2.11-3. In Fig. V.2.11-3, the red part and the blue part are the ON state and the OFF state, respectively. By using these the ON/OFF map of PIN diodes, the reflection angle θ_c of IRS can be adjusted to 15, 30, and 45 degrees, with the front of the incident direction set to 0 degrees.

Figure V.2.11-4 shows the simulated far-field patterns of the reflected wave at 58.32 GHz. The refectoin angle θ at horizontal axis indicates the angle of inclination from the +Z direction to the +X direction for the XZ plane. From the simulated results shown in Fig. V.2.11-4, it can be confirmed that

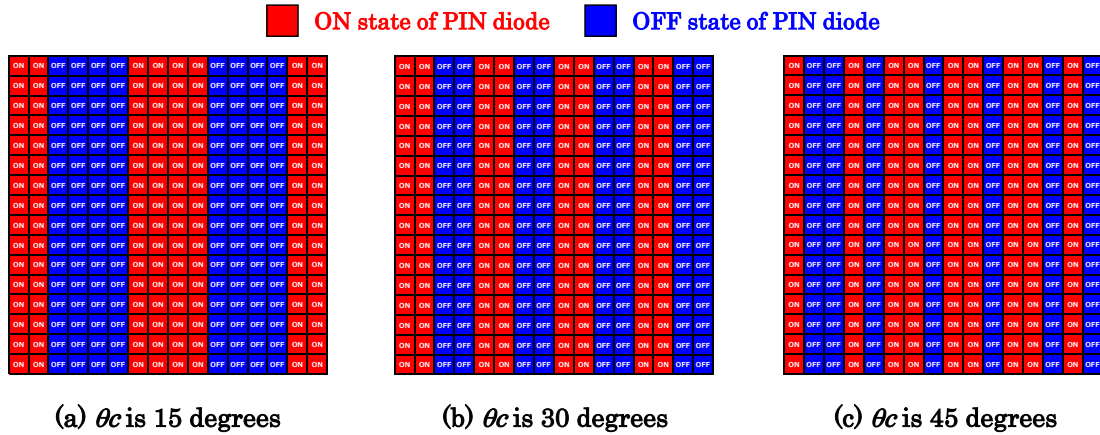


Fig. V.2.11-5 ON/OFF map of PIN diodes.

the reflected wave is tilted to the desired direction.

2.4. Characterization Experiments

2.4.1. Prototype IRS Outline

Prototype IRS shown in Fig. V.2.11-5 consists of a total of 6,400 elements, 80 each in the Y-axis vertical and X-axis horizontal directions. Element placement area is 200 mm x 200 mm, Element spacing is 2.5 mm, and Element size is 1.5 mm x 1.5 mm. Supported frequency is 58.32 GHz, and reflection phase control is a binary control of 0/180 degrees.

2.4.2. Experimental Environment and Methods

In this experiment, IRS, transmitter, and receiver are arranged as shown in Fig. V.2.11-6, and the reflection characteristics of the IRS are evaluated by changing the position of the receiver in the direction indicated by the arrow line. The transmitter is a communication device using 60 GHz band by Panasonic and the receiver is an Anritsu MS2762A spectrum analyzer. The direction of reflection of IRS is set to four patterns of 0, 15, 30, and 45 degrees, with the front of the incident direction set to 0 degrees. The receiving angle θ between the transmitter, IRS, and receiver is changed from 10 to 60 degrees in 1-degree increments. The distance between transmitter and IRS and between receiver and IRS are both 10 m. This experiment is conducted in a large anechoic chamber.

2.4.3. Experimental Results

Figure V.2.11-7 shows the experimental results. The angle θ_c shows the primary radiation direction of the reflected wave by the phase control of IRS. The results show that the received power peaks at 1 degree inside of each primary radiation direction. This is due to the characteristics of the device. The

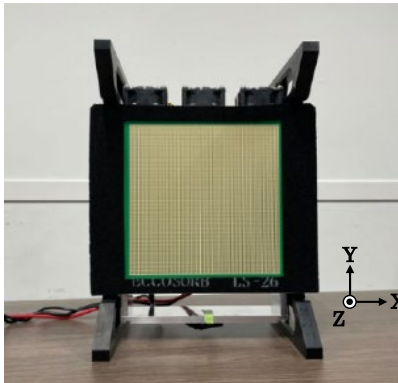


Fig. V.2.11-6 Prototype IRS.

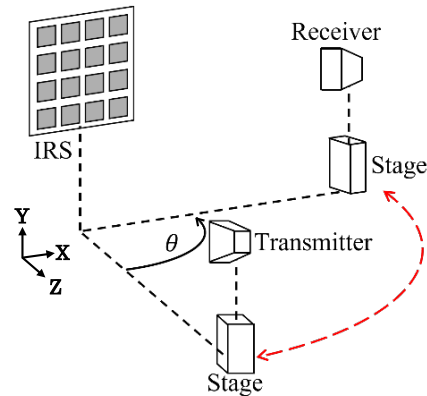
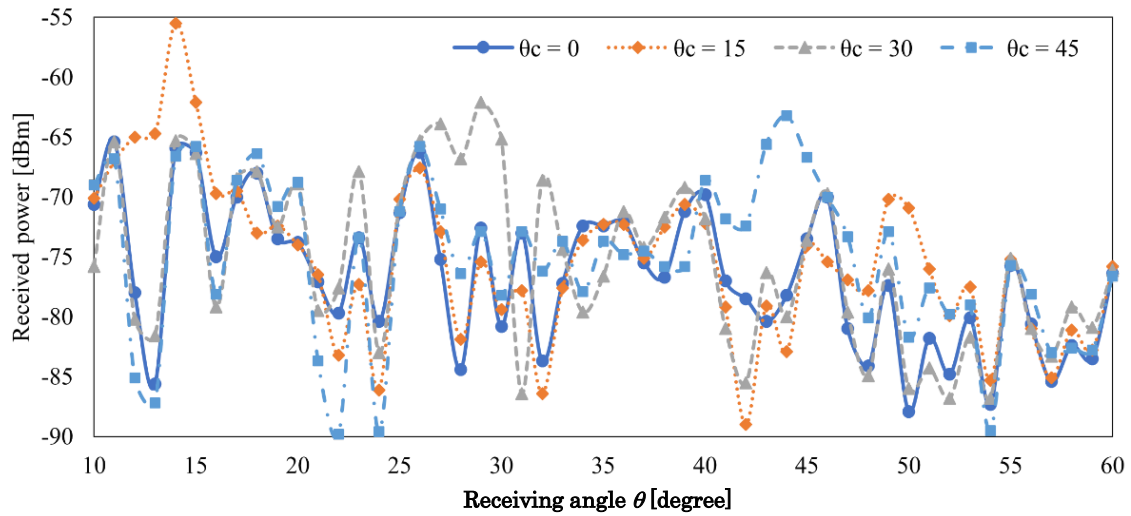


Fig. V.2.11-7 Experimental environment.

results also show that the peak in the primary direction is moderate and that the received power is not stable in the non-primary direction. This may be due to several factors. One of the major factors is that the experimental environment is small compared to the IRS, which is designed for long-distance communication.



V.2.11-8. Experimental results.

Additional video broadcasting experiments are conducted based on the characterization experiments. From this experiment, it can be confirmed that the video stopped and replayed in accordance with the operation of the IRS.

3. Conclusion

In this paper, we introduce the outline of the prototype IRS for 60 GHz band, the analyzed results by the EM simulation, and the results of characterization experiments. The development process and the experimental results show the effectiveness of the IRS as a device for improving the propagation path, and also reveal some issues, including the expansion of operating bandwidth, the reduction of beam squint, and the manufacturing cost. In the future, it will be necessary to consider the desirable equipment configuration for B5G/6G.

REFERENCE

- [V.2.11-1] Beyond 5G Promotion Strategy (Outline) (MIC, in Japanese)
https://www.soumu.go.jp/main_content/000702111.pdf
- [V.2.11-2] R. Hibi, Y. Kawamoto and N. Kato, "Standalone-Intelligent Reflecting Surface Control Method Using Hierarchical Exploration by Beamwidth Expansion and Environment-Adaptive Codebook," in IEEE Transactions on Vehicular Technology, vol. 72, no. 9, pp. 11990-12000, Sept. 2023.
- [V.2.11-3] H. Hashida, Y. Kawamoto, and N. Kato, "Selective Reflection Control: Distributed IRS-Aided Communication with Partial Channel State Information," IEEE Transactions on Vehicular Technology, vol. 71, no. 11, pp. 11949-11958, Nov. 2022.
- [V.2.11-4] D. Kitayama, D. Kurita, K. Miyachi, S. Itoh, and T. Tachizawa, "5G radio access experiments on coverage expansion using metasurface reflector at 28 GHz," 2019 IEEE Asia-Pacific microwave conference (APMC), pp. 435-437, Dec. 2019.

[V.2.11-5] L. Dai, B. Wang, M. Wang, X. Yang, et al., "Reconfigurable intelligent surface-based wireless communications: antenna design, prototyping and experimental results," IEEE access, vol. B, pp. 45913-45923, March 2020.

[V.2.11-6] A. Couch and A. Grbic, "A phase-tunable, liquid crystal-based metasurface," 10th International Congress on Advanced Electromagnetic Materials in Microwaves and Optics-metamaterials, pp. 94-96, Sept. 2016.

[V.2.11-7] Press release of Tohoku university, May 2023. (in Japanese)
tohokuuniv_press0524_01web_60ghz.pdf

V.2.12. Experimental evaluation of impact of intelligent reflecting surface for 60 GHz band on radio channel in Sub-6 GHz band

Kazuto Yano, Susumu Ano

Advanced Telecommunications Research Institute International

Yuichi Kawamoto, Hiroaki Hashida

Tohoku University

Abstract— If IRS causes an unintentional change of radio propagation in other frequency bands, independent resource allocation among multiple frequency bands may be disturbed if IRS causes an unintentional change of radio propagation in other frequency bands. To assess the impact of the reflection control of the IRS for the mmWave band on the radio propagation in the Sub-6 GHz band, an experiment evaluation was conducted using a prototype IRS for the 60 GHz band. This paper explains the experimental evaluation and its result.

1. Introduction

As described in the previous sections, Intelligent Reflecting Surface (IRS) is a key technology to enhance the coverage and flexibility of wireless communications in mmWave and higher frequency bands by changing radio propagation in communication areas. However, it may bring some restrictions in resource allocation among multiple frequency bands if IRS for a frequency band causes unintentional change of radio propagation in other frequency bands.

Therefore, using the prototype IRS for the 60 GHz band shown in Fig. V.2.11-6, an experiment was conducted to evaluate how the reflection control of the IRS changes the radio propagation in the Sub-6 GHz band. This section reports the results of this experimental evaluation.

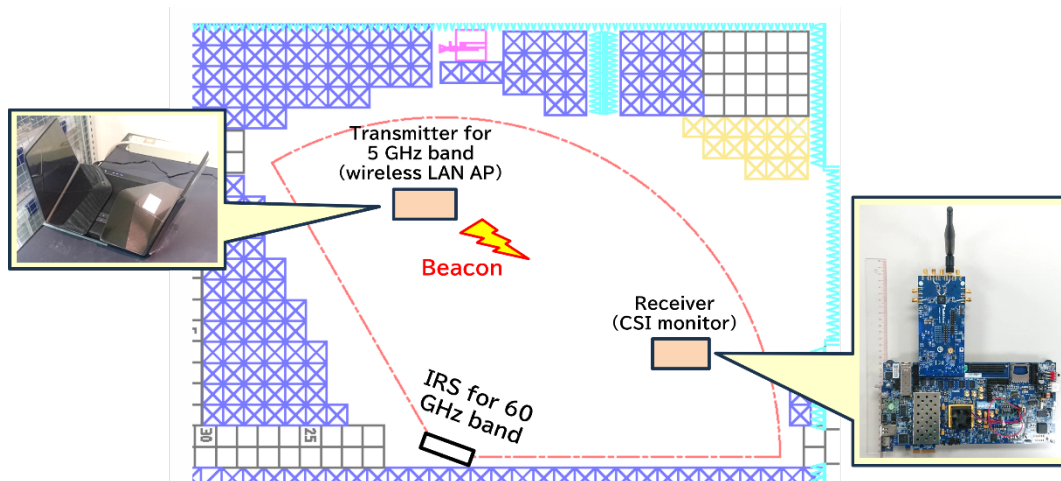


Fig. V.2.12-1. Overall configuration of prototype IRS.

2. Experimental evaluation of impact of reflection control of IRS for 60 GHz band on radio propagation in Sub-6 GHz band

2.1. Configurations of experiment

Fig. V.2.12-1 shows the configuration of the experiment. This experiment was conducted in an anechoic chamber as shown in Fig. V.2.12-2. In the anechoic chamber, a commercial access point of wireless LAN, a monitor of channel state information (CSI), and the IRS shown in Fig. V.2.11-6 are located. The access point has two omni-directional antennas, and it transmits beacon frames at Channel 48 of IEEE 802.11 wireless LAN (center frequency: 5.24 GHz) with a bandwidth of 20 MHz. The CSI monitor has one omni-directional antenna, and it records CSI of 52 subcarriers. The reflection direction of the IRS in the 60 GHz band was changed from -60 degrees to +50 degrees with a step of 10 degrees.

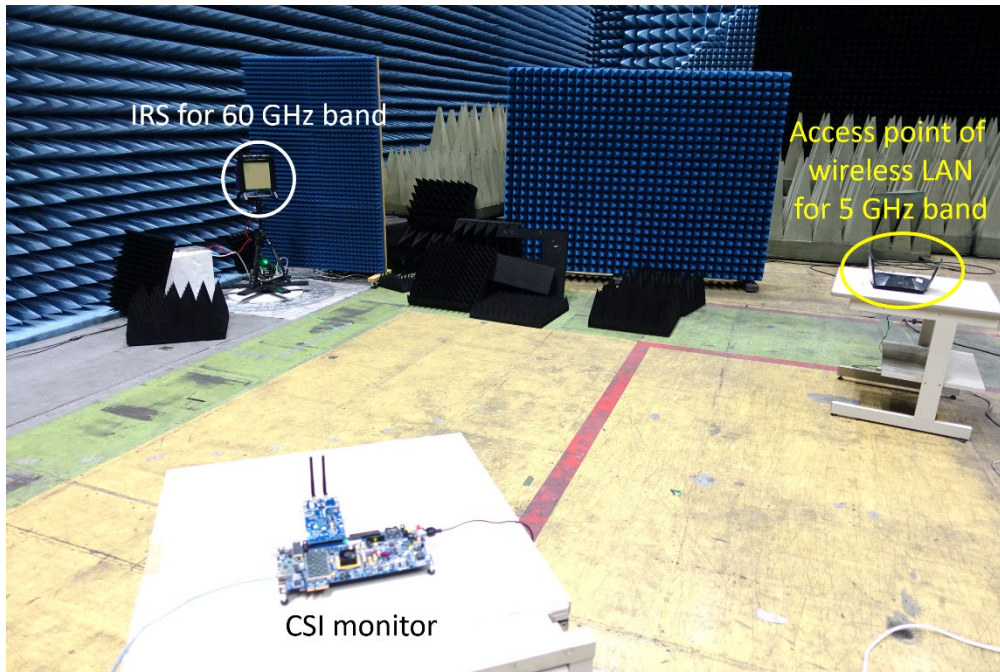


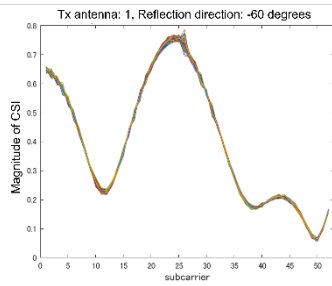
Fig. V.2.12-2. Experimental site.

2.2. Experimental results

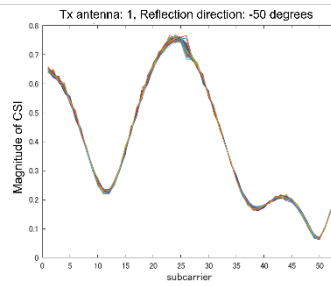
Fig. V.2.12-3 shows the measured magnitude of CSI between the first antenna of the access point and the CSI monitor with different reflection directions of the IRS. From the measurement results, it is found that multipath occurs, however, the change of reflection directions has a slight impact on the CSI in the 5 GHz band. Fig. V.2.12-4. shows the measured magnitude of CSI between the second antenna of the access point and the CSI monitor. A similar trend is found as in Fig. V.2.12-3. Therefore, it is expected that the resource allocation can be independently performed between Sub-6 band and the mmWave band in which IRS is employed.

3. Conclusion

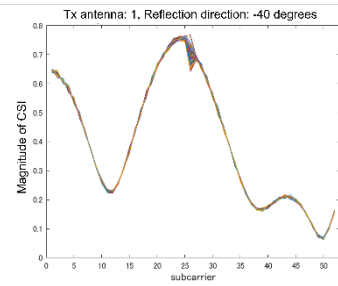
This section explained the experimental evaluation to assess the impact of the reflection control of the IRS for the 60 GHz band on the radio propagation in the 5 GHz band. Through the experimental evaluation, it was confirmed that the change of reflection directions has a slight impact on the CSI in the 5 GHz band. From this result, it is expected that the use of IRS will not disturb independent resource allocation among multiple frequency bands.



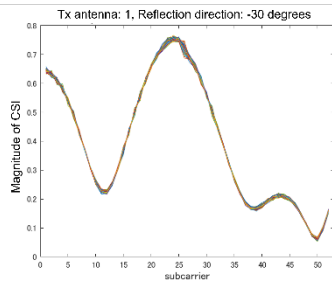
(a) Reflection: -60 deg.



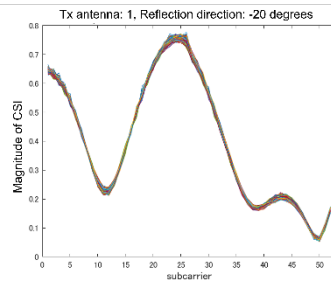
(b) Reflection: -50 deg.



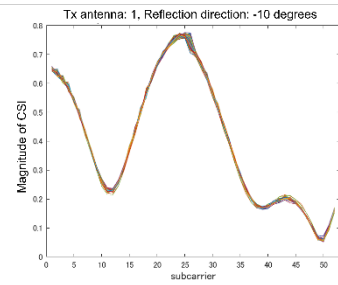
(c) Reflection: -40 deg.



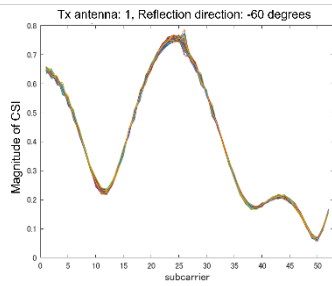
(d) Reflection: -30 deg.



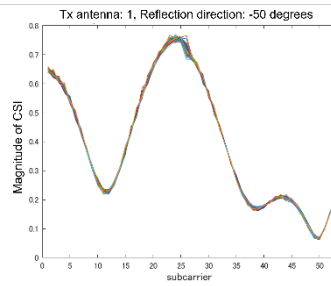
(e) Reflection: -20 deg.



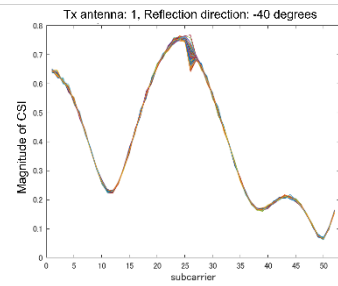
(f) Reflection: -10 deg.



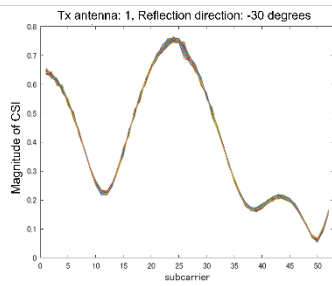
(g) Reflection: 0 deg.



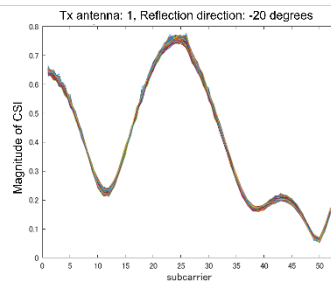
(h) Reflection: 10 deg.



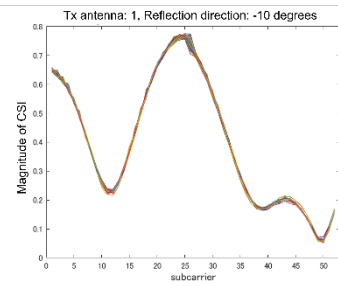
(i) Reflection: 20 deg.



(j) Reflection: 30 deg.



(k) Reflection: 40 deg.



(l) Reflection: 50 deg.

Fig. V.2.12-3. Measured CSI with different reflection directions of IRS. (First Tx antenna)

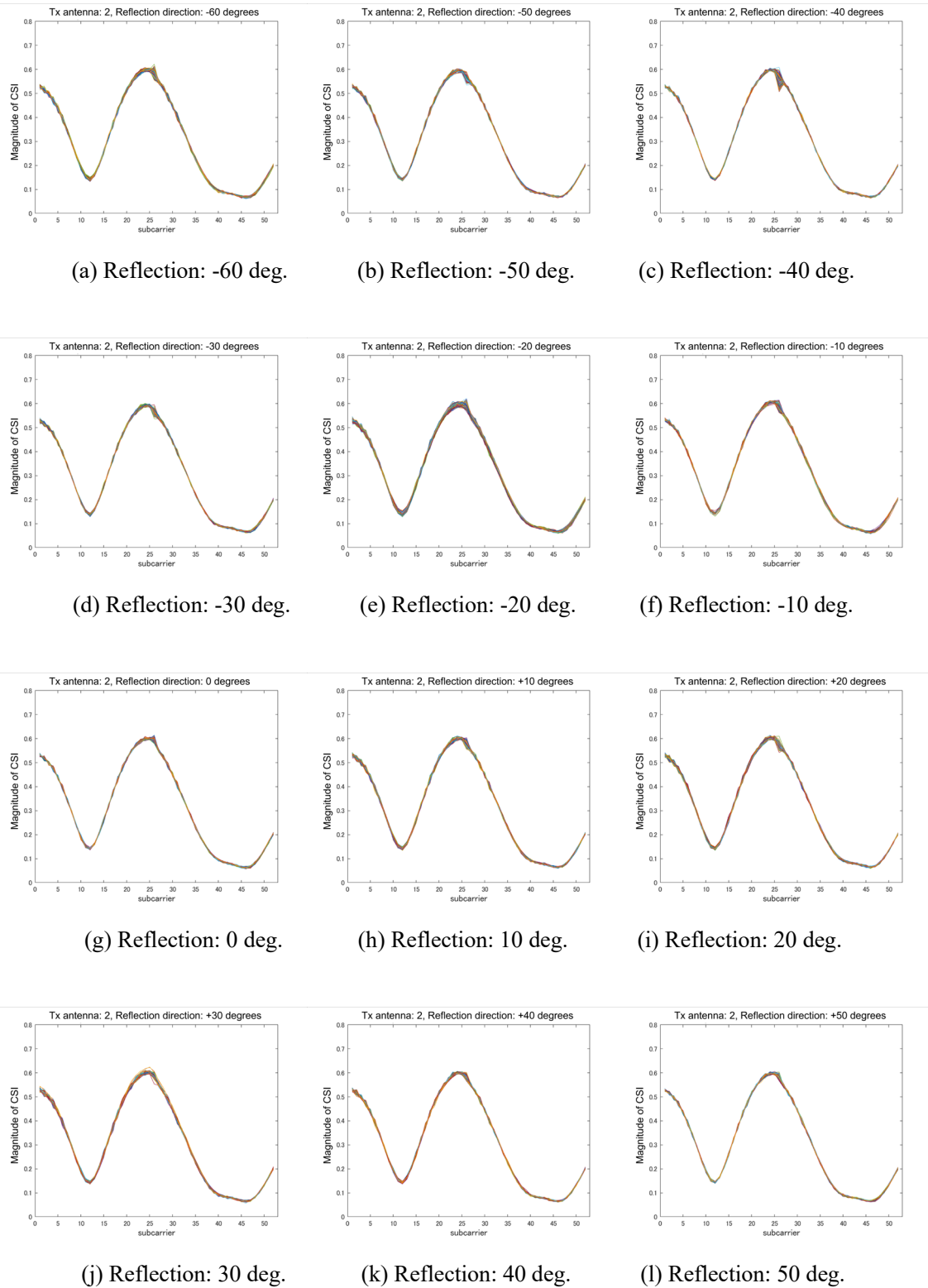


Fig. V.2.12-4. Measured CSI with different reflection directions of IRS. (Second Tx antenna)

Acknowledgements

These research results were obtained from the commissioned research (No.JPJ012368C03401) by National Institute of Information and Communications Technology (NICT) , Japan.

V.2.13. Performance evaluation of RIS-empowered 6G system by system-level and link-level simulations

Dan Mohri, Yuyuan Chang, Kiichi Tateishi, Satoshi Suyama, and Huiling Jiang
NTT DOCOMO, INC.

Abstract— In 6G, the goal is to provide extremely high-data-rate communications exceeding 100 Gbps, and to this end, the use of various frequency bands, such as sub-terahertz band and mid-band (FR3), is being studied. NTT DOCOMO has been developing a 6G system-level simulator (6G simulator) to evaluate the performance of 6G systems. New Radio Network Topology (NRNT) for constructing distributed radio network topologies in the space domain is becoming an important technical area [V.2.13-1] [V.2.13-2]. In NRNT, a variety of technologies are being studied, including distributed MIMO, the use of existing objects such as street lamps and lighting fixtures for mounting antennas, the development of advanced repeater technology, the use of Reconfigurable Intelligent Surface (RIS) reflectors that can dynamically control reflection intensity and direction, the use of mobile Base Stations (BSs), and Mobile Station (MS)-to-MS linking, all of which refer to nodes configuring a network topology and the technologies adopted for them [V.2.13-1]. On the other hand, when integrating NRNT and hybrid beamforming (BF), traditional beam selection algorithms, such as the maximum Reference Signal Received Power (RSRP) criterion, may struggle to select beams that support multiple propagation paths. To address this issue, we propose a novel method that enables beam selection toward previously unselected RIS directions. This is achieved by utilizing vectors from the kernel of the channel matrix, which includes the analog beams between the BS and the MS, as precoding vectors on the BS side. This approach generates beams with nulls in the directions of already selected RIS paths, thereby effectively enhancing multipath formation. This paper describes the 6G simulator that incorporates distributed MIMO in an outdoor urban environment. Additionally, we validate the effectiveness of our proposed method by MIMO link-level simulations, demonstrating its potential to improve 6G network performance.

1. Overview of 6G Simulator

The 6G simulator was developed to quantitatively test the 6G requirements and technical concepts described in NTT DOCOMO's 6G white paper [V.2.13-1] and to assess the feasibility of applying the sub-terahertz band or FR3 from a system perspective [V.2.13-3]-[V.2.13-5]. This simulator introduces distributed MIMO at the BS for both the Downlink (DL) and Uplink (UL). In distributed MIMO, a BS consists of multiple Transmission and Reception Points (TRPs), corresponding to the BS antennas, and a central station that consolidates those TRPs. Here, throughput can be improved through the cooperative transmission and reception at multiple TRPs. If distributed MIMO is not applied, the MS performs transmission and reception with only one TRP. This simulator installs multiple TRPs fixed to predetermined positions and evaluates DL and UL throughput characteristics of each MS during cooperative transmission or reception between those TRPs and the MS. Additionally, this simulator provides services while a drone TRP moves along a specific path to reduce propagation loss due to

blocking. Robots and self-driving vehicles are also arranged as MSs in addition to devices owned by individuals.

This simulator incorporates a massive MIMO antenna composed of multiple sub-arrays at each TRP. To simplify the evaluation, it is assumed that the reflection direction of the RIS reflector can be controlled ideally. In summary, the simulator uses the received power calculated in this manner to switch to the TRP that can communicate with the MS without delay. When distributed MIMO is applied, transmit precoding is executed for the sub-arrays of all TRPs under the control of the central station. Conversely, when distributed MIMO is not applied, transmit precoding is executed only among the sub-arrays within a single TRP.

2. 6G Simulator Utilizing Distributed MIMO in Outdoor Urban Environments

This simulator models an outdoor urban environment. It enables simulation-based evaluations at the system level for scenarios that deploy both 5G and 6G technologies within such settings. The urban scenario is illustrated in Figure V.2.13-1. This environment comprises an open public square surrounded by high-rise buildings, which, while lacking reflective objects, is adorned with trees. People, robots, and self-driving vehicles are present, either stationary or in motion. Fixed TRPs and RISs are installed on the walls of buildings or on streetlamps, while a drone TRP completes a round trip in the air along a roadside to provide services to MSs located away from the buildings in the square.

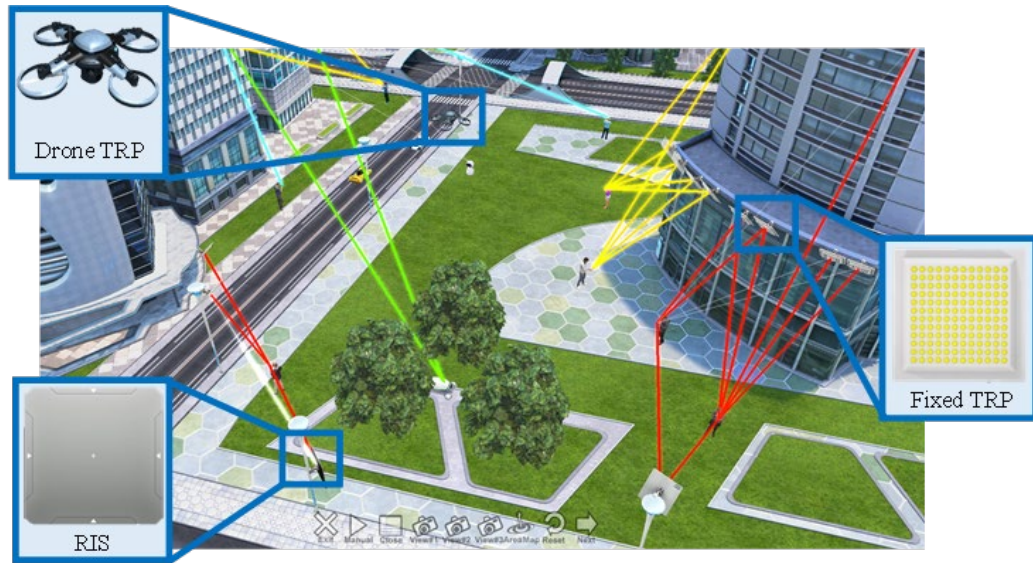


Figure V.2.13-1 6G simulator in an urban scenario.

Simulation assumptions are summarized in Table V.2.13-1. The center frequencies for Sub6, millimeter-wave, and sub-terahertz bands are 4.7 GHz, 28 GHz, and 100 GHz, respectively. Each TRP's massive MIMO antenna utilizes a planar array consisting of nine sub-arrays, with each sub-array performing analog beamforming (BF) for a single beam using an analog circuit. The duplex mode employed is Time Division Duplex (TDD), with a DL to UL time ratio of 7:3 across all slots. This evaluation environment comprises an arrangement of 22 MSs, including 18 individuals possessing MSs and the remaining four MSs mounted on two robots and two self-driving vehicles.

Table V.2.13-1 Simulation assumptions.

	Sub6	Millimeter wave	Sub-terahertz
Center frequency / Bandwidth	4.7 GHz / 100 MHz	28 GHz / 400 MHz	100 GHz / 8,000 MHz
Number of antenna elements in TRP (vertical × horizontal × sub-arrays)	144 (4 × 4 × 9)	2304 (16 × 16 × 9)	9216 (32 × 32 × 9)
Total transmission power in TRP	30 dBm		
Sub-array spacing	0.5 λ	4 λ	30 λ
TRP antenna element gain	5 dBi		
MS transmission power	23 dBm		
Number of antenna elements in MS (vertical × horizontal × sub-arrays)	144 (4 × 4 × 9)		
MS antenna spacing	0.5 λ		
Number of MIMO layers	1, 2, 3, 4, 8		

People and robots are moving at 3 km/h, while self-driving vehicles travel at 60 km/h, without stopping. In the sub-terahertz band, it is assumed that a throughput generally greater than 100 Gbps can be achieved with four or more layers. The propagation environment follows a multipath Rayleigh fading channel model, where spatial correlation among antenna elements is determined based on TRP and MS positions and antenna configuration.

The results of the MS throughput ratio without applying distributed MIMO are shown in Figure V.2.13-2. The graphs on the left side of the figure illustrate the throughput ratios for the DL and UL. Throughputs ranging from 0–1 Gbps, 1–10 Gbps, 10–50 Gbps, 50–100 Gbps, and 100 Gbps or greater are represented by five different colors, with the horizontal axis indicating time (slot number) and the vertical axis showing throughput ratio. The colors of the straight lines connecting a TRP to an MS in the figure correspond to these throughput categories. The graph on the right side of the figure depicts the throughput for User Equipment (UE) #22, which is positioned in front of a high-rise building and circled in black; here, the horizontal axis represents time (slot number) and the vertical axis shows throughput.

From Figure V.2.13-2, the graphs on the left side of the figure indicate that approximately 70% of the MSs achieved a throughput exceeding 1 Gbps in the DL, while about 9% were able to achieve a throughput greater than 100 Gbps. The graph on the right side of the figure demonstrates that UE #22 was able to consistently obtain a throughput exceeding 100 Gbps in the DL. Users in favorable environments could benefit from throughputs exceeding 100 Gbps, thanks to the advantages of greater bandwidths in the sub-terahertz band.

Next, Figure V.2.13-3 displays the evaluation results when applying distributed MIMO under the same installation conditions as shown in Figure V.2.13-2. The graphs on the left side of the figure indicate that approximately 90% of the MSs achieved a throughput exceeding 1 Gbps in the DL, while about 18% achieved a throughput greater than 100 Gbps. The graph on the right side of the figure illustrates that the throughput for UE #22 exceeded 100 Gbps in the DL, peaking at 190 Gbps. These results demonstrate that significantly higher throughput can be achieved compared to the case where distributed MIMO is not applied (Figure V.2.13-2).

The simulation results above indicate that throughput can be significantly improved by applying distributed MIMO, even in environments where the spatial multiplexing effects of MIMO may not be

fully realized due to a relatively small number of reflected waves and a predominance of line-of-sight (LOS) conditions, as seen in urban scenarios.

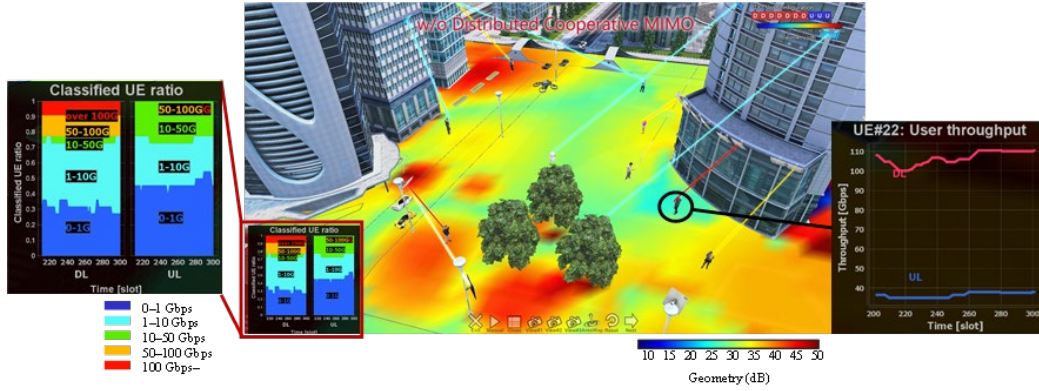


Figure V.2.13-2 Evaluation results without distributed MIMO.

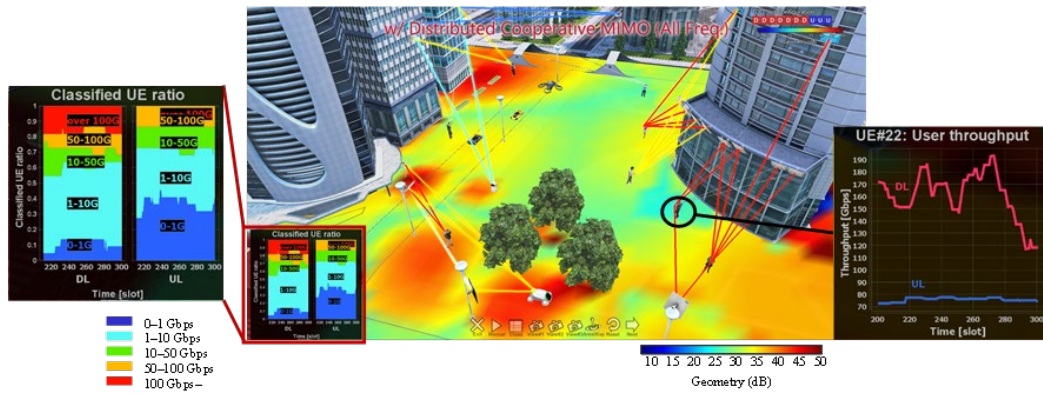


Figure V.2.13-3 Evaluation results without distributed MIMO including RIS.

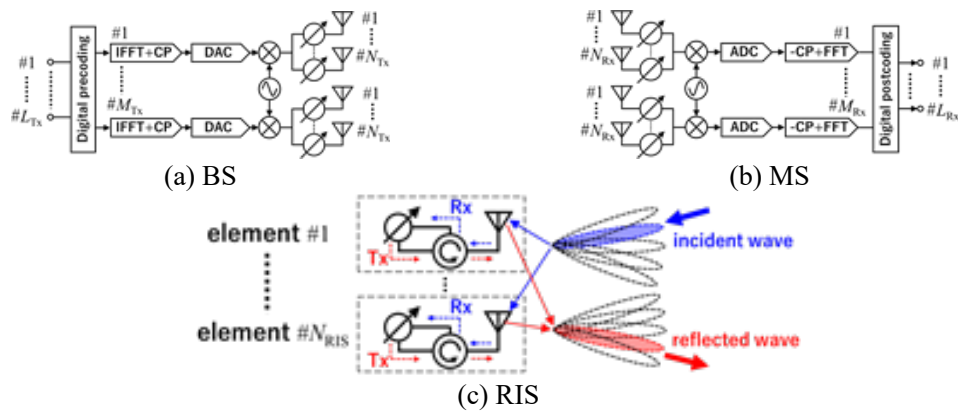
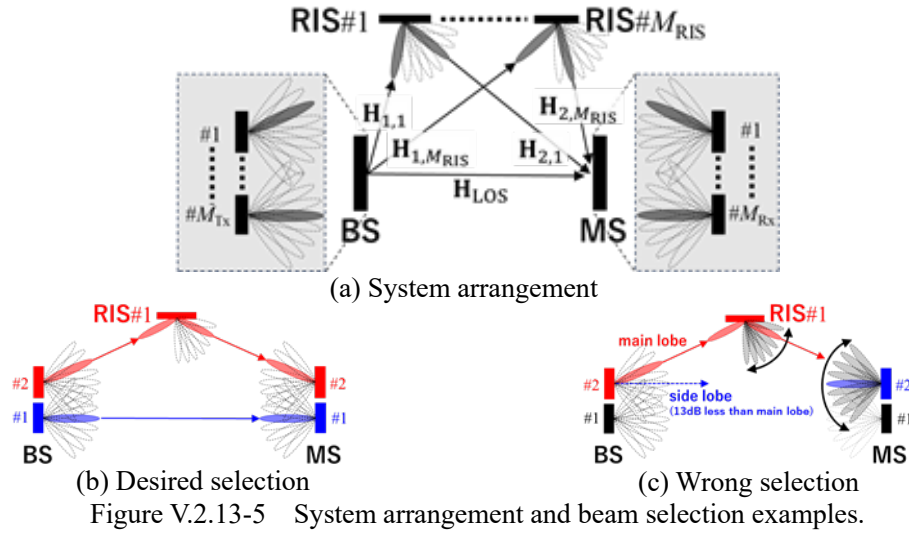


Figure V.2.13-4 System model using hybrid BF and RIS

3. System Model utilized in Link-Level Simulations for beam selection

The configurations of the BS and MS using hybrid beamforming (BF) are shown in Figures V.2.13-4(a) and (b), respectively. We assume that BSs act as transmitters (Tx) and MSs as receivers

(Rx). Analog BF is performed by the phase shifters of each antenna element. After analog BF, MIMO spatial multiplexing is conducted using fixed beamforming and Channel State Information (CSI)-based precoding (FBCP) for both the BS and MS based on CSI. The configuration including the RIS is shown in Figure V.2.13-4(c). Each antenna element of the RIS is equipped with a phase shifter that can adjust the phase of the incident wave for re-radiation as a reflected wave.



We assume that the position information of the BS and all RISs is known to the operator, allowing the beam direction to be set instantaneously from the BS toward any RIS. In contrast, the position information of the MS is unknown, and the beam directions from the BS or RIS toward each MS are determined based on the maximum received power criterion. The indices of the BS, RIS, and MS are indicated by their superscripts. The arrangement of the BS, MS, and RIS is shown in Figure V.2.13-5(a). We assume that: 1) the BS knows the positions of the RISs, and the RISs know the position of the BS; 2) the BS can immediately select the beam directed toward the selected RIS, and the RISs can similarly select the beam directed toward the BS; and 3) the BS, MS, and RIS select beams that maximize the RSRP at the MS.

Now, we will explain the challenges associated with beam selection for creating multiple propagation paths to enhance MIMO channel capacity in the system described above. For simplicity, we assume that $M_{Tx} = M_{Rx} = 2$ and $M_{RIS} = 1$, with no obstacles between the BS and MS. In this case, it is desirable for one beam from a BS subarray to be directed toward the MS and another toward the RIS, as shown in Figure V.2.13-5(b). This configuration would reduce the spatial correlation between the two subarrays of the BS and enhance MIMO channel capacity. Similarly, it is also desirable for one beam from an MS subarray to be directed toward the BS and another toward the RIS.

However, the beam directed toward the RIS may not be selected based on the assumption 3). This is because the propagation loss along the path from the BS to the RIS and then to the MS is greater than that along the direct LOS path from the BS to the MS. Even when the BS selects the beam directed toward the RIS, some power is still radiated in the LOS direction due to the side lobes of the BS

subarray antenna (in this work, the ratio of the main lobe to the side lobe is assumed to be 13 dB). Consequently, the MS may select the beam directed toward the BS (LOS), as illustrated in Figure V.2.13-5(c), which is not the desired outcome.

4. Proposed Beam Selection Algorithm with Null Steering [V.2.13-6] [V.2.13-7]

- Step A: Selection algorithm of the beams directed to RISs or MS

If there is a LOS path between the BS and MS, the beam directed toward the MS is selected; otherwise, the beam directed toward the RIS is chosen. The beam selection is based on the maximum RSRP criterion. On the other hand, the beam selection at the MS side is carried out in a similar manner.

Step B: Inductive selection algorithm of the beams directed to RISs

Using the channel matrix and its Singular Value Decomposition (SVD), we can obtain the kernel vector that points to the null space (null steering) of the channel matrix. By utilizing the kernel vector as the precoding vector, we can address the issue caused by the high level of sidelobes. Consequently, we can effectively redirect any incorrectly selected beams to the RIS.

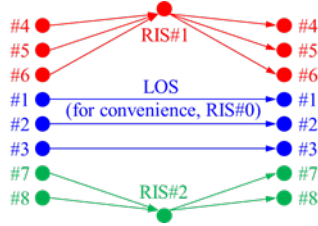


Figure V.2.13-6 Desired beam selection.

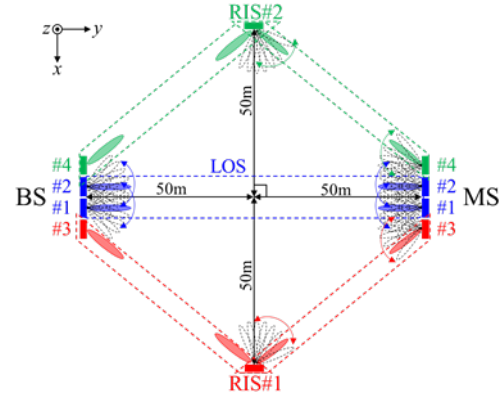


Figure V.2.13-7 Simulation topology.

Table V.2.13-2 Number of subarrays and MIMO streams

Pattern	A	B	C	D
BS subarrays ($M_{Tx,V}, M_{Tx,H}$)	(1, 2)	(1, 3)	(2, 2)	(2, 4)
MS subarrays ($M_{Rx,V}, M_{Rx,H}$)	(1, 2)	(1, 3)	(2, 2)	(2, 4)
Subarray directed to LOS $B[0]$	{1}	{1}	{1,2}	{1,2,3}
Subarray directed to RIS#1 $B[0]$	{2}	{2}	{3}	{4,5,6}
Subarray directed to RIS#2 $B[2]$	\emptyset	{3}	{4}	{7,8}
MIMO stream $L_{Tx} = L_{Rx}$	2	3	4	8

5. Evaluation Results for the Proposed Beam Selection Algorithm

To verify the effectiveness of the beam selection algorithm proposed in the previous section, we performed MIMO link-level simulations. The simulation topology is shown in Figure V.2.13-7. For comparison, the number of subarrays and the number of MIMO streams were simulated using four

patterns (A to D) as shown in Table V.2.13-2. The detailed simulation parameters can be found in our current works [V.2.13-6] [V.2.13-7].

The Signal to Noise Ratio (SNR) versus total throughput characteristics of all patterns in the simulation results are shown in Figure V.2.13-8. In patterns A and B, when the proposed method is used, the theoretical maximum throughputs 4.57 Gbps (A, 2 streams) and 6.86 Gbps (B, 3 streams) are achieved at SNR of 5 dB per Rx antenna element. On the other hand, when the conventional method is used, i.e., when beam selection is performed without using beams with null steering, the maximum throughput is not achieved even at an SNR of 30 dB. In pattern C, when the proposed method is used, the theoretical maximum throughput 9.14 Gbps (4 streams) is achieved at SNR of 30 dB. In pattern D, when the proposed method is used, the throughput is 17.38 Gbps at SNR of 30 dB, and the theoretical maximum throughput 18.28 Gbps (8 streams) cannot be achieved.

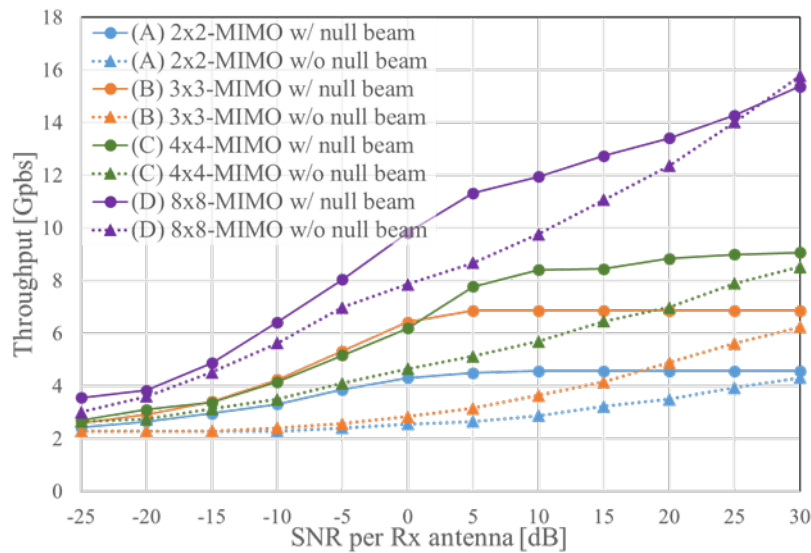


Figure V.2.13-8 SNR vs. throughput characteristics

6. Conclusions

In this paper, we described the development of the 6G simulator that incorporates distributed MIMO in the outdoor urban environment. Looking ahead, we will continue to enhance our 6G simulator to enable the evaluation and visualization of various 6G technologies at the system level, allowing users to virtually experience use cases of the 6G era based on this performance.

We also proposed the new beam selection based on the maximum RSRP in the environment with RISs to improve the spectrum efficiency. In addition, it has been confirmed by the MIMO link-level simulations in the 28 GHz band that the increasing effect of the MIMO capacity can be obtained by the proposed beam selection method in the environment with 2 RISs compared with the conventional beam selection method.

REFERENCE

- [V.2.13-1] NTT DOCOMO, Inc., 5G Evolution and 6G White Paper (Version 5.0), Jan. 2023.
https://www.docomo.ne.jp/english/binary/pdf/corporate/technology/whitepaper_6g/DOCOMO_6G_White_PaperEN_v5.0.pdf
- [V.2.13-2] Y. Kishiyama, S. Suyama, S. Nagata, “Trends and Target Implementations for 5G evolution & 6G,” NTT DOCOMO Technical Journal, vol. 19, no. 11, pp. 18–25, Nov. 2021.
- [V.2.13-3] T. Okuyama, S. Suyama, N. Nonaka, T. Asai, “6G System-level Simulator: Toward 100 GHz Band, 100 Gbps Extreme-high-data-rate Communications,” NTT DOCOMO Technical Journal, vol. 23, no. 3, pp. 13–26, Jan. 2022.
- [V.2.13-4] K. Tateishi, K. Kitao, S. Suyama, T. Yamada, “Enhancement of 6G System-level Simulators,” NTT DOCOMO Technical Journal, vol. 25, no. 2, Oct. 2023.
- [V.2.13-5] Y. Hayashi, K. Tateishi, S. Suyama, Y. Chang, H. Jiang, “Evaluation of Future Prediction Technology Using Machine Learning by 6G System Level Simulator,” IEICE Tech. Report, RCS2024-264, Mar. 2025.
- [V.2.13-6] D. Mohri, S. Suyama, Y. Chang, and H. Jiang, “Beam Selection Algorithm with BS Digital Null Beamforming in RIS-empowered 6G System,” IEICE Tech. Report, RCS2024-79, June 2024.
- [V.2.13-7] D. Mohri, S. Suyama, Y. Chang, and H. Jiang, “Hybrid Beamforming Algorithm with Null Steering for RIS-empowered 6G System,” IEEE VTC-Spring 2025, June 2025.

V.2.14. Liquid crystal reconfigurable intelligent surface

Takuya Ohto, Hiroki Aoki, Hiromi Matsuno, and Takahiro Hayashi
KDDI Research Inc.

Abstract— This paper describes the development and measurement results of liquid crystal reconfigurable intelligent surface (RIS); the design of the unit cell, scattering pattern, and experimental measurements using a local 5G system. The indoor experimental measurements show the LC RIS can improve the by 1.25 times at the median across the entire measurement range.

1. Introduction

The millimetre wave band suffers from high blockage loss, the received signal power in non-line of sight (NLOS) environments is significantly decreased. To overcome this problem, a metasurface reflector, which has an artificial surface for reflecting signals in the nonspecular direction [V.2.14-1], is expected to provide low-cost and low-power consumption coverage enhancement. This reflector comprises many passive elements, and it can reflect the incident wave towards the intended direction by adjusting the reflection phase of each element and establishing a reflection link between a transmitter and a receiver in NLOS environments. The authors focused on the low power consumption characteristics of liquid crystal and successfully realized and demonstrated a liquid crystal Reconfigurable Intelligent Surface (RIS), also known as intelligent reflecting surface (IRS). In this section, the implementation and measurements of the LC RIS are presented.

2. Unit Cell Design

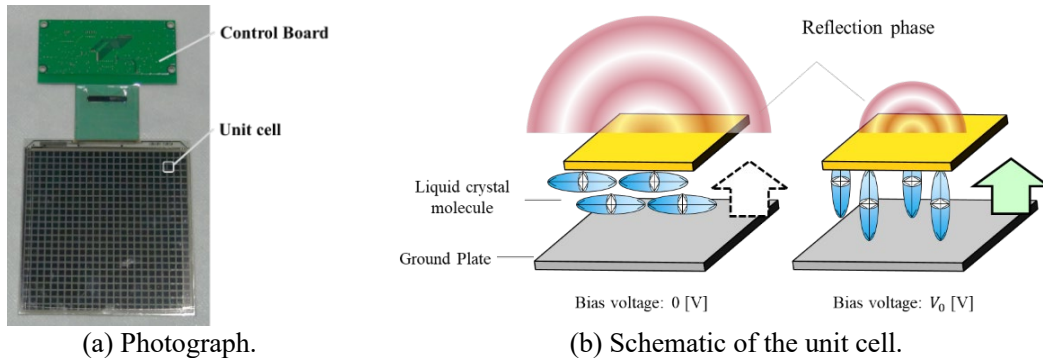


Fig. V.2.14-1 LC RIS.

In this section, the LC RIS is introduced. Although the reflection angle of the metasurface reflector in the former section is fixed once the reflector is developed, it is desirable to change the reflection angle based on the user's traffic and requirements. To address this issue, the LC RIS was developed in [V.2.14-2]. Fig. V.2.14-1 (a) and (b) show photographs of the LC RIS designed for 28 GHz and a schematic of its unit cell. The reflector utilizes LC for a reflection control functions. An LC is a molecule with anisotropy, and its electrical features, such as dielectric permittivity, depend on the direction of the molecule. The direction of the LC molecule's anisotropy is controlled by the bias voltage applied to the LC, which enables the reflector to control the reflection phase of each unit cell.

As shown in the figure, the patch element is utilized not only for reflecting elements but also for the electrode for bias voltage. The bias voltage of each reflecting element is controlled via the control board. By changing the distribution of the bias voltage, the reflection direction is controlled.

3. Scattering Pattern

Fig. V.2.14-2 shows the scattering pattern of the LC RIS. Each reflection direction is designed to reflect signals from 0 to 15, 30, 45, or 60 degrees, and the measurement results reveal that the reflector can reflect signals in the desired direction. Because polarized multiple-input-multiple-output (MIMO) is utilized in millimetre-wave communication systems to deliver high-speed data transmission, an RIS must also be applied for polarized MIMO. By changing the electric field length of the reflecting element, an asymmetric configuration is obtained in each polarization direction, and this reflector achieves a high cross-polarization discrimination (XPD) of more than 20 dB [2].

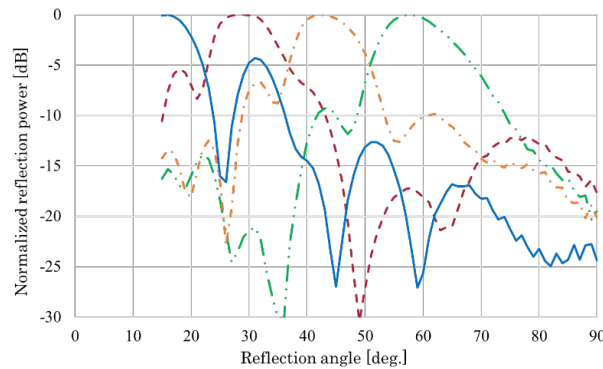
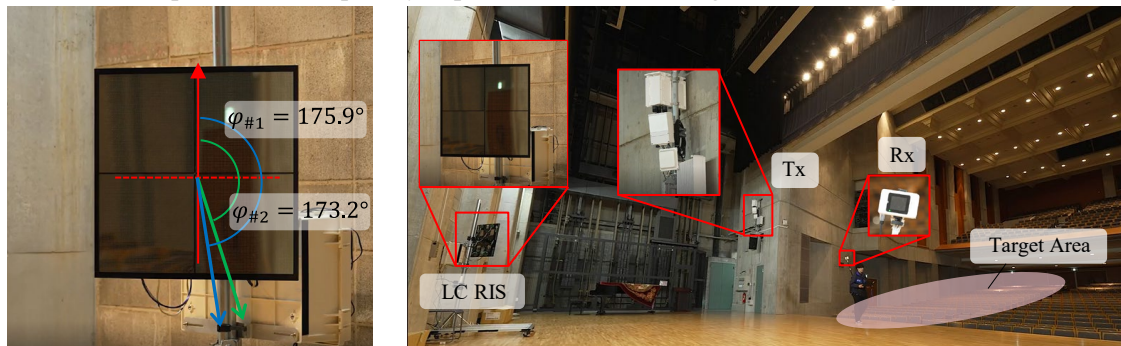


Fig. V.2.14-2 Measurement results of scattering pattern of LC RIS.

4. Indoor Trial

Fig. V.2.14-3 shows experimental validation of LC RIS in Indoor mmW system. We evaluated a large-scale prototype LC RIS (0.5m × 0.5m) in an indoor local 5G environment. The experiment was carried out using a local 5G base station of the 28 GHz band, situated within Tokyo Metropolitan University. The base station antenna was aimed at the stage in this experiment; however, certain areas of the audience seating existed coverage holes. Therefore, we improved the audience seating existed coverage holes using LC RIS. Additionally, the experiment demonstrated that by adjusting the beams of LC RIS, it is possible to temporally expand the mmW coverage in the coverage hole.



(a) Photograph of LC RIS

(b) Photograph of Measurement Environmental

Fig. V.2.14-3 Experimental Validation of LC RIS in Indoor mmW System

Fig. V.2.14-6 shows the measurement results of throughput without LC RIS and throughput with LC RIS. The results of this experiment indicated that the LC RIS improved the received signal power and throughput in coverage holes, even in this environment. Specifically, the received signal power improved by approximately 26% to 28% over the measurement range with the installation of this LC RIS. The median throughput without LC RIS was approximately 200 Mbps, which improved to around 250 to 260 Mbps with LC RIS, representing an increase of approximately 50 Mbps.

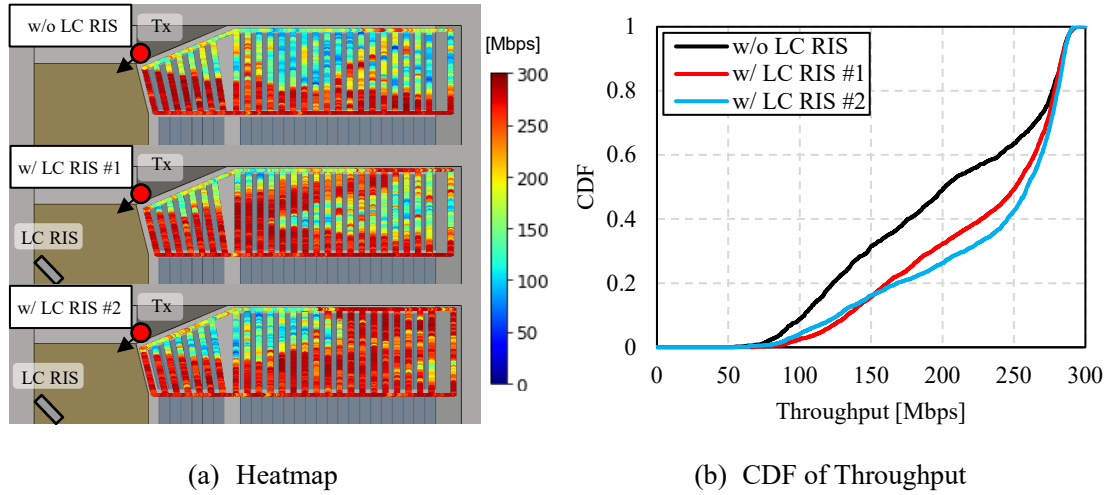


Fig. V.2.14-6 Measurement results of Throughput

5. Challenges of LC RIS

Although an LC RIS can achieve low power consumption, there are several challenges associated with this approach, including a high reflection loss and a long response time. To address the reflection loss, the author of [V.2.14-3] designed the unit cell of an LC RIS to mitigate the reflection loss, and the simulation and measurement results showed that the proposed LC RIS has a maximum reflection loss reduction of more than 10 dB. Another reference [V.2.14-4] similarly proposed a scattering pattern design in which the reflection phase with a high reflection amplitude was selected; moreover, experimental measurements with an LC RIS showed that the reflection power can increase at the desired angle. Moreover, to address its long response time, a user and passive beam scheduling scheme based on the response time of the LC RIS was proposed in [V.2.14-5]. The proposed scheme selects the passive beam that provides a high data rate for multiple users. Numerical simulations show that the proposed scheme achieves a higher throughput than does the conventional scheduling scheme, if consideration of the response time is neglected.

6. Conclusion

This section describes the implementation and measurement results of previously developed LC RIS. To efficiently reflect signals towards intended users, it is essential to mitigate hardware limitations associated with such reflectors. This section also introduces works addressing the challenges of the LC RIS, namely, high reflection loss and long response time.

ACKNOWLEDGEMENT

A part of this research was supported by the Ministry of Internal Affairs and Communications in Japan (JPJ000254).

REFERENCE

- [V.2.14-1] KDDI, Beyond 5G/6G White Paper ver.2.0.1, Oct. 2021.
https://www.kddiresearch.jp/tech/whitepaper_b5g_6g/
- [V.2.14-2] H. Matsuno, et al., "Development of a Dual-Polarized Direction-Variable Liquid-Crystal Meta-Surface Reflector for Intelligent Reflecting Surface," in *IEEE Access*, , vol. 11, pp. 95757-95767, May 2023.
- [V.2.14-3] Y. Cui, et al., "A Low-Cost Structure for Reducing Reflection Loss in Intelligent Reflecting Surface of Liquid Crystal," in *IEEE Antennas and Wireless Propagation Letters*, vol. 22, no. 12, pp. 3027-3031, Dec. 2023.
- [V.2.14-4] T. Ohto, et al., "Reconfigurable Meta-surface Reflectors: Practical Phase adjustment method and Experimental Validation," in *Proc VTC2022-Spring*, Helsinki, Finland, June 2022.
- [V.2.14-5] K. Yoshikawa, et al., "User and Passive Beam Scheduling Scheme for Liquid Crystal IRS-assisted mmWave Communications" in *Proc 2024 18th European Conference on Antennas and Propagation (EuCAP)*, Glasgow, United Kingdom, 2024.

V.2.15. Multishape radio and its experimental studies using Airy and Bessel beams in Sub-THz bands: RIS perspective on beam manipulation

Doohwan Lee, Yasunori Yagi, Kosuke Suzuoki, Riichi Kudo
NTT Network Innovation Laboratories, NTT Corporation

Abstract— Reconfigurable Intelligent Surface (RIS) technology is a key innovation in beam manipulation for next-generation wireless communication. By dynamically adjusting electromagnetic wave propagation, RIS improves signal performance, mitigates interference, and enhances spectral efficiency. Multishape radio, an application of RIS-based beam manipulation, utilizes Airy beams and Bessel beams as representative examples to optimize wireless communication in sub-terahertz (sub-THz) bands. Experimental results demonstrate three key advancements: Airy beams enable low-interference transmission for parallel data streams, and Bessel beams enhance signal-to-noise ratio (SNR) by 10 dB, ensuring robust communication in challenging environments. The integration of RIS-based beam manipulation with multishape radio techniques significantly improves data rates, spectral efficiency, and resilience, paving the way for highly adaptive next-generation communication networks.

1. Introduction

The evolution of 6G networks aims to revolutionize wireless communication by introducing unprecedented improvements in speed, latency, and connectivity. Unlike previous generations, 6G seeks to integrate advanced technologies such as non-terrestrial networks, AI-driven network management, and ultra-dense connectivity to support applications like immersive extended reality (XR), autonomous systems, and real-time sensing. As wireless technology progresses towards terahertz (THz) bands, optimizing signal transmission and mitigating propagation challenges become critical [V.2.15-1]–[V.2.15-3].

A key enabler for overcoming these challenges is Reconfigurable Intelligent Surface (RIS) technology, which allows for dynamic beam manipulation to enhance signal strength, reduce interference, and improve spectral efficiency. RIS consists of programmable metamaterials that can intelligently steer, focus, and reshape electromagnetic waves, offering a cost-effective and energy-efficient alternative to conventional network infrastructure. By dynamically adjusting beam trajectories in real time, RIS mitigates interference, reduces signal fading, and minimizes propagation loss, significantly improving communication quality. This capability surpasses conventional beamforming techniques, offering a higher degree of adaptability in directing electromagnetic waves [V.2.15-4] [V.2.15-5].

2. Multishape Radio

Multishape radio expands the potential of radio technologies by leveraging unique electromagnetic wave properties that are underutilized in conventional wireless communication. The term multishape radio reflects how distinct beam shapes arise from different wave properties, enabling novel

approaches to transmission, interference management, and signal robustness [V.2.15-6]. As an application of RIS-based beam manipulation, multishape radio demonstrates how structured electromagnetic waves enhance wireless communication. It leverages RIS to modify wave properties dynamically, optimizing beam trajectories, reducing interference, and improving signal resilience in high-frequency bands. This integration facilitates advanced beam control, improving spectral efficiency and enabling adaptive wireless transmission.

One example of multishape radio is the Airy beam, which exhibits curved power distribution along their propagation. This property allows for improved obstacle avoidance and low-interference propagation. The asymmetric sidelobe distribution of Airy beams can be leveraged for low-interference transmission, enhancing the reliability of multiple data streams [V.2.15-7]. The Bessel beam is another type of multishape radio that remains non-diffractive over long distances. This characteristic enables enhanced signal retention and self-healing properties, making Bessel beams ideal for robust transmission in obstructed environments. Their high power efficiency and non-diffractive nature also make them suitable for wireless power transfer applications [V.2.15-8].

By integrating these wave manipulation techniques with RIS-based beam steering, multishape radio offers a novel approach to optimizing wireless transmission. This synergy enhances data capacity, reduces interference, and improves communication reliability in challenging environments.

3. Experimental Study of Multishape Radio

The experiments in this section were conducted using dielectric lenses to evaluate the effect of RIS, particularly in the context of RIS-based beam manipulation. These experiments could serve as examples of beam manipulation technology.

3.1. Airy Beams for Low-Interference Transmission

Airy beams are generated using the paraxial approximation of the wave equation, where the initial condition is an Airy function. These beams exhibit a unique curved power distribution along their propagation path while maintaining intensity due to their non-diffractive nature [V.2.15-9]. However, ideal Airy beams require infinite power, making practical implementation challenging. Instead, truncated Airy beams, which consume finite power, are utilized in wireless communication. A key property of Airy beams is their asymmetric sidelobe distribution, which allows multiple data streams to be transmitted with minimal interference. By carefully positioning sidelobe-free regions, multiple Airy beams can coexist without significant signal degradation. This property is particularly advantageous for low-interference transmission in sub-THz bands [V.2.15-10].

To generate an Airy beam, a truncated Gaussian beam is processed through a phase modulation lens (PML), which applies cubic phase modulation, and then transmitted through a Fourier transform lens (FTL), forming an Airy beam in real space. This method enables beam generation using only phase manipulation without altering intensity. The PML and FTL are fabricated using 3D printing techniques, providing flexibility in beam control. We extend the concept from 1D to 2D Airy beams for practical implementation. The PML design incorporates a 2D Airy beam in the k-space, reducing transmitter

size while maintaining beam-shaping capabilities. The FTL is similarly designed to operate in k-space, ensuring efficient beam propagation. The fabricated lenses, shown in Figure V.2.15-1(a), have a focal length of 10 cm, with phase modulation achieved through depth control and modulo arithmetic to minimize volume.

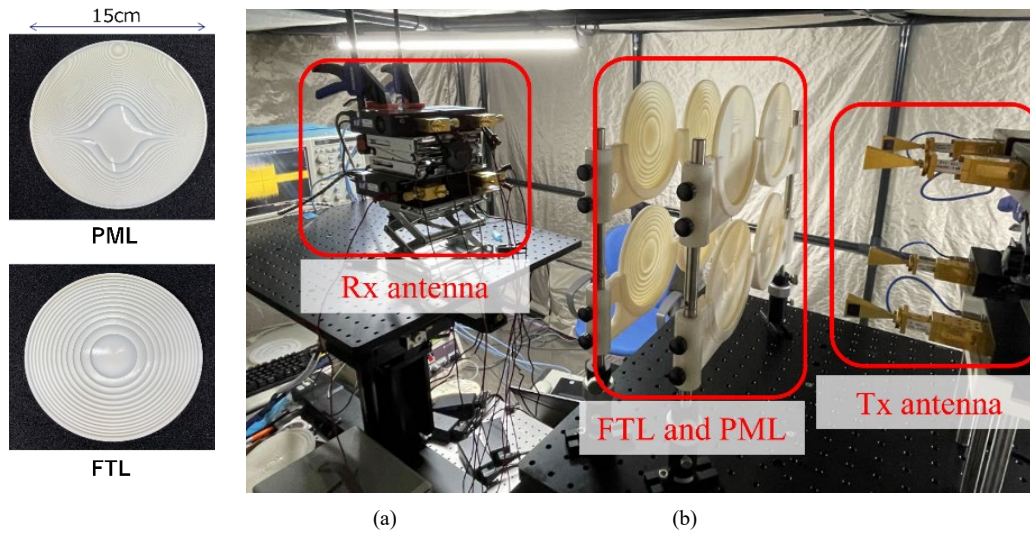


Fig. V.2.15-1 (a) Fabricated PML and FTL, (b) Experimental setup for four Airy beams transmission.

TABLE V.2.15-1. Experimental parameters

Parameter	Values	Parameter	Values
Frequency	136–152 GHz, 152–168 GHz	Code rate	1/2, 3/5, 2/3, 3/4, 4/5, 5/6
Bandwidth	32 GHz	Modulation	16 QAM, 64 QAM
Tx power	–15 dBm	Waveform	SC-FDE
Antenna gain	25 dBi (Tx) 10 dBi (Rx)	Frame length	64,800 bits
Forward error correction	BCH (Outer), LDPC (Inner)	Diameters of PML and FTL	12 cm
Frequency	136–152 GHz, 152–168 GHz	Code rate	1/2, 3/5, 2/3, 3/4, 4/5, 5/6

TABLE V.2.15-2. Experimental results of Airy beams.

Stream Number	Transmission Rate (132–152 GHz)	Stream Number	Transmission Rate (152–168 GHz)
1	48 Gb/s	1	48 Gb/s
2	53.33 Gb/s	2	48 Gb/s
3	57.6 Gb/s	3	53.33 Gb/s
4	53.33 Gb/s	4	53.33 Gb/s
Sum: 414.94 Gb/s			

Table V.2.15- 1 and Figure V.2.15-1(b) illustrate the experimental parameters and setup for four Airy beams transmission. Each beam passes through two lenses—PML and FTL—both fabricated via 3D printing. By positioning PMLs strategically, sidelobes of the four Airy beams appear in distinct quadrants, minimizing interference. The distances between Rx antennas and FTLs, FTLs and PMLs, and PMLs and Tx antennas were set to 40, 10, and 15 cm, respectively. Table 2 presents the wireless transmission results, conducted across two 16 GHz sub-THz frequency bands. The low-interference properties of Airy beams enabled successful transmission of four simultaneous data streams without significant crosstalk. Additionally, MIMO channel estimation and equalization processing were simplified, reducing computational costs significantly [V.2.15-10].

3.2. Bessel Beams for Rx SNR Enhancement

To address the significant propagation losses encountered in higher frequency bands, more efficient beamforming techniques are required. Bessel beams have gained considerable attention due to their ability to enhance received power [V.2.15-11]. These beams provide a nondiffractive solution to the Helmholtz equation, meaning their shape remains unchanged during propagation. They continue to improve received power up to a certain distance from the source. Since generating an ideal Bessel beam would require infinite power, practical implementations use pseudo Bessel beams, which can be produced with a finite power supply. However, the key characteristic of an ideal Bessel beam—its invariant distribution during propagation—is subject to distance limitations [V.2.15-12]. A Bessel beam is typically generated by directing a planewave Gaussian beam through an axicon lens, as detailed in our previous work [V.2.15-13].

Figure V.2.15-2(a) illustrates the experimental setup, which consists of a signal generator, a six-times multiplication upconverter, and an arbitrary waveform generator. A 141 GHz continuous wave was generated, followed by spatial phase modulation applied through a programmed control system. A 15 cm dielectric axicon lens was used, assuming a Gaussian beam as its input. The horn antenna was placed 20 cm away from the lens to ensure that the intensity distribution remained within the lens. To mitigate the spherical wave effects caused by the close proximity between the antenna and lenses, the phase characteristics of a spherical lens with a focal length of 20 cm were incorporated into the axicon lens. As a result, a Bessel beam was successfully generated using a single lens. On the receiving side, the planar distribution of received power was measured at various propagation distances with a spatial resolution of 2 mm in both the vertical and horizontal directions. The peak power values were obtained for each propagation distance. When measuring the received power, the time-domain waveform was first acquired, followed by a fast Fourier transform to extract only the 141 GHz component, which was then analyzed as the received power.

For comparison with conventional techniques, an additional experiment was conducted without a collimated beam and lens, using only a spherical lens with a focal length of 20 cm to compensate for spherical wave effects. Figure V.2.15-2(b) presents a comparison between the experimental results and simulation results obtained using the angular spectrum method. Although the received power of the Bessel beam decreased in the region close to the lens, the overall trend remained consistent. The results confirmed that at a propagation distance of 42.5 cm, the received power improved by 10 dB.

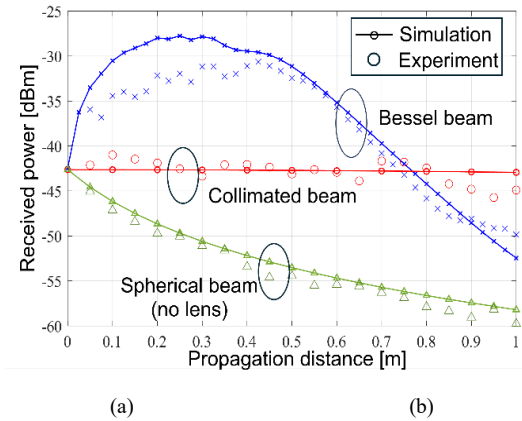
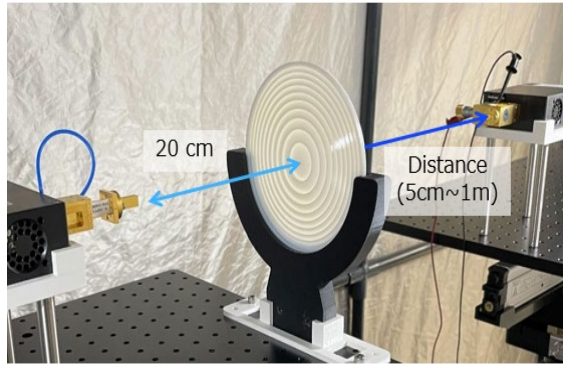


Fig. V.2.15-2 (a) Experimental setup, (b) Experimental results of received power on lens center axis at each beam when using dielectric lenses.

4. Conclusion

This study explores the concept of multishape radio, leveraging the unique propagation characteristics of structured electromagnetic waves to enhance wireless communication in sub-THz bands. As an application of RIS-based beam manipulation, multishape radio demonstrates how controlled beams can optimize mitigate interference and improve signal robustness in challenging environments. Airy beams demonstrated their potential for low-interference transmission, with four simultaneous beams achieving a total transmission rate of 414 Gb/s. By precisely controlling the sidelobe distribution, interference was minimized, enhancing reliability in dense wireless environments. Bessel beams, with their non-diffractive nature, improved received power by over 10 dB, making them particularly effective for robust communication in obstructed environments.

REFERENCE

- [V.2.15-1] W. Saad, M. Bennis, and M. Chen, "A Vision of 6G Wireless Systems: Applications, Trends, Technologies, and Open Research Problems," *IEEE Network*, vol. 34, no. 3, pp. 134–142, 2020.
- [V.2.15-2] M. M. Elshaer, M. M. E. Mohamed, and S. H. A. Begg, "Reconfigurable intelligent surfaces: A new era for wireless communication," *IEEE Transactions on Wireless Communications*, vol. 22, no. 4, pp. 1910–1923, 2023.
- [V.2.15-3] T. Zhang, Y. Yang, and J. Li, "Channel estimation and beamforming in RIS-based wireless networks," *IEEE Wireless Communications Letters*, vol. 28, no. 9, pp. 1144–1147, 2022.
- [V.2.15-4] H. Yang, C. Zhang, and X. Hu, "RIS-aided beamforming for 6G wireless communication," *Journal of Communications and Networks*, vol. 44, no. 2, pp. 58–72, 2025.
- [V.2.15-5] J. C. Liang, L. Zhang, Z. W. Cheng, P. Zhang, and T. J. Cui, "Flexible Beam Manipulations by Reconfigurable Intelligent Surface With Independent Control of Amplitude and Phase," *Frontiers in Materials*, vol. 9, p. 946163, 2022.
- [V.2.15-6] D. Lee, Y. Yasunori, and H. Shiba, "Multishape radio: New approach to utilizing the physical properties of electromagnetic waves," *IEICE Communications Express*, vol. 11, no. 9, pp. 571–576, 2022.

- [V.2.15-7] N. K. Efremidis, Z. Chen, M. Segev, and D. N. Christodoulides, "Airy beams and accelerating waves: An overview of recent advances," *Optica*, vol. 6, pp. 686–701, 2019.
- [V.2.15-8] S. Paković, et al., "Bessel–Gauss Beam Launchers for Wireless Power Transfer," *IEEE Open Journal of Antennas and Propagation*, vol. 2, pp. 654–663, 2021.
- [V.2.15-9] Y. Yagi, H. Sasaki, R. Kudo, and D. Lee, "Parabolic Reflector for UCA-based OAM Multiplexing in sub-THz Band and Transmission Experiment," in *Proc. 2023 IEEE GLOBECOM Workshops*, 2023.
- [V.2.15-10] D. Lee, Y. Yagi, K. Suzuoki, and R. Kudo, "Experimental demonstration of wireless transmission using Airy beams in sub-THz band," *IEEE Open Journal of the Communications Society*, vol. 6, pp. 1091–1102, 2025.
- [V.2.15-11] J. Durnin, J. J. Miceli Jr., and J. H. Eberly, "Diffraction-free beams," *Phys. Rev. Lett.*, vol. 58, pp. 1499–1501, 1987.
- [V.2.15-12] I. V. A. K. Reddy, D. Bodet, A. Singh, V. Petrov, C. Liberale, and J. M. Jornet, "Ultrabroadband terahertz-band communications with self-healing bessel beams," *Communications Engineering*, vol. 2, no. 70, 2023.
- [V.2.15-13] K. Suzuoki, Y. Yasunori, R. Kudo, and D. Lee, "Experimental evaluation of received-power improvement using sub-THz Bessel beam," *Electronics Letters*, vol. 61, 2025.

VI. Summary

This white paper is intended for telecom operators and vendors worldwide who will develop and deploy repeaters, RIS/IRS, and metasurfaces for Beyond 5G and 6G. Based on insights gained from the deployment of mmWave 5G by four telecom operators in Japan since 2020, the 6G Radio Technology Project of XGMF has decided to publish this white paper as a comprehensive guide for the use of repeaters, RIS/IRS, and metasurfaces in mmWave deployment for Beyond 5G and 6G.

This white paper covers use cases and scenarios, technology trends, relevant standards, and all Japanese activities related to repeaters, RIS/IRS, and metasurfaces, particularly for mmWave frequency bands. The use cases and scenarios include coverage enhancement, spectral efficiency, reliability, security, sensing, and energy efficiency enabled by repeaters, RIS/IRS, and metasurfaces, with details summarized in Sect. II. Section III provides a comprehensive survey of global technology trends up to the end of 2024, categorized into topology, system architecture, materials, and frequency aspects of repeaters, RIS/IRS, and metasurfaces.

Recent standards and related documents discussed in 3GPP NCR and ETSI RIS are summarized in Sect. IV, including the history of standardization and control plane functions supported by existing standards to orchestrate repeaters, RIS/IRS, and metasurfaces. Finally, Sect. V compiles all Japanese activities related to mmWave repeaters, RIS/IRS, and metasurfaces, including system design, theoretical analysis, hardware prototyping, and field measurements. We believe the content of this white paper will contribute to the successful utilization of mmWave frequency bands in Beyond 5G and 6G.

Although this white paper does not specifically cover network orchestration using AI, such orchestration will be essential for optimizing the operation of Beyond 5G and 6G networks that utilize mmWave along with repeaters, RIS/IRS, and metasurfaces, helping to minimize both CAPEX and OPEX. If you are interested, we welcome you to join our group in creating future white papers on the integration of repeaters, RIS/IRS, and metasurfaces with AI.

Abbreviation list

Abbreviation	Explanation
AI	Artificial Intelligence
AF	Amplify and Forward
AMC	Adaptive Modulation and Coding
AoA	Angle of Arrival
AR	Augmented Reality
ASIC	Application Specific Integrated Circuit
AWG	Arbitrary Waveform Generator
BER	Bit Error Rate
BF	BeamForming
BS	Base Station
CC	Component Carrier
CI	Close-in
CMOS	Complementary Metal Oxide Semiconductor
CPS	Cyber Physical System
CSI	Channel State Information
DC	Direct Current
DF	Decode and Forward
DFT	Discrete Fourier Transform
DL	Down Link
DNN	Deep Neural Network
DOA	Direction of Arrival
DSP	Digital Signal Processing
DU	Donor Unit
EIRP	Effective Isotropic Radiated Power
EVM	Error Vector Magnitude
eWLB	embedded Wafer Level Ball grid array
FDD	Frequency Division Duplex
FDE	Frequency Domain Equalize
FR	Frequency Range
FSPL	Free Space Path Loss

Abbreviation	Explanation
HARQ	Hybrid Automatic Repeat Request
HPBW	Half Power Beam Width
IAB	Integrated Access and Backhaul
IBO	Input Back Off
IFFT	Inverse Fast Fourier Transform
InH	Indoor hotspot cell
IRS	Intelligent Reflecting Surface
ISAC	Integrated Sensing and Communication
ITU-R	International Telecommunication Union Radiocommunication Sector
KPI	Key Performance Indicator
LAN	Local Area Network
LC	Liquid Crystal
LNA	Low-Noise Amplifier
LOS	Light of Sight
LTE	Long Tern Evolution
MCM	Multichip Module
MEMS	Micro Electro Mechanical Systems
MIMO	Multiple-Input and Multiple-Output
MMIC	Monolithic Microwave IC
MS	Mobile Station
MOS	Metal Oxide Semiconductor
MOS-HEMT	Metal-Oxide-Semiconductor Eigh-Electron-Mobility Transistor
MSL	Microstrip Line
NCR	Network Controlled Repeater
NLOS	Non-Line of Sight
NR	New Radio
NRNT	New Radio Network Topology
NSA	Non-Stand Alone
OAM	Orbital Angular Momentum
OFDM	Orthogonal Frequency Division Multiplexing
PA	Power Amplifier

Abbreviation	Explanation
PCB	Printed Circuit Board
PCM	Phase Change Material
PLE	Path Loss Exponent
QMH	Qualitative Microwave Holography
RAN	Radio Access Network
RAT	Radio Access Technology
RD	Relay Device
RF	Radio Frequency
RIS	Reconfigurable Intelligent Surface
RMSE	Root Mean Square Error
RS	Relay Station/Repeater
Rx	Receiver
SAG	Selective-Area Growth
SC	Single Carrier
SiP	System-in-Package
SISO	Single-Input Single-Output
SIW	Substrate-Integrated Waveguide
SNR	Signal to Noise power Ratio
STAR	Simultaneously Transmitting and Reflecting
SU	Service Unit
TDD	Time Division Duplex
TDS	Time Domain Spectroscopy
THz	Tera Hertz
TMA	Trimethylaluminum
TSV	Through-silicon Via
Tx	Transmitter
UCA	Uniform Circular Array
UE	User Equipment
UL	Up Link
VR	Virtual Reality